SEDIMENTOLOGY, PETROGRAPHY, AND TECTONIC SIGNIFICANCE OF CRETACEOUS TO LOWER TERTIARY DEPOSITS IN THE TINGRI-GYANGTSE AREA, SOUTHERN TIBET

By

Bin Zhu

A Dissertation

Submitted to the University at Albany, State University of New York

in Partial Fulfillment of

the Requirements for the Degree of

Doctor of Philosophy

College of Arts & Sciences

Department of Earth & Atmospheric Sciences

2003

Abstract

Cretaceous and Lower Tertiary sedimentary rocks are well exposed in the Tingri-Gyangtse area, tectonically belonging to the central Tibetan Himalayas, to the south of the Indus-Yarlung-Zangbo suture. The Cretaceous Tianba flysch in the Tianba-Jiabula region is correlative with the Giumal Group sandstone in Zanskar, northwestern Himalayas. There are significant amounts of chrome-rich spinels in turbiditic sandstones from the upper part of Tianba Flysch, which might suggest ophiolite derivation and a Cretaceous ophiolite obduction event on the northern Indian continental margin in southern Tibet. However the compositional range of these detrital spinels closely matches that of spinels from intra-plate basalts. About 5% of the spinels contain melt inclusions. The compositions of melt inclusions correlate well with those of host spinels. Melt inclusion geochemistry also suggests a source of hotspot basalts. It is concluded that the Rajmahal volcanics were the source for these Cr-rich spinels. The continuous Cretaceous to Lower Eocene marine sedimentary series in the Gamba and Tingri areas suggest that the Indian-Asian collision must have started after the deposition of the youngest marine shelf sediments. Petrographical analysis of sandstones reveals that the monocrystalline quartz grains of cratonic origin are dominant in the Paleocene Jidula Formation; in contrast there are significant amounts of immature framework grains with a distinct ophiolitic and volcanic arc influence present in the Eocene Youxia Formation and the younger Shenkeza Formation. Geochemistry in both sandstones and shales complement the petrographic data indicating that the source of the Jidula Formation primarily consisted of quartzose basement rocks, while the Youxia and Shenkeza Formations are mainly derived from the uplifted Gangdese arc-trench system. The compositions of Cr-rich spinels in the Youxia and Shenkeza sandstones are similar to those from fore-arc peridotites, most likely from the arc and ophiolite rocks along the Yarlung-Zangbo suture to the north. No spinels have been observed in the Jidula sandstones. Therefore the early Tertiary detrital sediments in Tingri record a marked change in provenance in the early Tertiary, which indicates that the onset of India-Asia collision was at ~47 Ma in southern Tibet.

I would like to dedicate this dissertation

to my parents, Weilan Jiang & Shouqing Zhu,

who would have been proud to have seen its completion.

Acknowledgements

Without the help and encouragement of numerous people, the successful completion of this work would have been impossible. I owe a great deal of gratitude to the Department of Earth and Atmospheric Science. To each of the members of the Department who have worked with me, I express my most sincere thanks. In particular, members of my committee, Drs. John Delano, Greg Harper, Bill Kidd, and David Rowley, are greatly thanked for continuous support, inspiring discussions during my graduate studies in Albany, and for meticulously reading and correcting my early draft of this thesis. Their criticisms and concerns were sometimes difficult to overcome, but this thesis and I clearly benefited. Special thanks go to the two faculty members who have given me the most in terms of their time, advice and support. Bill Kidd introduced me to the fantastic world of the Himalayan geology, and supervised this thesis with much patience during its ups and downs. I especially appreciate him for his financial support through my graduate career. I learned a tremendous amount from him, including the importance of self-reliance, accuracy, organization, logic, and imagination. His support for this project and for me is immeasurable. John Delano introduced me to the geochemistry of melt inclusion and chrome spinel, and provided working facilities in the Petrology Lab. His expertise at geochemistry of melt inclusion gave form and substance to the melt inclusion chapter of this thesis. He also taught me, both in words and by example, how to be careful and dedicated in a scientific research.

Two field trips in southern Tibet laid the foundation of this thesis. I am highly grateful to the help and support from Drs. Binggao Zhang and Yugan Jin in Nanjing. Successful fieldwork would have been impossible without their well-made preparation and organization. I will never forget the ‘bear’ cave in the top of the Zhepure Shan Mountain, where we spent a night on October 22, 2000 without winter coats and tents. Special thanks go to Drs. Brian Currie, Bill Kidd, David Rowley and Binggao Zhang for their help in the field.

Moral support and encouragement also came from other faculty members, staff and fellow students. Students’ seminars were part of my graduate experience here, and very important for me to develop this thesis. I appreciate Drs. Win Means, John Arnason, Brad Linsley for their thought-provoking questions and inspiring discussions in the seminars. Special thanks go to Diana Paton, our department secretary, for taking care of my administrative and family troubles in Albany. I greatly benefited from almost daily discussions with my fellow graduates. They are Adam, Barbara, Chul, Elizabeth, Fasong, James, Lei, Steffi, Stefan, Taohong, Vera, Youshe, who help me to maintain my motivation and excitement for this project.

The electron microprobe results in this thesis were generated at RPI Probe Lab, and I am grateful to Kiera Becker and David Ward for their insight and patience during endless hours of probe analysis. Special thanks are due to Steve Howe for his advice on heavy mineral separation.

None of this would have been possible without the love and support from my family. My wife Weiwei is something very special. I want to thank her for the patience and understanding during my adventurous graduate career over the past years. My son Frank makes a difference in my life every day, and I am sorry for I cannot be with him during many weekends and evenings. Wutong Miao and Zhanme He, my in-laws, are thanked for their moral support and encouragement. Very special thanks go out to my brother, Tao Zhu, his wife, Meihua He, and his daughter Xiaomin. They have helped me in many ways, both large and small. I am very happy to have them as part of my life. Thank you all for your love and support.

This research was supported by National Science Foundation grant to Bill Kidd and David Rowley. Microprobe work was partially supported by SUNY Benevolent Association Research Grant and SUNY GSO Research Grant to Bin Zhu.

TABLE OF CONTENTS

LIST OF TABLES

LIST OF FIGURES

CHAPTER THREE

CHAPTER FOUR

Chapter 1. Introduction of the Himalayas in south Tibet

Introduction

The Himalayan-Tibetan orogenic system (Figure 1.1), the "Roof of the World", is one of the most spectacular tectonic events of the Cenozoic time on our planet (Dewey et al., 1989). The Himalaya, a type continent-continent collision, stretch between two structural syntaxes: Nanga Parbat on the west and Namche Barwa on the east, defining a 2500-km-long arc of mountain ranges, that are the result of collision between the India and Eurasian continents (Gansser, 1964; Hodges, 2000). This system provides an excellent opportunity to study the complicated processes by which continents respond to collisional orogenesis, because the Himalaya are one of the youngest and ongoing continent-continent collision zones in the world (Monlar and Tapponnier, 1975, 1977, 1978, 1985; Tapponnier, et al., 1981, 1982, 1986;Yin and Harrison, 2000; Hodges, 2000). Consequently, tectonic models proposed for the evolution of the Himalayan-Tibetan orogenic system have been widely used in our interpretation of the tectonics of older mountain belts, such as the Appalachian belt in North America and the Ural Mountains in central Eurasia (Dewey and Bird, 1970).

Furthermore, recent studies have shown that the uplift of the Himalayan and Tibetan plateau have affected not only the immediate environment but also the development of Asian climatic patterns, the chemistry of the ocean, and the motion of at least some of the Earth's lithospheric plates through the last 50 Ma (Richter et al., 1993;

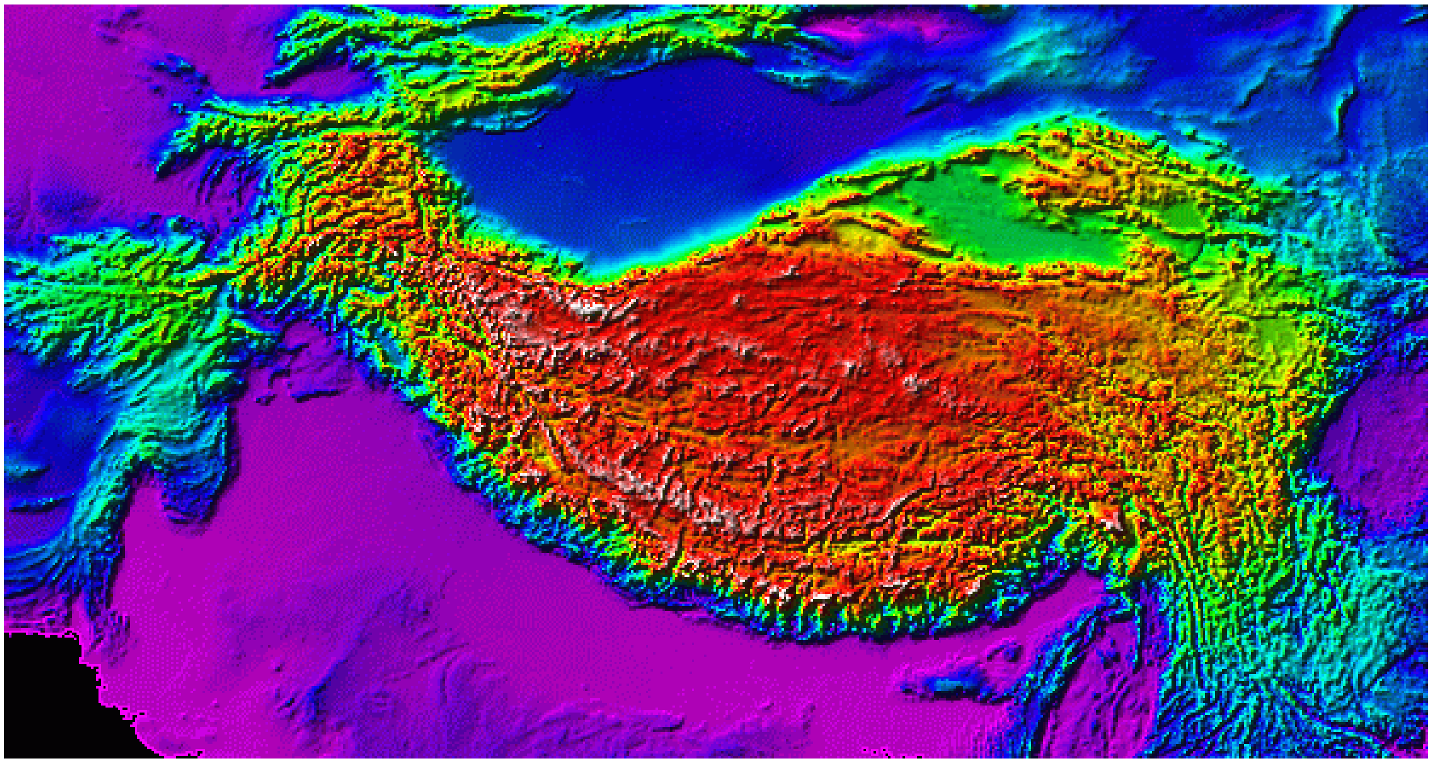

Figure 1.1 Himalayas-Tibetan Plateau Topography (from http://www.geo.cornell.edu).
This image is a false-color, shaded relief image with illumination from the northwest. The shadowing gives an indication of local relief while color indicates elevation as follows: magenta=sea-level; blue=1000m; cyan=2000m; green=3000m; yellow=4000m; red=5000m; white=6000m and above.

Butler, 1995; Beck et al., 1995; Clift et al., 2000, 2001, 2002). It has been suggested that India-Asia collision and closure of the Neo-Tethyan sea led to a marked change in climate from wet equatorial in Paleocene to tropical semiarid in Eocene, with formation of a major unconformity and widespread development of red beds, as well as pedogenic carbonates (caliche) and local evaporates (Garzanti et al., 1987, 1988; Wang et al., 2002).

This study focuses on the Tethyan Himalaya, lying between the High Himalayan Crystallines to the south and the Indus-Zangbo Suture and the Lhasa block to the north (Figure 1.2). The Tethyan Himalaya consist of late Precambrian to early Eocene sedimentary rocks. The Neo-Tethyan Ocean started with rift-stage in the Triassic (Sengor et al., 1988), and formed a relatively wide passive continental margin along the north rim of the Indian continent in the Mesozoic. During the Mid-Cretaceous, a forearc basin (Xigaze Forearc Basin) evolved along the southern margin of the Lhasa block (Durr, 1996; Einsele et al., 1992), when this ocean started to close by northward-directed subduction beneath it (Figure 1.3). The analyses of magnetic anomalies from the Indian ocean have shown that India drifted northward at least 4000 km, and perhaps as much as 7000 km (Van der Voo et al., 1999), with drift rates up to 150-200 km/Ma (Klootwijk and Peirce, 1979; Patriat and Achache, 1984; Besse et al., 1984; Besse and Courtillot, 1988; Patzelt et al., 1996). The India-Asia collision started somewhere in the interval of late Cretaceous and early Tertiary (Molnar and Tapponnier, 1975; Jaeger et al., 1989; Beck et al., 1995; Rowley, 1996, 1998, and references therein; Garzanti et al., 1987, 1996; Yin and Harrison, 2000; Najman and Garzanti, 2000; Xu, 2000; Li et al., 2000; de Sigoyer et al., 2000, 2001; Searle, 2001; Aitchison et al., 2002, 2003; Wan et al., 2002;

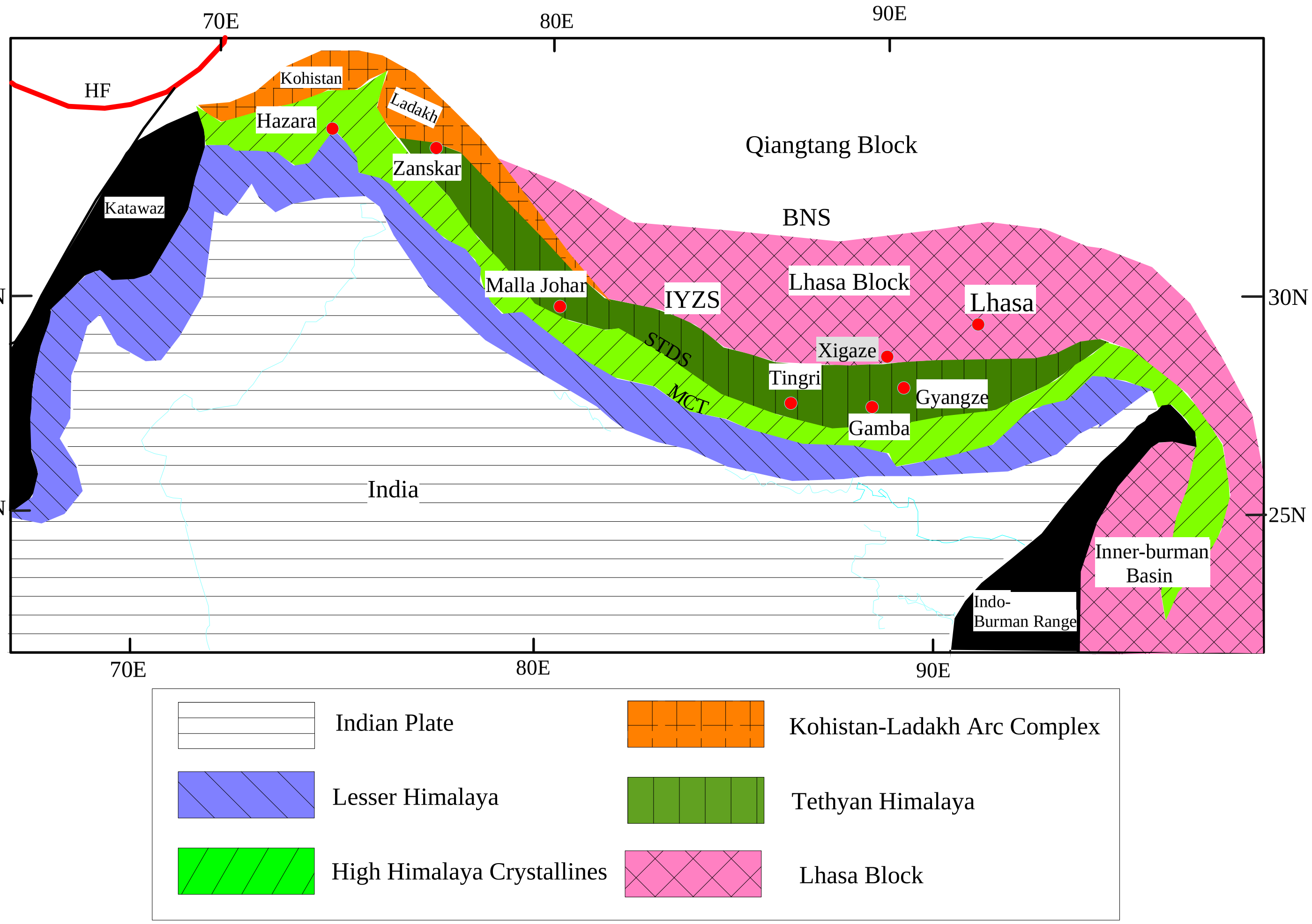

Figure 1.2 Regional geological map of Tethyan Himalaya (modified after Rowley, 1996)
BNS: Banggong-Nujiang Suture IYZS:Indus-Yarlung-Zangbo-Suture, MCT:Main-Central-Thrust, STDS:Southern-Tibet-Detachment-System

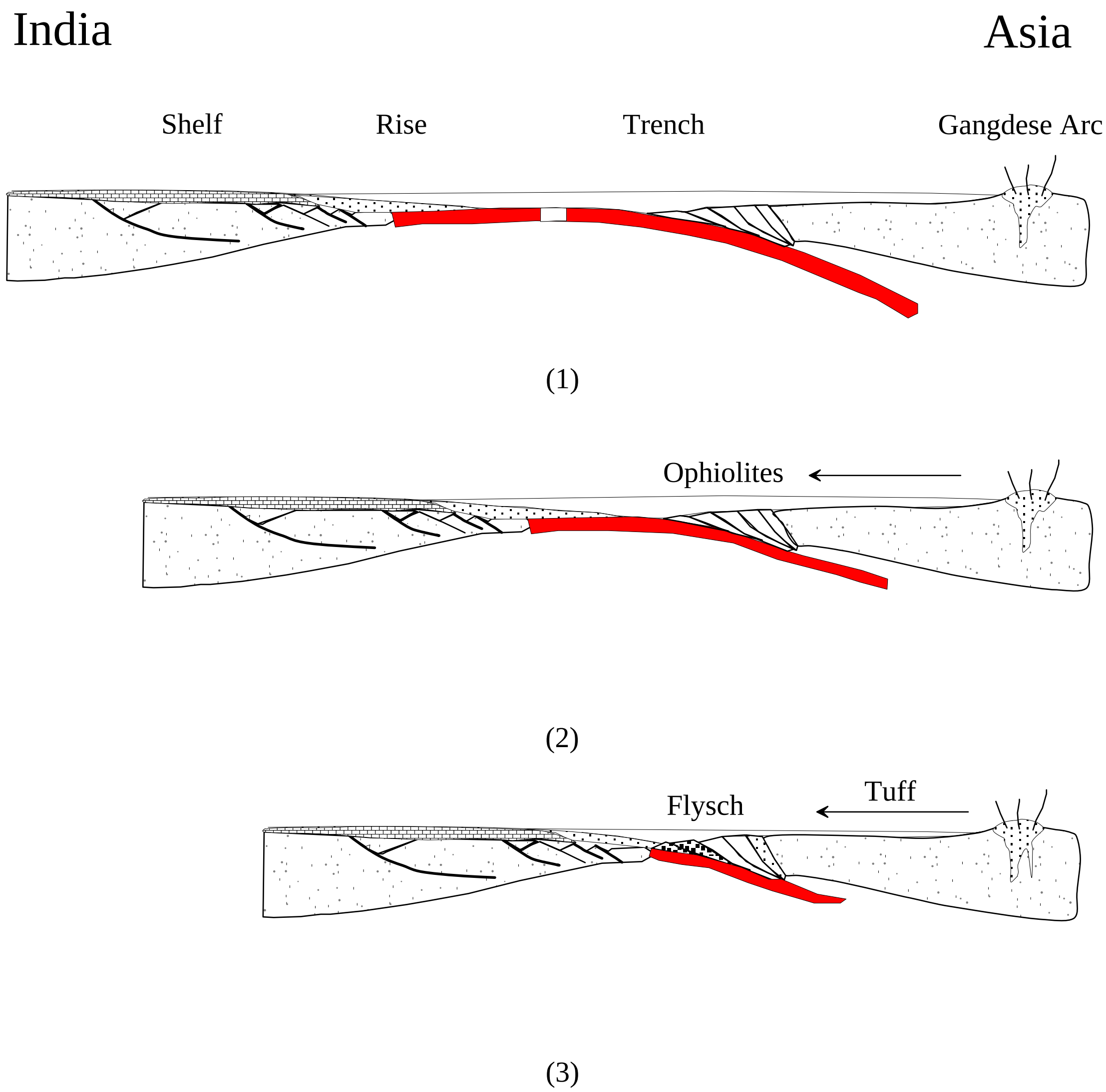

Figure 1.3 Schematic cross-sections of the India-Asia convergence up to the initiation of collision (modified after Rowley and Kidd, 1981). (1) Cretaceous; (2) Paleocene; (3) Eocene.

Wang et al., 2002, Najman et al., 2002), giving rise to the Indus-Yarlung-Zangbo suture (IYZS), which contains remnants of material that once lay between India and Asia prior to continental collision (Nicolas, 1989; Chang, 1996). Therefore the Mesozoic and lower Tertiary sedimentary series of the Tethyan Himalaya record the drift history of peninsular India and its collision with the Eurasian continent.

Two tectonic problems in southern Tibet

As the Himalayan orogeny is considered to be an icon for modern continent-continent collision (Dewey and Bird, 1970; Molnar, 1984), the geology of southern Tibet has been a main focus of studies for the past three decades, which have significantly improved our understanding of the evolution of the Himalayas, and hence of collisional processes in general (Allegre et al., 1984; Burg and Chen, 1984; Tapponnier et al., 1981; Molnar and Tapponnier, 1978; Searle et al., 1987; Dewey et al., 1988, 1989; Harrison et al., 1992; Burchfiel et al., 1985, 1991, 1992; Liu, 1992, 1994; Zhao et al., 1993; Nelson et al., 1996; Chang, et al., 1996; Hao et al., 1995, 1999; Matte et al., 1997; Chemenda et al., 2000; Yin and Harrison, 2000, Hodges, 2000). Despite Tibet's geological significance, and some excellent preliminary investigative work, the area is vast and remains poorly understood, and most of its geology is known largely from sketchy reconnaissance. For the Tethyan Himalaya in southern Tibet, a number of important aspects still remain unclear or controversial: 1. When did the Indian continent start to collide with Asian continent in the eastern Tethyan Himalayas? 2. Is there any record of an ophiolite-obduction event in the Cretaceous in the southern Tibet? This study concentrates on the well-exposed Cretaceous to lower Tertiary sedimentary rocks of the Tethyan Himalaya collision in the Tingri-Gyangtse area to try to answer these questions about the tectonic and sedimentary evolution before and up to the start of the India-Asia.

Approach to the problems

Petrographic studies and detrital modes of sandstones

Sediment composition is obviously controlled by the source rocks from which the sediment is derived. As such, the composition of sediment correlates well with the source rocks under many conditions. Since tectonic setting in turn controls source rock composition, the conjunction of plate tectonics and sandstones composition has shown that sandstones from a variety of tectonic settings exhibit considerable diversity that is related to tectonic association (e.g., Dickinson et al., 1979, 1980, 1983, 1985, 1988; Ingersoll et al., 1979, 1984; Yerino and Maynard, 1984; Valloni and Maynard, 1981). Accordingly it is possible to reconstruct the plate tectonics settings of source areas by analyzing the detrital modes of siliciclastic strata in diverse depositional basins (e.g., Garzanti, 1987, 1996; Ingersoll et al., 1995). In the work of Dickinson (1985), the ternary plots of quartz-feldspar-lithics distinguish three major provenance terranes; they are continental blocks, magmatic arcs, and recycled orogens (Figure 1.4). The continental blocks include stable cratons and basement uplifts, which are tectonically, consolidated regions of amalgamated ancient orogenic belts that have been eroded to deep levels. The magmatic arcs include the volcanic chain, granite plutons and metamorphosed sediments

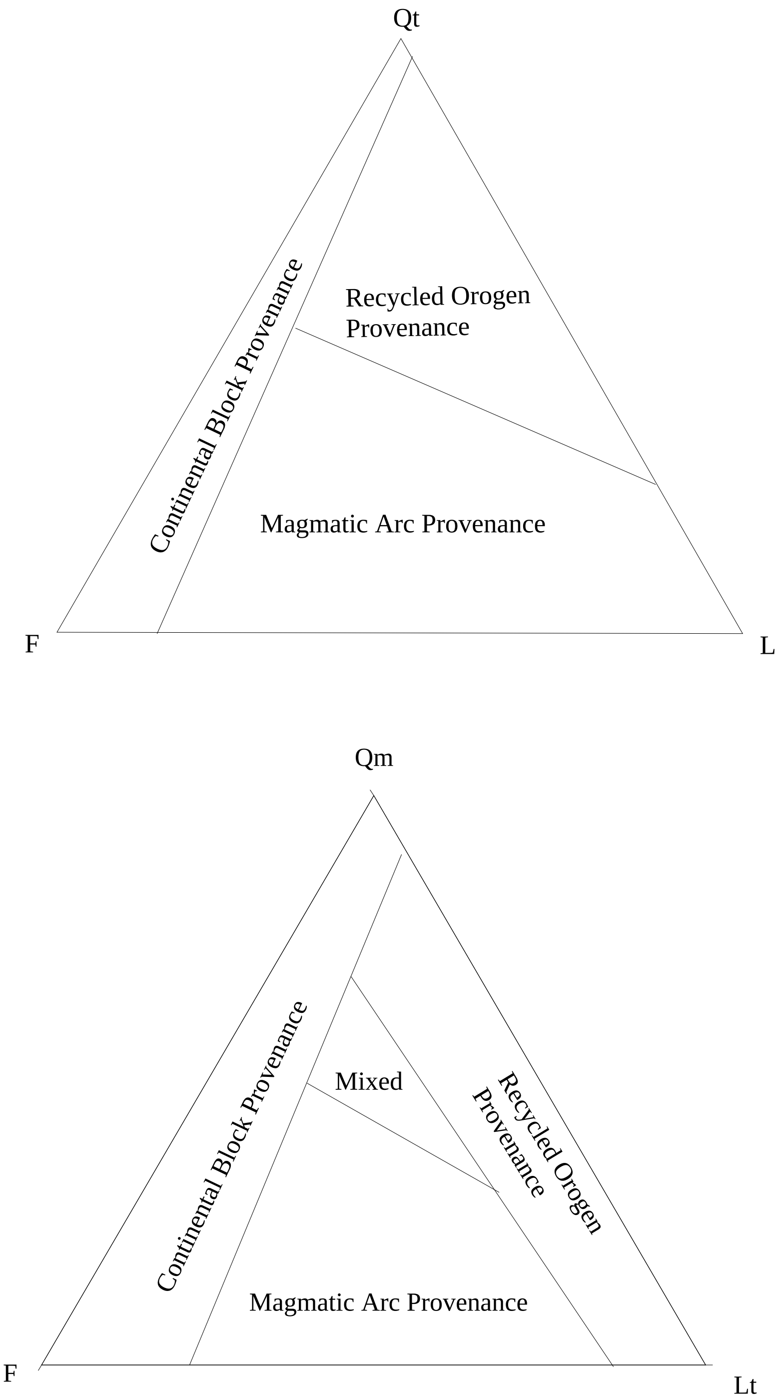

Figure 1.4 Detrital mode distribution in three major tectonic settings. After Dickinson et al. (1983).
Qt: monocrystalline quartz+polycrystalline quartz; Qm:monocrystalline quartz; F: feldspar, L:rock fragments; Lt: rock fragments+polycrystalline quartz.

in arc-trench systems. Recycled orogens contain uplifted and deformed sedimentary and volcanic rocks, which are exposed to erosion by orogenic uplift of fold-and-thrust belts, and they mostly consist of sediments, but include volcanic rocks and metasediments.

Heavy mineral analysis

A large number of heavy mineral species with specific gravity > 2.80 have been recorded from sandstones, and many of these are exceptionally source-diagnostic (Morton, 1985, 1991; Mange and Maurer, 1992; Evans and Mange, 1991). They are extracted from disaggregated sand by separation in dense liquids, such as bromoform, and examined in grain mounts. Much use, therefore, has been made of these heavy minerals in provenance studies, even though most sands typically contain less than 1% by weight.

The content and composition of a heavy mineral assemblage is controlled not just by provenance, but also by various modifying factors in the sedimentary environment that alter the heavy minerals from those present in the source rock to those identified under the microscope (Morton, 1985; Morton and Hallsworth, 1999). The most influential of these is source-area weathering, processes of transportation and deposition, and post-deposition alteration. Their behavior during diagenesis is in accord with their chemical stability and is manifested by the progressive decline of individual heavy mineral species with increasing depth of burial. Thus the use of the heavy mineral assemblage of a sand as a provenance indicator must be used with caution, noting that it will also reflect the hydraulics of sediment transport and deposition and burial history. For correct interpretation of provenance, it is critical that the parameters used are inherited from the source area and are not modified to any great extent by process operative during the sedimentation cycle.

Conventional, species-level, heavy mineral studies carried out on low-diversity assemblages are often problematic, leading in many cases to erroneous conclusions (Morton, 1991, Mange, 1995). Considering the fact that heavy minerals with similar densities and hydraulic behavior are not affected by changes in hydraulic conditions during sedimentation, Morton and Hallsworth (1994) proposed a number of mineral ratios that largely reflect provenance characteristics. Ratios such as apatite/tourmaline, rutile/zircon, chrome spinel/zircon are useful indicators of changing provenance in deeply-buried sandstones, and the garnet/zircon ratio is also useful providing that garnet can be demonstrated to be stable within the sequence under investigation.

By contrast, a ‘high-resolution heavy mineral analysis’ (HRHMA) subdivides heavy minerals into varietal types based on the recognition that rock-forming and accessory minerals crystallize within a range of pressure-temperature conditions, which determine both their chemistry and morphology (Mange, 1995; Dewey and Mange, 1999). The majority of minerals show a diversity of habit, color, internal structure, chemistry and optical properties that are signatures of geophysical and geochemical parameters during crystallization. Heavy mineral species in sediments are therefore represented by several varietal types which provide extremely valuable information about their parent rock lithologies, as well as providing important clues to the identification of lithostratigraphic units with a common provenance and differentiating them from those with different sedimentary histories.

Distinguishing the varietal types of the chemically highly resistant minerals, such as zircon, tourmaline, and apatite, proves most useful since they are ubiquitous and remain stable during diagenesis. An important advantage of HRHMA is that, because it deals with each particular species, the influence of modifying factors (especially hydraulic and diagenetic) is considerably reduced. According to Dewey and Mange (1999), differentiation of provenance using HRHMA concentrates on parameters are acquired from the petrographic microscope, such as color, habit and internal structure. For zircon, they suggest that the euhedral-subhedral grains are derived from granitoids, migmatites, and some mafic rocks; anhedral and rounded elongated crystals can be from reworked sedimentary or metasedimentary sources; rounded to well-rounded, pink and purple grains are derived from the Precambrian shield; and zoned crystals with overgrowths are from a high-grade metamorphic paragenesis and contact metamorphic rocks.

The advent of electron microprobe analysis has added a new dimension to heavy mineral analysis by allowing the geochemical characterization of individual mineral suites (Morton, 1991). This type of information enables direct mineralogical comparison between source and sediment since the microprobe provides confirmation of optical identifications and greater accuracy in identifying source lithologies. This approach can be applied to many mineral species, but is best used on minerals that are stable.

In short, there are three techniques to characterization of sediment provenance using heavy minerals. Three stages have been undertaken on the heavy minerals separated from sandstones in the Tingri-Gyangze area: 1. Using conventional heavy mineral analysis to characterize, differentiate and map sand types, which provides important information on the nature and location of source areas; 2. Using HRHMA to study varieties of zircon, tourmaline, apatite, providing direct mineralogical comparison with potential source areas; 3. Using microprobe analysis to acquire geochemical characterization of individual grains (e.g., spinel, garnet), which gives direct chemical composition constraints on the source region. This integrated approach provides a through evaluation of sediment provenance in the work area.

Geochemical analysis

The geochemical composition of clastic sediments is also controlled by the composition of source rocks and has often been successfully applied to provenance studies, which significantly adds accuracy to detrital modal analysis. A number of major oxide and trace element-based diagrams may indicate the plate tectonic setting of sediments (Bhatia, 1983, 1985; Taylor and McLennan, 1985; Bhatia and Crook, 1986; Roser and Korsch, 1986, 1988; McLennan et al., 1990, 1993). The best discrimination parameters are provided by ratios of stable trace elements that are quantitatively transferred from source to sink.

One of important advantages of geochemical analysis for studies on sedimentary provenance is that geochemical approaches are equally applicable to coarse- and fine-grained sedimentary rocks (Roser and Korsch, 1986; McLennan et al., 1990, 1993). Because of being better mixed and more homogenous than coarser grained fractions, argillite-mudrock members of sedimentary sequences commonly preserve the source signature most accurately (Najman and Garzanti, 2000). In addition, given the fact that most provenance-diagnostic, but commonly less resistant grains (e.g., olivine, volcanic rock fragments), may have been preferentially broken down into matrix, there is great potential for evaluating the origin of sandstones with substantial amounts of secondary matrix where alteration does not affect bulk chemistry and trace element abundances.

Organization of Text

The organization of the thesis is as follows. Chapter two is a review of the Cretaceous and early Tertiary stratigraphy of the study area based on recently published data (both English and Chinese). Results of mid Cretaceous Tianba Flysch in the Tianba-Jiabula region are presented in Chapters three, four, and five. Studies on early Tertiary clastic rocks are presented in Chapter six.

Chapter three is a manuscript submitted to Journal of Geology, with co-authoirs William S.F. Kidd, David B. Rowley, and Brian S. Currie. We reported that there are abundant Cr-rich spinels in the Tianba Flysch. From the chemical compositions of the Cr-rich spinel data, likely source rocks for these spinels are not arc-complexes or plutons or ophiolites but flood basalts associated spatially and temporally with Kerguelen hotspot activity at 117 Ma. This event is related to the break-up of India, Australia, and Antarctica in the early-mid Cretaceous.

Chapter four is a manuscript submitted to Earth & Planetary Science Letter, with co-authors John W. Delano, William S.F. Kidd, and Brian S. Currie. This is a report of the study on the melt inclusions trapped in Cr-rich spinels in the Cretaceous Tianba Flysch in southern Tibet. The compositions of homogenized melt inclusions correlate well with the compositions of hosted spinels, which show a possible co-crystallization of olivine and spinel in the parental magma. The discriminant diagrams show that these melt inclusions were most likely sourced from hot-spot basalt. As such, this study confirms the inference that the volcanics of Rajmahal provide significant volcanic components to the Tianba Flysch based on the Cr-rich spinel characteristics presented in Chapter three.

Chapter five reports geochemical data of the Tianba Flysch in southern Tibet. The geochemistry of sandstone-shale suites indicates a passive margin provenance, and constrains the Tianba Flysch to have been predominately derived from quartzose basement and mature sedimentary rocks most likely the Indian subcontinent to the south. However, there is geochemical evidence of a significant volcanic input in the upper part of the Tianba Flysch, which is consistent with the petrographic and heavy mineral studies reported in chapters three and four.

Chapter six is a manuscript on the provenance and tectonic significance of lower Tertiary clastic rocks in the Tingri region, with co-authors William S.F. Kidd, David B. Rowley, and Brian S. Currie. The provenance of sandstone/shale in the well-exposed lower Tertiary section of Zhepure Shan Mountain has been constrained using petrographic, geochemical whole-rock and single-grain analyses. Our data indicate that there is a marked change in sediment character during the deposition of early Tertiary detrital sediments. The Jidula sandstones are characterized by dominant mono- and poly-crystalline quartz of cratonic origin while the Youxia and Shenkeza sandstones are enriched in immature framework grains such as plagioclase and volcanic lithics. This change indicates that the onset of India-Asia collision and development of the foreland basin occurred at ~47 Ma in eastern Tethyan Himalaya.

Chapter 2. Stratigraphy of the Cretaceous and lower Tertiary Strata in the Tethyan Himalaya of southern Tibet

Abstract

Cretaceous and Lower Tertiary sedimentary rocks are well exposed in the Tingri-Gyangtse area, tectonically belonging to the central Tethyan Himalayas (originally Indian continental margin), to the south of the Indus-Yarlung-Zangbo suture. The E-W trending Gyirong-Kangmar thrust divides the sedimentary sequences into two subzones of different lithological compositions. The southern zone consists of stable continental shelf deposits of massive limestones, reefal limestones, and sandstones, as well as subordinate shales, and dolomites, that are continuously exposed in the Gamba-Tingri area to the south of the Lhago-Kangri mountains. The frequent occurrence of fossils well constrain the relative age of these rocks. In the northern zone, sediments in the Gyangze-Kangmar area are characterized by dark shales, deep-sea chaotic clastics, pelagic radiolarites, cherts, and marls, that were deposited in a continental slope and rise setting. Chaotic deposits, mainly derived from the passive margin, are well developed in the late Cretaceous. Detailed studies on these sediments in southern Tibet should provide important information on the early geology of the Himalayan system.

Introduction

The Tethyan Himalayas in the southern Tibet can be divided into two subzones of different lithological compositions (Figure 2.1), separated by the East-West trending Gyirong-Kangmar thrust (Burg and Chen, 1984; Liu, 1992). The northern zone is dominated by slightly metamorphosed deposits of outer shelf, continental slope, and deeper-water deposits of the continental rise, and the southern zone is characterized by non-metamorphic, shallow water shelf calcareous and terrigenous deposits with gentle and subtle lateral changes in lithofacies and thickness, which range from Cambrian to Eocene without any significant angular unconformity (Wen, 1987; Xu et al., 1989; Liu, 1992; Willems et al., 1993, 1996).

1.1. Southern zone

The marine Cretaceous sequence of the southern Tethyan Himalayan zone is best exposed in the mountain ranges east of Gamba, and west of Tingri (Willems et al., 1996), which are regarded as local stratotypes for the Cretaceous and lower Tertiary in southern Tibet (Zhang and Geng, 1983; Xu et al., 1989).

Gamba area

The Gamba area is geologically dominated by a syncline striking approximately E-W with a southward vergence and overthrusting (Willems and Zhang, 1993) (Figure 2.2).

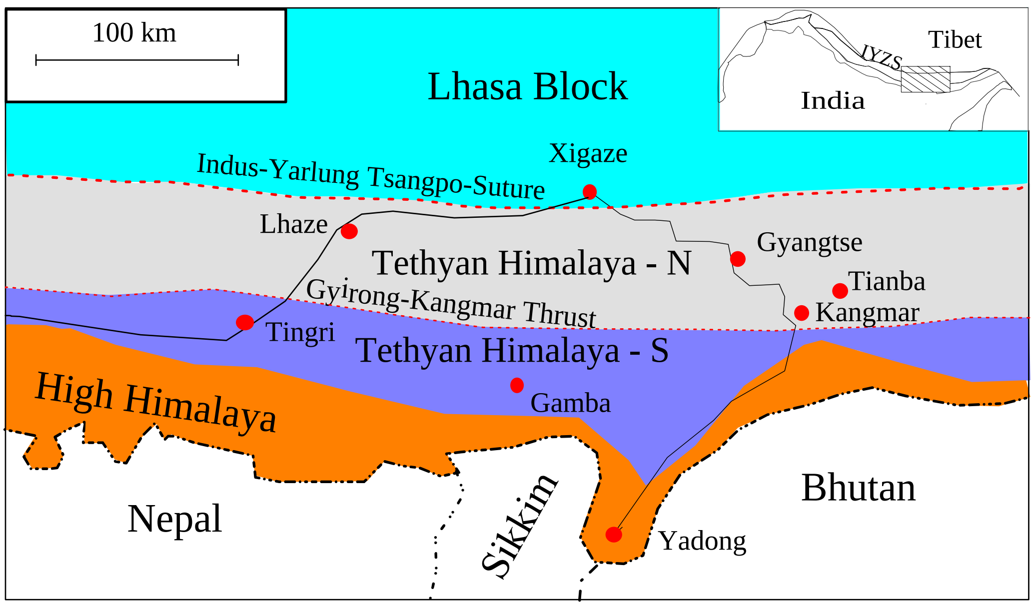

Figure 2.1 Simplified geologic map of Tingri-Gyangtse area, southern Tibet (modified after Willems et al., 1996). The inset map shows this region located in the Himalaya system.

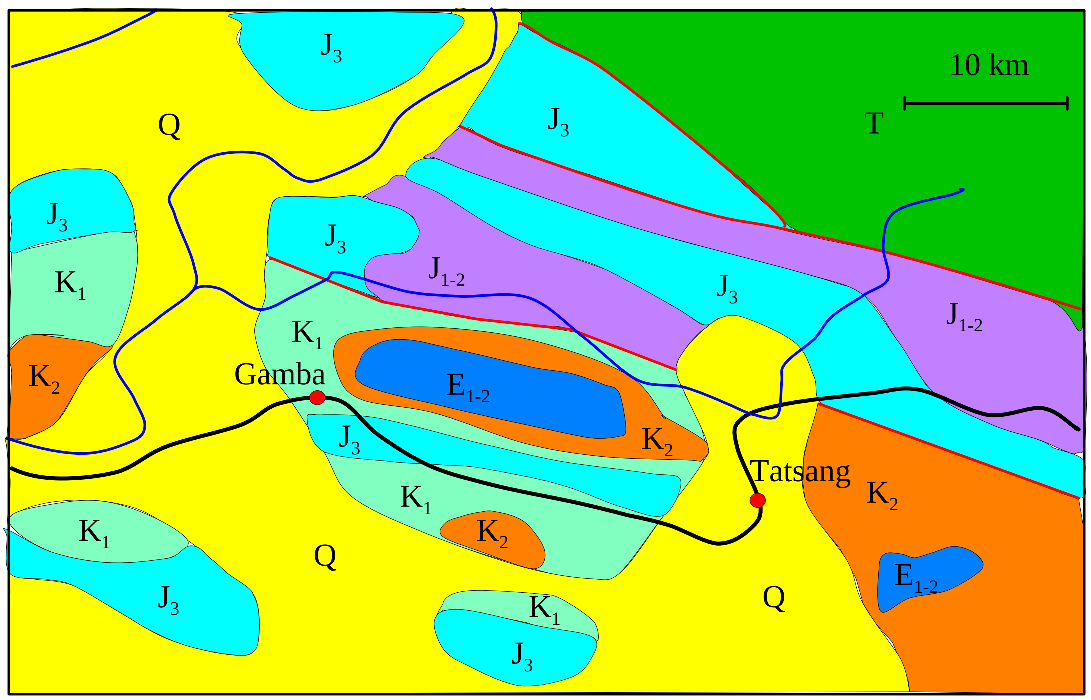

Figure 2.2 Simplified geologic map of the Gamba region (modified after geologic map (1:1,500,000) in Xizang BGMR, 1992).

The syncline has become a morphologic feature by relief inversion and it forms a 25-km long mountain chain continuing eastward from Gamba to Tatsang. The Cretaceous sediments here are classic sections that have been known for more than a century (Willems and Zhang, 1993; Rowley, 1996). Since the 1960s, the Academia Sinica, the Tibet Geological Survey and different Chinese academic institutions have worked on these sections. As a result, a relatively detailed stratigraphic system has been established in the Gamba region.

Gamba Group

Mu et al. (1973) first introduced the term 'Kampa Group' comprising units the formerly called: the 'Giri Limestone', the 'Kampa Shales' and the 'Hemiaster Shales' of Hayden (see Willems and Zhang, 1993). Now this unit in the southern zone of the Tethys Himalayas is commonly termed "Gamba Group" (Willems et al. 1996).

Lithologically, the Gamba Group consists of shales and sandy shales intercalated with thin-bedded marls and sandstones (Mu et al., 1973, Wen, 1987; Liu, 1992; Willems and Zhang, 1993). The lower part is composed of black shales and silty shales with intercalated thin beds of siltstone and fine sandstone. The black shales are characterized by well-developed lamination and abundant concretions, which are dominated by siderite, subordinate pyrite and phosphate. Fossils are rare. These features indicate a restricted depositional setting, i.e., an anoxic and stagnant water environment, mostly below the oxygenation level. The middle part consists of platy- and graded-bedding sandstone turbidites with incomplete Bouma sequences and sandstone dykes. The sandstones contain a high percentage of detrital quartz, associated with scattered breccias and banks rich in bivalves. The calcareous content and the amount of fossils increase continuously upward, and the bedding structures are disturbed upward by bioturbations, indicating an improved supply of oxygen to the sea floor in comparison with the lower part. With a significant upward increase of carbonate content, the upper part contains laminated black shales, calcareous shales with intercalated very thin micritic limestones. The biofacial feature is the dominance of planktonic foraminifera, bivalves and ammonites.

Farther south, west of Tuna along the road from Gamba to Yadong, the lower Cretaceous lithologies appear to be coarser grained (Liu, 1992). Rocks consist mainly of massive black mudstones and siltstones with abundant concretions. Strongly bioturbated, medium- to fine-grained dark and black sandstones, up to 0.5 m in thickness, are observed frequently. In-situ brachiopods and bivalves are common in the interbeds, representing a shallow-marine setting. The coarse grain sizes imply that Tuna is closer to the source area relative to the Gamba region, that is, the source rocks for the Gamba Group were in the south, most likely the Indian craton.

In summary, the Gamba Group is characterized by a great thickness of dark shales and sandstones with an increasing proportion of calcareous content and a decreasing proportion of ferruginous concretion-bearing black shales upward, representing a transition from a restricted environment to a relatively open shelf setting. The formation of thick black shales may have been caused by both high organic production in response to the warm Cretaceous climate, and relatively oxygen deficient bottom water related to the global anoxic event of early and middle Cretaceous time (Liu, 1992). The abundant ammonites and planktonic foraminifera indicate an age of the middle and late Albian to the Santonian for the Gamba Group (Wen, 1987; Willems et al, 1996).

Zhongshan Formation

The Zhongshan Formation constitutes the ridge-forming unit of Gamba-Tatsang Range, and is equivalent with the three formerly called 'Scarp Limestones' in the Hayden system (Willems and Zhang, 1993). The Zhongshan Formation can be subdivided into three limestone horizons separated by two marly units (Willems and Zhang, 1993). The two lower limestones occur morphologically as prominent scarps in the Gamba-Tatsang Range. Limestone 3 appears less clearly because it is thinner and grades upward into increasingly marly limestone and marl. It is in turn overlain by a diversified series dominated by calcareous algae.

According to Liu (1992) and Willems and Zhang (1993), the lower part of the Zhongshan Formation is very rich in planktonic foraminifera including *Globotruncana, Heterihelix, Boliving*, etc., which are typical of a relatively deep open shelf setting. Liu (1992) recognized the slope-toe and talus facies in the Zhongshan Formation. With abundant planktonic foraminifera and bioturbation, the slope-toe face appears as thin to medium-bedded wackstone and mudstone, while the talus consists of poorly sorted intraclastic limestone with many fragments of bivalves. The limited thickness and relatively fine-grained clasts of talus show that the slope was not very steep. The transition into the calcareous marls of 'Member Rhodolite' (Willems and Zhang, 1993) is characterized by a striking increase in organism diversity, such as corals, sponges, and red algae. This calcareous sequence was probably formed predominantly in a terrigenously influenced, more near shore platform area (Liu, 1992).

Generally, the Zhongshan Formation is composed of skeletal-limestones and calcareous marls and records a typical carbonate platform setting. Vertically, it reflects a clear shoaling upward succession ranging from open shelf to supratidal conditions (Liu, 1992; Willems and Zhang, 1993). The Zhongshan Formation in Gamba ranges from the early Campanian to Maastrichtian based on planktonic foraminifera (Willems and Zhang, 1993).

Jidula Formation

The Jidula Formation named after its main occurrence in the Jidula village, north of Gamba, consists of quartzose sandstones with minor amounts of sandy carbonates (Mu et al., 1973; Wen, 1987; Willems and Zhang, 1993). The sandstones are dominated by quartz greywackes and quartz arenites, and contain well-rounded to sub-rounded grains showing a high mineralogical maturity. In the lower half, the sandstones contain medium- to large-scale cross-bedding with a bimodal paleocurrent orientation (Liu, 1992). Vertical burrow-dominated trace fossils and intense bioturbation are prominent in the medium- to thin-bedded, fine-grained sandstones and occasionally in coarse sandy channel fills. A gradation from coarse to fine sand is common in one layer or throughout several layers. These features indicate a tidal-dominated environment. The middle part of Jidula Formation consists of black limestones rich in micrite, intercalated with quartz sandstones in some places, containing abundant Chlorophycean algae (Willems and Zhang, 1993). The sedimentary structure shows strong bioturbation in the more quartz sandy strata, whereas there is no bioturbation in the terrigenously unaffected limestones. The upper part of sandstones is similar to the lower part except that distinctly graded sedimentary cycles are rarely developed. Medium to small scale cross-bedded units prevail, and the grain size ranges between fine and medium. The Jidula Formation is topped by sandstones about one meter thick, which are very intensely ferruginous and brown-red.

Laterally, along the continuous outcrop eastward, the thickness of sand bodies in the Jidula Formation tends to decrease. According to Liu (1992) and Willems and Zhang (1993), the total sandstone thickness in the Zhongshan section is about 180 m, but about 20 km east of Gamba no sandstone has been found, and the corresponding lithologies are dominated by cross-bedded calcarenite and skeletal limestones intercalated with thin-bedded, medium- to fine-grained quartzose sandstones.

Generally the Jidula Formation reflects a very shallow, tide-dominated inner shelf to shoreline zone. The lenticular geometry of this sandstone interval shows that during the early Danian a major tidal inlet belt developed in the Gamba region (Liu, 1992). The high mineralogical maturity of the sandstones implies that this area was still a tectonically stable setting during the early Paleocene. The abundant calcareous algae and ostracods in limestones intercalated in the lower part of sandstones, and the appearance of planktonic foraminifera of the *angulata* zone in marls of the Zongpu Formation just above the top of upper sandstones of the Jidula Formation indicate that the Jidula Formation ranges from late Maastrichtian to middle Paleocene in age (Willems and Zhang, 1993, Wan et al., 2002). As such, the Cretaceous/Tertiary boundary lies with in the Jidula Formation in the Gamba region.

Zongpu Formation

The Zongpu Formation was introduced by Mu et al. (1973) for the marine strata in the Zongpu valley, NE of Gamba for a unit primarily consisting of limestone. The lower part shows a diversified facial development, and forms a sharp lithofacial boundary with the sandstones of the Jidula Formation, characterized by an abrupt lack of terrigenous quartz accretion (Willems and Zhang, 1993). The brown-grey marls poor in fossils in the lower Zongpu Formation reflect a relatively deep water and lower energy setting. Upward the carbonate content tends to increase with the decreasing siliciclastic supply. The dominant part of the Zongpu Formation consists of nodular micritic limestones, which represent a quiet stable sedimentary environment (Willems and Zhang, 1993). The dominant organisms of this facies are foraminifera, ostracodes, bivalves, gastropods, cephalopods, corals, and calcareous algae, which point to an age of middle Paleocene to early Eocene for the Zongpu Formation (Wen, 1987; Willems and Zhang, 1993; Wan et al., 2002). Large benthic foraminifera are locally enriched to form foraminifera limestones, indicating shallow a marine environment (Liu, 1992).

Zongpubei Formation

The Zongpubei Formation is the highest unit preserved in Gamba, which was first defined by Willems and Zhang (1993). The succession consists of greenish-grey mudstones and marls in the lower part, grading upward into reddish siltstone and mudstone, and then into fine sandstone, a lithologic equivalent to the ‘Dzongbuk Shale’ of Hayden (Wen, 1987).

The lower 40 m of the Zongpubei Formation is intercalated at irregular intervals by thin-bedded, ferruginous calcareous marls and oolitic limestones, containing biogens of the underlying Zongpu Formation redeposited as oolid cores. The upper monotonous red shale is intercalated at several levels by lenticular oolitic limestones, indicating temporary marine ingressions or storm events during deposition (Liu, 1992). According to Willems and Zhang (1993), the basal part of Zongpubei Formation can be dated as Ilerdian (Paleocene/Eocene boundary), based on the stratigraphic position of the topmost strata of the foraminifera-bearing limestones in the Zongpu Formation. However, recently Li et al. (2003) and Xu (2000) reported abundant planktonic foraminifera and calcareous nannofossils in the shale and limestone of the Zongpubei Formation in the Gamba region, which point to an age interval of middle-late Eocene.

In summary, the end of the marine sedimentary history in Gamba is dated as middle Eocene by a distinct and rapid lithologic change: the carbonate rocks of the upper Zongpu Formation rich in large foraminifera are replaced by marlstone, mudstones, and siltstones. So the lower Tertiary sequence of the Gamba records a transition from the sedimentary setting of the open marine platform to restricted remnant marine.

Tingri area

Similar to the geological framework in the Gamba region, the dominant structural element is an E-W striking syncline in the area west of Shekar Dzong (New Tingri). The syncline also forms an orographically prominent massif; i.e., the Zhepure Mountain (Figure 2.3), which is composed of massive limestones that are resistant to weathering. The Cretaceous strata crop out on both flanks of the syncline. Recently, six stratigraphic units have been measured on the north slope of the Zhepure Mountain, west of New Tingri (Willems et al., 1996). They are described from base to top as follows.

Gamba Group

The Gamba Group in the Tingri region is 625 m think, consisting of marls, marls, and to a less extent, limestones (Willems et al., 1993, 1996). Generally there is an upward increase in carbonate content.

According to Willems et al. (1996), the lower Gamba Group comprises dark grey marls and less frequent marls, containing calcareous dinoflagellates, radiolaria, spicules, as well as benthic and planktonic foraminifera. The middle part consists of grey marls, greenish-grey calcareous marls, and a few intercalated marly limestones with a general decrease in the microfossil content. The upper part consists of marls, marly limestones, and increasing intercalation of light grey to beige limestones.

In the outcrops at Kema, about 35 km west of Tingri, there is a continuous section of the Cretaceous (Liu, 1992). The lower part is about 150 m thick and consists of mixed siliciclastics and carbonate grainstones. The middle part of grey silty shales and siltstones shows offshore sedimentary structure, such as parallel lamination, ripple cross-lamination and wavy bedding. The relatively deep offshore facies are made up of grey silty shales and calcareous shales in the upper part of the section. The tendency of an upward

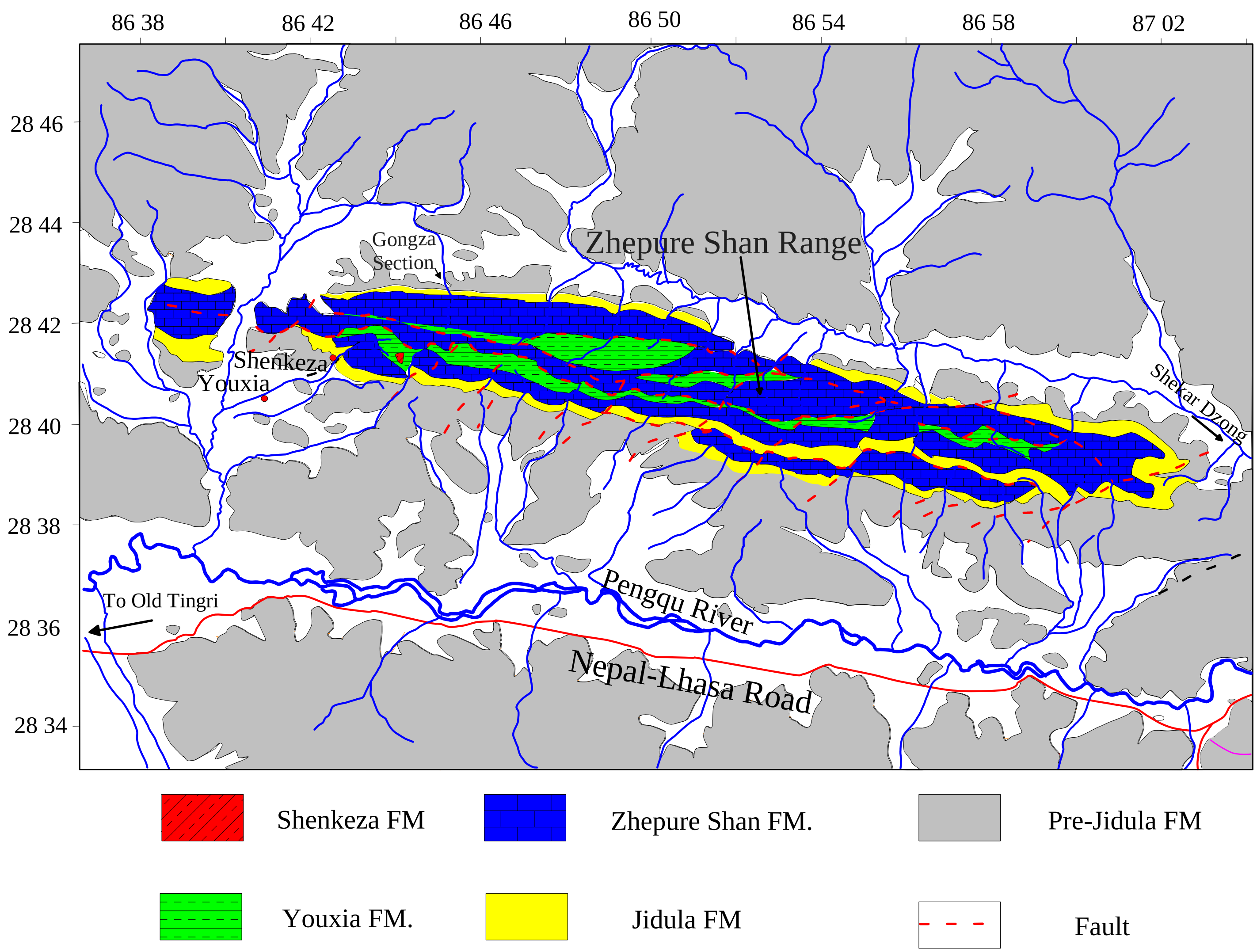

Figure 2.3 Geologic map of the Zhepure Shan Mountain (based on field observations and image interpretation (Kidd)). Geographic coordinates in degrees, minutes.

increase in calcareous content is seen in both sections, in the Zhepure Mountain and Gamba areas, implying that carbonate production increased upward with increased water-depth (Liu, 1992).

Based on the abundant planktonic foraminifera, the Gamba Group in Tingri is dated as late Albian-early Santonian (Willems et al., 1993, 1996). Therefore the vertical facies association in the Tingri region reflects a clear sea-level rise during the deposition of the Gamba Group. The major part of the sediments of Gamba Group in this region were deposited in a pelagic to hemi-pelagic environment in an open marine basin and its slope (Willems et al., 1996).

Zhepure Shanbei Formation

Because of the litho- and biostratigraphic differences of the Zhepure Mountain compared to that in the Gamba region, Willems et al. (1993, 1996) introduced the name Zhepure Shanbei Formation for the well-bedded limestones interbedded with very thin layers of calcareous marls which conformably overlie the Gamba Group. The boundary between the Zhepure Shanbei Formation and the Gamba group is marked by the last appearance of marls and the clear dominance of limestones (Willems et al., 1996).

Evenly bedded, dark-grey limestones interbedded with very thin layers of marl dominate the Zhepure Shanbei Formation. Unlike the underlying Gamba Group, the input of detrital quartz is more or less absent. There is a significant increase in the content of planktonic foraminifera and calcispheres in the upper part of the limestones (Willems and Zhang, 1993). The uppermost 10.5-m of the Zhepure Shanbei Formation begins with a 0.5 m thick layer of polymict limestones, dominated by: wackestones with planktonic foraminifera and calcisphere from the underlying pelagic facies, and pack- and grainstones with orbitoid foraminifera from the neritic facies of the Gamba region (Willems et al., 1996). Overlying this are limestones, in which there is a clear change in the biogenic assemblage compared with underlying strata. Besides planktonic foraminifera and calcisphere, these biomicrites are characterized by high quantities of reworked carbonate extraclast and by the first appearance of intraformationally reworked *Orbitoides meia* and *Omphalocyclus macroporu.* In the matrix of these layers, the content of detrital quartz is the highest within the Zhepure Shanbei Formation. All these features indicate a transition is recorded from an open shelf to a proximal continental slope environment.

Willems et al. (1996) identified abundant planktonic foraminifera (e.g., *Globotruncanita elevata, D. asymetrica, Globotruncana dupeublei,* etc.) in the Zhepure Shanbei Formation, which are clearly indicative of an age of early Santonian to middle Maastrichtian for this formation. The depositional environment for most of the Zhepure Shanbei Formation is pelagic, which was also developed in the Gamba Group. The occurrence of abundant calcispheres is clear evidence for an outer shelf environment during deposition of the Zhepure Shanbei limestones.

The litho- and micro-facies of the Zhepure Shanbei Formation are directly correlative with the lower part of the Zongshan Formation in the Gamba area (Willems et al., 1993, 1996). However the upper part of limestones and rhodolite facies of Zongshan Formation in Gamba are totally absent in Tingri. Given the fact that Tingri is located north of Gamba, it is not surprising that Tingri should be in a more offshore sedimentary environment than Gamba. Therefore the different depositional settings between Gamba and Tingri result in a reduced thickness of the Zhepure Shanbei Formation in Tingri, which reflects a pelagic sedimentary environment and reduced sedimentation rate, whereas a shallow water carbonate platform was formed in the Maastrichtian with a much higher accumulation rate in Gamba (Willems et al., 1996).

Zhepure Shanpo Formation

The Zhepure Shanpo Formation is also a newly established formation named by Willems et al. (1993), referring to more heterogeneous calciturbities and siliciclastic sediments than those of the overlying Jidula Formation. This formation is restricted to the Tingri region.

The lower part is dominated by siliciclastic turbidites with minor calcareous cemented quartz sandstones. Most of the sandtones show distinct fining upward and thinning upward cycles (Willems et al., 1996). These cycles begin with medium to thick bedded layers and successively change upwards to thinner platy layers, in which sediments start with quartz pebbles and gradually become fine sandy, to partly silty at the top. The pelagic/hemipelagic background sedimentation, which consists of marlstones, is characterized by a low-diversity fossil association, dominated by calcispheres. The upper part is composed of a varied sequence of brownish grey and black marlstone, sandy limestone, and very often nodularl calcareous marlstone with indistinct bedding planes. The sandy limestones and calcareous sandstones show fine lamination, flaser bedding, and cross bedding (Willems et al., 1996). The characteristic sedimentary cycles of lower part are not present in this upper part. There is generally a slight increase in the carbonate content as well as the successive occurrence of calcareous extraclasts derived from different shallower water sequences. The fossil diversity is clearly higher than in the lower part (Willems et al., 1996). Pelagic organisms, such as calcispheres and less frequently planktonic foraminifera, that are typical in the lower part, are diluted in this part due to the heavy input of detrital material.

Thus the sediments of the Zhepure Shanpo Formation record a transition from a more distal continental slope in the lower part, to a proximal continental slope turbitite fan system in the upper part (Willems et al., 1996). This reflects an overall shallowing upward trend. The Zhepure Shanpo Formation in the Tingri region ranges from middle Maastrichtian to Danian based on the abundant planktonic foraminifera (Willems and Zhang, 1993).

Jidula Formation

The Jidula Formation in the Tingri region consists nearly exclusively of quartz sandstones which conformably overlies the Zhepure Shanpo Formation. It is about 100-m-thick.

The lower part is primarily composed of calcareous quartz sandstones intercalated with some layers of glauconitic sandstones. Some thin sandy and marly intercalations contain re-deposited calcispheres and fragments of echinoderms and corallinacean algae (Willems and Zhang, 1993). There is a 24-m-thick zone of sandy marl containing argillaceous ironstone concretions in the upper half of this part. The upper part is made up of nodular limestones and calcareous marlstones with abundant large-sized macrofossils (e.g., gastropod, bivalve, echinoderm, etc.), and marked by increasing carbonate content. Thin layers of marls, sandy limestones, and calcareous sandstones are intercalated.

The quartzose sandstones here can be correlated not only in terms of their stratigraphic position but also sedimentologically and petrographically with the upper sandstone of the Jidula Formation in the Gamba area. The fossils of the underlying Zhepure Shanpo Formation and the overlying Zhepure Shan Formation delimit the age of the Jidula Formation as the early Paleocene (Willems and Zhang, 1993; Wan et al., 2002; Xu et al., 1989). This suggests that he Jidula Formation of the Tingri area is correlative with the upper sandstones of the Jidula Formation of the Gamba area.

Trace fossils of the *Skolithos* ichnofacies occurring in the top layer are indicative of a subtidal shore face zone (Willems et al., 1996). The whole succession of the Jidula Formation in the Tingri area records a continuation of the overall shallowing upward tendency, which started in the Zhepure Shanpo Formation.

Zhepure Shan Formation

The Zhepure Shan Formation is named after its main occurrence along the mountain crest of Zhepure Mountain (Willems and Zhang, 1993), and consists of massive limestones. It is correlated with the limestones of the Zongpu Formation in the Gamba region (Mu et al., 1973; Wen, 1987; Xu et al., 1989).

The 440-m-thick Zhepure Shan Formation is made up of massive limestones and nodular limestones, with minor marls and marlstones. Willems et al. (1996) divided the Zhepure Shan Formation into six members: Member 1, dolomitic limestones and dolomites; Member 2, massive limestones with rhodoids; Member 3, thick-bedded limestones with calcareous algae; Member 4, nodular limestones with larger foraminifera; Member 5, massive limestones composed of rock-forming quantities of *Nummulites and Alveolina*; Member 6, massive limestones with abundant foraminifera (e.g., *Asterocyclina, Assilina, and Discocylina)*.

The sedimentary development of the Zhepure Shan Formation shows establishment of a stable carbonate-producing platform, characterized by prominent bio- and microfacial changes and sedimentary stages rapidly succeeding one another. It started with the stage of high-energy shoals on a platform margin. A high diversity of calcareous algae, in addition to smaller benthic foraminifera, dominated these shallow subtidal areas. Finally, it evolved into an open marine platform with changing water depth shifting between areas above and below the normal wave base.

Based on the abundant occurrence of large foraminifera, Willems et al. (1996) assigned an age of Danian to Lutetian to the Zhepure Shan Formation. As such, they concluded that the marine sedimentary history in the Tingri area ended in the Lutetian.

Zongpubei Formation

According to Willems et al. (1993, 1996), the highest known stratigraphic level in the Tingri region is the Zongpubei formation, which is made up of unfossiliferous greenish-gray marls in the lower part and red clay and siltstone with intercalations of fine sands above. No diagnostic fossils or microfossils are reported by Willems et al. (1996), and the Zongpubei Formation is Lutetian or younger based on its stratigraphic position above the Lutetian Zhepure Shan Formation.

Willems et al. (1996) interpreted these sediments as representing lagoon and hypersaline coastal ponds, and finally a continental sedimentary environment. However, the transition between the marine limestones of Zhepure Shan Formation and the sediments of the Zongpubei Formation is not exposed in the Gongza section they studied (Willems and Zhang, 1993). This manifests itself in a radical change from the massive grey limestones rich in fossils of the Zhepure Shan Formation deposited in normal marine conditions of the open marine platform, to greenish-grey and reddish mudstones and siltstones poor in carbonate content and fossils. The abrupt change in sedimentary pattern in the basal part of Zongpubei Formation may be linked to a tectonic event, possibly the final closure of Neo-Tethys Ocean and start of collision between India and Asia.

The overall sedimentary history shows a sea level high at the Cenomanian/Turonian boundary corresponding to a global highstand (Haq et al., 1987; Willems et al., 1996). The following sequence covering the time period from the Turonian to the Danian in the Gamba Group, Zhepure Shanbei Formation, Zhepure Shanpo Formation, and Jidula Formation, represents an overall shallowing-upward mega-sequence. This regression was followed by a new transgression-regression cycle during the Paleocene and Eocene. It began in the Danian documented by the carbonate platform limestones of the Zhepure Shan Formation, and ended in the Lutetian Zongpubei Formation, which is only locally preserved.

Gyangze-Kangmar Area

As a result of being closer to the IYZS than the Tingri and Gamba sections, the sediments of the Gyangze-Kangmar area are characterized by deeper water facies. The

Cretaceous sequence is divided into two formations: the Jiabula Formation, and the Zhongzuo Formation (Wen, 1987; Xu et al., 1989; Liu, 1992).

Jiabula Formation

The Jiabula Formation is composed of a series of black shales with intercalated turbiditic sandstones, lenticular limestones and pyrite nodules. Marls and dark-grey to black shales point to an oceanic basin setting (Liu, 1992). Abundant foraminifera, radiolaria, ammonites, belemnites and thin-shelled bivalves (Wen, 1987; Liu, 1992; Wang et al. 2000) point to an early Cretaceous age for the Jiabula Formation.

The sediments of the Jiabula Formation in its type locality, i.e., Jiabula village, are interrupted by three horizons of olistostromes with accompanying turbidites (Liu, 1992). Olistostrome horizon 1 consists of various shallow-water sedimentary clasts, ranging in size from several mm to over ten meters, and a deep water-dominated matrix of black shale and sandstone. The clasts are irregular in shape. Some contain shallow-water fossils of the same age as the surrounding deep-water matrix. The long axes of elongate boulders or gravels are mainly parallel with bedding surfaces implying an origin of loose or semi-consolidated shallow water deposits. All these features indicate that the majority of the clasts were derived from the continental rise and slope, which represents sediments deposited in shallow-water environments, at least much shallower than the enclosing matrix material. The matrix in the lower part is black laminated marl, shale and siliceous shale, while that of the upper part consists of chaotic shale and sandstone containing sandstone and limestone pebbles. The other two olistostrome horizons do not appear as complete as the lower olistostrome horizon. However, it is clear that all three chaotic deposits were mainly caused by gravity sedimentation, implying relatively steep slope that repeatedly developed during the early Cretaceous at Jiabula (Liu and Einsele, 1996).

In the section of Tianba, the Jiabula Formation is made up of fine clastic-dominated sediments of a slope apron and radiolarian siliceous shale of pelagic plain, as well as turbiditic sediments of distal deep-sea fans (Liu, 1992). The lower part consists of thin-bedded grey shale, silty shale and siltstone. Considerable amounts of nektonic organisms including ammonites, belemnites, bivalves and some brachiopods and gastropods, are found in these sediments. The depositional environment deepened upward and formed an abyssal plain facies between 200 and 400 m thickness in Liu's measured-section (1992), characterized by radiolarian-bearing siliceous shale, foraminifera calcareous shale intercalated with tuff. Secondary pyrite concretions of cubic shape are common (Liu, 1992). At the top there is a 10-m-thick section of grey-green cherts with well-developed lamination. All these are indicative of a period of deposition within a sediment-starved basin. As a result of the influence of terrigenous turbidites, the pelagic sediments tend to become increasing siliceous upward. The upper part is dominated by thin-bedded turbitite sandstones, siltstones, silty and sandy shales with some intercalated limestone. Divisions of the typical Bouma sequence are common. The grey to green siliceous shales and red limestones, rich in planktonic foraminifera and radiolaria, represent a deepening oceanic setting, which according to Liu (1992), may have resulted from rapid subsidence caused by faulting and/or bending of the outer continental rise.

Zhongzhuo Formation

The Zhongzhuo Formation is characterized by olistostrome horizons interbedded with radiolarian-rich siliceous shale and chert (Liu, 1992). The matrix in the olistostrome contains dark grey to black calcareous and siliceous shales with abundant pyrite concretions reflecting suboxic bottom-water conditions. The clasts are irregular in shape and derived from limestone, siliceous shale, sandstone and chert. This indicates that the source rocks are of both continental and ocean origin. Abundant foraminifera (e.g., *Globotruncana linneiana, G. elevata, Marginotruncana stuarti, M. stuartiformis, Heterohelix sp*.) and some radiolaria (Tapponnier et al., 1981) point to an age of late Cretaceous (Campanian-Maastrichtian) for the Zhongzhuo Formation (Wang et al., 2000).

In the Weimei section (Liu, 1992), the Zhongzhuo Formation can be subdivided into three parts. The lower part consists of dark-grey shales, showing convolute structure, intercalated with irregular clasts of sandstones. Flattened clasts are probably derived from a semi-consolidated turbidite sequence. The percentage of sandy gravel or blocks, which display cross-bedding structure, increases upward. The middle part is characterized by coarse gravel and blocks, up to 4 m in size, made up of siliceous shales, cherty limestones and turbiditic rocks. Some limestone blocks and gravel are derived from shallow-water deposits. The largest block is about 100m by 25m in size, and consists of metamorphosed quartz sandstones, which appear to be much older than the matrix. The various clastic sources suggest that syn-depositional faults incised not only contemporary sediments, but also older strata. The upper part consists of laterally continuous pelagic thin-bedded red siliceous shale and limestone rich in radiolaria and planktonic foraminifera, passing upward into coarse to fine-grained sandstones.

In summary the sedimentary sequence of the Gyangze-Kangmar area in the Cretaceous is characterized by chaotic deposits and associated turbidites. The proportion of oceanic detritus is greater relative to that of the Indian passive continental shelf and slope. In contrast to the relatively stable southern zone, the Gyangze-Kangmar area was transformed into a faulted slope and rise (Liu, 1992).

Discussion

Correlation of lithostratigraphy between Gamba and Tingri

The Cretaceous and lower Tertiary sedimentary sequence of Gamba and Tingri represents part of the sedimentary evolution of the Indian passive margin that bordered the southern margin of the Neo-Tethys ocean (Willems et al., 1993, 1996; Liu et al., 1994). The almost conformable succession is strong evidence to support the interpretation that the collision between India and Asia did not affect the Gamba-Tingri area until the Lutetian (Rowley, 1996, 1998).

Although the sediments of Gamba and Tingri can be correlated with each other, there are some differences between them (Willems et al., 1996). The lower part of the Gamba Group in the Tingri area is more calcareous and fossiliferous than that of the type section in the Gamba area. Although the Zhepure Shanbei Formation of Tingri can be correlated litho- and biostratigraphically with the lower limestones of the Zhongshan Formation of Gamba, the upper limestones and the rhodolite facies of the Zhongshan Formation are not represented in the Zhepure Mountain section. The upper part of the Zhepure Shanpo Formation is characterized by pelagic and hemipelagic sediments interrupted by turbidites containing abundant reworked Maastrichtian shallow-water carbonate, whereas a stable carbonate platform was established in the Gamba region at that time. Two quartz sandstone units interbedded with a layer of black limestone developed in Gamba from the late Maastrichtian to the middle Paleocene, which is different from the sequence in Tingri where the Jidula Formation is only composed of the lower Tertiary sandstones.

The above-mentioned differences between Gamba and Tingri are consistent with the more landward position of Gamba than that of Tingri. It is apparent that the stratigraphy of Tingri generally has a deeper marine environment relative to Gamba during the evolution of the Neo-Tethys Ocean.

Gyangze-Kangmar area

The lithostratigraphy of the Gyangze-Kangmar area is characterized by continental slope and abyssal plain deposits. During the early Cretaceous this area was dominated by slope apron and submarine fan sediments (Jiabula Formation). Locally, chaotic deposits, mainly derived from the passive margin, perhaps formed as a result of growth faulting along the toe of the continental slope and outer-shelf. This was followed by limestones and radiolarian siliceous rocks containing oceanic volcanics, representing a relatively starved ocean basin environment (Zhongzhuo Formation). The olistostromes contain older rocks derived not only from shelf and slope sediments, but also from rocks of oceanic crust, which suggests that chaotic deposits may have been formed in a deep-sea graben. The graben appears to have developed on the continental rise where continental crust passed into oceanic crust (Liu, 1992).

Due to intense tectonic deformation and difficult working conditions in the Tethyan Himalayas, the map units here are generally over-extended (Rowley, 1996), and detailed chrono-stratigraphic division and correlation are relatively poor. Therefore the exact time of the closure of the Neo-Tethys ocean, that is, the start of collision between the Indian and Asian continents, remains poorly-dated in the Tethyan Himalayas of southern Tibet, where it needs detailed work in field mapping, stratigraphic section measuring and biostratigraphic analysis.

Chapter 3. Chemical compositions and tectonic significance of chrome-rich spinels in Tianba Flysch, southern Tibet

Abstract

Significant amounts of chrome-rich spinels occur in turbiditic sandstones from the well exposed, mid-Late Cretaceous "Tianba Flysch" sequence in the north Nieru Valley, southern Tibet. Microprobe results indicate that the spinels have a well-developed Fe-Ti trend, and have Cr/(Cr+Al) between 0.4 and 0.65, Mg/(Mg+Fe^{2+}) between 0.3 and 0.9, and TiO_2 wt% values above 1%. The presence of melt inclusions, subhedral-euhedral grain boundaries on some grains, and well above 0.2 wt% TiO_2 contents suggests that the source of these Cr-rich spinels was a volcanic suite of rocks. Comparison with spinels from published literature suggests that the compositional range of the detrital spinels closely matches those from intra-plate basalts and is very similar to the composition of spinel inclusions in olivine from volcanic rocks of Hawaii and Disko Island, western Greenland. Based on the regional tectonic history of southern Tibet, there are two possible sources for the Tianba chrome-rich spinels: ophiolitic ultramafic or gabbroic material of an intra-oceanic subduction system associated with the closing of the Neo-Tethys; or the Rajmahal basalts associated spatially and temporally with Kerguelen hotspot activity on India about 117 Ma ago. Based on palaeo-tectonic reconstruction, the presence of mid-Late Cretaceous fossils in the strata, and the limited range of chemical compositions, the Cretaceous volcanics of the Rajmahal/Kerguelen hot spot were most likely the source for the chrome-rich spinels in the Tianba Flysch.

Introduction

It is generally accepted that understanding the petrologic, mineralogical, and geochemical characteristics of a basin-fill sequence attached to a past active hinterland is essential for the reconstruction of tectonic evolution (Dickinson and Suczek, 1979; Ingersoll et al., 1984; Garzanti et al., 1996; Dickinson, 1985; Zuffa, 1980; Pearce, 1987; Dewey and Mange, 1999). Original composition of the source rocks, however, may be obscured by many factors, including climate, relief, transport mechanism, post-burial diagenesis, and regional metamorphism, all of which may yield potentially ambiguous interpretations (Morton, 1985, 1991). Given the fact that the most diagnostic but chemically and mechanically unstable minerals are eliminated by post-depositional dissolution, studies of ultrastable minerals in sedimentary rocks are applied in the palaeo-tectonic reconstruction with increasing frequency (Morton 1991, Dewey and Mange, 1999; Lihou and Mange-Rajetsky, 1996, Sciunnach and Garzanti, 1996; Caironi et al., 1996). Of these minerals, chromian spinel is of particular significance to sedimentary provenance studies for a variety of reasons: spinels crystallize from mafic and ultramafic magmas over a wide range of conditions, and therefore are a sensitive indicator of the host rock composition (Irvine, 1967; Roeder, 1994) and crystal-liquid equilibrium and disequilibrium processes (Allan et al., 1988). Being one of the first phases to crystallize, compositional analysis of spinels is routinely applied in petrologic studies of spinel-bearing igneous rocks, and a large volume of microprobe data is available in the literature (Barnes & Roeder, 2001; Kamenetsky et al., 2001; Dick et al., 1984; Arai & Okada, 1991; Lee, 1999); the unusual chemical durability of chromian spinel makes its original composition more likely to be preserved after burial, particularly when compared with other high temperature igneous minerals such as olivine; and the lack of cleavage and high degree of hardness makes the spinels physically resistant to lower grade alteration and mechanical breakdown, and as such they may be enriched in some sedimentary rocks and may even form placer deposits (Ganssloser, 1999; Pober et al., 1988; Cookenboo et al., 1997; Lenaz et al., 2000).

Recently there has been a great deal of interest in the early tectonic history of the Himalaya, the orogenic product of continent-continent collision between Asia and India. Much of the pre-Middle Tertiary record of this tectonism is recorded in the sedimentary rocks situated south of the Indus-Yarlung-Zangbo Suture in southern Tibet (Tapponnier et al., 1981; Allegre et al., 1984; Garzanti et al., 1987; Garzanti, 1993, 1999; Garzanti et al., 1996; Beck et al., 1995; Rowley, 1996, 1998; Yin and Harrison, 2000; Wang et al., 2001; Davis et al., 2002; Wan et al., 2001; Ziabrev et al., 2001). In order to better understand the tectonic history of the region, we report provenance data from the Cretaceous Tianba Flysch from the northern part of the Nieru Valley in the Tethyan Himalaya. The Tianba Flysch consists of a section of lithic-rich turbidite sandstones and interbedded shales, which in terms of its lithology and bedding characteristics appears in outcrop to be a typical collision-related flysch (Rowley & Kidd, 1981; Garzanti et al., 1987). Our data provide insight into the early evolution and timing of initiation of the India-Asia collision, and allow a clear test of the hypothesis that there was mid-Late Cretaceous ophiolite-obduction event in the eastern Tethyan Himalaya.

Geologic Overview

The Tethyan Himalaya, lying between the High Himalayan Crystalline belt to the south and the Indus-Yarlung-Zangbo Suture and the Lhasa block to the north (Figure 3.1), consist primarily of late Paleozoic to early Eocene sedimentary rocks, originally deposited along the northern edge of the Indian continent. Deposition began with late Paleozoic-Triassic rifting (Sengor et al., 1988; Sciunnach and Garzanti, 1996; Garzanti, 1999) during the initial development of the Neo-Tethyan Ocean, and a relatively wide passive continental margin subsequently developed along the north rim of the Indian continent. During the mid-Cretaceous, northward-directed subduction of the Neo-Tethyan oceanic crust beneath the southern margin of Asia resulted in the development of a magmatic arc and a forearc-related basin (Xigaze Forearc Basin) along the southern margin of the Lhasa block (Durr, 1996; Einsele et al., 1992). With continued subduction, the India-Asia collision initiated in the early Tertiary, which gave rise to the Indus-Yarlung-Zangbo suture (IYZS). Therefore the strata of the Tethyan Himalayas record the entire depositional history of the northern Indian passive margin.

In southern Tibet, the Tethyan Himalaya can be divided into two subzones of different lithological assemblages (Figure 3.2) that are separated by the East-West trending Gyirong-Kangmar thrust (Burg and Chen, 1984; Liu, 1992). The northern zone is dominated by slightly metamorphosed deposits of outer shelf, continental slope, and possible trench basin environments, while the southern zone is characterized by non-metamorphic, shallow water shelf carbonate and terrigenous deposits ranging from late Paleozoic to Eocene, except that the latest Permian is partly missing due to uplift in

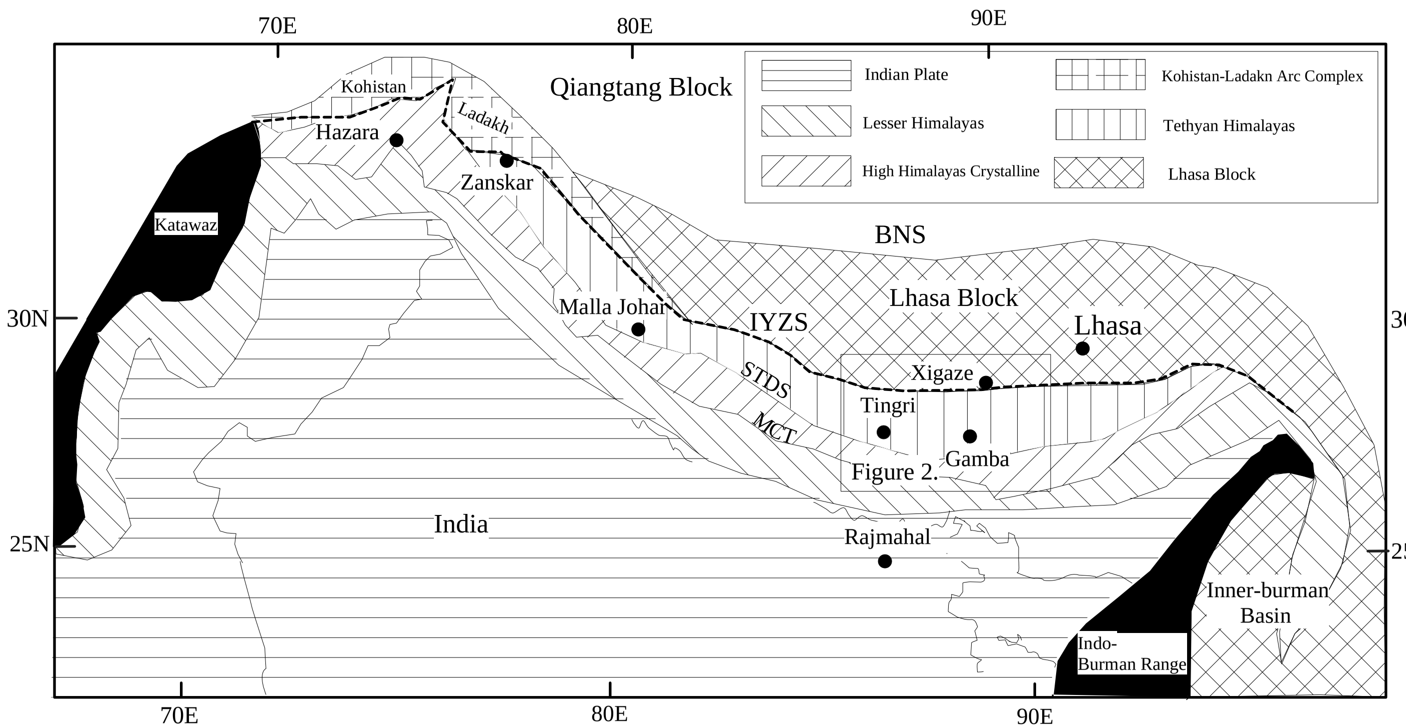

Figure 3.1 Regional geological map of Tethyan Himalaya (after Rowley, 1996). BNS: Banggong-Nujiang Suture IYZS:Indus-Yarlung-Zangbo-Suture, MCT:Main-Central-Thrust, STDS:Southern-Tibet-Detachment-System.

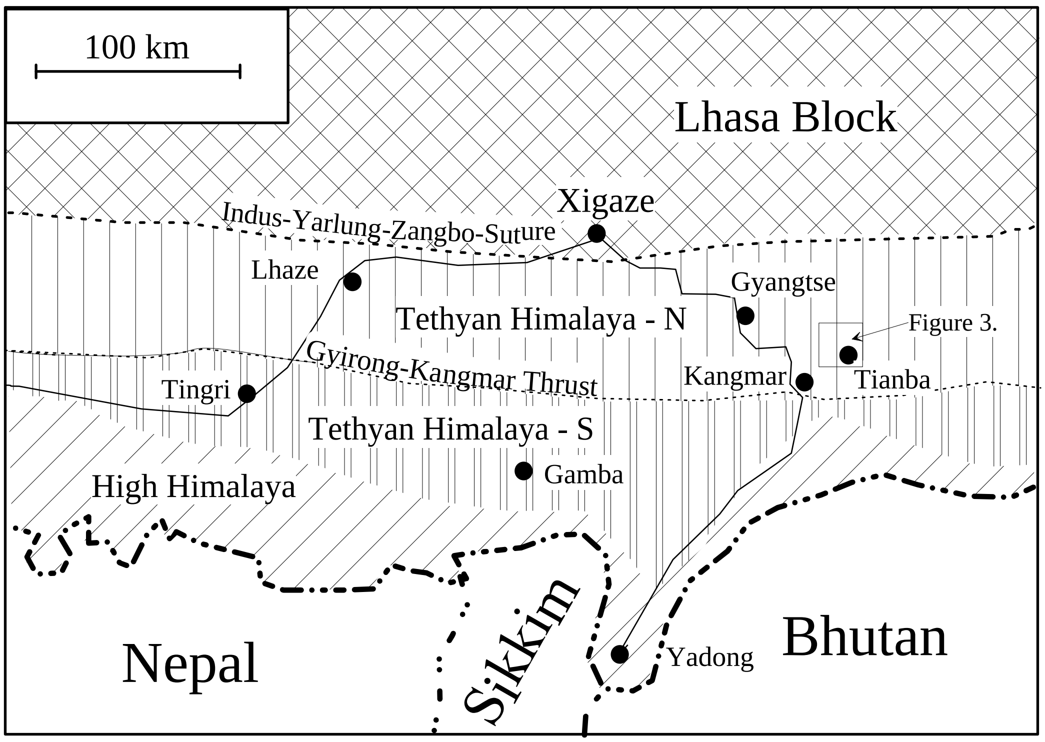

Figure 3.2 Simplified tectonic map of the study area (after Willems et al, 1996)

conjunction with the initial rift-stage of the Neo-Tethys (Wen et al., 1980; Willems et al., 1996; Xizang BGMR, 1992).

This study concentrates on the well-exposed lithic rich arenites at the northern end of the Nieru Valley (Figure 3.3), which belong to the northern zone of the Tethyan Himalayas. Near Tianba, the lower part of the section consists of thin-bedded grey shales, silty shales, and cherts of the Jiabula Group (Xizang BGMR, 1992; Liu, 1992). These rocks contain abundant fossils of nektonic organisms including ammonites, bivalves, and belemnites, which indicate a Berriasian to Aptian age (Wang et al., 2000; Zhang Binggao, personal communication, 2000). The Jiabula Group also contains pyrite concretions, dark shales, and laminated grey-green cherts indicating deposition within a sediment-starved basin (Liu, 1992; Wang et al., 2000).

The upper part of the Jiabula Group in the northern Nieru Valley is made up of the Tianba Flysch. In this area, the Tianba Flysch is about 220 m thick (Figure 3.4-5) and consists primarily of well-bedded sandstone, siltstones and shales. The contact between the Tianba Flysch and the underlying dark shales and cherts is conformable. The basal interval of the flysch is characterized by rapid disappearance of black cherts and appearance of olive-colored argillites and mica-rich siltstones that coarsen up rapidly into graded sandstones. Individual sandstone beds fine upwards into siltstones and shales, and contain abundant sedimentary structures including sole marks, horizontal laminations, small-scale cross bedding, in a Bouma sequence indicating a turbidite depositional environment for the Tianba flysch (Figure 3.6-7).

The top of the Tianba Flysch is characterized by an abrupt termination of the turbiditic sandstones, which are conformably overlain by greenish-grey burrowed shales

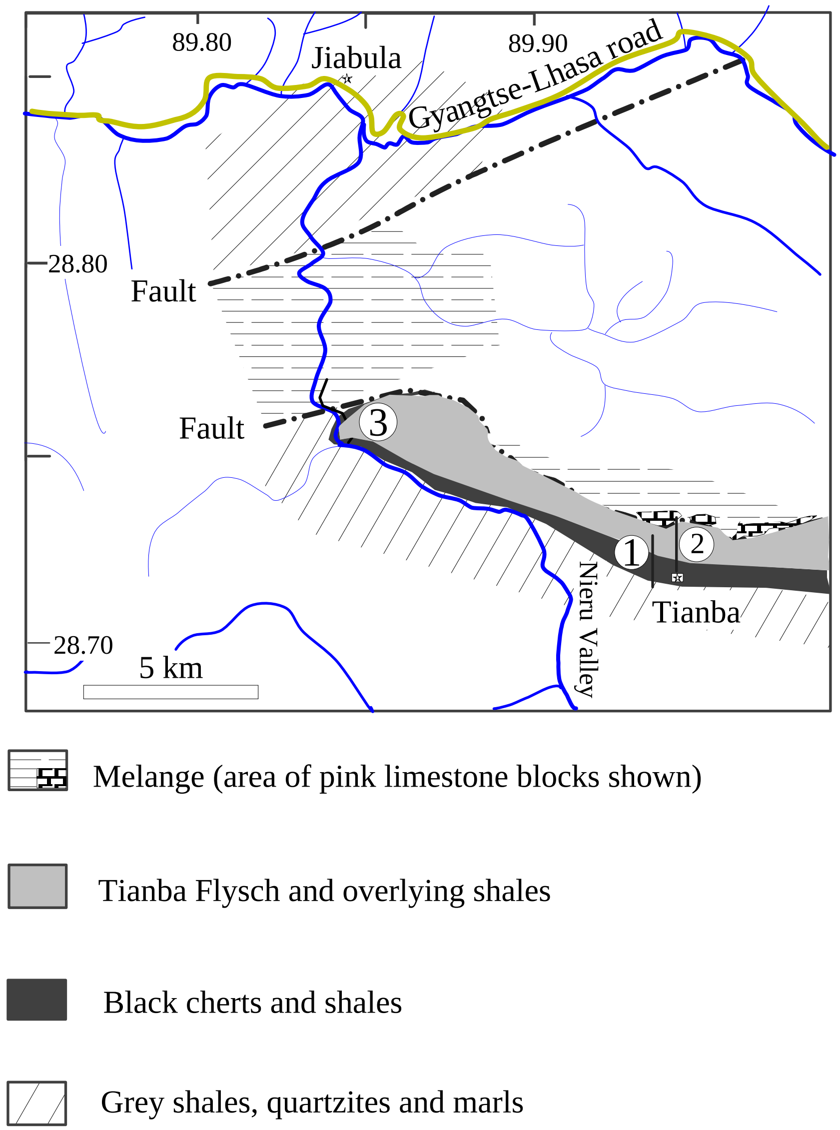

Figure 3.3 Sketch geologic map at Tianba showing three measured sections 1-3.Note: Rivers are traced from the 1:100,000 topographic map

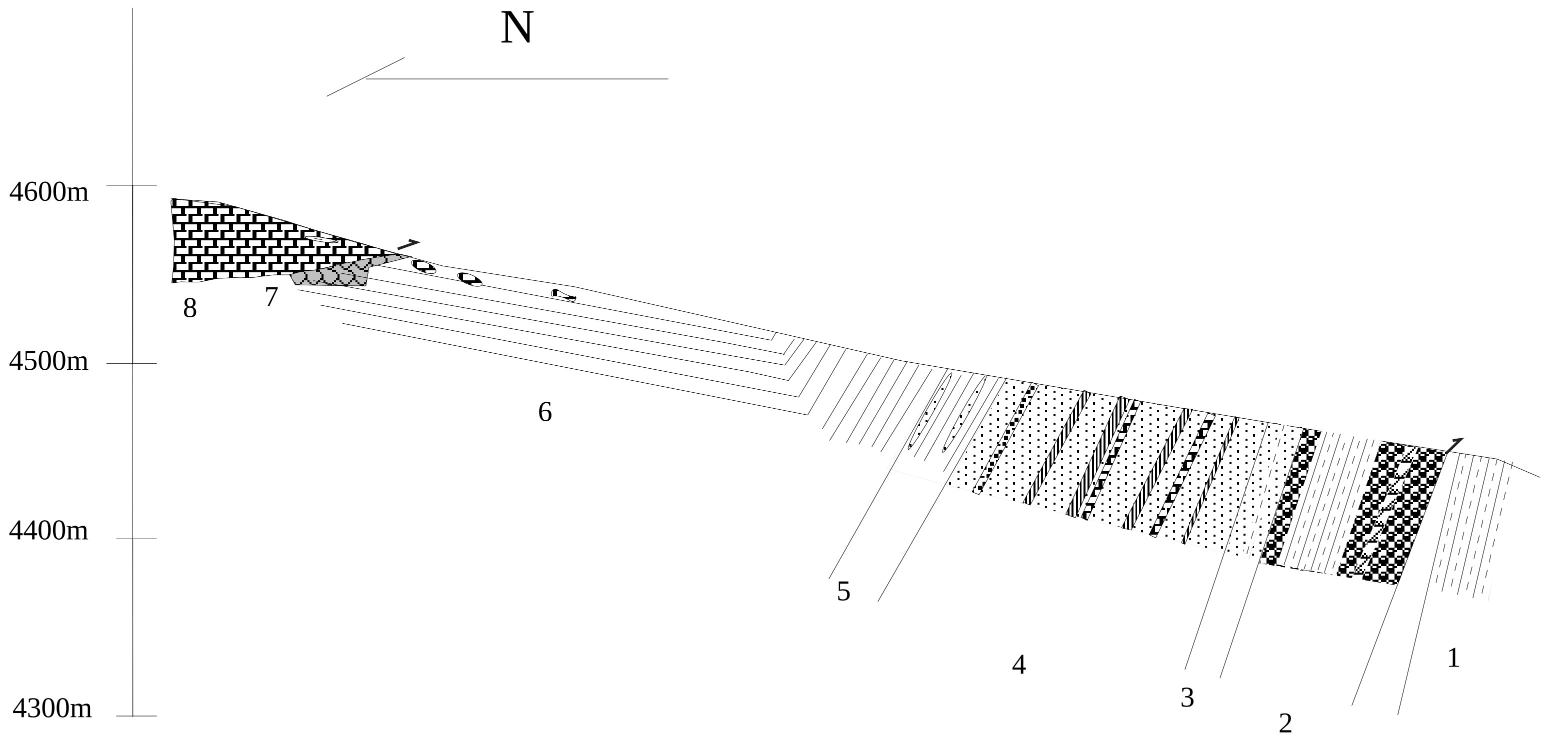

Figure 3.4. Tianba cross-section (section 2, see figure 3.3 for location) Horizontal scale=vertical scale
See Figure 3.11 for explanation of lithologic units and ornaments.

Figure 3.5 View to north of Tianba section. Dark grey shales and cherts are of early Cretaceous sediments in the river valley and the lower slopes of the hills beyond; tan-orange band is the Tianba Flysch; pink-purple rocks above this are fault-juxtaposed late Cretaceous limestones and shales. [The author, Bin Zhu, in this picture]

(1)

(2)

Figure 3.6 Sedimentary structures in the Tianba Flysch
(1) Ripple marks; (2) Sole marks.

Figure 3.7 Well-bedded turbidite sandstones with shale interbeds in the center part of the Tianba Flysch. View to east, section youngs to north (left).

(Figure 3.8). These shales also contain a few thin sideritic sandstone beds (Figure 3.9); and an interval containing some large (up to 1-meter diameter) calcareous nodules (Figure 3.10), one of which yielded an ammonite. Some belemnites are found in the shales above the flysch, and preliminary investigation of radiolaria fossils present in the sideritic sandstones points to a Late Cretaceous age of deposition (N. Shafique, personal communication, 2002).

In this section, above the interval with large calcareous nodules, a significant fault places mélange, including blocks of pink limestones (so-called Chuangde Formation by Wang et al., 2000), over the dipping, and folded Cretaceous rocks described above (Figure 3.4, 3.11). The pink limestone blocks in the hanging wall of this fault contain abundant foraminifera (*Globotruncana linneiana, G. elevata, Marginotruncana stuarti, M. stuartiformis, Heterohelix sp*) that indicate a Campanian depositional age (N.Shafique, personal communication, 2002; Willems, et al., 1996; Wang, et al., 2000). Based on the sedimentologic, structural, and biostratigraphic data, the Tianba Flysch was deposited during mid-Late Cretaceous time in a deep-water setting of the outer Indian passive margin.

Detrital modes of Tianba flysch

Petrographic examination of the sandstone samples from the northern Nieru Valley indicates that there are two types of sandstone associated with the Tianba Flysch. In the lower part of the unit, and mostly in the western sections, sandstones are primarily quartz rich lithic arenites. Most of the sandstones, by contrast, are lithic wackes.

Figure 3.8 Top of the Tianba Flysch, north of Tianba village. The uppermost thick-bedded sandstone of the Tianba Flysch is on the right. View to ENE, section youngs to north (left).The dark grey shales conformably overlie the Tianba flysch.

Figure 3.9 Sideritic sandstone bed showing graded-bedding. Abundant Cr-rich spinels are found in these sandstones.

Figure 3.10 Outsized (up to 1 m across) calcareous nodules in the greenish-grey shales, north of Tianba village. View to NE. One small nodule (10 cm across) yielded an ammonite. [Dr. B. Zhang in this picture]

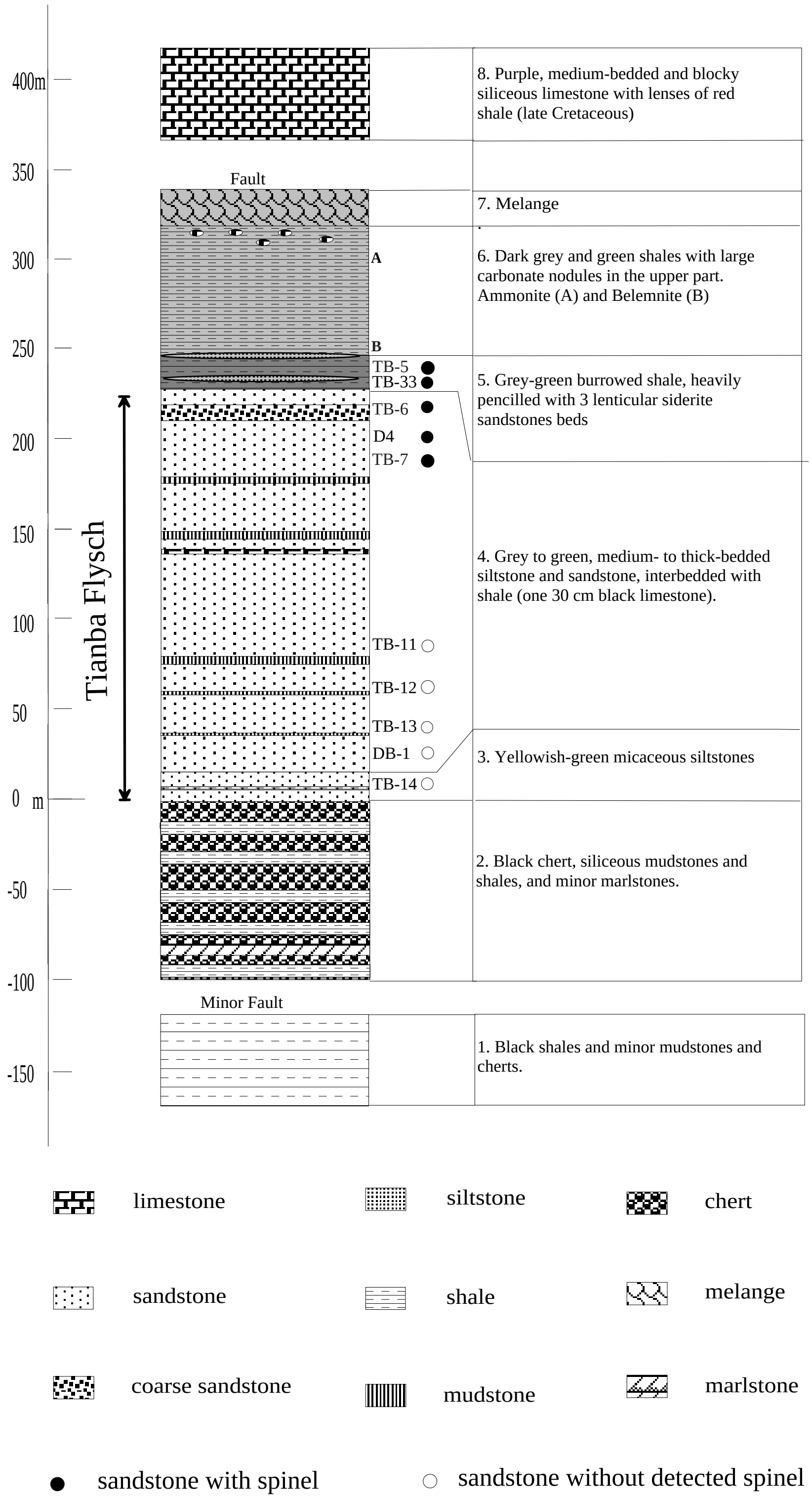

Figure 3.11 Measured Section (2), north of Tianba village. See Figure 3.3 for location.

In the basal part of the western section (section 3, Figure 3.12), sandstones are greenish in color, and occur as strongly channeled lensoidal bodies within the uppermost 25 meters of the dark cherts and siliceous shales of the Jiabula Group. Quartz constitutes 52% to 81% of the total framework grains (Figure 3.13). Matrix content is generally less than 15%. Average percentages of monocrystalline and polycrystalline quartz (Qm, Qp) are 70%, 1% respectively. Lithic fragments, the second-most abundant constituent, comprise 5% to 28% of the total framework grain population. These lithic grains can be further divided into volcanic (Lv), metamorphic (Lm) and sedimentary (Ls) types on the basis of the relict features (Figure 3.14). The recalculated mean value of LvLmLs parameters of quartz rich arenites are 8%, 80%, 12%, respectively, showing that the sandstones are most likely derived from a metamorphic terrane. Feldspar content is minor, averaging 1% of the total grain population. The recalculated mean value of QtFL plots along the total quartz-lithic leg in recycled orogen area in the conventional triangular compositional diagram (Figure 3.15). The presence of well-sorted, round quartz and relatively abundant metamorphic lithics may indicate derivation from the initial unroofing of an uplifted quartz- and metamorphic lithic-rich Gondwana sedimentary assemblage due to the final break-up event of Gondwanaland in the Cretaceous.

The lithic wackes (Figure 3.16) are characterized by poorly sorted, subangular quartz with significantly more lithic content. Quartz is dominant (average percentage 62%), and inclusions of feldspar, biotite and zircon in quartz grains are common. Matrix is generally abundant (10% to 30%). Feldspar comprises 1% to 6% of the total grain population (Figure 3.17). On the basis of extinction angles, plagioclase composition

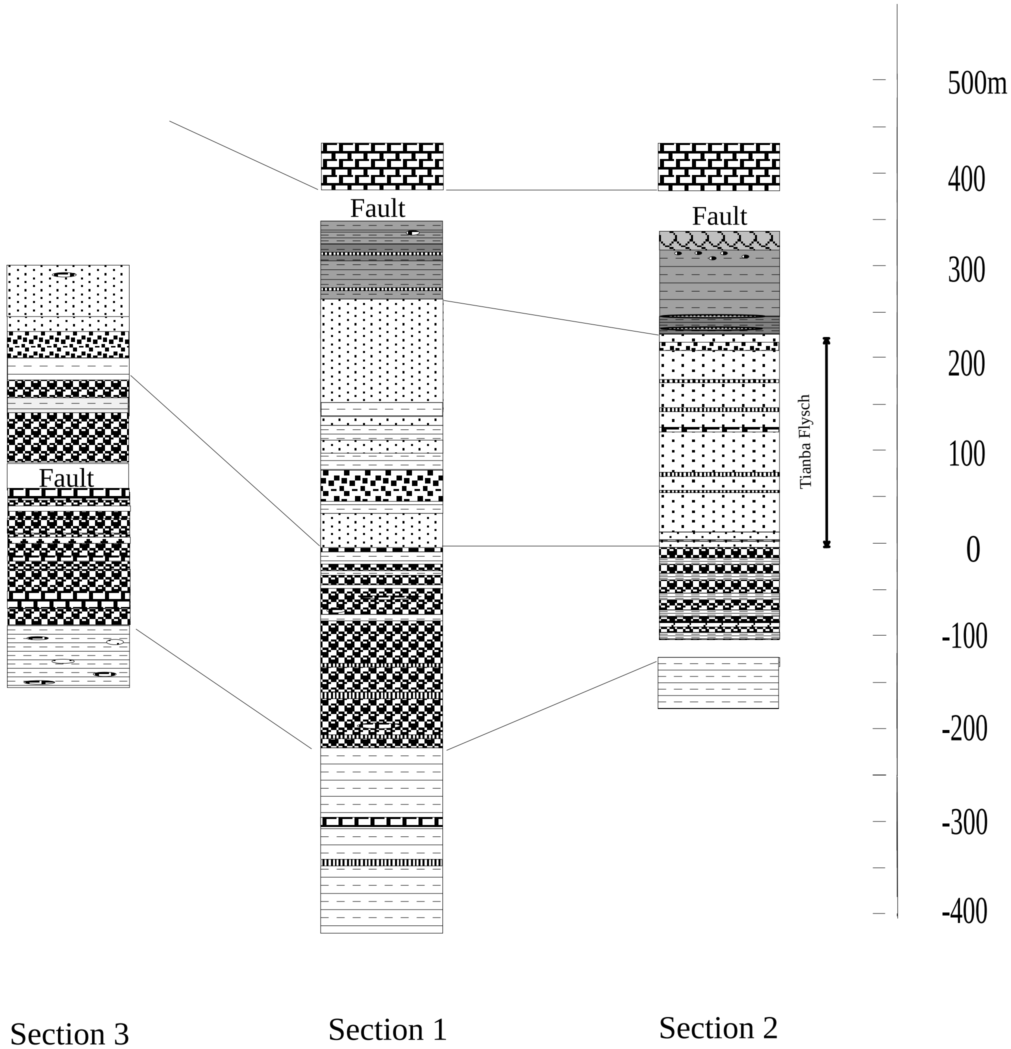

Figure 3.12 Measured stratigraphic sections at Tianba. Section locations are shown in Figure 3.3 See Figure 3.11 for explanation of the lithologic ornaments.

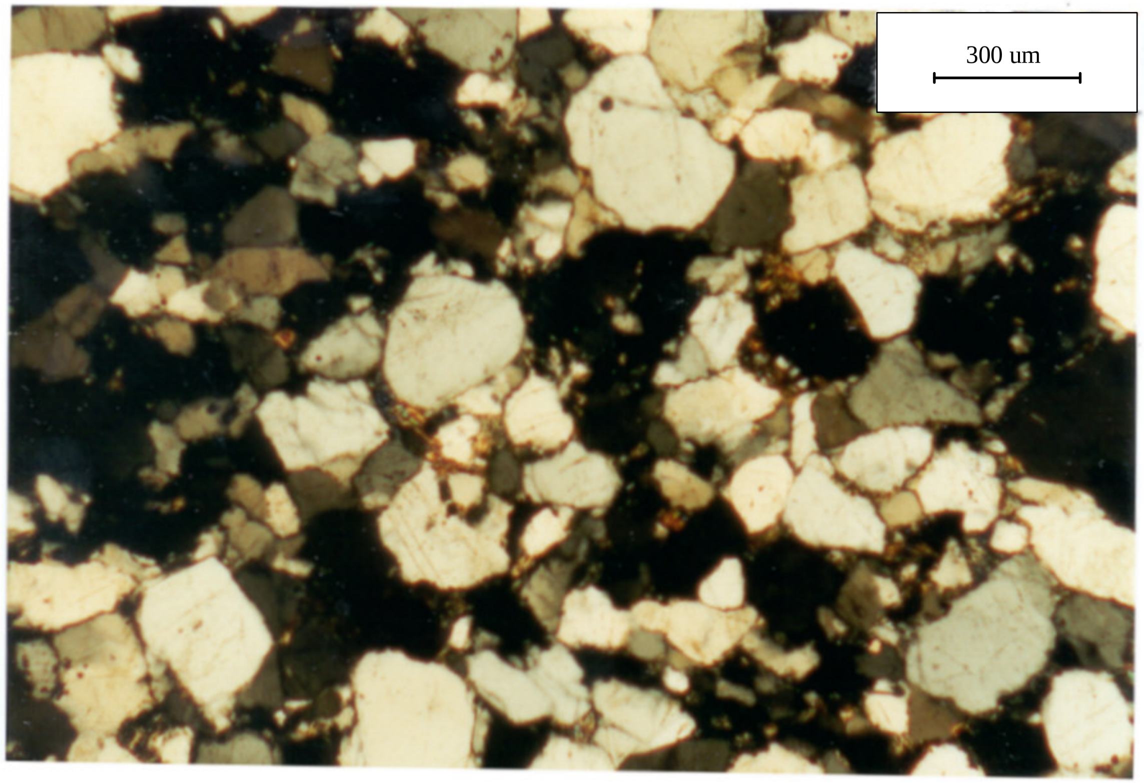

Figure 3.13 Photomicrograph (crossed polars) of quartz-rich sandstone in the basal part of western section (section 3 in Figure 3.3). Quartz grains are mostly monocrystalline,and the rock is well-sorted.

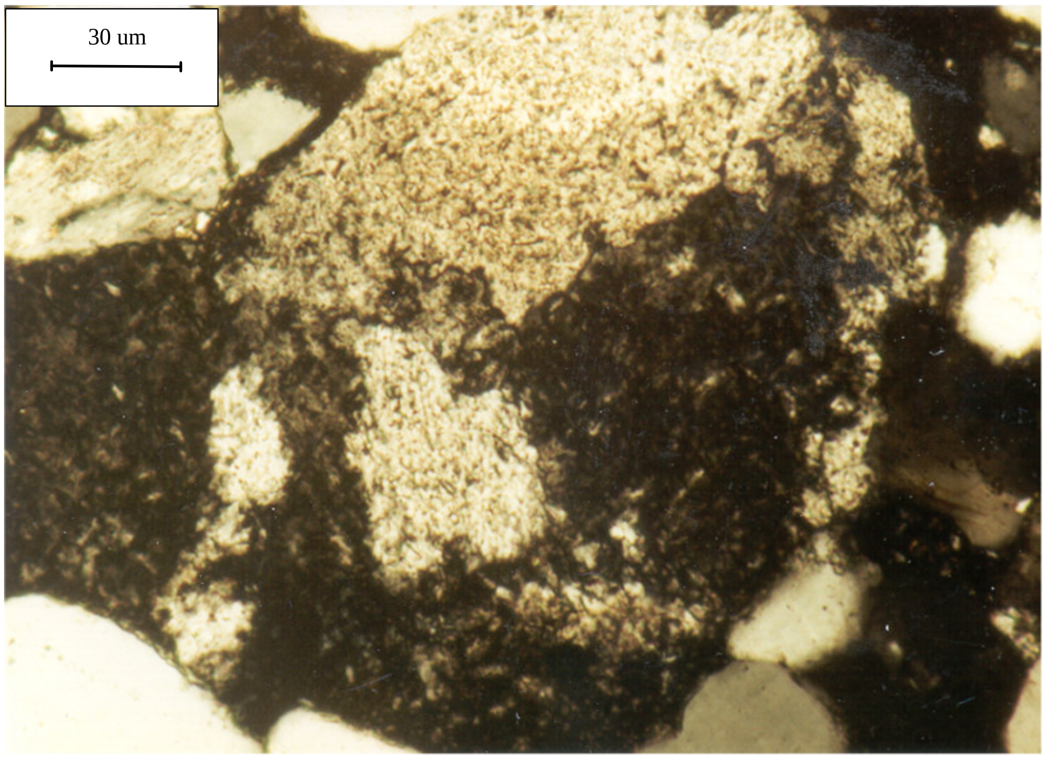

Figure 3.14 Photomicrograph (crossed polars) of a metamorphic rock fragment in the quartz-rich sandstones in the basal part of western section (section 3, see figure 3.3 for location.

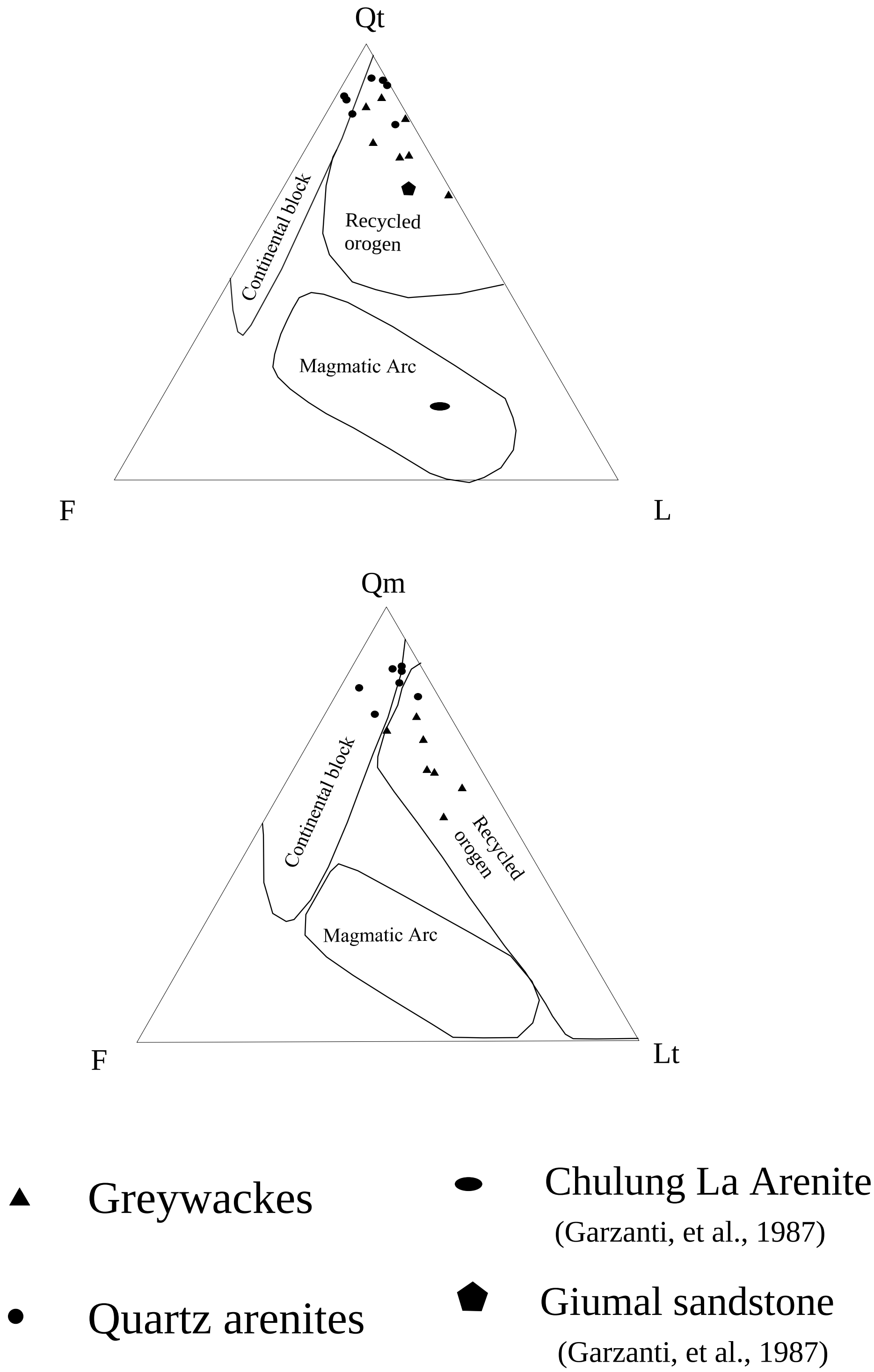

Figure 3.15 Detrital mode plot of sandstones in the Tianba sections. Tectonic fields from Dickinson and Suczek, 1979. Giumal sandstones and Chulung La Arenite from Zanskar are shown for reference on the QtFL plot.

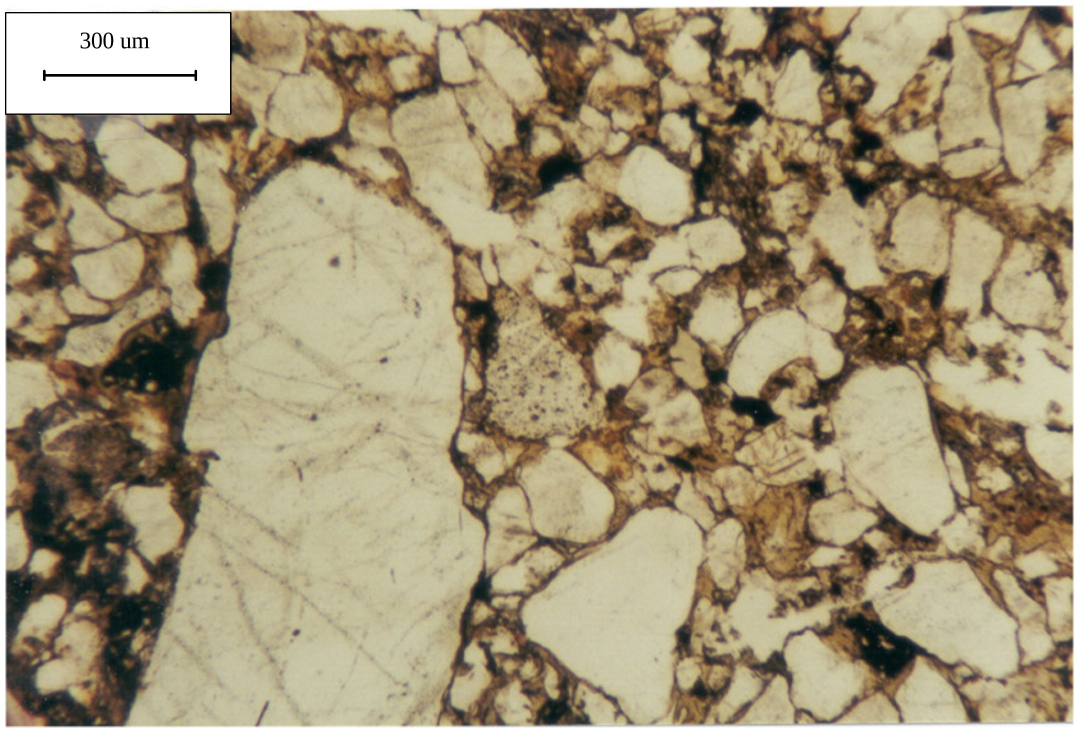

Figure 3.16 Photomicrograph (plane polars) of greywackes in the Tianba measured section. Note angular quartz grains are poorly-sorted,and there are some feldspar grains (dusty/dirty looking compared with clearer quartz grains).

range from albite to andesine and K-feldspar consists of either microcline or perthite. Sedimentary rock fragments (siltstone, shales, micritic limestones) are generally abundant (2% to 3%) in medium and coarser sandstones. Metamorphic grains (1% to 4%) are present in relatively smaller amounts. Volcanic clasts (2%-5%) contained in the wackes are both mafic and silicic in composition, although the larger clasts tend to be mafic (Figure 3.18). The presence of clear trachytic textures (Figure 3.19) in some lithic grains indicates that the lithic wackes were derived from a terrane that included volcanic rocks. The recalculated mean values of QtFL and QmFLt (Figure 3.15) of the lithic wackes also plot in the recycled orogen area. The presence of poorly sorted, subangular quartz suggests a short distance to the source area from the site of final deposition.

In summary, these sandstones have similar quartz contents (Figure 3.20). However, lithic wackes have more matrix, feldspar, and volcanic lithic clasts and less metamorphic lithics. This change may indicate progressive unroofing of a metamorphic lithic sedimentary assemblage, eventually with erosion into the crystalline basement, while at the same time having a more significant volcanic component relative to the quartz-rich lithic arenites.

Heavy mineral analysis of Tianba Flysch

As stated earlier, many important works have demonstrated that heavy mineral analysis is a sensitive and well-proven technique for determining the provenance of clastic sediments (Morton 1991, Dewey and Mange, 1999; Lihou and Mange-Rajetsky, 1996, Sciunnach and Garzanti, 1996; Caironi et al., 1996). Given the fact that some species derive from restricted lithologies, their detrital occurrence points to a clear source

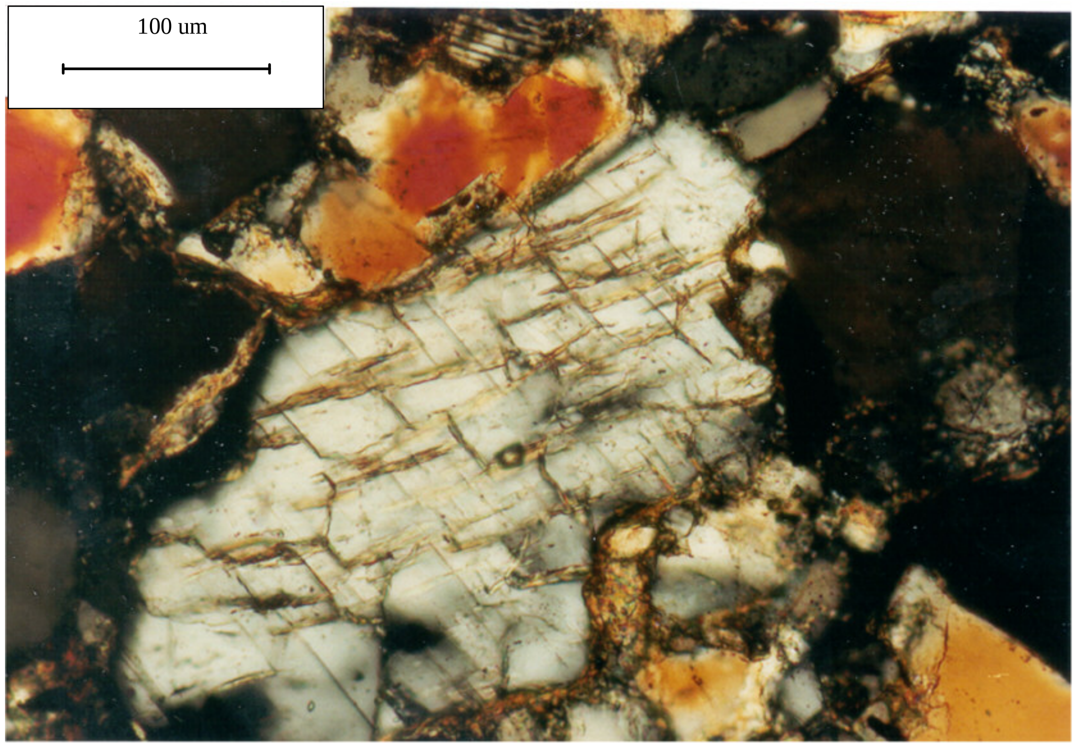

Figure 3.17 Photomicrograph (crossed polars) of feldspar (perthite) in the greywackes of the Tianba section 2 (see figure 3.3 for location).

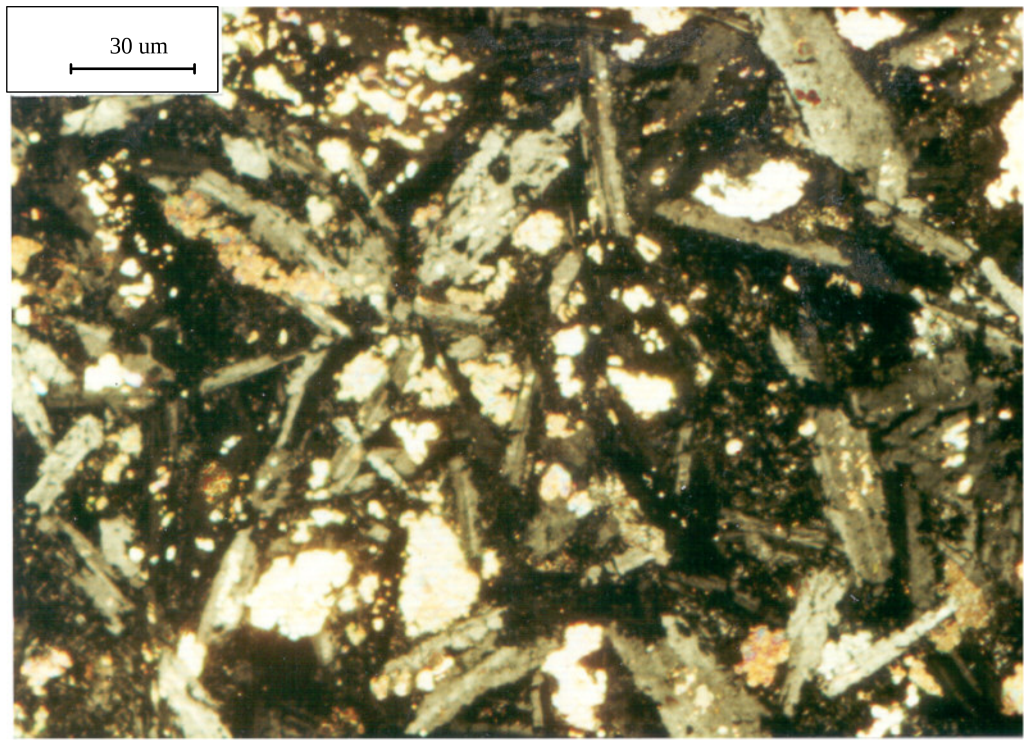

Figure 3. 18 Photomicrograph of a volcanic rock fragment composed of plagioclase phenocrysts within fine-grained ground mass. This indicates that there was a significant volcanic source for the Tianba Flysch.

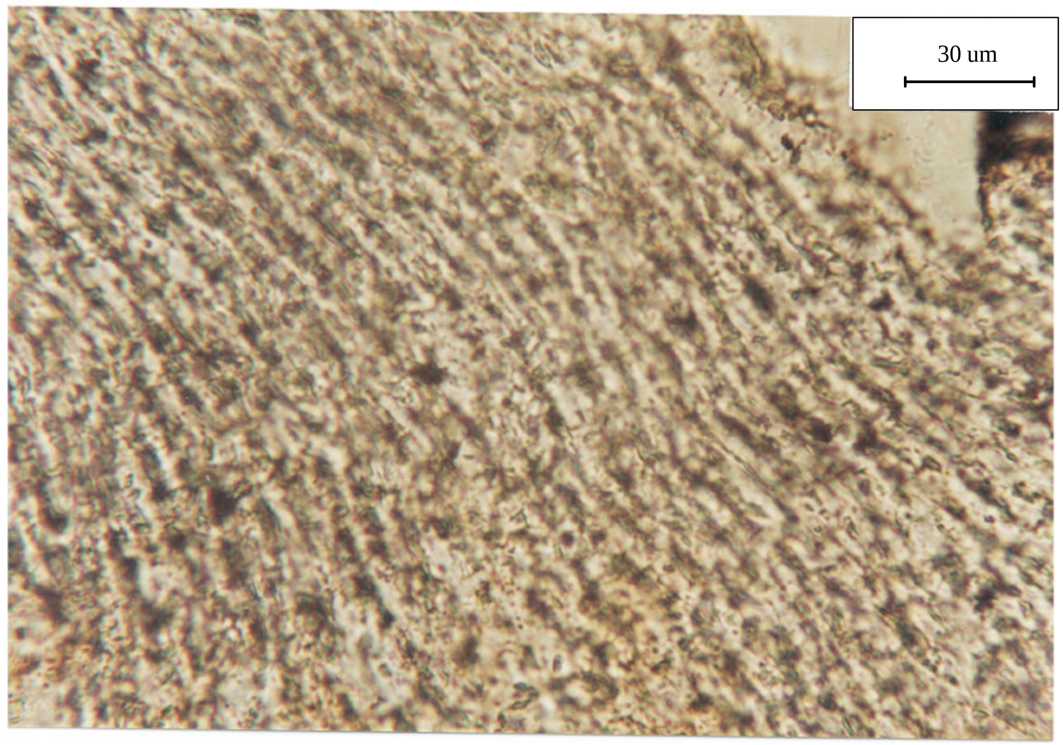

Figure 3.19 Photomicrograph (crossed polars) of a rock fragment with trachytic texture in TB6 sample in the Tianba section 2 (see figure 3.3 for section location).

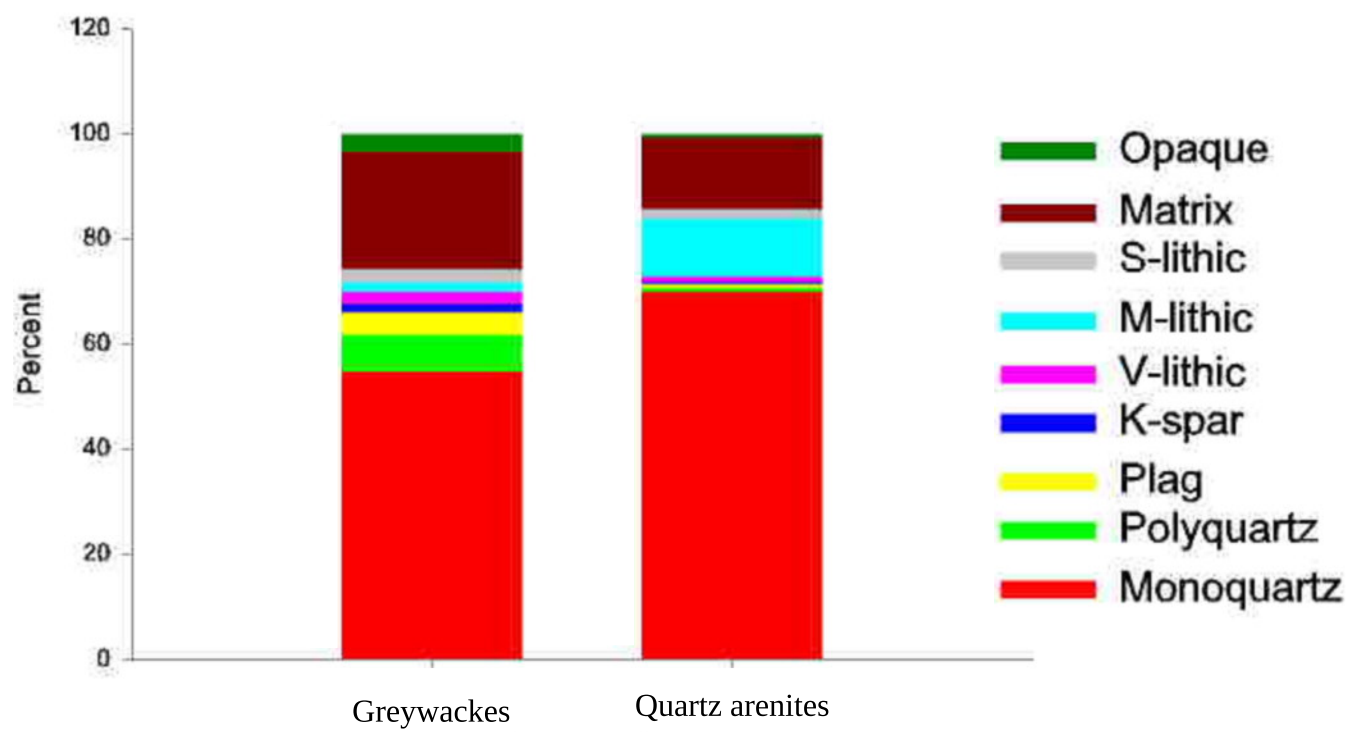

Figure 3.20 Histogram showing the different detrital modes between quartzite and greywackes in the Tianba sections. These sandstones have similar quartz contents, while there are more matrix, feldspar, volcanic lithics and less metamorphic lithics in the greywackes compared to the quartzites.

Monoquartz: monocrystalline quartz; Polyquartz: polycrystalline quartz; Plag: plagioclase; K-spar: K-feldspar; V-lithic: volcanic lithics; M-lithic: metamorphic lithics; S-lithic: sedimentary lithics; opaque: opaque minerals.

affinity (Dewey and Mange, 1999). To date, no studies have reported quantitative and temporal variations in heavy mineral assemblages from the Cretaceous sandstones in southern Tibet. Therefore a study of heavy minerals in the Tianba Flysch was performed in order to better understand the tectonic history in southern Tibet during the Cretaceous.

Samples preparation and analytical method

Ten samples were selected for heavy mineral analysis. Samples were prepared using the standard laboratory technique described by Mange and Maurer (1992), separating out the heavy minerals from the 62.5-250 μm disaggregated fine-sand fraction using bromoform (tribromoethane, density 2.89). The heavy mineral analysis indicates a low-diversity, zircon-rich assemblage with varying amounts of mica, tourmaline, apatite, rutile, magnetite, calcite, pyrite, and Cr-rich spinel. The significant volcanic component of Tianba Flysch is reflected by the abundance of sharp euhedral, colorless zircons in the upper part of the unit. Four samples (TB6, TB7, TB5, and TB33) were found containing Cr-rich spinels. TB6 and TB7 are in the upper part of the flysch while TB5 and TB33 are in the sideritic sandstone beds overlying the flysch unit (Figure 3.11). There are predominant amounts (more than 50%) of Cr rich spinels in the heavy mineral population from TB5 and TB33, indicating a prominent ultramafic and/or mafic magmatic event occurring before the deposition of these sediments. This is, to our best knowledge, the first report of Cr-rich spinels found in the mid-Late Cretaceous sandstones in southern Tibet. The study of these detrital spinels hence provides a more specific and detailed understanding of tectonic setting of the source area for the Tianba Flysch, which in outcrop appearance closely resembles a syn-collisional flysch.

81 spinel grains were handpicked from TB6, TB7, TB5 and TB33. They are dark brown to dark reddish-brown and are up to 0.2 mm in diameter with the majority 0.1 mm in size. Thicker grains are weakly translucent at the edges. Grain margins commonly show conchoidal fractures, suggesting mechanical breakage, but some grains are subhedral-euhedral and preserve the original crystal boundary. The preservation of original crystal margins is important because any changing environment of the parental melts during crystallization can be reflected by the microprobe measurements of core-to-rim variation for the spinel crystal. Samples were mounted in epoxy resin and ground and polished to expose the spinels for microprobe analysis.

All analyses were performed in six sessions using a JEOL 733 Superprobe (fully automated, five Wavelength Dispersive Spectrometers) in the department of Earth and Environmental Sciences at Rensselaer Polytechnic Institute. The elements Al, Mg, Cr, Fe, Ni, V, Mn, Zn and Ti were analyzed under the following conditions: accelerating voltage 15 keV, a beam current 15 nA, and a beam diameter of 1 micron, using ZAF correction model. The major elements were counted for 40 s and minor elements Ti, Mn, Ni, V, and Zn for 100 s each. USNM 117075 from Tiebaghi Mine, New Caledonia was used as standard for Cr, Al, Fe and Mg. Other element standards were as follows: Zn on pure gahnite; Ti on rutile; Mn on tephroite, V on synthetic V_2O_5 and Ni on diopside glass. Analysis of standard (USNM 117075) as unknown was done at the beginning, middle and end of each analytical session to ensure proper calibration throughout, and the compositions of the standard between six probe sessions show no statistically significant differences. For each analyzed grain, 2-6 analytical points were used to calculate average composition and the data normalized to 4 oxygen atoms.

All Fe is expressed as FeO except for the first session, and the ferric iron content of each analysis was determined by assuming stoichiometry and an ideal XY_2O_4 formula, where X=Fe^{2+}, Mg, Ni, Zn, and Y=Cr, Al, Ti, Fe^{3+}, following the methods of Barnes and Roeder (2001). A recent study of Kamperman et al (1996), using direct oxygen measurement of Cr-rich spinel, revealed that spinels from the volcanic rocks of Hunter Fracture Zone, Ca-rich boninites from the Tonga Trench, and metamorphosed volcanics from the Peak Hill-Glengarry Basin and the Heazlewood River Ultramafic Complex show a range of nonstoichiometry because of the cation deficiency in the spinel crystal structure. Barnes and Roeder (2001) also mentioned that the propagation of errors in the stoichiometry-based calculations might give rise to a significant error in the observed variance in trivalent ions. Given the fact that there are few analyses using direct oxygen measurement in spinels available and most concentrations of ferric and ferrous iron were calculated assuming ideal stoichiometry in the literature, we can only recognize this as a limitation in the interpretation of the chemical composition of spinels (Barnes and Roeder, 2001).

Cr-rich spinel chemical compositions

The microprobe results (Table 3.1) indicate that the spinels can be characterized as a complex solid solution of the oxides of chromium, magnesium, aluminum, ferric iron, ferrous iron and titanium with 15-26 wt% Al_2O_3, 36-45 wt% Cr_2O_3, 10-12 wt%

Table 3.1 Representative analyses of Cr-rich spinels from Tianba Flysch

Sample	TiO2	V2O5	Al2O3	Cr2O3	MnO	MgO	NiO	ZnO	FeO	Fe2O3	total	Cr/3+	Fe/3+	Al/3+	Mg/(Mg+Fe2+)	Cr/(Cr+Al)
TB33	2.81	n.a.	17.10	39.09	0.23	12.26	0.18	0.09	15.43	13.20	100.37	0.49	0.19	0.32	0.52	0.61
TB33	1.64	n.a.	16.18	44.24	0.26	10.93	0.15	0.09	16.74	11.52	101.76	0.55	0.15	0.30	0.48	0.65
TB33	2.33	n.a.	17.58	37.95	0.30	8.84	0.15	0.18	19.55	12.39	99.25	0.49	0.17	0.34	0.39	0.59
TB33	2.34	n.a.	18.39	37.46	0.30	9.06	0.15	0.17	19.47	12.18	99.52	0.48	0.17	0.35	0.40	0.58
TB33	1.84	n.a.	19.69	37.94	0.20	11.84	0.14	0.00	15.69	12.85	100.19	0.46	0.18	0.36	0.51	0.56
TB33	3.36	n.a.	16.32	38.71	0.43	12.29	0.14	0.13	14.74	10.86	96.98	0.52	0.16	0.32	0.54	0.61
TB33	1.47	n.a.	16.45	42.11	0.22	11.47	0.13	0.06	15.27	12.53	99.71	0.52	0.17	0.30	0.51	0.63
TB5	2.34	0.32	22.77	36.00	0.33	20.78	0.16	n.a.	5.09	12.27	100.06	0.42	0.19	0.39	0.82	0.52
TB5	1.61	0.36	16.36	40.71	0.31	9.89	0.13	n.a.	17.80	12.85	100.03	0.51	0.18	0.31	0.44	0.63
TB5	1.46	0.18	17.64	41.92	0.25	11.70	0.11	n.a.	15.67	12.14	101.06	0.51	0.16	0.32	0.51	0.61
TB5	1.37	0.18	18.91	42.52	0.23	11.35	0.15	n.a.	16.40	9.26	100.37	0.53	0.12	0.35	0.50	0.60
TB5	1.40	0.28	19.47	39.00	0.25	11.42	0.14	n.a.	16.21	12.73	100.90	0.48	0.17	0.35	0.49	0.57
TB5	1.53	0.17	20.09	37.77	0.21	13.68	0.16	n.a.	12.88	13.18	99.68	0.46	0.19	0.36	0.58	0.56
TB5	1.95	0.48	17.43	40.61	0.37	10.02	0.10	n.a.	18.33	10.48	99.78	0.52	0.14	0.34	0.44	0.61
TB5	1.27	0.28	19.18	40.53	0.38	8.23	0.11	n.a.	20.78	9.40	100.16	0.52	0.12	0.36	0.37	0.59
TB5	4.24	0.73	18.74	32.15	0.30	7.97	0.21	n.a.	23.23	11.66	99.24	0.45	0.17	0.39	0.34	0.54
TB5	1.85	0.29	18.28	37.89	0.27	10.87	0.14	n.a.	16.83	13.61	100.03	0.47	0.19	0.34	0.47	0.58
TB5	1.96	0.32	17.80	39.41	0.21	13.08	0.20	n.a.	13.77	12.91	99.66	0.49	0.18	0.33	0.56	0.60
TB5	1.08	n.a.	23.03	39.24	0.17	14.09	0.19	0.00	12.81	10.26	100.87	0.46	0.13	0.40	0.60	0.53
TB5	1.83	n.a.	18.41	38.19	0.24	11.21	0.16	0.06	16.29	14.21	100.59	0.47	0.20	0.34	0.48	0.58
TB5	1.79	n.a.	16.08	41.28	0.24	11.27	0.14	0.06	15.36	12.02	98.23	0.53	0.17	0.31	0.50	0.63
TB5	1.59	0.31	18.81	37.32	0.33	8.11	0.14	n.a.	20.47	12.06	99.13	0.48	0.16	0.36	0.36	0.57
TB5	2.02	0.45	16.64	39.75	0.24	11.37	0.20	n.a.	16.44	14.19	101.30	0.49	0.20	0.31	0.48	0.62
TB5	2.06	0.35	17.32	41.20	0.26	12.48	0.17	n.a.	14.87	11.46	100.17	0.52	0.16	0.32	0.54	0.62
TB5	2.07	0.40	18.20	38.00	0.26	11.10	0.17	n.a.	16.85	13.25	100.30	0.48	0.18	0.34	0.48	0.58
TB5	1.51	0.32	16.97	41.79	0.24	11.27	0.17	n.a.	15.96	11.65	99.88	0.52	0.16	0.32	0.50	0.62
TB5	2.10	0.61	17.62	40.51	0.26	10.49	0.14	n.a.	18.00	10.02	99.76	0.52	0.14	0.34	0.46	0.61
TB6	1.17	0.16	23.44	38.16	0.19	15.04	0.20	n.a.	11.16	9.27	98.79	0.46	0.12	0.42	0.65	0.52
TB6	1.30	n.a.	23.63	37.95	0.22	14.14	0.17	0.00	12.43	8.62	98.46	0.46	0.11	0.43	0.62	0.52
TB6	0.47	n.a.	39.34	26.82	0.22	17.88	0.02	0.00	9.62	5.22	99.58	0.29	0.06	0.65	0.73	0.31

note: The ferric iron content of each analysis was determined by assuming stoichiometry, and an ideal XY_2O_4 formula, where X=Fe^{2+}, Mg, Ni, Zn, and Y=Cr, Al, Ti, Fe^{3+}, following the methods of Barnes and Roeder (2001).

MgO, 20-30 wt% FeO_t, and 1.5-2.0 wt% TiO_2 (Figure 3.21). There is an obvious reciprocal relationship between Cr and Al, which may be indicative of different degrees of partial melting in the mantle (Dick and Bullen, 1984). Mn, Ni, V, and Zn are present in only trace amounts, generally less than 0.5 wt% oxides. No rim of "ferritchromit" was found in the spinels probed, and grains are generally homogeneous and show no obvious signs of zoning in line scans. This indicates that (1) parental lavas had undergone little or no magma mixing or significant crustal assimilation (Allan et al, 1988), (2) there was no extensive subsolidus reequilibration between spinels and other silicate minerals (Scowen et al, 1991), (3) no major metamorphism event occurred after the crystallization of these spinels. This also suggests that the Cr-rich spinels were not xenocrystals from unknown magma or residual mantle. It appears that there is no significant stratigraphic variation in the chemistry of Cr-rich spinels within these samples except relatively high contents of MgO (up to 17.88 wt %) in TB6 and TB7.

Volcanic source for the detrital spinels

Most spinel-peridotites have spinels with low or negligible TiO_2 contents (except spinels in the plagioclase-peridotites from Romanche Fracture Zone and St. Paul's Rocks (Dick and Bullen, 1984)), while volcanic spinels with TiO_2 <0.2 are uncommon (some suites of low-Ti MORB, arc tholeiites and boninites (Kamenetsky et al, 2001)). Lenaz et al (2000), therefore, set a compositional boundary between peridotitic and volcanic spinels at TiO_2 =0.2 wt%. Given the fact that TiO_2 contents of our spinels are well above 0.2 wt% (Figure 3.21), we conclude that the detrital spinels from Tianba Flysch were derived from volcanic rocks.

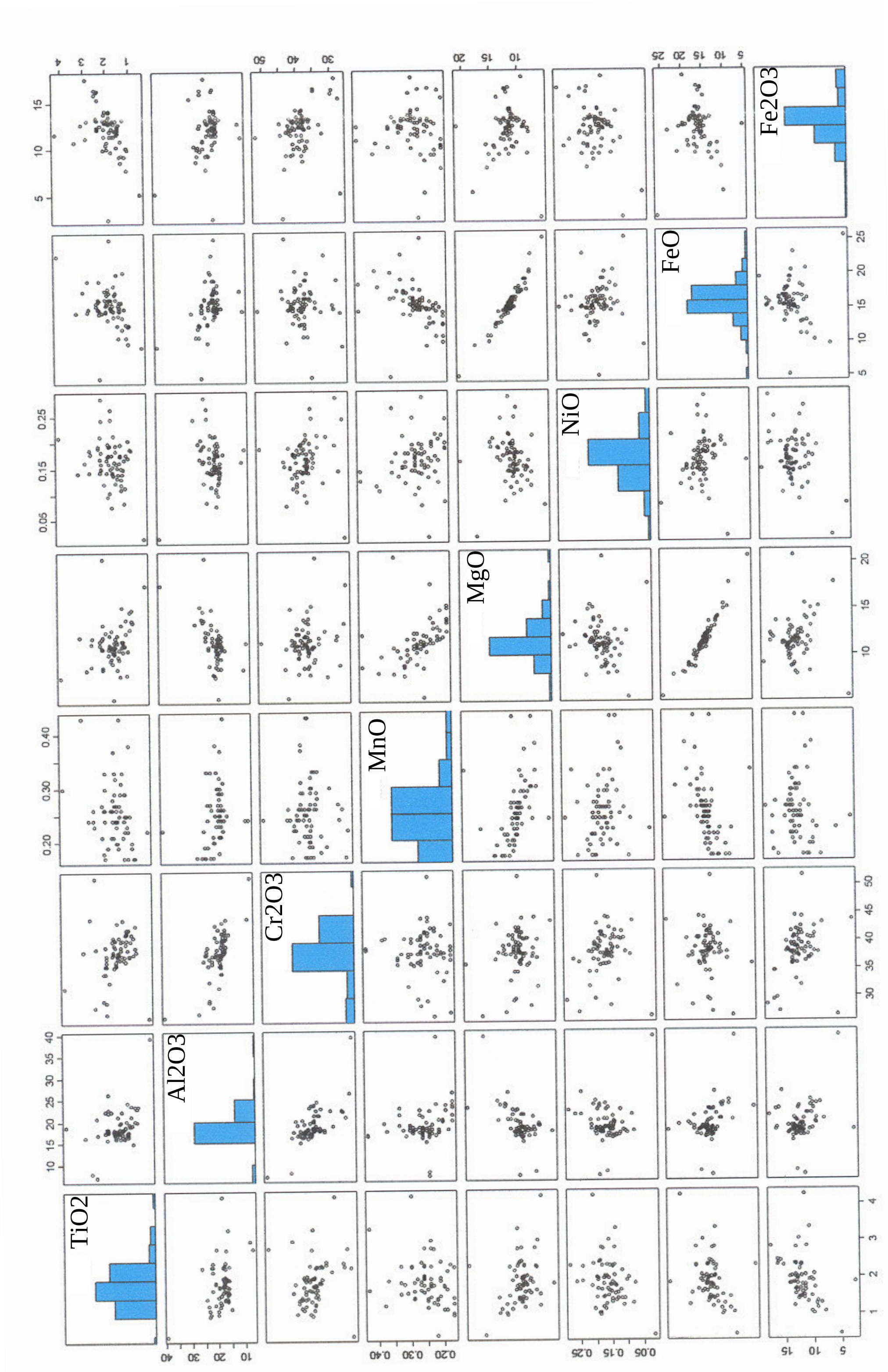

Figure 3.21 Chemical compositions of detrital Cr-rich spinels using pairs plot from S-plus

About 5% of the spinel grains contain melt inclusions, and are thus clearly volcanic in origin. They are variable in size (10-40 um), showing negative crystal shapes. Some of them are glass with some shrinkage bubbles (Figure 3.22a). Two melt inclusions (40 μm) are made up of pyroxene blebs (bright), residual glass (black), shrinkage vapor bubbles and minor sulfide droplets (Figure 3.22b), and clinopyroxene. The presence of well-crystallized clinopyroxene (Figure 3.22b) indicates that there was a relatively long cooling history after entrapment. The compositions of four pyroxenes in this inclusion show that they have significantly different contents in the major oxides, as expected from closed-system crystallization; this is consistent with the interpretation that the pyroxenes are not xenocrystals but true daughter crystals after entrapment in the spinel. One spinifex-like texture was found, defined by acicular clinopyroxene crystals (Figure 3.22c). The observed crystals at exposed surfaces of melt inclusions are randomly oriented relative to the crystallographic axes of host chromites, suggesting that there is similar arrangement in three dimensions. This distribution is very similar to the olivine-enriched melt inclusions in chromites from low-Ca boninites, Cape Vogel, Papua New Guinea (Kamenetesky et al., 2002)

Trace elements in the detrital spinels

Manganese concentrations in the detrital spinels range from 0.17 to 0.43 wt% with a mean value of 0.25 wt%. There is a strong linear negative correlation between MnO and MgO (Figure 3.21). Almost all of our data (96 %) plot (Figure 3.23a) below the 'filter' line (Barnes, 1998) in the plot of MnO vs Mg# (Mg/(Mg+Fe^{2+})), suggesting that

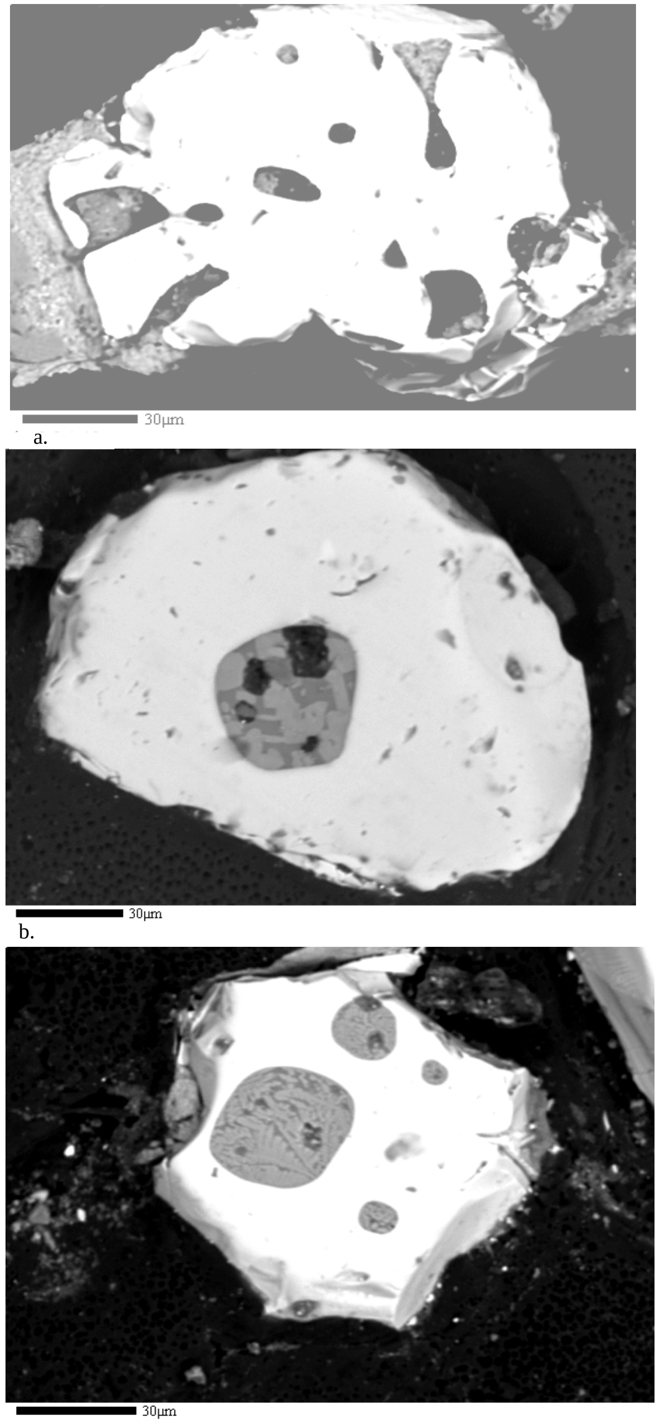

Figure 3.22 Backscattered electron images of melt inclusions in the detrital spinels from Tianba Flysch.

there were no significant chemical changes after crystallization of these spinels, in agreement with the lack of obvious zoning in the euhedral spinel grains. All the detrital spinels analyzed contain measurable quantities of Ni, varying from 0.076 to 0.285-wt%, with positive linear correlation with MgO (Figure 3.21). It appears that the content of Ni increases with decreasing Cr/(Al+Cr+Fe^{3+}) ratio and increasing Mg# (Figure 3.23b.) due to Ni having a large octahedral site preference in the chromian spinel structure (Paktunc and Cabri, 1995). This is consistent with the studies of Stosch (1981), who concluded that the composition of magma and coexisting olivine and spinel predominantly control Ni partitioning between Cr-rich spinels and mantle silicates. Zn contents measured in 20 grains are consistently low with a range from the detection limit of about 0.04 wt% to 0.18 wt%. There is negative correlation between ZnO and Mg# for spinels containing >0.04 wt% ZnO (Figure 3.23c.), which may be indicative of Zn having a strong tetrahedral site preference in the crystal lattice of Cr-rich spinels (Paktunc and Cabri, 1995). Of the 46 probed spinels, vanadium contents measured display a good correlation with Mg# as well (Figure 3.23d.), and implies that V may also favor the tetrahedral site when entering the normal spinel structure.

In summary, Mn, Zn, and V are negatively correlated with Mg# while Ni correlates positively with Mg# because of different site preference in the crystal structure of studied spinels. The relatively strong linear correlations between these elements and Mg# suggest that their concentrations in the spinels are sensitive to changes in the compositions of parental magma and coexisting early crystal phases, consistent with the limited ranges of major oxide contents.

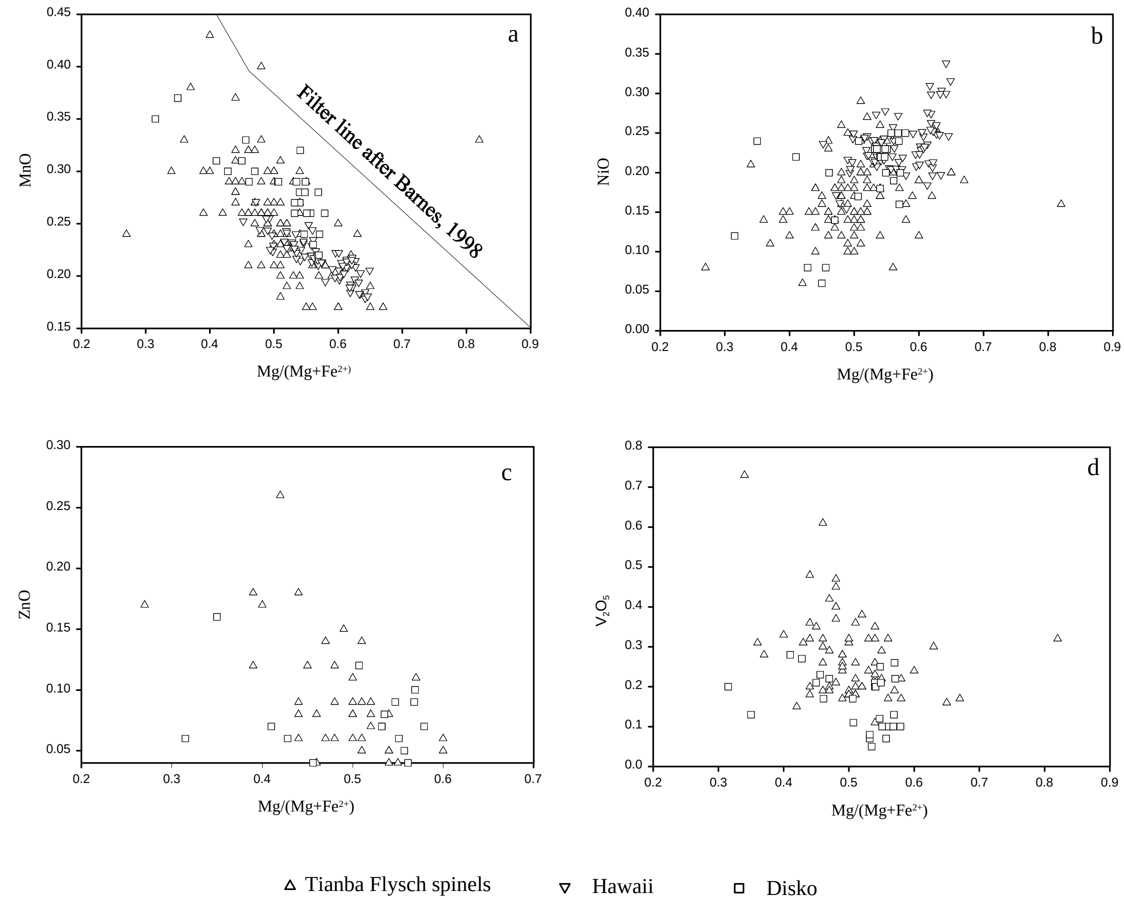

Figure 3.23 Covariation of minor elements with $Mg/(Mg+Fe^{2+})$ in spinel (For comparision, data from Hawaii and Disko are also shown):
a. MnO vs. Mg#; b. NiO vs. Mg#; c. ZnO vs. Mg#; d. V_2O_5 vs. Mg#.

Possible source rock lithology

In the spinel nomenclature (Barnes and Roeder, 2001), the detrital spinels we analyzed have a well-developed Fe-Ti trend and have Cr#(Cr/(Cr+Al)) between 0.4 and 0.65, Mg# (Mg/(Mg+Fe^{2+})) between 0.3 and 0.9, and Fe3+/(Al+Cr+Fe^{3+}) close to 0.2. In terms of origin and tectonic setting, Cr-rich spinels from a variety of types of ultra-mafic and mafic complexes can be discriminated by plotting different major-element concentrations (Irvine, 1967; Dick and Bullen, 1984; Arai, 1992; Kamenetsky et al., 2001; Barnes and Roeder, 2001). Overlaps among various tectonic settings on some plots (Dick and Bullen, 1984), however, are not uncommon because only selected aspects of the total chemical variation of the spinels are reflective in the binary plot of individual elements (Cookenboo et al., 1997). All major elements and, if possible, trace elements, therefore should be considered to determine the possible parental magma of the studied spinels.

In the plot of Cr# vs Mg# (Figure 3.24a), there is a slightly negative correlation between Cr# and Mg#, and the Mg# values are significantly scattered along the higher Cr# (close to 0.6). This may be a possible path of spinel crystallization due to the cocrystallization of olivine, plagioclase and spinel (Roeder, 1994) or a result of the prolonged crystallization of spinel and/or low-temperature re-equilibration with olivine in host rocks (Kamenetsky et al., 2001; Lenaz et al., 2000). We favor the first interpretation because there is no evidence for significant low-temperature re-equilibration observed as discussed above. Comparison of our spinels with those coexisting with olivine in modern submarine volcanics (Kamenetsky et al., 2001) suggests that the studied spinels were most likely sourced from primitive basalts with olivine phenocrysts at least as Mg-rich as

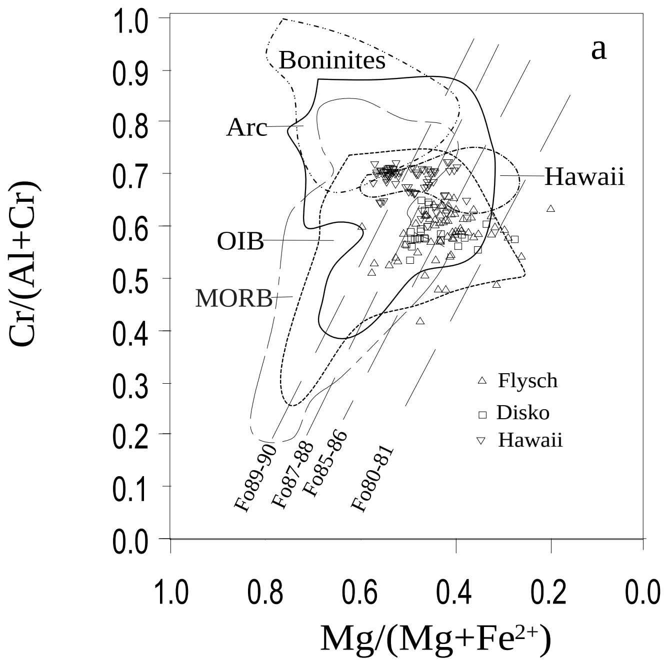

Isopleths of olivine Fo (dashed lines) from Kamenetsky et al, 2001

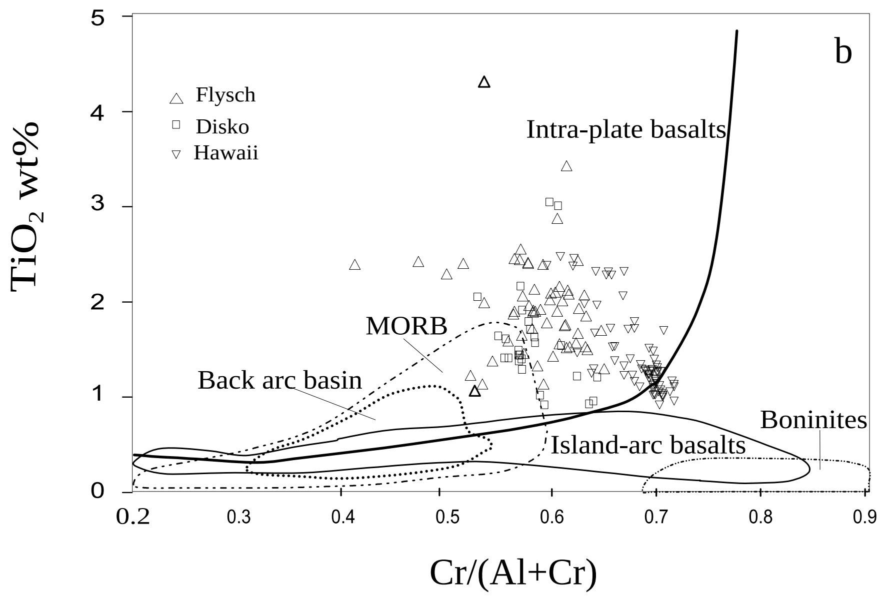

Figure 3.24 Major element contents of spinels and tectonic setting discriminant plot:
a. Cr/(Cr+Al) vs. Mg/(Mg+Fe^{2+}) after Barnes and Roeder, 2001;
b. TiO_2 vs. Cr/(Cr+Al) after Arai, 1992.

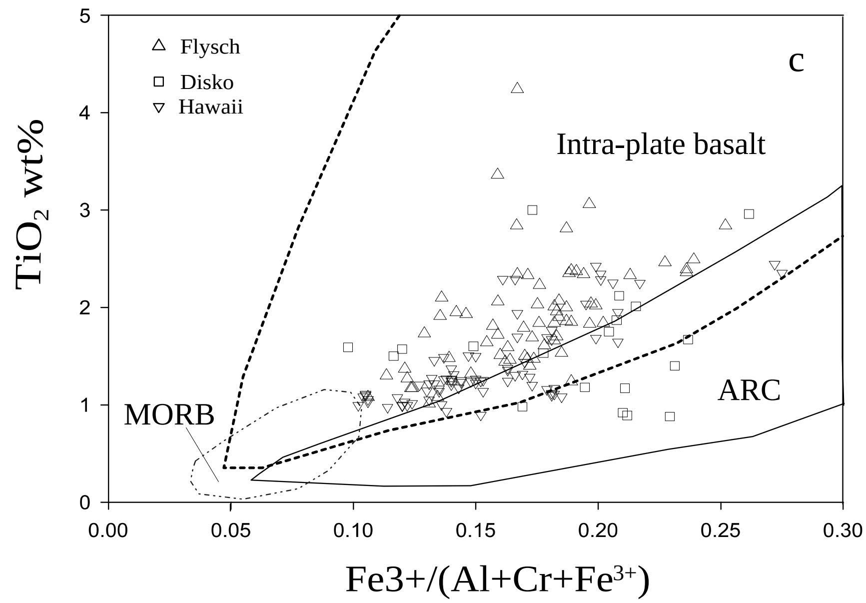

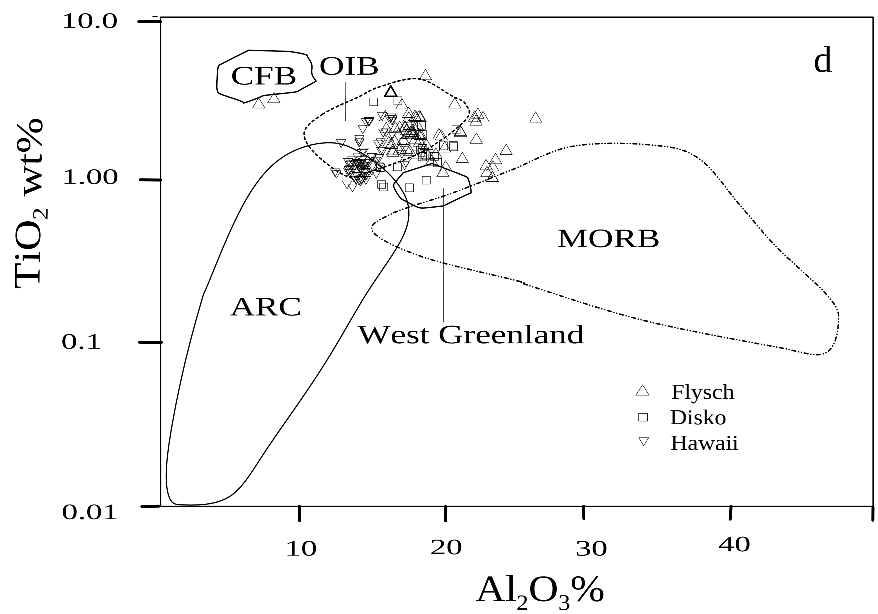

Figure 3.24(continued) Major element contents of spinels and tectonic setting discriminant plot:
c. TiO_2 vs. $Fe^{3+}/(Al+Cr+Fe^{3+})$ after Arai, 1992;
d. TiO_2 vs. Al_2O_3 after Kamenetsky et al, 2001.

Fo80-86 (Figure 3.24a), which is also supported by the evidence of strong linear correlation between trace elements and Mg# described above. In the conventional fields (Figure 3.24a) of tectonic settings for spinels (Barnes and Roeder, 2001; Dick and Bullen, 1984; Irvine, 1967), our data plot in the overlap field of oceanic island basalts (OIB) and MORB. As such island arc tholeiites and boninites did not significantly contribute to these sedimentary strata.

Given the fact that the diffusivity of Ti, Al and Cr through olivine is low (Scowen et al., 1991; Kamenetsky et al., 2001) and the contents of TiO_2 in the volcanic spinels increase from boninites and island arc basalts to intra-plate basalts through MORB and back-arc basin basalts (Arai, 1992), it is possible that these magma affinities can be distinguished by the relationship between Ti, Al and Cr. In the plot of TiO_2 vs. Cr# (Figure 3.24b), >90% of studied flysch spinels plot in the field of intra-plate basalts with a few in the MORB field, but no points plot in island-arc basalt and boninite fields. A similar result is shown in the plot of TiO_2 vs. $Fe^{3+}/(Al+Cr+Fe^{3+})$ except no points for the flysch fall in MORB and only one in arc field (Figure 3.24c).

It appears that TiO_2 and Al_2O_3 are negatively correlative in Cr-rich spinels (Figure 3.21), which may be indicative of reducing the partitioning of Ti into spinel with increasing Al activity in the system of melt-spinel because both favor the octahedral sites in the spinel structure (Kamenetsky et al., 2001). Using 400 melt inclusion-spinel pairs from 36 igneous suites from oceanic, arc and intra-plate tectonic environments, Kamenetsky et al. (2001) discriminate four fields of different geodynamic settings: Large Igneous Province (LIP), Oceanic Island Basalt (OIB), Oceanic Ridge Basalt (MORB), and Island-arc Magmas (ARC) based on the relative contents of TiO_2 and Al_2O_3 in the studied spinels (Figure 3.24d). They also found that there is a strong positive correlation between TiO_2 and Al_2O_3 contents in spinel and coexisting melt inclusions, indicating that their contents in spinels are primarily dependent on the magmatic TiO_2 and Al_2O_3 abundances, consistent with experimental studies of Roeder and Reynolds (1991). Plotting our flysch Cr-spinel data on their diagrams (not shown) for spinel-melt pairs (in terms of TiO_2 and Al_2O_3 abundances) indicates that the detrital spinels crystallized from a melt containing 13-15 wt% Al_2O_3 and 1.5-2.5 wt% TiO_2 (Zhu et al., in preparation), consistent with preliminary data of homogenized compositions of melt inclusions in the spinels. Most detrital spinels plot in the field of OIB (Figure 3.24d), consistent with the results of discriminant diagrams described above.

Considered together, the binary plots of Mg# vs. Cr#, TiO_2 vs. Cr#, TiO_2 vs. $Fe^{3+}/(Al+Cr+Fe^{3+})$, and TiO_2 vs. Al_2O_3 demonstrate that the compositional range of the detrital spinels closely matches that of spinels from ocean-island basalts and excludes island arc basalt, MORB, boninites, and ophiolites as major sediment sources. Also shown (Figure 3.24a, b. c. d) are spinels from Hawaii (spinel inclusions in olivine from Green Sand Beach, Delano, unpublished data) and Disko Island, Greenland (Paktunc and Cabri, 1995). It is clear that there are significant overlaps between spinels from Tianba Flysch, Hawaii and Disko Island in these plots. Similar abundances (Figure 3.23) and similar trends in trace elements between the Tianba Flysch, Hawaii and Disko Island, Western Greenland discussed above are also good indicators of close affinities of parental magma between these suites. Therefore we conclude that our detrital spinels were derived from plume related, intra-plate basalts.

Discussions

Correlation of Tianba flysch with the Giumal Group sandstones in Zanskar

Lithic rich arenites and mudrocks of the Cretaceous are widely exposed in the Tethyan Himalaya from Zanskar in the west to southeastern Tibet (Durr and Gibling, 1994; Garzanti, 1993). Comparisons of our stratigraphic data and sandstone detrital mode (Figure 3.15) with the well-documented Cretaceous sedimentary sequence in the northwest Himalayas show that the Giumal Group sandstones of the Zanskar region are analogous to the Tianba flysch in many aspects (Figure 3.25). In Zanskar, the Upper Jurassic to Lower Cretaceous Spiti Shale is dominated by ammonite-bearing soft black calcareous shales, and is conformably overlain by the Giumal Group. The latter has been subdivided into two formations (Garzanti, 1993). The Upper Necomian? to Aptian Takh Formation is characterized by quartzo-feldspathic sandstones, while the Albian Pingdo La Formation consists of volcanic arenites and is capped by the Nerak and Oma chu Glauco-phosphorites. In the plot of QtFL (Figure 3.15), the Giumal sandstones plot in the recycled orogen field, similar to those of Tianba Flysch. The Giumal Group is immediately overlain by mudstones and shales with pelagic foraminifera (Chikkim Formation), beginning in the Late Albian or early Turonian and reaching up to the Campanian/Maastrichtian boundary. The Cretaceous succession is completed by Maastrichtian marls and limestones (Kangi La and Marpo Fromation).

Abundant fossils including ammonites (*Spiticeras, Neocosmoceras, Neocomites, Killanella*), and bivalves (*Inoceramus everesti, Oxytoma*) are reported in the upper part of the Spiti Shale (Sinha, 1988; Wen, 1980), indicating a Berriasian-Valangian age of deposition. There are also similar faunal assemblages in the lower part of the calcareous

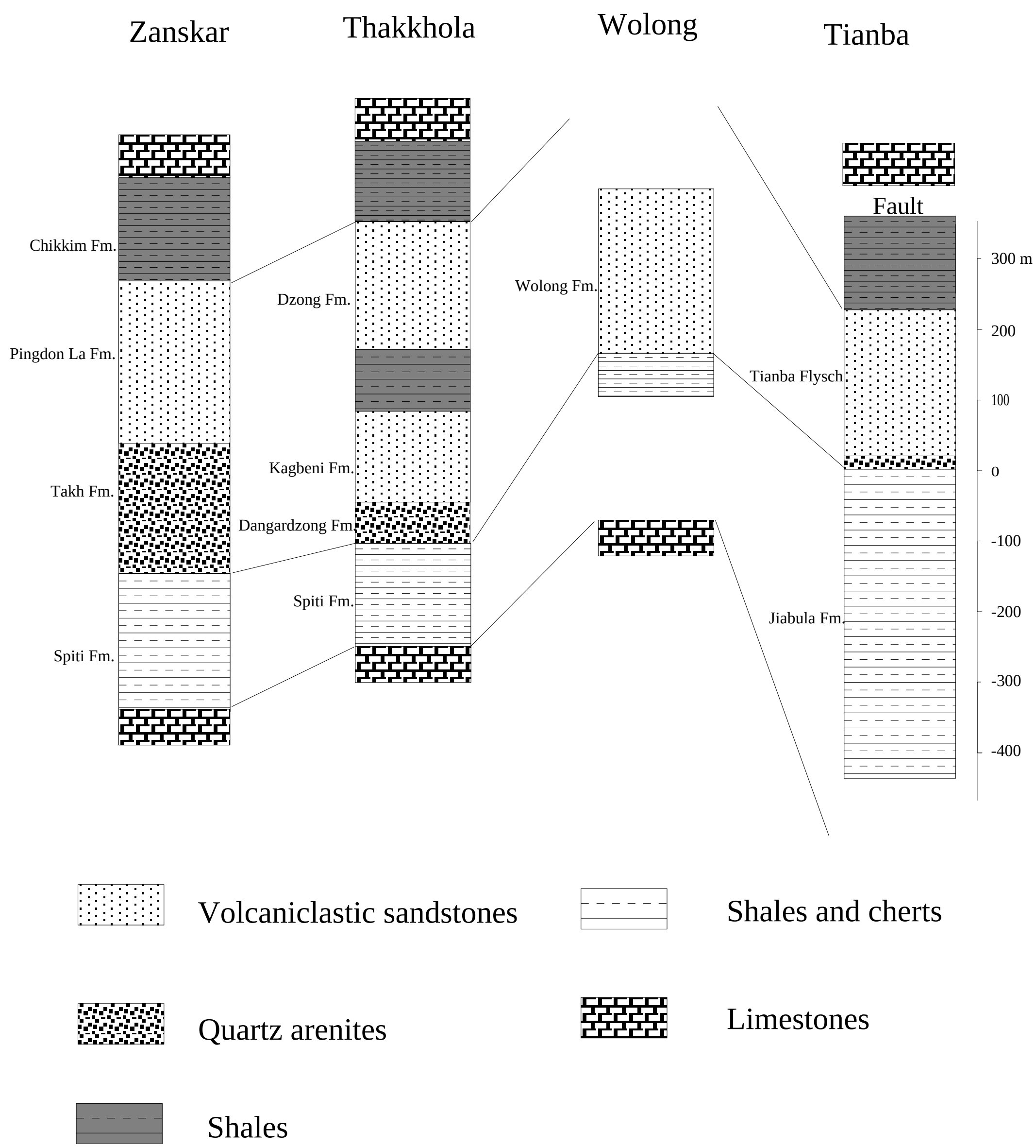

Figure 3.25 Comparison of lithostratigraphy between Tianba, Zanskar (after Garzanti, 1993), Thakkhola (Garzanti, 1999) and Wolong (Jadoul, et al. 1998).

shales of the Jiabula Group in the eastern Himalaya. Therefore available fossil evidence indicates that Cretaceous sedimentary rocks in the north Nieru Valley and Zanskar are both lithologically and biostratigraphically correlative.

Continent-wide, Early-Mid Cretaceous volcanic event

Clastic wedges correlative with the Tianba flysch and Giumal Group are deposited all along the Himalayas, from the Trans-Indus Salt Range, where they overlie glaucontic ironstone intervals, to the Malla Johar and Thakkhola regions, where two >400-m-thick lithic wacke sections accumulated during a large part of the Early Cretaceous (Sinha, 1988; Gibling et al., 1994). The geochemical composition of a basaltic pebble fragment found in the Valanginian to Aptian volcaniclastic sandstones in the Thakkhola region (Durr and Gibling, 1994) indicates a source of alkali basalts of within-plate affinity. Our preliminary microprobe data of melt inclusions in the detrital spinels show a composition of 49-52 wt% SiO_2, 13-15 wt% Al_2O_3, 1.5-2.5 wt% TiO_2, 1.6-4.1 wt% Na_2O, 0.5-1.5 wt% K_2O and 0.3-0.5 wt% P_2O_5, also points to a close affinity of those spinels to alkali basalts. All basins of the East India coast are characterized by Hauterivian to Aptian sandstones, pointing to rejuvenation of the craton ascribed to lithospheric doming (Garzanti, 1993). A sudden burst of flood-basalt magmatism, linked to the activity of the Kerguelen mantle plume, took place at 117 Ma (Baksi, 1995; Kent, 1997), as recorded in the Rajmahal-Sylhet-Bengal Trap Province of northeast India (Kent, 1991, Garzanti, 1993). Therefore tectonic extension affected both the western and eastern margins of the Indian continent in the Early Cretaceous, which was separating from Antarctica.

The rapid increase in sand-sized quartzose detritus at the base in the Tianba flysch indicates a source from the uplifted Indian continent during final fragmentation of Gondwanaland, while relatively abundant ‘trachytic’ detritus in some layers in the lithic wackes point to sudden outpouring of plume-related magmas onto northern India. This temporal evolution is consistent with the classic sequence of tectono-sedimentary episodes during plume related rifting: initial doming is followed by erosion, tectonic extension and break-up of a continent which reduce the thickness of the lithosphere, followed by volcanic eruption at the climax when rifting above uprising hot plumes gives rise to basaltic magma by extensive decompression melting of the asthenosphere (Campbell and Griffiths, 1990; Garzanti, 1993).

Late Jurassic to Early-Mid Cretaceous oceanic island arc and ophiolite obduction

The presence of chrome-rich spinels in sedimentary rocks of a basin in and adjacent to an orogenic belt is generally interpreted as an indicator of a source from ophiolitic rocks, especially peridotites of the oceanic upper mantle (Ganssloser, 1999; Pober et al., 1988; Cookenboo et al., 1997). As such the presence of significant mafic volcanic detritus and uncharacterized chrome-rich spinels in the Tianba Flysch might suggest ophiolite derivation and a Cretaceous ophiolite obduction event on the northern Indian continental margin.

It has been proposed that there was a late Cretaceous ophiolite-obduction event in the Zanskar region, northwestern Himalaya (Searle, 1983). Recent work by Aitchison et al. (2000), McDermid et al. (2002), Davis et al. (2001) and Aitchison et al. (2002) points out that there was a Late Jurassic to Early-Mid Cretaceous intra-oceanic magmatic arc between the Indian passive margin and Lhasa Block in southeastern Tibet. The Zedong terrane comprises basaltic-andesites, andesites, andesitic breccias, rare dacites and other intrusives, as well as radiolarian cherts. South of it lies the Dazhuqu terrane, consisting chert, siliceous mudstone, felsic tuffs and fine-grained volcaniclastic turbidites, and the Bainang terrane which consists of a series of south-directed imbricate thrusts including slices of red ribbon-bedded cherts, fine-grained siliciclastics and tuffaceous cherts of Tethyan origin (Aitchison et al., 2000, McDermid et al., 2002). This terrane assemblage is interpreted as representing the arc massif, the fore-arc basin and the subduction complex of a deformed arc-trench system of Late Jurassic to Early-Mid Cretaceous age within the Neo-Tethys (Aitchison et al., 2000; McDermid et al., 2002).

It is generally accepted that a Cr# ratio > 0.7 in spinel is indicative of arc-related setting (Dick and Bullen, 1984), in contrast to the generally lower values of this ratio in spinel from MORB and OIB. Given the fact that abyssal ocean crust may be finally transported to a subduction zone and "so become tectonically intermingled with arc ophiolites" (Stowe, 1994), a wide variation in the chemical compositions would be commonly expected for the spinels derived from arc complexes and associated accretionary complexes. TiO_2 content in arc spinels is generally below 1 wt % (Figure 3.24d). As described above, there is, however, a narrow range of parameters for chemical compositions of the Tianba Flysch detrital spinels; most of them have TiO_2 abundance around 2 wt %, and they consistently plot in the discriminant field of OIB or intra-plate basalts. No significant contribution of spinels to Tianba flysch from arc-trench complexes has been detected.

The close proximity of our sampled section to the Zedong-Dazhuqu-Banang region (Figure 3.1) argues that these arc volcanics and ophiolites did not affect this area until after deposition of the Tianba Flysch. Based on the detrital mode and chemical composition of sandstones in the Upper Cretaceous rocks of the study area (Zhu et al., in preparation), any interactions most likely occurred after the Campanian. As such the northeastern Indian passive margin was not involved in tectonic interactions with Neo-Tethyan oceanic arc terranes during the Mid-Late Cretaceous period when the Tianba Flysch was deposited.

Conclusion

There are significant amounts of chrome-rich spinels in turbiditic sandstones from the upper part of mid-Cretaceous Tianba Flysch in the northern Nieru Valley, southern Tibet. Based on the presence of melt inclusions, and > 1 wt% TiO_2 in the probed spinels, we conclude that the spinels were derived from a volcanic source. No significant compositional zoning is present suggesting that there was little or no magma mixing and/or the spinels were erupted shortly after their crystallization from the parental lava. From the chemical compositions of the Cr-rich spinel data, likely source rocks for these spinels are not arc-complexes or plutons but flood basalts associated spatially and temporally with Kerguelen hotspot activity at 117 Ma, which are related to the break-up of India, Australia, and Antarctica in the Early-Mid Cretaceous. Although the Tianba Flysch looks in the field like a typical collisional product, and the presence of Cr-rich spinels might suggest an ophiolitic source and a Cretaceous ophiolite-obduction on the northeastern Indian continental margin, our detailed work shows clearly that the Tianba Flysch is neither ophiolite-derived, nor related to the start of the India-Asia collision.

Chapter 4. Melt inclusions in Detrital Cr-rich Spinels from the Cretaceous greywackes of the eastern Tethyan Himalayas: evidence for hotspot-related volcanic event

Abstract

Cr-rich spinel is a detrital component in turbidites from the well-exposed, mid-late Cretaceous Tianba Flysch sequence in the Nieru Valley, southern Tibet. Microprobe analyses show that the spinels have a well-developed Fe-Ti trend, Cr/(Cr+Al) 0.4-0.65, Mg/(Mg+Fe^{2+}) 0.3-0.9, and TiO_2 >1 wt.%. The compositional range of these detrital spinels closely matches that of spinels from intra-plate basalts, and is very similar to spinel inclusions in olivine from hotspot basalt like Hawaii and Disko Island. About 5% of the spinels contain melt inclusions, 5-60 μm diameter. Compositions of melt inclusions are (in wt.%): SiO_2 (42-53), TiO_2 (1.5-3.9), Al_2O_3 (11.5-15), MgO (6-13), CaO (6-12), Na_2O (0.5-4), K_2O (0.3-1.1), and CaO/Al_2O_3 (0.7-1.0). The compositions of melt inclusions correlate well with those of host spinels, and both show a possible co-crystallization of olivine and spinel in the parental magma. Melt inclusion geochemistry suggests a source from hotspot basalts. Based on palaeo-tectonic reconstruction, presence of mid-late Cretaceous fossils in the strata, and the chemical compositions of spinels and associated melt inclusions, we conclude that volcanics of the Rajmahal, which are associated spatially and temporally with Kerguelen hotspot activity on India about 117 Ma ago, were the likely source for these Cr-rich spinels.

Introduction

It is well known that the chemical characteristics of primary melt can be completely or partially obliterated from the compositions of the final igneous rock product by physical changes (pressure and temperature) and the processes of fractional crystallization, magma mixing, hydrothermal alteration, degassing, and assimilation of wall rocks before the original melt appears at the surface (Sobolev, 1996). Melt inclusions found in minerals as tiny droplets trapped during crystal growth offer unique way of catching instantaneous melt composition as magma cools due to their effective isolation from the influence of these later processes (Watson, 1976; Roeder and Poustovetov, 2001), and thus they can reveal the melt evolution that may not be recorded in bulk-rock data. The studies of the melt inclusions in the earliest crystallized phenocrysts (olivine, chromian rich spinel) therefore have provided significant advances in determining the primitive melt composition and evolutionary environments of parental magma (Sobolev and Shimizu, 1993, 1994; Sobolev et al., 1994, 2000; Kamenetsky et al., 1997; Danyushevsky et al., 2000, 2002). Given the fact of low chromium solubility in basaltic melts (Roeder and Reynolds, 1991; Barnes, 1986) and thus absence of significant crystallization of the Cr-rich spinel on the walls of melt inclusions, the compositions of melt inclusions trapped in Cr-rich spinels should be a better approximation of original magma than those hosted in silicate minerals (Kamenetsky et al., 1998, 2001, 2002; Schiano et al., 1997; Shimizu et al., 2001; Lorand and Ceuleneer, 1989; Sigurdsson et al., 2000). Chrome spinel may be enriched in some sedimentary rocks because of their unusual chemical durability, lack of cleavage, and resistant to lower grade alteration and mechanical breakdown (Pober et al., 1988; Cookenboo et al., 1997; Ganssloser, 1999; Dewey and Mange, 1999). Therefore the studies of Cr-rich spinels with melt inclusions in ancient sediments may provide important information on provenance and tectonic evolution in a complex orogenic system (Kamenetsky, 1996; Lenaz et al., 2000).

In this paper we present chemical compositions of melt inclusions (Figure 4.1) trapped in Cr-rich spinels from the Cretaceous Tianba Flysch at the north end of Nieru Valley, southern Tibet (Figure 4.2). A key objective of this study is to demonstrate how the compositions of melt inclusions in Cr-rich spinels can be used to constrain the provenance of the host sedimentary or volcano-sedimentary rocks in the Himalayan fold-belt. This is the first study of melt inclusions in detrital spinels in the Himalayan orogen, the product of continent-continent collision between Asia and India. The compositional data of Cr-rich spinels associated with melt inclusions have the potential to provide a direct constraint on the tectonic setting in source area, especially with respect to the type of basalt, and therefore can both strengthen provenance studies based on detrital modal analyses and improve our understanding of the tectonic history of the Tethyan Himalaya during the Cretaceous.

Geologic Setting

Cretaceous sedimentary rocks are well exposed in the Tianba-Jiabula area to the south of the Indus-Yarlung-Zangbo Suture (Figure 4.2), tectonically belonging to the central Tethyan Himalaya (originally the outer part of the Indian passive continental margin). In general, these rocks are interbedded variegated shales, cherts, argillaceous limestones, turbiditic sandstones and siltstones.

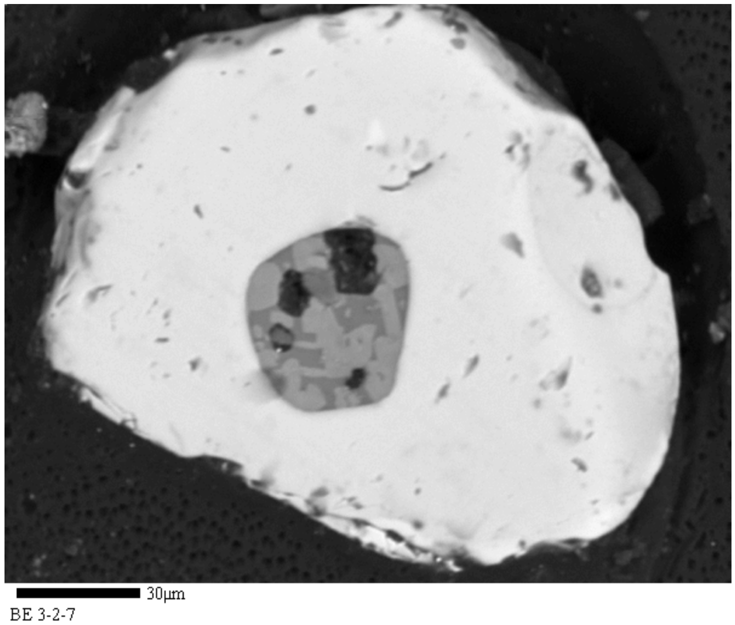

(a)

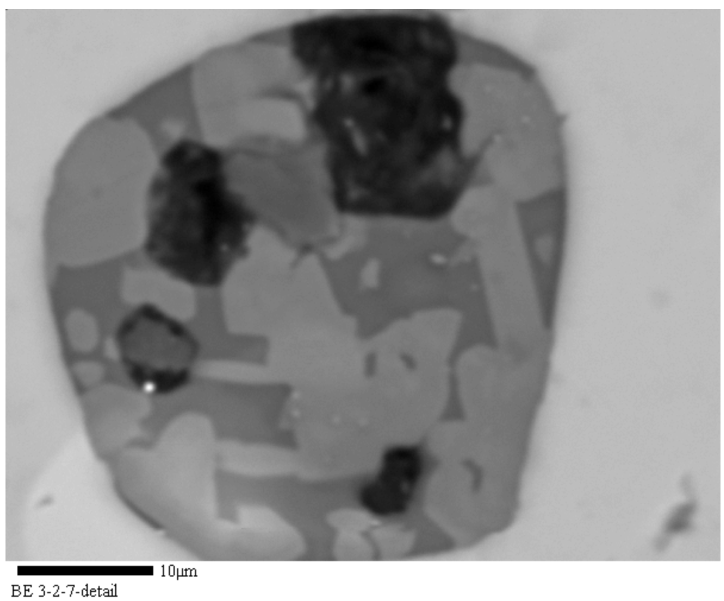

(b)

Figure 4.1 (a) Backscattered electron images of a crystallized melt inclusion (grey) in Cr spinels (white) from Tianba Flysch (Scale bar=30 μm);
(b) Enlarged melt inclusion consisting of pyroxene crystals (light grey), residual glass (dark grey), and minor sulfide droplet (bright spot).
The pyroxenes are compositionally zoned (Scale bar=10 μm).

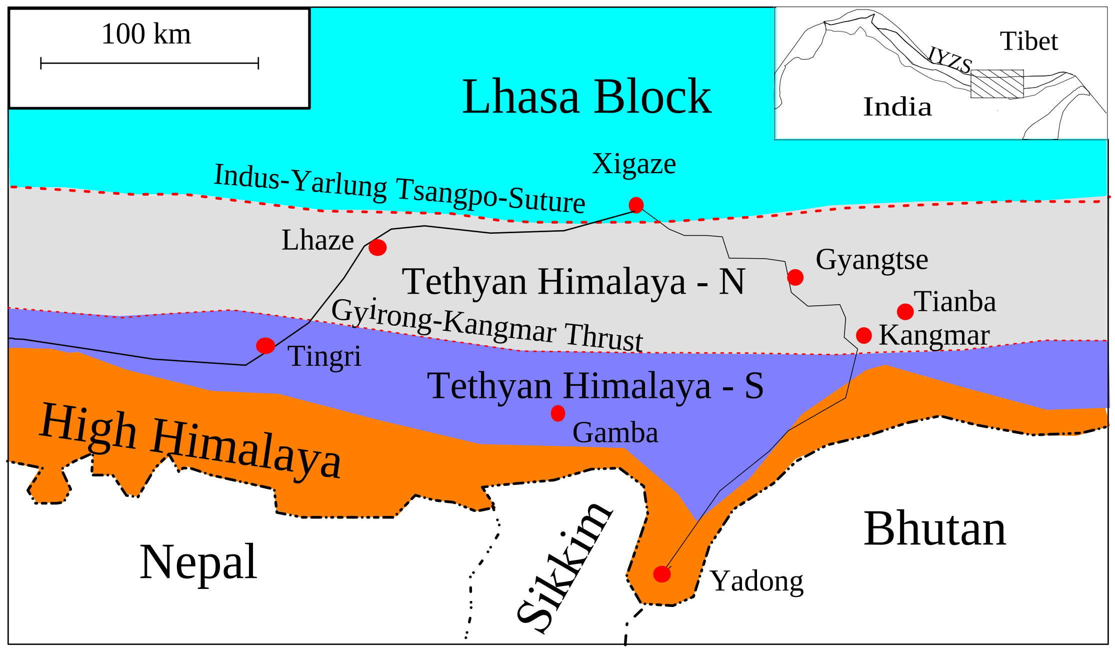

Figure 4.2 Simplified tectonic map of the study area (after Willems et al, 1996). The inset map shows the Tingri-Gyangtse area in the Himalayan system.

Ammonite, belemnite, and bivalve fossils are abundant in the lower part of the Cretaceous section of shales and thin-bedded limestones of a Valanginian-Aptian age (Wen et al., 1987; Xizang BGMR, 1992; Wang et al., 2000). The overlying cherts and siliceous shales indicate a pelagic setting (Willems et al., 1996).

The transition of those series to the overlying Tianba Flysch is conformable, with the contact marked at the base by an interval of mica-rich siltstone. Thick-bedded, massive sandstones dominate Tianba Flysch. Individual sandstone beds fine upwards into siltstones and shales, and contain abundant sedimentary structures including sole marks, horizontal laminations, small-scale cross bedding; these features indicate a turbidite depositional environment for the Tianba Flysch (Zhu et al., in preparation).

The top of the Tianba Flysch is characterized by an abrupt termination of the turbiditic sandstones that are conformably overlain by greenish-grey burrowed shales. These shales also contain a few thin sideritic sandstone beds and some large (up to 1 meter diameter) calcareous nodules in the interval ~60-70 m above the flysch, one of these nodules yielded an ammonite. Some belemnites are found in the shales above the flysch, and preliminary investigation of radiolaria fossils present in the sideritic sandstones indicates deposition sometime within the late Cretaceous (N. Shafique, personal communication, 2002). Therefore the Tianba Flysch was deposited during mid-late Cretaceous time in a deep-water setting of the outer Indian passive margin.

Samples preparation and analytical method

Thin-section examination and point-counting analyses show that significant amounts of opaque minerals are present in the upper sandstones of Tianba Flysch and in the sideritic sandstones (Zhu et al., in preparation). To obtain detailed information of the opaque minerals, these samples were crushed, separated in bromoform following the standard laboratory technique described by Mange and Maurer (1992). Individual grains were handpicked and mounted in epoxy resin, polished and examined under the optical microscope and electron microprobe.

Microprobe results show that Cr rich spinels constitute more than 50% of the heavy mineral population from the sideritic sandstones and about 5% of the spinel grains contain melt inclusions. To obtain the original composition of partially crystallized melt inclusions, high-temperature experiments on 400 spinel grains were performed with an atmospheric furnace in the Petrology Lab of University at Albany. The sample loader was suspended on a Fe-doped Pt-wire in the center of the furnace with a layer 2 mm thick of mantle olivine (~Fo92) powder to prevent any contaminations from the loader; the oxygen fugacity at the FMQ buffer was controlled by CO +CO_2 gas flow during heating. Following the studies of Roeder and Reynolds (1991), spinels were heated in two separate experiments at 1200°C and 1250°C for 96 hours to obtain equilibrium between spinel and melt, and homogenize the melt inclusions (Figure 4.3a-b, Figure 4.5). Each experiment was terminated by electrically cutting the Pt-wire causing the sample to fall into water, and thus the effective time of quenching was less than 1 sec. These spinels were also mounted in epoxy resin, polished and analysed by electron micrprobe. This procedure is similar to that described by Kamenetsky (1996), Sigurdsson et al. (2000), and Shimizu et al. (2001) except that we used 96 hours heating period, and CO+CO_2 mixture instead of 10 minutes and pure He.

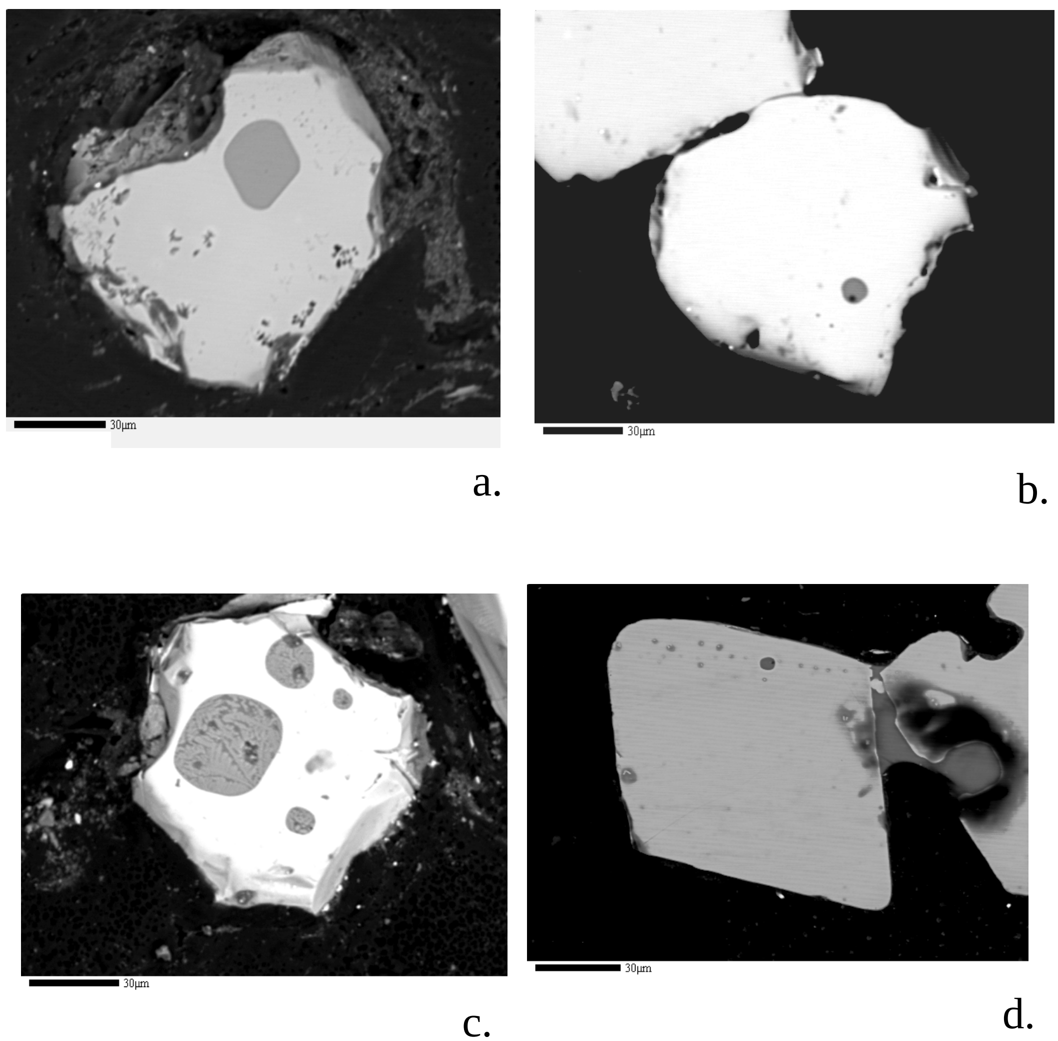

Figure 4.3 Backscattered electron image of melt inclusions (grey) in Cr spinels (white) from Tianba Flysch

(a) Homogenized melt inclusion heated 96 hours at 1250 C.
(b) Homogenized melt inclusion heated 96 hours at 1200 C.
(c) Melt inclusions are randomly distributed in Cr-rich spinel.
(d) Numerous melt inclusions form a band parallel with the outline of an euhedral Cr-rich spinel.
Scale bar=30 µm

All microprobe analyses were performed using a JEOL 733 Superprobe (fully automated, five Wavelength Dispersive Spectrometers) in the department of Earth and Environmental Sciences at Rensselaer Polytechnic Institute. Standard procedures (accelerating voltage 15 keV, a beam current 15 nA, and a beam diameter of 1 micron, using ZAF correction model) were used to analyze the spinels with natural minerals and glasses as standards. Melt inclusions were analyzed for the elements Si, Ti, Al, Ca, Fe, Mg, Mn, Na, K, and P; five x-ray spectrometers were tuned and calibrated for each element. Forty seconds counting time was used, with an accelerating voltage 15 keV, a beam current 15 nA. The VG-2 basaltic glass standard was analyzed at intervals throughout the probing session to ensure that calibration did not drift. Na_2O was analyzed first in order to minimize the possible effect of Na loss during analyses. Backgrounds were collected for each element on each analysis. Relative errors were generally less than 1% for major elements (Si, Fe, Al, Mg, Ca), and less than 5% for minor elements (Ti, Na, K, P).

Cr-rich spinel

The detrital spinels (Figure 4.1) are up to 0.2 mm in diameter with the majority-approximated 0.1 mm in size. They are dark brown to dark reddish-brown, a typical color for Cr-rich spinel (Ganssloser, 1999). Some grains are weakly translucent at the edges. Grain margins commonly show conchoidal fractures, suggesting mechanical breakage, but some grains are subhedral to euhedral.

The microprobe results indicate that the detrital Cr-rich spinels from Tianba Flysch can be characterized as a complex solid solution of the oxides of chromium, magnesium, aluminum, iron and titanium with 15-26 wt% Al_2O_3, 36-45 wt% Cr_2O_3, 10-12 wt% MgO, 20-30 wt% FeO_t, and 1.5-2.0 wt% TiO_2 (Zhu et al., in preparation). There is an obvious reciprocal relationship between Cr and Al, which may be indicative of different degrees of partial melting in the mantle (Dick and Bullen, 1984). MnO, NiO, V_2O_5, and ZnO are present in only trace amounts, generally less than 0.5 wt%. Spinel grains are generally homogeneous and show no obvious signs of zoning in line scans. This indicates that most of the parental lavas had undergone little or no magma mixing or significant crustal assimilation (Allan et al., 1988), that there was no extensive subsolidus re-equilibration between spinels and other silicate minerals (Scowen et al., 1991), and/or that no major metamorphism event occurred after the crystallization of these spinels. This also suggests that the Cr-rich spinels were not xenocrystals from another magma or residual mantle. In the spinel discriminant plots (Figure 4.4), the detrital spinels from Tianba Flysch consistently plot in the ocean island basalt field (Zhu et al., inpreparation), suggesting that there was a significant hotspot volcanic event in the source area for these arenites.

Melt inclusions

About 5% of the Cr-rich spinels contain melt inclusions. They are variable in size (10-40 um), showing negative crystal shapes. Some inclusion-bearing spinels contain numerous melt inclusions (Figure 4.3c), which are randomly distributed throughout the host spinel. However inclusion-rich bands along peripheral zones of the host mineral are

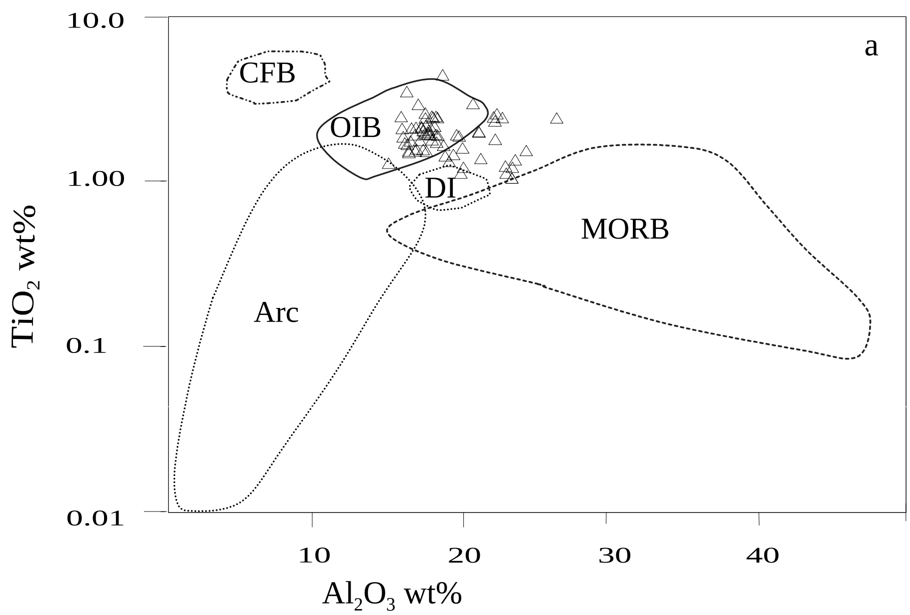

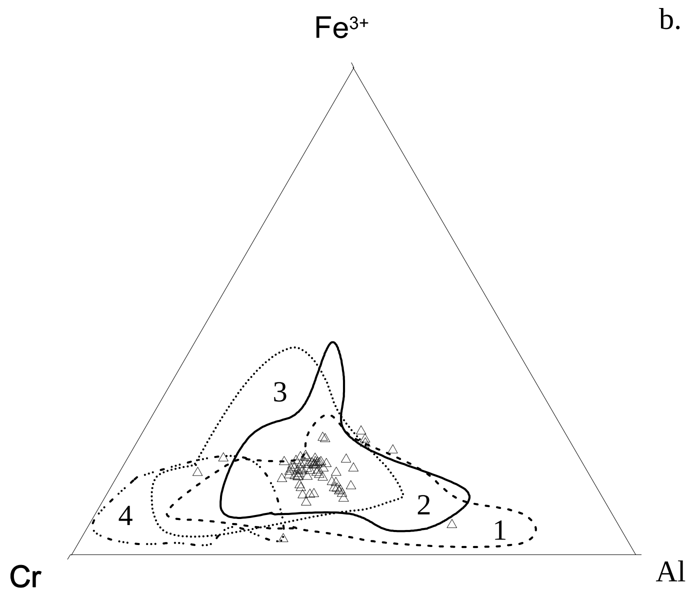

Figure 4.4 Major element contents of spinels and tectonic setting discriminant plots:
a.TiO_2 vs. Al_2O_3 after Kamenetsky et al[14]. Studies of Cr-rich spinel compositions from different tectonic settings show that TiO_2 and Al_2O_3 contents of spinel form a linear trend for those from Continental Flood Basalts (CFB), OIB, DI (Disko Island, W. Greenland), and MORB. Our data mostly plot in the middle of this trend, mainly in the OIB field.
b.Cr-Al-Fe^{3+} ternary plot. 95% of the detrital spinels plot in the 90th percentile contours of OIB field. Different fields are from Barnes and Roeder[33]: 1-MORB; 2-OIB; 3-Island Arc; 4-Boninites.

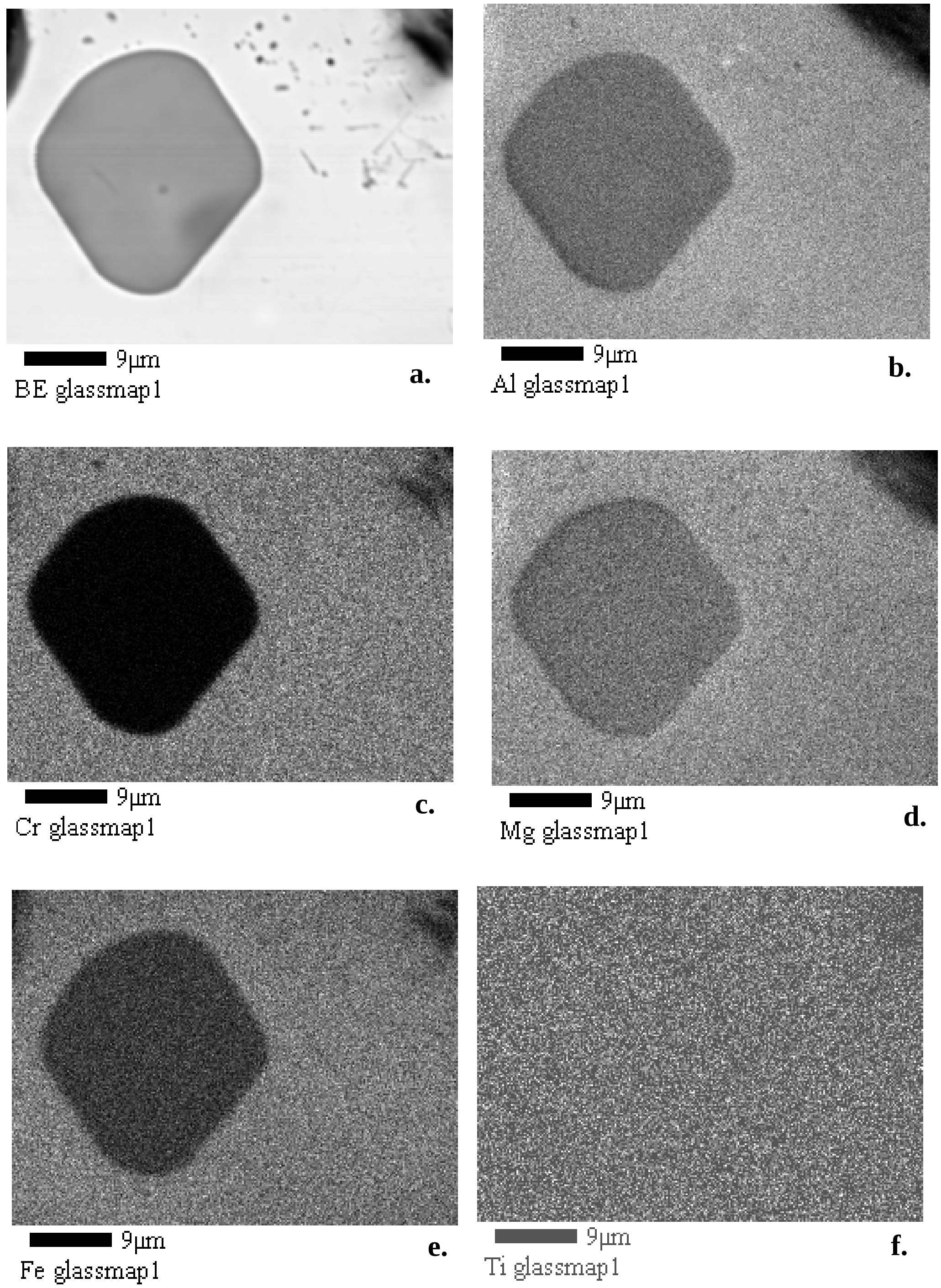

Figure 4.5 Elemental maps of a melt inclusion quenched from 1250C, showing the homogenised melt inclusion.
a. Backscatter image of the melt inclusion; **b**. X-ray image of Al distribution;
c. X-ray image of Cr distribution; **d.** X-ray image of Mg distribution;
e. X-ray image of Fe distribution; **f.** X-ray image of Ti distribution.

found in one euhedral Cr-rich spinel (Figure 4.3d). Most of the melt inclusions are subhedral to subround, and their crystal shapes align with the host spinel crystallographic direction. These features are common for melt inclusions trapped during the crystallization of the Cr-rich spinel (Roeder and Poustoveto, 2001). Two melt inclusions (40 μm) found are made up of pyroxene blebs (bright), residual glass (black), shrinkage vapor bubbles, and minor sulfide droplets (Figure 4.1b). The presence of well-crystallized clinopyroxene (Figure 4.1b) indicates that there was a relatively long cooling history after entrapment. Line scans on one spinel with a melt inclusion show that there is a significant compositional change of the spinel at the melt/spinel interface where Al_2O_3 increases from 18.04% to 29.17% while Cr_2O_3 decreases from 36.24% to 26.11%. This is good evidence that crystallization of Cr-rich spinel continued on the inclusion walls after entrapment of melt inclusions (Sigurdsson et al., 2000).

Representative major element compositions of the melt inclusions and host Cr-rich spinels are given in Table 4.1 and illustrated in Figure 4.6. For comparison, unheated melt inclusions were probed using broad beam analysis (a beam diameter of 10 microns). It appears that there is no clear correlation between the quench temperature and melt inclusion compositions except for Mg content. Higher temperature experiments (1250 C) yield higher MgO content (>8 %) than 1200°C experiments (<8 %). This may be indicative of higher Mg in melts at 1250°C equilibrium between melt inclusion and host spinel.

Table 4.1 Representative analyses of melt inclusions and host spinel from the Tianba Flysch

	unheat	unheat	unheat	unheat	unheat	1200	1200	1200	1200	1250	1250	1250	1250	1250	1250	1250	1250
Glass																	
SiO_2	52.25	49.39	52.05	46.69	47.86	46.14	46.71	45.91	45.19	44.17	51.87	42.75	46.18	44.16	47.96	45.51	41.5
MgO	11	8.34	6.74	6.18	6.28	6.12	4.66	7.72	5.89	8.89	12.46	10.94	10.77	8.75	10.24	10.68	9.79
FeO	4.01	10.67	10.39	9.35	9.71	5.43	9.06	12.22	5.69	12.06	9.24	11.31	13.1	11.91	10.16	12.18	13.55
CaO	14.21	12.9	10.91	12	11.74	13.93	11.55	11.85	13.84	11.89	9.01	12.38	12.33	11.68	16.67	13.1	11.66
Al_2O_3	11.03	13.85	14.56	14.86	14.79	15.76	15.38	13.31	15.18	13.86	13.53	15.19	12.38	13.65	10.19	15	11.54
Na_2O	0.78	0.45	0.55	2.96	2.17	3.27	3.24	2.37	4.07	2.33	0.46	2.22	2.34	2.12	0.21	2.72	2.26
TiO_2	1.85	1.54	1.5	1.79	1.79	4.02	2.12	1.78	3.98	3.19	1.88	1.68	1.78	3.08	1.71	1.93	1.82
MnO	0.09	0.16	0.21	0.16	0.14	0.11	0.13	0.18	0.1	0.22	0.2	0.18	0.22	0.21	0.13	0.14	0.22
K_2O	0.82	0.5	0.29	0.93	0.84	0.76	1.64	0.66	0.73	1.14	0.14	0.6	0.67	1.21	0.09	0.56	0.7
P_2O_5	0.44	0.31	0.36	0.34	0.36	0.51	0.24	0.26	0.52	0.62	0.08	0.2	0.24	0.7	0.23	0.2	0.34
Cr_2O_3	0.67	0.64	1.22	1.03	1.01	1.06	1.4	1.27	1.02	0.87	1.06	1.22	1.6	0.9	0.91	1.4	1.31
Total	97.16	98.76	98.78	96.3	96.68	97.22	96.26	97.54	96.22	99.23	99.95	98.67	101.59	98.37	98.71	103.41	94.7
CaO/Al_2O_3	1.29	0.93	0.75	0.81	0.79	0.88	0.75	0.89	0.91	0.86	0.67	0.82	1	0.86	1.64	0.87	1.01
Na_2O+K_2O	1.6	0.95	0.84	3.88	3.01	4.03	4.88	3.04	4.8	3.47	0.6	2.82	3.01	3.33	1.28	3.28	2.96
Spinel																	
Al_2O_3	21.17	17.31	17.33	17.77	17.77	18.5	18.38	16.86	16.04	21.7	17.53	16.85	18.17	22.37	16.84	17.68	21.2
TiO_2	1.93	2.75	1.38	1.9	1.74	2.75	1.71	2.06	2.72	2.56	1.62	1.66	1.64	2.53	1.57	1.96	1.62
MgO	11.17	12.48	12.48	9.53	10.39	12.12	10.65	10.72	9.57	12.57	13.52	12.97	12.48	13.51	12.85	12.56	12.74
MnO	0.27	0.24	0.28	0.29	0.21	0.2	0.32	0.25	0.27	0.25	0.21	0.2	0.26	0.29	0.24	0.27	0.29
FeO	16.62	15.69	14.09	17.72	16.95	16.2	17.26	16.73	19.15	15.49	13	13.38	14.55	14.49	13.73	14.4	14.61
Fe_2O_3	10.99	10.3	12.57	13.09	13.96	9.08	10.42	13.21	8.8	12.97	11.55	12.02	11.85	11.47	15.7	11.5	11.66
NiO	0.25	0.16	0.19	0.15	0.12	0.05	0.24	0.18	0.12	0.27	0.14	0.18	0.17	0.21	0.18	0.24	0.23
V_2O_5	0.12	0.38	0.32	0.19	0.19	n.a.	0.26	0.19	n.a.	0.2	0.22	0.19	0.37	na	n.a.	0.22	0.32
Cr_2O_3	36.35	41.14	41.25	36.26	37.38	40.68	40.86	38.98	41.93	34.15	42.07	41.61	40.43	35.41	39.89	40.77	37.58
Total	98.86	100.45	99.89	96.91	98.7	99.59	100.1	99.19	98.6	100.15	99.87	99.05	99.93	100.28	100.99	99.61	100.25
Fe3+/Fe	0.35	0.35	0.42	0.37	0.4	0.3	0.33	0.39	0.26	0.4	0.42	0.42	0.4	0.39	0.47	0.39	0.39
Mg/(Mg+Fe2+)	0.49	0.53	0.54	0.43	0.46	0.52	0.47	0.47	0.43	0.52	0.58	0.57	0.54	0.39	0.54	0.54	0.54
Cr/(Cr+Al)	0.54	0.61	0.61	0.58	0.59	0.6	0.6	0.61	0.64	0.51	0.62	0.62	0.6	0.56	0.61	0.61	0.54

Note: The ferric iron content of each analysis was determined by assuming stoichiometry.

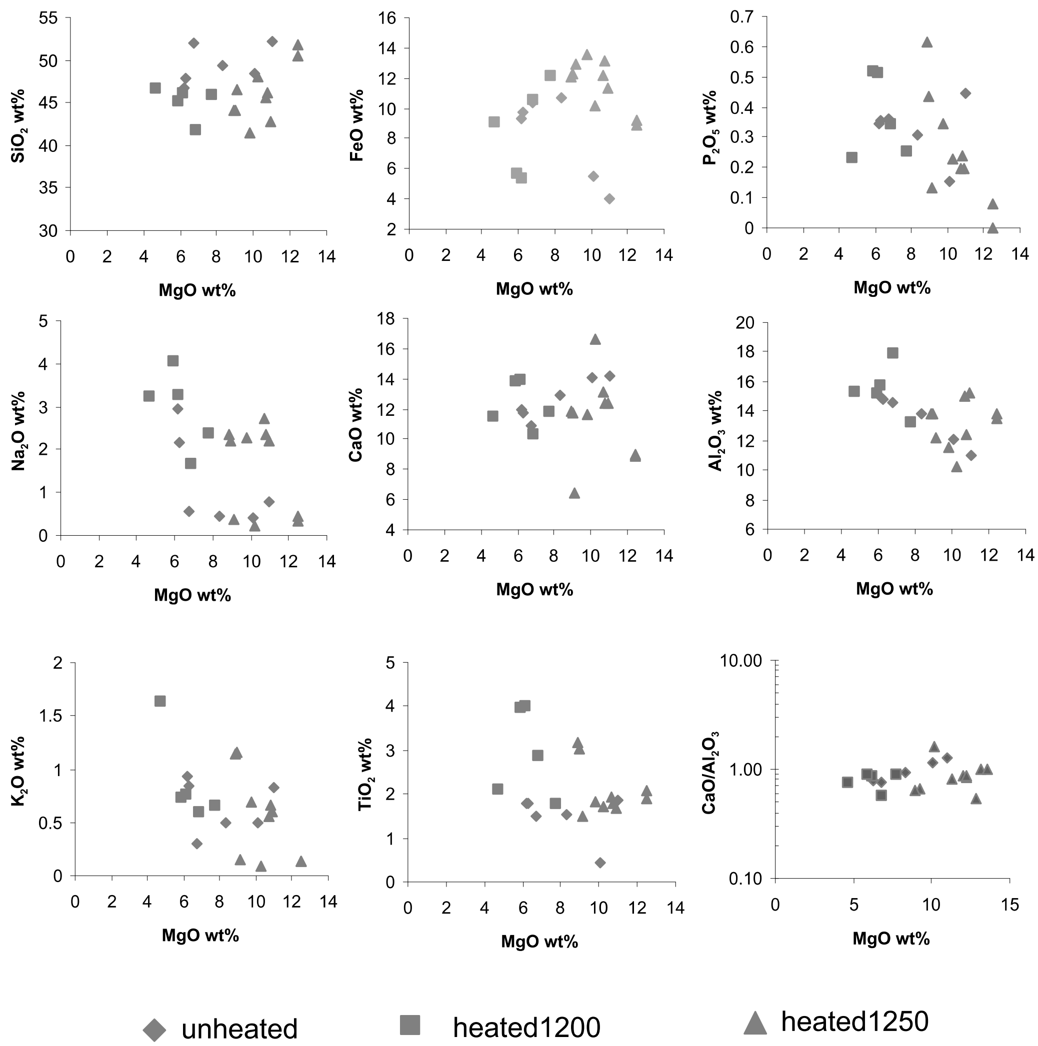

Figure 4.6 Major-element compositions of melt inclusions in the detrital spinels from Tianba Flysch. Note K_2O, TiO_2, Al_2O_3, P_2O_5, and Na_2O are increasing with dereasing MgO, showing relative enrichment of incompatible elements consistent with the crystallization of olivine and spinel.

Compositions of melt inclusions (Table 4.1) are: 42-53 wt% SiO_2, 1.5-3.9 wt% TiO_2, 11.5-15.8 wt% Al_2O_3, 4.66- 12.46 wt% MgO, 9.01-16.67 wt% CaO, 0.45-4.07 wt% Na_2O, 0.3-1.1 wt% K_2O, and 0.7-1.0 CaO / Al_2O_3. The Na_2O content in five analyses (Table 4.1) is lower than 1%. This is a common problem due to sodium loss from glass through heating by the electron beam. We repeated some glass analyses using lower current and defocused beam (for size>20um), but obtained similar values in three probe sessions. Another possible reason for Na loss is the small size of the probed melt inclusions (most are less than 20 um). Therefore we consider the sodium content we obtained for these five analyses may not be real, and the rest analyses suggest that the parental magma is most likely alkali rich, which is consistent with relatively enrichment of incompatible elements (Ti, P, K) in the glass analyses (Table 4.1). The alkali-silica diagram (Figure 4.7) shows that these melt inclusions (excluding the five analyses of lower Na content) were from alkali basalt and tholeiitic basalt.

The Cr_2O_3 content in melt inclusions (0.6-1.2 %) is significantly higher than that in typical basalts (Roeder and Reynolds, 1991). Since no Cr-rich minerals were found in the partially crystallized melt inclusions from our samples, we think the high Cr_2O_3 content in these melt inclusions is not real. We follow Sigurdsson et al. (2000) and Roeder & Reynolds (1991) in attributing this to secondary fluorescence that interferes with analyses of low-Cr content melt inclusions hosted in Cr-rich spinels.

In a plot of major element compositions (Figure 4.6), there is a negative correlation between the incompatible elements Ti, Na, K, and P and Mg, which may suggest that there was a relative enrichment of these elements due to crystallization of olivine and spinel in the magma. The relatively constant CaO content with MgO implies

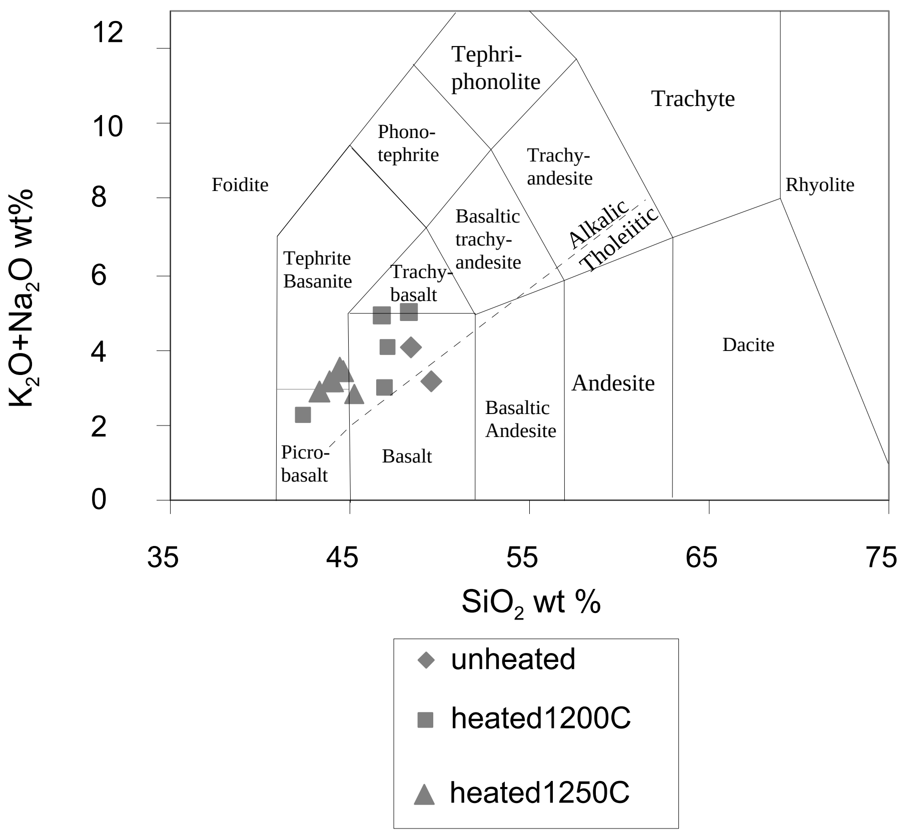

Figure 4.7 Total alkalis vs silica plot after Le Bas et al. [34]. The Macdonald-Katsura line that divides the tholeiitic series from the alkalic series is from Macdonald and Katsura[35]. In our glass data, there are 13 analyses with Na_2O content >1 wt%, and only one plots in the tholeiitic area, hence the parental magma of these melt inclusions must be alkali basalt.

that there was no significant clinopyroxene or plagioclase crystallization in the parental magma, and the well-crystallized clinopyroxene found in some melt inclusions (Figure 4.1) must have formed after entrapment in spinel, rather than being trapped together with the melt. There are significantly different contents in the major oxides of probed pyroxenes in one melt inclusion as expected from closed-system crystallization, which also suggest that the pyroxenes are true daughter crystals of the melt inclusion.

Due to possible diffusion of Fe and Mg between olivine and spinel, Mg-number ($Mg/(Mg+Fe^{2+})$) in trapped melt and spinel should be used with caution (Kamenetsky, 2001; Sigurdsson et al., 2000; Danyushevsky et al. 2001). However the abundances of Al and Ti cations in the melt inclusions and spinel would not change significantly during the crystallization of olivine because of their low contents, if any, in the olivine. Kamenetsky et al. (2001) observed that there are high positive correlations for TiO_2 and Al_2O_3 between melt inclusions and hosted spinel from a variety of magma types and tectonic environments (Figure 4.8). Our data are very close to or aligned with their best-fit lines. The relatively restricted range of the data and proximity to the OIB field suggest a single source for these Cr-rich spinels, and, in particular, shows that no spinel from arc complexes have contributed to the Tianba Flysch.

In the TiO_2-MnO-P_2O_5 plot (Mullen, 1983), 12 of our glass data (Na_2O >1 wt%) plot in or very close to the ocean-island alkalic basalt field (Figure 4.9). I have developed a discriminant plot based on compositions of 600 basalts from well-studied areas (Zhu et al. in preparation), and most of the melt inclusions (SiO2 40~55%, Na2O>1%) in spinel from Tianba Flysch plot in the hotspot basalt field (Figure 4.10). Therefore we conclude

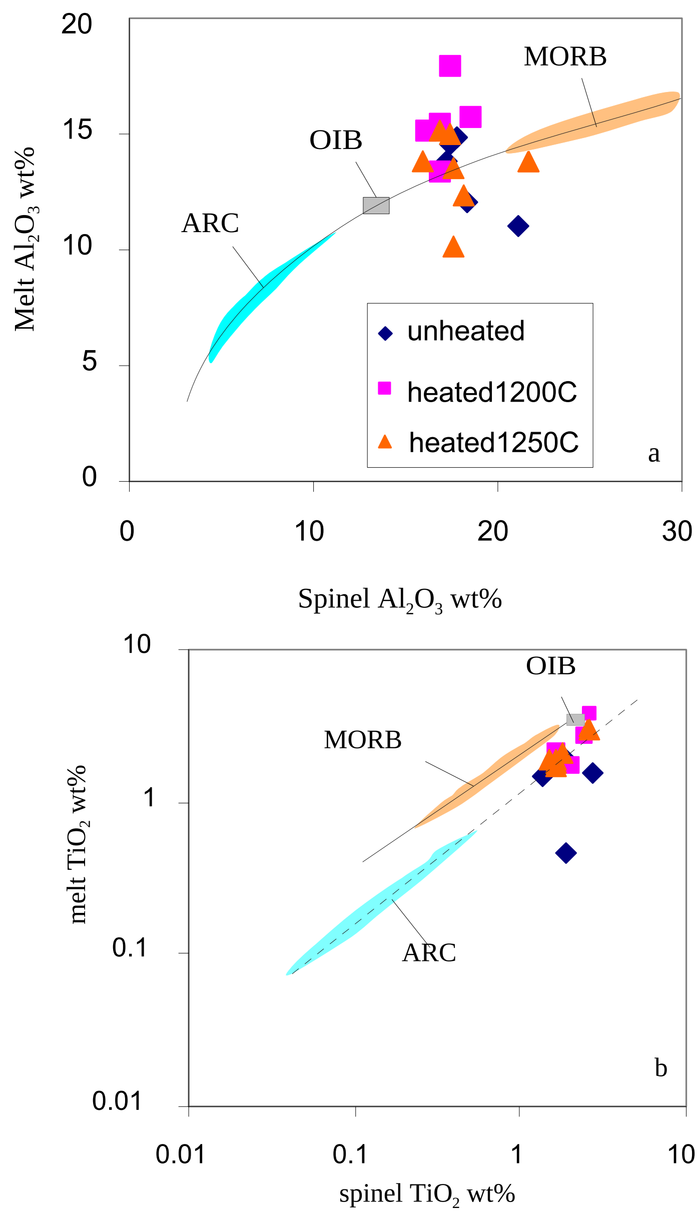

Figure 4.8 Positive correlation between Al_2O_3 and TiO_2 contents in melt inclusions and hosted spinels (the best fit lines and fields are from Kamenetsky et al., 2000). Continuous line in **a**. is a power law best fit through published data; Continuous and dashed lines in **b**. are best fit through the high-Al (Al_2O_3 in melt >14 wt%) and low Al (Al_2O_3 in melt<14 wt%) data, respectively. Our data are either close to, or aligned with their best fit lines. The relatively narrow range of our data and proximity to the OIB point suggest a single tectonic provenance for these detrital spinels.

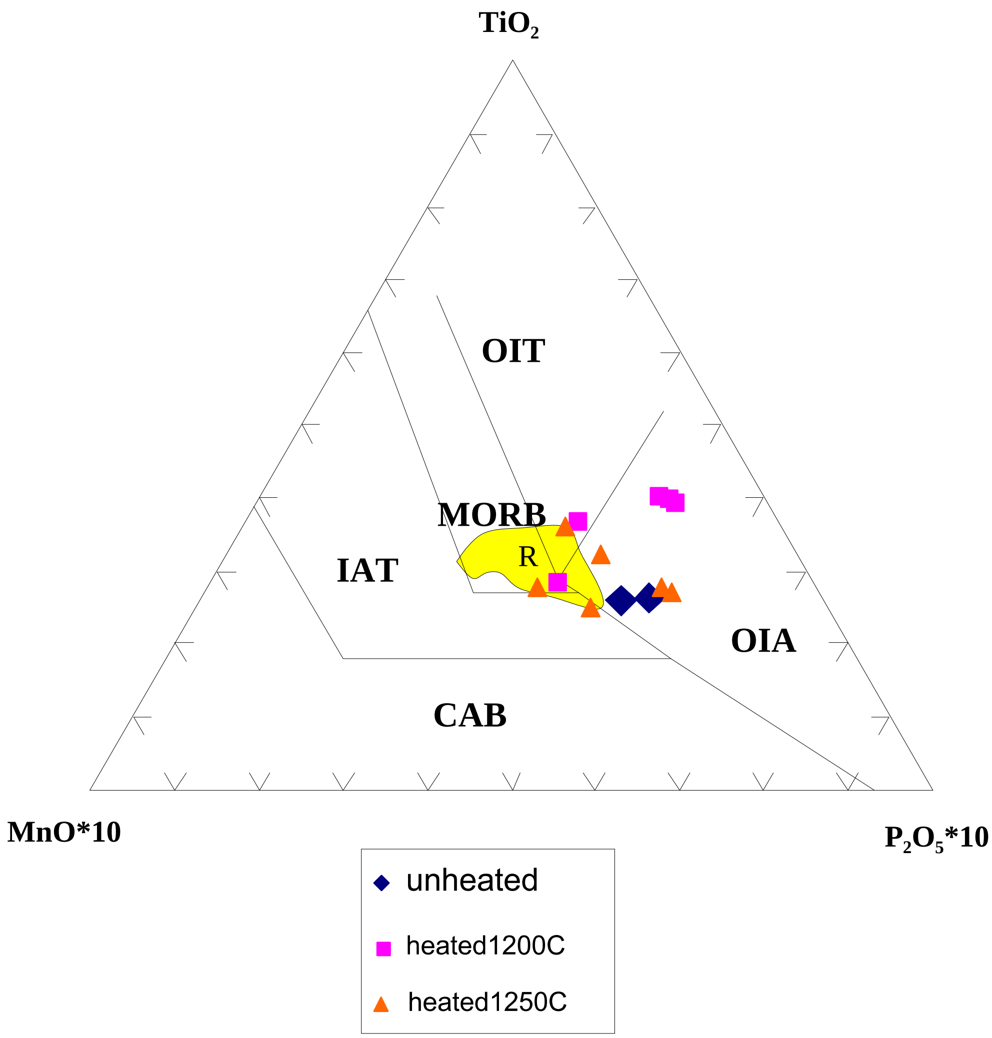

Figure 4.9 TiO_2-MnO-P_2O_5 plot (after Mullen, 1983). CAB: Calc-Alkaline basalts; IAT: Island Arc Tholeiites; OIA: Ocean Island Alkali basalt or Seamount Alkali Basalt; OIT: Ocean Island Tholeiites. 13 of data (Na_2O>1 wt%) plot in, or very close to, the OIA field. Therefore the melt of the spinel melt inclusions was most like oceanic island basalt. R represents the field of Rajmahal Traps (data from Storey et al., 1992).

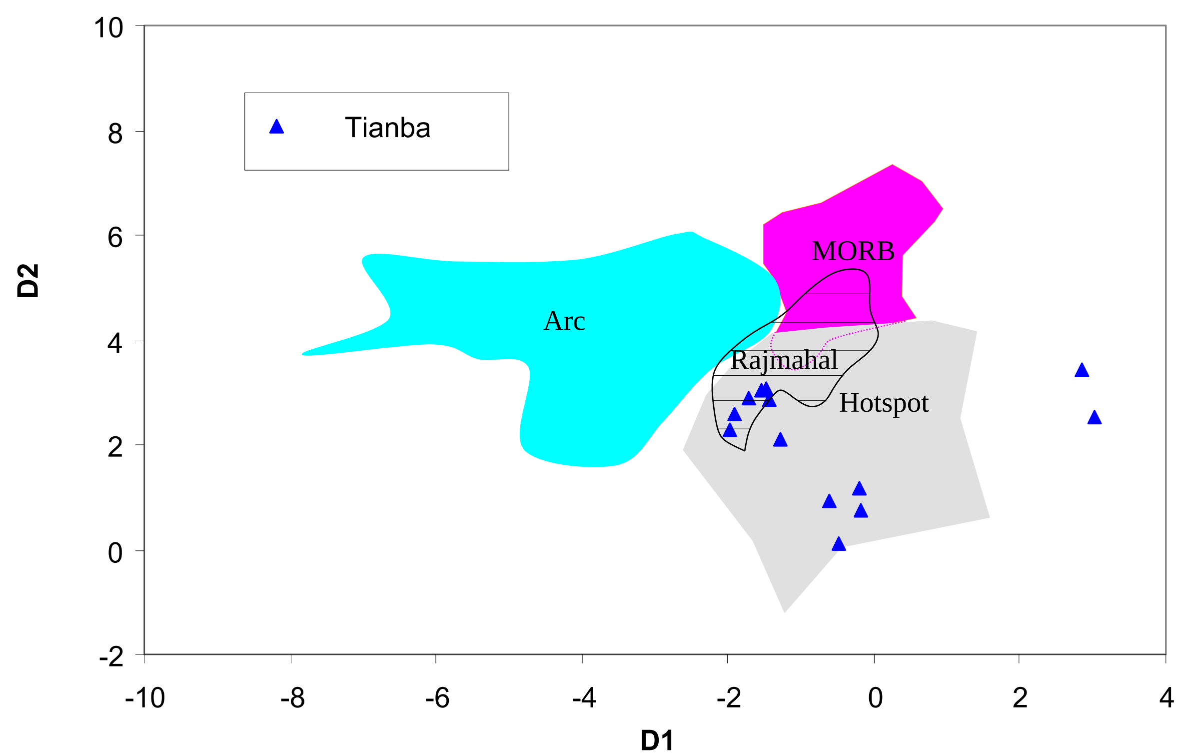

Figure 4.10 Discriminant function plot of basalt from three tectonic settings. The compositions of basalt (SiO_2:40-55 wt%) from Izu Island Arc (50), Andean Arc(50), Mariania Arc (50), Honshu Arc(50), MORB(200), Hawaii(50), Iceland(50), Kerguelen Island (50), and Canary Island (50) are used to develop this plot using linear discriminant function(lda) in Splus [29]. 11 of 13 melt inclusions in Tianba Flysch plot in Hotspot basalt field, and no points plot in arc field. Rajmahal data from Kent et al.,1997; Storey et al., 1992.

$D1=2.02*\log(SiO_2/TiO_2)-2.15*\log(Al_2O_3/TiO_2)-3.14*\log(FeO/TiO_2)+0.82*\log(CaO/TiO_2)+0.41*\log(MgO/TiO_2)$
$-1.07*\log(K_2O/TiO_2)-0.37*\log(Na_2O/TiO_2)+0.53*\log(P_2O_5/TiO_2)$

$D2=1.69*\log(SiO_2/TiO_2)-2.88*\log(Al_2O_3/TiO_2)-0.09*\log(FeO/TiO_2)+0.85*\log(CaO/TiO_2)-0.49*\log(MgO/TiO_2)$
$-1.15*\log(K_2O/TiO_2)+3.48*\log(Na_2O/TiO_2)-0.17*\log(P_2O_5/TiO_2)$

that the parental melt of the spinel melt inclusions was most like oceanic island basalt, consistent with the Cr-rich spinel compositions (Figure 4.4).

Discussion

Heating time of homogenization experiment

A key question in this study is whether the re-homogenized melt inclusions represent the composition of the parental magma. Most workers heat glass-bearing spinel for only 10 to 30 minutes because of suspicions that there may be some re-equilibration between the melt inclusions and spinel, and/or in situ crystallization of spinel, during longer heating interval (Kamenetsky, 1996; Sigurdsson et al. 2000; Shimizu et al, 2001).

Danyushevsky et al. (2002) argued that during homogenization experiments the phenocrysts may control the compositions of melt inclusions due to their dominant size, and that the composition of a melt is a function of the physical conditions of the experiment and the phenocryst composition when chemical equilibrium is established. In contrast, during crystallization in natural magma systems, the melt composition controls the composition of crystallizing phases, that is, the composition of a phenocryst is a function of the physical conditions and melt composition. Therefore they suggested that "melt inclusions should be kept at high temperatures for a minimum possible time during an experiment". However, no one knows with certainty the history of melt inclusions trapped in spinels before eruption and quenching. It is reasonable to assume that there was equilibrium between melt inclusions and host spinel in the parental magma before eruption, and that there were a few days between eruption and entrapment of melt inclusions in Cr-rich spinel because the crystallization of Cr-rich spinel in basaltic melt is very slow (Roeder and Poustovetov, 2001). This assumption is consistent with the presence of euhedral crystals and the absence of zoning in the Cr-rich spinel grains (Figure 4.1). Also, Cr solubility in melt is very low, about 0.05% at 1200 °C and 0.08% at 1250 °C for FMQ oxygen fugacity buffer; Cr-rich spinel that contains 30-40 wt % Cr_2O_3 can be in equilibrium with a melt containing 0.02-0.06 wt % Cr_2O_3 (Roeder and Reynolds, 1991), so there should be no significant composition change of melt inclusions during heating experiments. Therefore we consider it is a better approach to recover the original melt composition in our experiments, and that is why we chose to heat glass-bearing spinels in a FMQ buffered furnace for four days.

Source of the volcanic clastics for Tianba Flysch

The presence of Cr-rich spinels in sedimentary rocks of a basin within and/or adjacent to an orogenic belt is generally interpreted as an indicator of derivation from the peridotites of an ophiolite (Ganssloser, 1999; Pober et al., 1988; Cookenboo et al., 1997). Hence the presence of significant mafic volcanic detritus and uncharacterized chrome-rich spinels in the Tianba Flysch might suggest ophiolite derivation and a Cretaceous ophiolite obduction event on the northern Indian continental margin. However, in this scenario, it would generally be expected that a wide variation in the chemical compositions of spinel from arc complexes would be found, because Cr-spinel from obducted ophiolite and associated subduction/accretionary materials of arc complexes is likely to be of diverse origins. Additionally the TiO_2 contents in arc spinels are generally below 1%. Our detrital spinels have a limited range of chemical compositions, and most of them have TiO_2 content around 2%, and they consistently plot in the discriminant fields of ocean island (hotspot) basalts (Figure 4.4). As such, no significant contribution of spinels from an arc-trench system to the Tianba Flysch has been detected.

Clastic wedges correlative to the Tianba Flysch were deposited all along the region which became the Himalayas, from the Trans-Indus Salt Range, where they overlie glaucontic ironstone intervals, to the Malla Johar and Thakkhola regions, where two >400-m-thick lithic wacke sections accumulated during a large part of the Early Cretaceous (Sinha, 1988; Gibling et al., 1994). The geochemical composition of a basaltic pebble fragment found in the Valanginian to Aptian volcaniclastic sandstones in the Thakkhola region (Durr and Gibling, 1994) indicates a source of alkali basalts having within-plate affinity. All basins of the East India coast are characterized by Hauterivian to Aptian sandstones, pointing to rejuvenation of the craton ascribed to lithospheric doming (Garzanti, 1993). A large flood-basalt event (Figure 4.11), linked to the activity of the Kerguelen mantle plume, took place at 117 Ma (Baksi, 1995; Kent, 1997), as recorded in the Rajmahal-Sylhet-Bengal Trap Province of northeast India (Kent, 1991, Garzanti, 1993). This provided volcanic clastics to Cretaceous turbiditic sandstones along the north Indian passive margin, now locally preserved in the Tethyan Himalaya sedimentary sections.

Conclusion

There are significant amounts of Cr-rich spinels derived from volcanic rocks in turbiditic sandstones from the upper part of Mid-Cretaceous Tianba Flysch in the

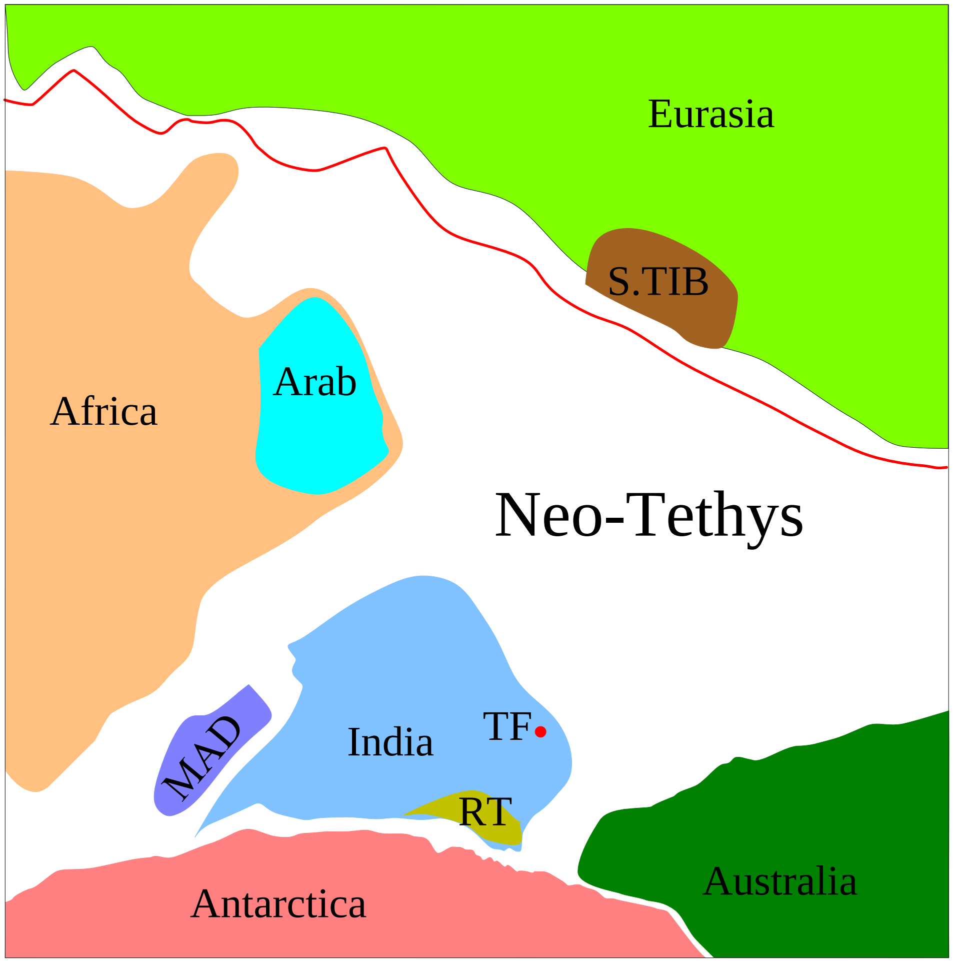

Figure 4.11 Reconstruction map at about 117 Ma (modified after Besse and Courtillot, 1988). MAD, Madagascar block; S.TIB, southern Tibet; RT, Rajmahal Traps; TF, Tianba Flysch. The red line is the major subduction zone.

northern Nieru Valley, southern Tibet. Microprobe results indicate compositions of detrital spinel are similar to those of spinel inclusions in olivine from hotspot basalt. About 5% of the spinels contain melt inclusions of 5-60 μm in diameter. The compositions of melt inclusions correlate well with those of host spinels, and both indicate a possible co-crystallization of olivine and spinel in the parental magma. These results, combined with palaeo-tectonic reconstruction, for the time given by the mid-late Cretaceous fossils in the strata, suggest that volcanics of the Rajmahal, which are associated spatially and temporally with Kerguelen hotspot activity on India about 117 Ma ago, were the source for these Cr-rich spinels. The geochemical data of spinels and their melt inclusions in the Tianba Flysch do not support derivation from ophiolite or a contemporaneous volcanic arc.

Chapter 5. Geochemistry and provenance of the Tianba Flysch, southern Tibet

Introduction

Studies on the composition of sedimentary rocks have significantly improved our understanding of the tectonic history of the earth (Taylor and McLennan, 1985; Dickinson, 1988, and references therein). Tectonic environment has been advocated as the primary control on sedimentary composition, which is supported by the fact that modern sands of known tectonic settings have been shown to have a systematic variation of composition as a function of provenance type (Dickinson and Valloni, 1980; Valloni and Mezzadri, 1984; McLennan et al., 1990). The considerable increase in the precision and rapidity of whole rock major-, and trace- element analysis with the development of automated analytical equipment has produced abundant chemical data for sedimentary rocks derived from well-known tectonic settings, which have been used to developed a series of geochemical discriminant diagrams (Bhatia, 1983, 1985; Bhatia and Crook, 1986; Roser and Korsch, 1986, 1988; Floyd et al., 1991; McLennan et al., 1990, 1993).

Geochemical analyses (Table 5.1) of the shales (N=5) and sandstones (N=6) from the Tianba section was done at the GeoAnalytical Laboratory of Washington State University using X-ray fluorescence (XRF) and inductively coupled plasma mass spectrometry (ICP-MS) techniques. Detailed analytical methods are given in Johnson et al. (1999) and Knaack et al. (1994), respectively. The precision was assessed through repeat analyses of samples: errors for major elements vary between 1 and 2% of the amount present, and accuracy of the trace elements and REE analyses is

Table 5.1 Geochemical data of the Tianba Flysch, southern Tibet

	TB-1 shale	TB-4 shale	TB-8 shale	TB-10 shale	TB-11 shale	TB-5 sand	TB-6 sand	TB-7 sand	TB-14 sand	TB-13 sand
SiO2	69.41	64.41	69.67	52.33	59.11	30.50	83.34	85.72	60.21	91.19
Al2O3	13.52	18.51	15.71	27.25	23.71	7.85	6.93	6.22	18.88	4.21
TiO2	0.93	0.92	0.85	1.20	1.15	1.19	0.78	0.77	1.32	0.52
FeO*	7.60	7.56	5.46	8.69	6.73	9.46	4.96	3.36	12.55	2.07
MnO	0.03	0.02	0.03	0.05	0.05	1.61	0.03	0.02	0.05	0.01
CaO	1.53	0.58	0.55	0.86	0.63	45.04	0.26	0.85	0.58	0.25
MgO	3.37	2.77	1.97	1.66	1.55	2.57	1.76	1.09	1.93	0.36
K2O	2.15	4.73	5.25	7.27	6.39	0.60	0.26	1.04	3.21	0.73
Na2O	1.13	0.17	0.18	0.16	0.23	0.72	1.50	0.72	0.81	0.46
P2O5	0.17	0.09	0.11	0.21	0.16	0.28	0.08	0.08	0.22	0.05
LOI (%)	6.32	6.70	5.75	9.01	7.57	27.55	1.90	2.68	5.56	1.43
total	99.84	99.77	99.78	99.68	99.71	99.82	99.91	99.87	99.76	99.86
Ni	48	84	29	60	52	197	25	22	85	12
Cr	80	107	80	176	136	320	59	61	94	52
Sc	23	24	17	34	28	0	16	13	32	5
V	129	178	98	295	208	139	82	78	158	25
Ba	487	921	943	1410	1349	372	186	541	1001	425
Rb	76	182	209	238	223	18	10	30	145	26
Sr	88	64	69	132	111	369	56	49	113	25
Zr	174	145	284	174	231	98	249	337	197	612
Nb	21.7	19.9	20.8	31.4	28.7	20.4	12.2	13.7	28.2	10.3
Ga	18	26	20	35	32	12	9	9	25	3
Cu	131	140	54	56	51	40	11	11	44	14
Zn	108	172	83	163	131	66	45	39	125	24
Pb	20	38	28	51	37	4	14	11	32	12
Th	16	19	19	37	27	3	10	13	21	18
La	40.06	49.49	53.30	83.77	70.80	20.74	23.38	29.00	55.24	30.78
Ce	87.25	121.12	126.56	188.94	154.01	43.84	47.54	56.94	166.00	58.58
Pr	8.19	9.97	11.57	18.61	14.97	4.27	4.98	6.07	11.68	6.03
Nd	31.10	38.32	44.40	70.97	56.40	18.45	19.49	23.38	45.84	22.29
Sm	6.51	8.38	9.76	15.47	11.89	4.66	4.18	4.89	10.10	4.24
Eu	1.56	1.78	1.86	3.28	2.40	1.68	0.91	0.99	2.27	0.61
Gd	5.51	7.13	7.85	12.62	9.73	5.27	3.55	4.03	8.89	3.30
Tb	0.86	1.14	1.23	2.02	1.55	0.84	0.55	0.63	1.40	0.49
Dy	5.07	6.43	6.95	11.23	8.91	5.03	3.12	3.56	7.81	2.87
Ho	1.01	1.28	1.36	2.10	1.76	1.02	0.61	0.70	1.52	0.58
Er	2.67	3.37	3.52	5.30	4.56	2.54	1.53	1.85	3.89	1.64
Tm	0.39	0.49	0.52	0.76	0.66	0.35	0.23	0.27	0.54	0.25
Yb	2.36	3.03	3.25	4.55	4.01	2.00	1.45	1.65	3.17	1.64
Lu	0.36	0.47	0.50	0.68	0.62	0.30	0.22	0.26	0.48	0.28
Y	27.13	32.50	33.46	47.50	42.15	31.11	15.17	18.13	38.64	16.09
Eu*	23.10	29.78	33.94	54.10	41.64	18.70	14.85	17.17	36.39	14.57
Eu/Eu*	0.77	0.69	0.63	0.70	0.66	1.03	0.70	0.66	0.72	0.48

Note: total iron expressed as FeO.

within 5%. All data discussed in this paper have been recalculated to 100% on a volatile-free basis.

Major elements

The influence of weathering processes on compositions of sedimentary rocks can be evaluated in terms of the molecular percentage of the four major oxides (Nesbitt and Young, 1982, 1984), which is commonly calculated as the chemical index of alteration ($CIA=100*Al_2O_3/(Al_2O_3+CaO^*+K_2O+Na_2O)$, where CaO^* is the amount of CaO in silicate minerals only). The CIA gives a measure of the degree of alteration of feldspars to clay minerals during weathering because feldspar makes up > 50% of the upper crust (Taylor and McLennan, 1985). In general, fresh igneous rocks or unweathered upper crust have CIA values of about 50, whereas extremely weathered rocks have values of near 100 (Figure 5.1). Shales or mudstones commonly show higher CIA values than do the associated sandstones, which reflects more severe weathering histories for the shales/muds (McLennan et al., 1990). The shales in the Tianba Flysch have moderate to high CIA values between 69 and 76 with an average of 74, which is in the range of typical shales that average about 70 to 75 (McLennan et al., 1993). Sandstones have relatively lower values than shales, with a range between 64 and 72. It is interesting to note that four samples (TB7, TB13, TB 1, and TB14) define a linear trend in the ternary diagram Al_2O_3-($CaO+Na_2O$)-K_2O, parallel to the Al_2O_3-($CaO+Na_2O$) join, which would be expected if the trend was caused solely by weathering (Nesbitt and Young, 1982). Four shales (TB4, TB8, TB10, TB11) plot slightly below this trend, towards the K_2O

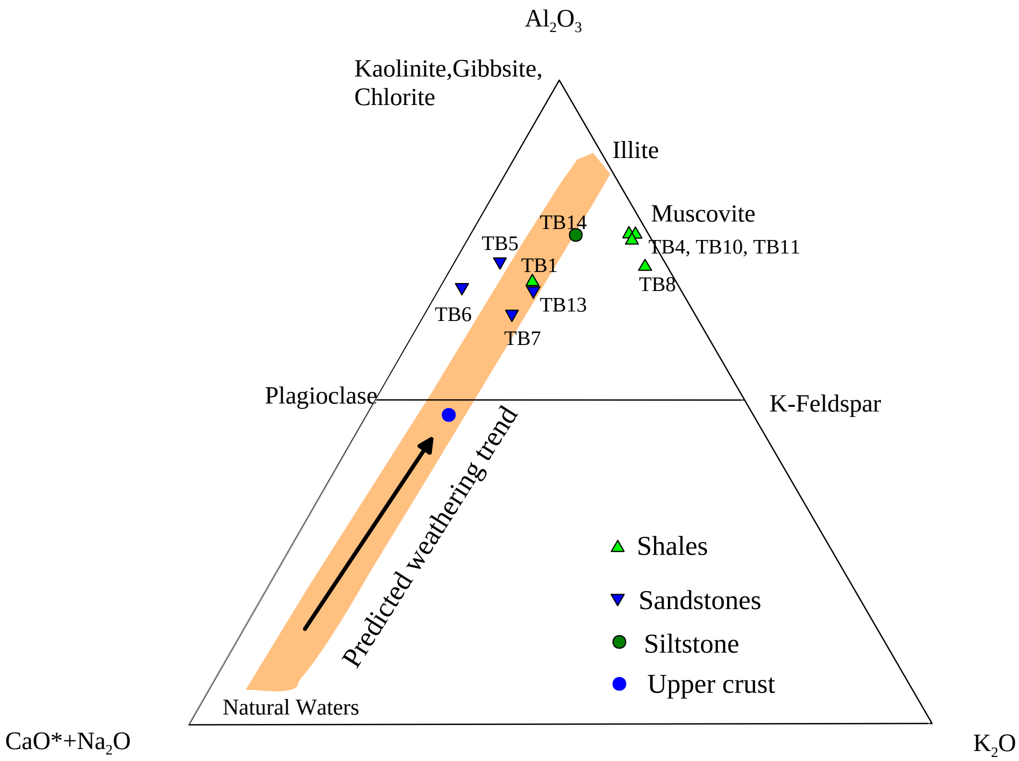

Figure 5.1 CIA ternary plot of the Tianba Flysch. Modified after Bock et al. (1998). The enrichment in Al_2O_3 and depletion of CaO+Na_2O+K_2O reflect the degree of chemical weathering to which the materials have been subjected. Four analyses (TB1, TB7, TB13, TB14) defined a linear trend encompassed in the predicted weathering trend for the average upper crustal composition. Four shales do not follow the predicted weathering trend, indicating processes in addition to the weathering have affected these sediments. TB6 and TB5 plot close to the Al_2O_3-CaO+Na_2O join, which may indicate a signficant volcanic input.

apex. A possible explanation may be the loss of Al_2O_3 or the addition of K_2O during diagenesis (Bock et al., 1998). TB5 and TB6 do not follow a predicted weathering trend for the average upper crustal composition (Taylor and McLennan, 1985), indicating mixing of provenance components for them. This is consistent with the presence of significant amounts of volcanic rock fragments, and Cr-rich spinels in TB5 and TB6 (see chapter 3).

Detrital sediments from the Tianba Flysch define a linear trend on a SiO_2-Al_2O_3 graph (Figure 5.2), with shales containing < 70% SiO_2 and > 10% Al_2O_3, and sandstones (TB6, TB 7 and TB13) containing > 80 % SiO_2 and < 8% Al_2O_3. This trend appears to be typical of many other sedimentary rocks (Young et al. 1998; Condie et al., 2001), which suggests that there was a significant size fractionation of sands and shales during the deposition of the Tianba Flysch, and there was no significant difference in provenance for the shales and sandstones in the Tianba Flysch. In particular, SiO_2/Al_2O_3 values in the sandstones (TB6, TB7, and TB13) lie in the range of 12 to 22. Such values are more typical of modern passive margin tectonic settings (5.2-28.5) than active margins (<6.0) (Roser and Korsch, 1986; McLennan et al., 1990). The relatively high SiO_2 content and the highest SiO_2/Al_2O_3 ratio (~22) of the lowest sandstone (TB13) indicate mineralogical and textural maturity of the minerals making up the basal part of the Tianba Flysch. As expected, sample TB14 (siltstone) plots in the range of shales due to the high mica content, TB5 does not follow the overall linear trend because of abundant calcite in this sample. The K_2O/Na_2O ratios of TB5 and TB6 (0.83 and 0.18) are less than the rest of the samples in the Tianba Flysch (1.5-45.1). Considering that sands from volcanically active setting commonly have K_2O/Na_2O <1, whereas sands from passive margins exhibit

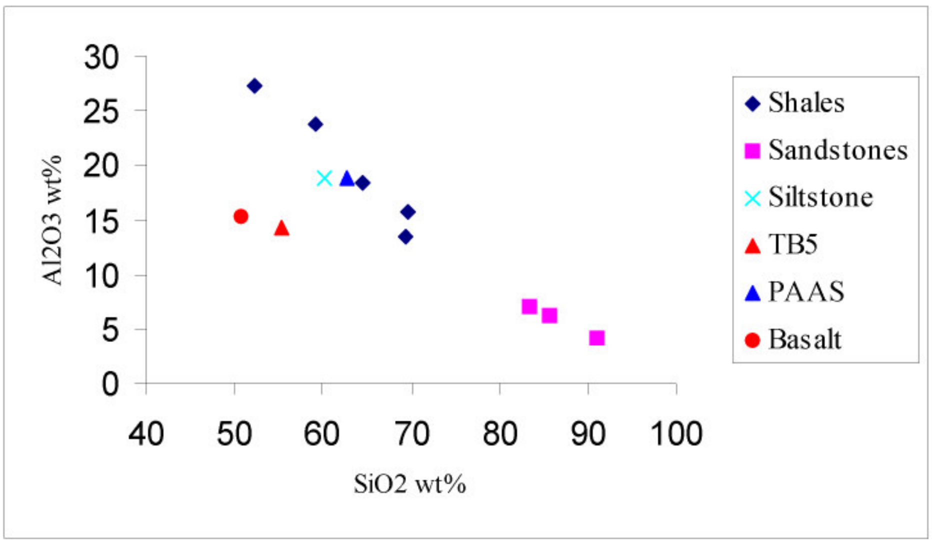

Figure 5.2 SiO_2-Al_2O_3 plot of the Tianba Flysch. TB5 (based on CaO and LOI-free recalculation) is not in the linear trend formed by the rest of analyses in Tianba Flysch.
PAAS from Taylor and McLennan (1985), average basalt composition from Condie (1993).

ratios > 1 (McLennan et al., 1990), it is concluded that there is a significant volcanogenic component for the top sandstones of the Tianba Flysch while the major part of the Tianba Flysch was deposited in an overall passive margin setting. The relative enrichments of Mg, Mn, Ni and V in TB5 and TB6 compared TB13 and TB7 also suggest that there was a mafic/ultramafic component in the source area (Bock et al., 1998; McLennan et al., 1990). This agrees with petrographic characteristics described above: well-sorted and subround-subangular quartz is the primary framework grain in TB 7 and TB13 whereas significant amounts of labile rock fragments and Cr-rich spinels are present in TB6 and TB5.

Although data are somewhat scattered, especially for shales, there is a suggestion of a linear relation between MgO and FeO_t in the Tianba Flysch (Figure 5.3). Shales have higher values of MgO and FeO_t than sandstones, which is consistent with high contents of clay and mica minerals in shales. TB14 has an unusually high Fe content, falling off the Fe-Mg trend defined by the rest of the samples, which may reflect abundant mica minerals or diagenesis effect in this sample. TB5 and TB6 plot in or very close to the range of shales with high Mg and Fe contents, indicating a significant volcanic source.

A number of studies (Young and Nesbitt, 1998; Hayashi et al., 1997; Rahman and Faupl, 2003) have shown that Ti and Al are generally stable chemical constitutes of sedimentary rocks during most weathering, transportation and diagenesis processes. There is a considerable variation for the Al_2O_3/TiO_2 ratio for sediments from different source rocks because this ratio is generally higher in more acidic igneous rocks (Sugitani et al., 1996). Accordingly the Al_2O_3/TiO_2 ratio of a sedimentary rock would be essentially the same as that of its source rock, and may be used as a provenance indictor. Figure 5.4

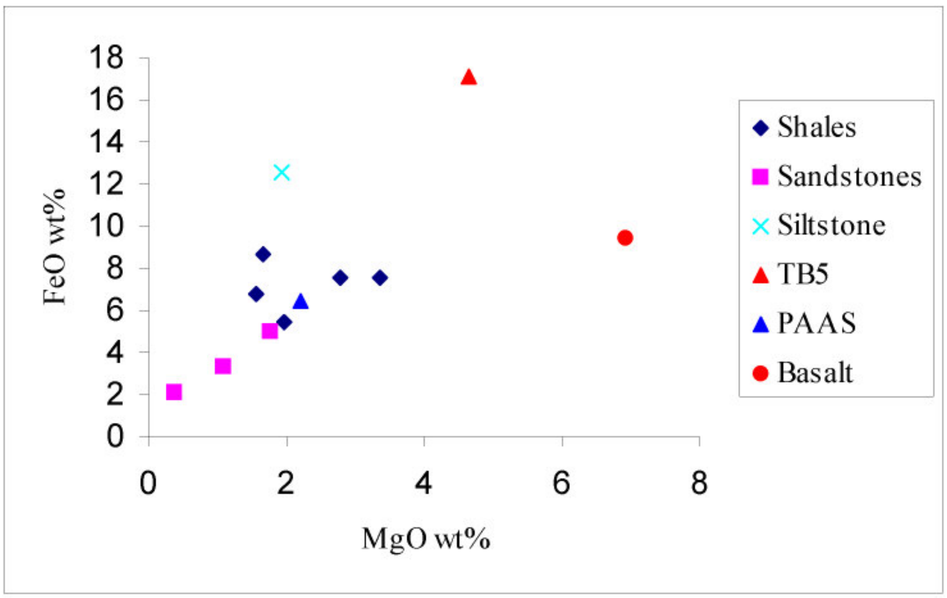

Figure 5.3 MgO-FeOt plot of the Tianba Flysch.TB14 (siltstone) has high Fe content falling off the Fe-Mg trend of the other analyses. PAAS from Taylor and McLennan (1985), basalt from Condie (1993).

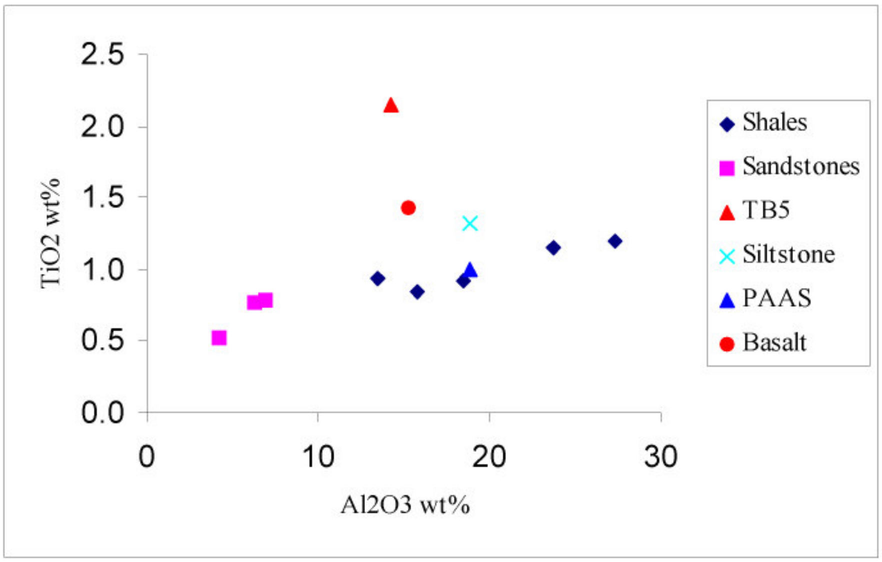

Figure 5.4 Al_2O_3-TiO_2 plot of the Tianba Flysch.There is a approximate linear relationship between Al_2O_3 and TiO_2 in the analyses from the Tianba Flysch. PAAS from Taylor and McLennan (1985), basalt from Condie (1993).

shows a roughly linear distribution between Al_2O_3 and TiO_2 in the Tianba Flysch samples, except for TB5. Note the Al_2O_3/TiO_2 ratios for shales are considerably higher than those of sandstone (14.5-22.8 vs. 6.6-8.9), which is inconsistent with the observation that the fractionation of Al and Ti is minimal between associated sandstones and shales/mudstones (Hayashi et al., 1997). This may suggest that there was significant loss of highly aluminous materials in the sandstones of Tianba Flysch due to separation of the fine-grained clay minerals from quartz and feldspar during transportation (Young and Nesbitt, 1998). However, both sandstones and shales in the Eocene section in the Tingri region have Al_2O_3/TiO_2 ratios similar to sandstones in the Xigaze fore-arc basin (Zhu et al., in preparation), reflecting a source from volcanic arc complex for clastic rocks in the Eocene in the Tingri region. A possible explanation may be that there were variably mixed provenances for the Tianba Flysch including both stable continental craton and volcanic rocks.

Trace elements

Different tectonic settings give rise to volcanic rocks of different compositional suites and thus result in sedimentary provenance difference that are reflected in variation in trace element geochemistry (Bhatia et al., 1986). During fractional crystallization of a silicate melt, many trace elements become incorporated into the major silicate phases, often as isomorphous replacement for a major element (Krauskopf and Bird, 1995). For example, Rb, Ba, and Pb commonly substitute for K due to the similarity in their ionic radii, and are concentrated in rocks formed late in the crystallization sequence; in contrast, Ni, Cr, Mn, V, and Ti are expected to be enriched in rocks formed early in this sequence because of their substitution for Fe and Mg. Therefore the incompatible elements including the large-ion lithophile (LIL) elements (K, Rb, Pb), high field strength elements (HFSE), and light rare earth elements (LREE) are typically enriched in felsic rocks; while the compatible elements (V, Cr, Ni, Sc) are enriched in the mafic rocks. On the other hand, according to Taylor and McLennan (1985), certain trace elements (e.g., Zr, Sc, Nb, Ga and REE) remain essentially constant in abundance during weathering because of their relatively low solubility in aqueous solutions at surface conditions and their short residence time in seawater. These elements are thus transferred quantitatively into terrigenous sediments during sedimentation, and can record the signature of source rocks. Furthermore the ratios of some trace elements can rule out the possible concentration/dilution effects of sorting or winnowing during sediment transport (Bhatia and Crook, 1986; McLennan et al., 1990, 1993). As such, they are more reliable provenance indicators.

The Th/Sc ratio indicates the degree of igneous differentiation because Th and Sc are incompatible and compatible, respectively, in igneous differentiation processes, and both elements are quantitatively transferred from source to sink (Taylor and McLennan, 1985; McLennan et al., 1990). As a result, this ratio has been widely used in provenance studies (e.g., McLennan et al., 1993; Young et al., 1998). In the plot of Th/Sc vs. Zr/Sc (Figure 5.5), with the exception of TB5, all samples of the Tianba Flysch plot in the passive margin field or follow the linear trend of sediment recycling: Zr/Sc of both sandstones and shales increase substantially, with Th/Sc increasing far less, which points to a considerable zircon addition trend (McLennan et al., 1993). This also confirms that sorting processes did not significantly affect the Th/Sc (Young et al., 1998). The relatively moderate Th/Sc ratios in the Tianba Flysch are close to the average present-day

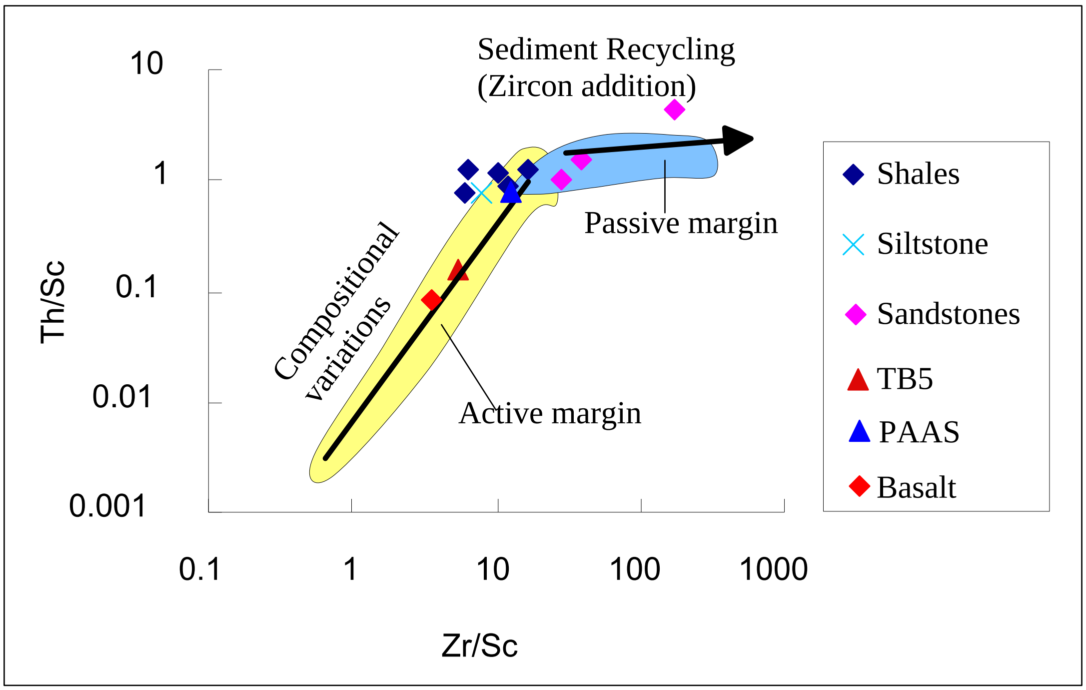

Figure 5.5 Th/Sc-Zr/Sc plot of the Tianba Flysch.
Passive margin and Active magin fields, and trends of compositional variations and sediment recycling are from McLennan et al. 1990. PAAS from Taylor and McLennan (1985), average basalt composition from Condie (1993).
There is a signficant enrichment of Zircon (high Zr/Sc) in passive margin setting resulting from sedimentary sorting and recycling.

upper crust with Th/Sc ratio close to 1 (Taylor and McLennan, 1985), which reflects input from continental sources and deposited on a passive continental margin. However TB5 has a significantly lower Th/Sc ratio (0.16), indicating substantial incorporation of materials derived from mafic sources.

Considering that U may be lost to the oceans due the soluble U^{6+}state under oxidized conditions, the resultant increases in the Th/U may indicate weathering and recycling histories for sedimentary rocks (McLennan et al., 1990). Sediments derived from most active margins have Th/U ratios (1.0-4.0) because of the sampling of depleted mantle sources of island arc provenances (McLennan et al., 1990), which are notably lower than the present upper continental crustal value of 3.8 (Taylor and McLennan, 1985). The Th/U ratios of the Tianba Flysch range from 6.84 to 11.88 (Figure 5.6) which suggests that the Tianba Flysch clastic input was significantly affected by sedimentary processes involving derivation from old upper crustal sources, that may have included recycled sedimentary sources. This is consistent with the presence of sedimentary rock fragments, the quartz-rich nature of the sands, and round-subround zircon grains, especially for the basal sandstone (TB13).

During mafic fractional crystallization, Cr and Ni commonly substitute for Fe and Mg in early-crystallized minerals, including spinel and olivine, and to a lesser extent diopside and augite (Najman and Garzanti, 2000). Given the fact that most mafic neosilicates and inosilicates are less resistant due to preferential breakdown, and that Cr and Ni are immobile (Condie and Wronkiewicz, 1990) during weathering and diagenesis processes, the geochemical abundances of Cr and Ni therefore are a very useful complement to the sedimentary petrology results. In particular, the relative enrichments

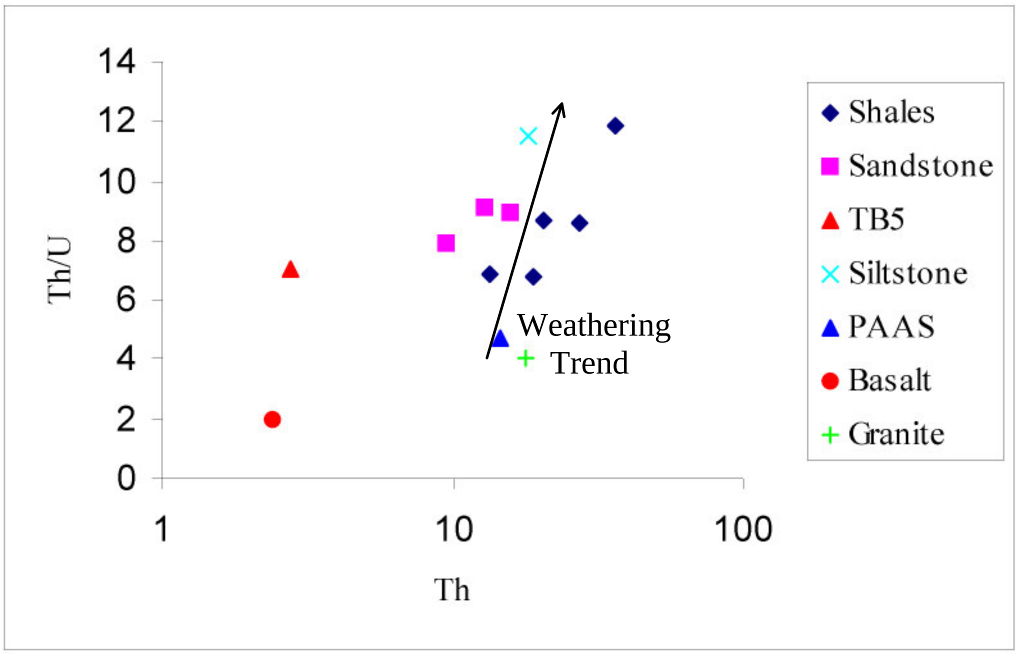

Figure 5.6 Th/U-Th plot of the Tianba Flysch. Arrow indicates a weathering trend.Note analyses (except TB5) from the Tianba Flysch follow the weathering trend, similar to Australian Shales with cratonic provenance (McLennan et al., 1990). PAAS from Taylor and McLennan (1985), average basalt and granite compositions from Condie (1993).

of Cr (e.g., >150 ppm) and Ni (e.g., >100 ppm) may indicate an ultra-mafic/mafic provenance for sediments (Hiscott, 1984; Garver et al., 1996; Bock et al., 1998). With the exception of TB5, the relatively low concentrations of Cr (80-176 ppm in shales, and 52-61 in sandstones) and Ni (29-84 ppm in shales, and 12-25 in sandstones) are notable in the Tianba Flysch. In particular, the Cr and Ni abundances in the shale samples are very close to those of Post-Archean Average Shale (PAAS, Cr=110 ppm, Ni=55 ppm, Taylor and McLennan, 1985), indicating a dominantly continental crustal. Considering that the Cr/V ratio indicates the relative enrichment of Cr over other ferromagnesian trace elements, and Y/Ni reflects the general level of ferromagnesian trace elements (Ni) compared to a proxy for HREE (Y), the plot of Cr/V vs. Y/Ni (Figure 5.7) may be used to distinguish sediments derived from an active margin or a passive margin (McLennan et al., 1990, 1993; Bock et al., 1998). Samples in the Tianba Flysch plot with low Cr/V (mostly between 0.59 and 0.81) and variable Y/Ni ratios, which is a typical range for sediments from passive margins. However, TB5 has significantly higher Cr and Ni abundances (320 and 197, respectively), which is strong evidence for significant amounts of mafic or ultramafic lithologies in the source area. This is consistent with abundant Cr-rich spinels found by heavy mineral separation. The presence of Cr-rich spinels is commonly used as a good indicator of an ophiolitic source component (Rowley and Kidd, 1981; Bock et al., 1998). However, detailed studies of the spinel compositions in the Tianba Flysch have shown that they were derived hotspot-related basalts, not from obducted ophiolites (Zhu et al., in review).

Rare earth elements (REE) are considered to be essentially constant in abundance during sedimentary processes because of their relatively low mobility. As such, REE

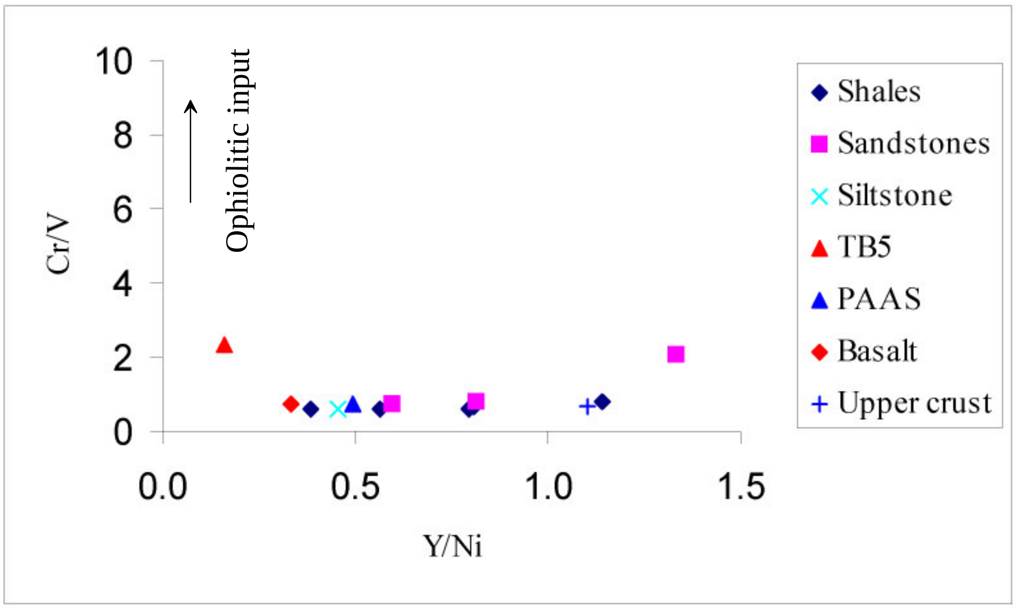

Figure 5.7 Cr/V-Y/Ni plot of the Tianba Flysch.
Note Cr/V ratios of the Tianba Flysch are constantly low with the increase in Y/Ni ratios.Mafic-ultramafic sources tend to have high Fe, Cr, Ni abundances with low Y/Ni and high Cr/V ratios. TB5 has high Cr and Ni abundances indicating a volcanic provenance. PAAS and Upper Crust from Taylor and McLennan (1985), average basalt composition from Condie (1993).

variation in sedimentary rocks is widely used to determine the tectonic setting of deposition (e.g., Taylor and McLennan, 1985; Bhatia et al., 1986; McLennan et al., 1990, 1993). With the exception of sample TB5, the chondrite-normalized REE abundance patterns of the Tianba Flysch are similar to REE pattern of PAAS (Taylor and McLennan, 1985) although the shale samples are all enriched relative to PAAS while the sandstone samples are depleted due to quartz dilution (Figure 5.8). All the samples are LREE enriched relative to HREE with flat HREE patterns (La_N/Yb_N=10.9-12.7), and apart from TB5 described below, display negative Eu anomalies (Eu/Eu* values between 0.49 and 0.79). TB13 with the most marked negative Eu anomaly has high silica and high Zr contents (SiO2=91.19%, Zr=612 ppm). Comparison with the REE pattern of PAAS reinforces the similarity of the major part of Tianba Flysch to the average upper crust, indicating the Tianba Flysch is composed of sediments derived from old upper continental crust. TB5 exhibits a very different chondrite-normalized REE pattern: there is no significant LREE enriched relative to HREE (La_N/Yb_N=7.02), and a slightly positive Eu anomaly (Eu/Eu*=1.03), suggesting notable contribution from immature source. TB14 (siltstone) has similar chondrite-normalized REE pattern to the shales except there is a significant positive Ce anomaly. The reason for this discrepancy is not understood at present, but it may be related to high abundance of mica in this sample.

Geochemical discrimination of tectonic environment

According to Roser and Korsch (1988), major oxide compositions can be utilized to distinguish clastic sediments derived from four provenance and tectonic setting areas including primarily mafic, intermediate or felsic igneous, and recycled-mature polycyclic

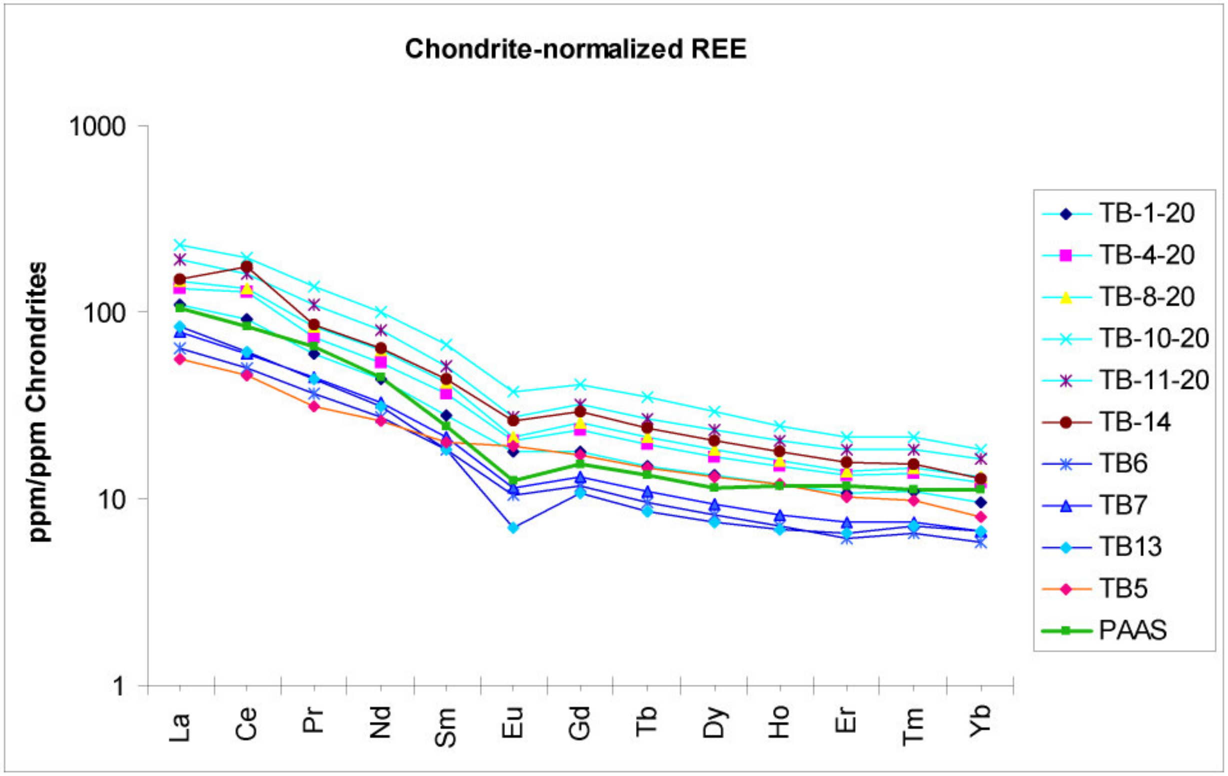

Figure 5.8 Chondrite-normalized REE plot of the Tianba Flysch, north of Tianba village.
All analyses except TB5 show LREE enrichments and negative Eu anomalies, similar to PAAS, indicating a common cratonic provenance. Relatively flatten REE trend of TB5 points to a signficant volcanic source. PAAS from Taylor and McLennan (1985).

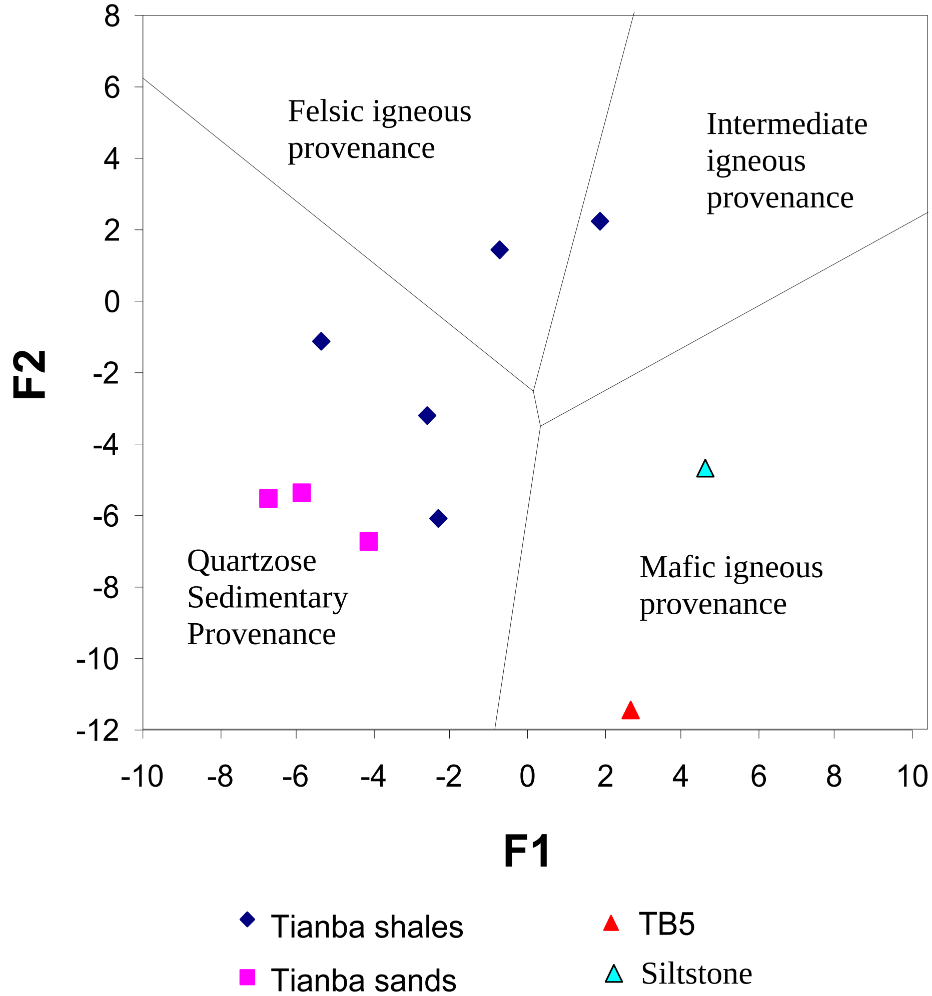

Figure 5.9 Tectonic discriminant diagram for the Tianba Flysch. Tectonic setting fields are from Roser and Korsch (1988).
$F1=-1.773TiO_2+0.607Al_2O_3+0.76Fe_2O_3-1.5MgO+0.616CaO$
$+0.509Na_2O-1.224K_2O-9.09$
$F2=0.445TiO_2+0.07Al_2O_3-0.25Fe_2O_3-1.142MgO+0.438CaO$
$+1.475Na_2O+1.426K2O-6.86$
Data from Roser and Korsch (1988).

quartzose sedimentary material (Figure 5.9). Three sandstones and three shales from the Tianba Flysch plot in the quartzose sedimentary provenance, equivalent to a passive margin tectonic setting. Two shales fall in the fields of felsic-intermediate provenances. Sample TB14 (siltstone) plots in the mafic igneous provenance, which may be explained by the unusually enriched mica resulting in high Al and Fe contents. TB5 contains 45.04% CaO, consistent with considerable amounts of calcareous cement and calcite grains observed in the thin section. Recalculated values for this sample based on 100% CaO and LOI-free plot well in the mafic igneous provenance. Therefore this plot suggests that the Tianba Flysch was deposited primarily at a stable continental margin with a significant volcanic input in the upper part of the sequence.

In the K_2O/Na_2O-SiO_2 discrimination diagram (Roser and Korsch, 1986), as expected, five shales and two sandstone analyses of the Tianba Flysch fall into the passive continental margin (Figure 5.10). TB6 (sandstone in the upper part of the Flysch) plots in the active margin, which may indicate the volcanic component. Again, the recalculated values based on 100% CaO and LOI-free for TB5 plot in the arc field, indicating a notably volcanic input.

Conclusion

In summary, geochemical data are broadly consistent with the petrographic interpretations. The relatively high SiO_2, Zr, SiO_2/Al_2O_3, K_2O/Na_2O, Th/Sc, Th/U, and La_N/Yb_N, and pronounced Eu anomalies suggest that the Tianba Flysch is dominated by mature cratonic detritus, and most likely was deposited on the Indian passive margin. Therefore, the Tianba Flysch, as discussed above, possesses similar geochemical characteristics to that of a passive margin tectonic setting as described by many workers (e.g., Bhatia, 1985; Taylor and McLennan, 1985; Roser and Korsch, 1986, 1988; McLennan et al., 1990, 1993). It is also evident that there was a significant volcanic source in the upper part of the Tianba Flysch. Despite the appearance, based on the bulk geochemical data alone, of arc or active margin influence, it is clear based on the more refined and precise data from spinels and their melt inclusions that these volcanics were exclusively of hot-spot origin (Zhu et al., in preparation).

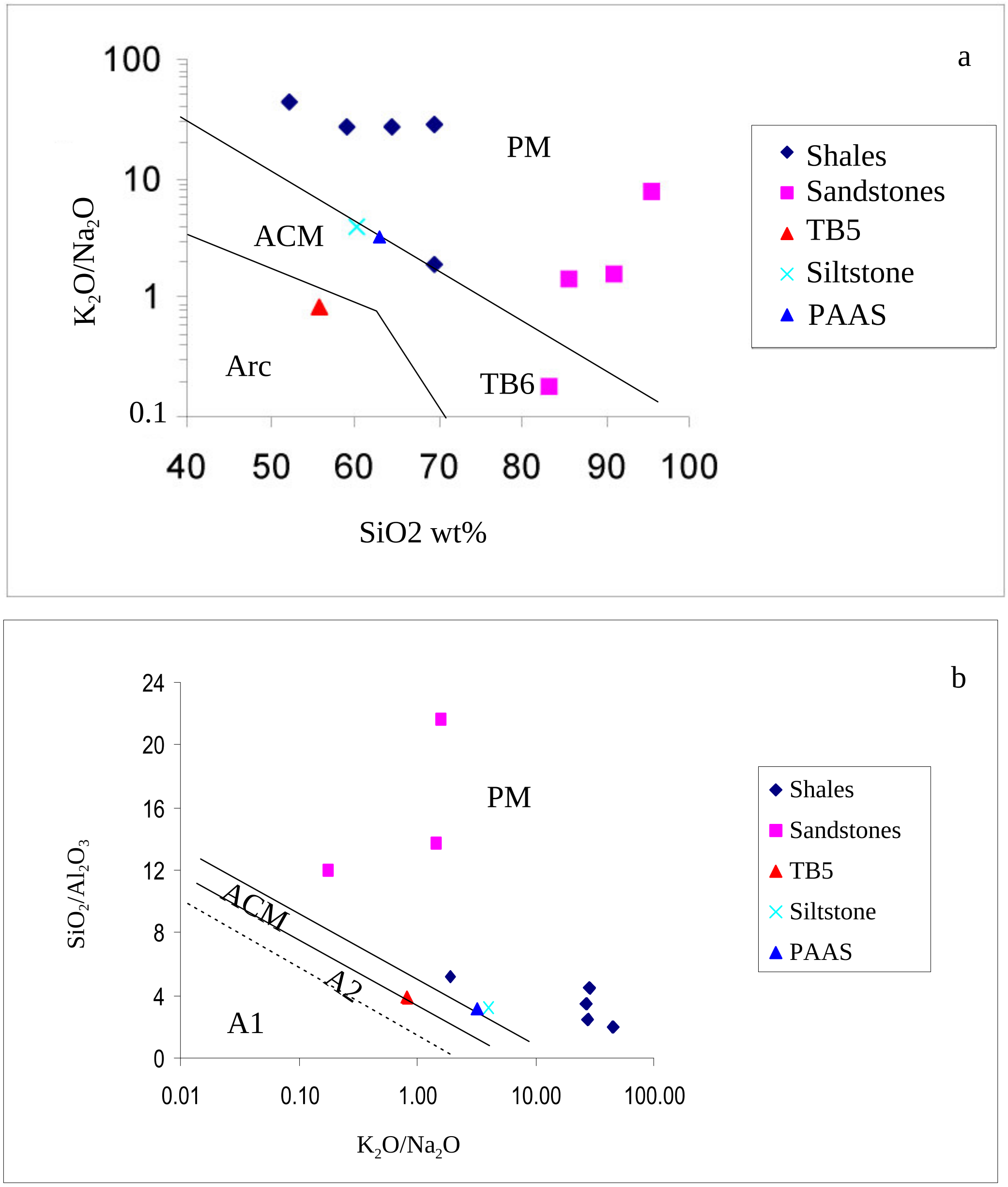

Figure 5.10 K_2O/Na_2O-SiO_2 (a) and SiO_2/Al_2O_3-K_2O/Na_2O (b) plots of the Tianba Flysch.

Tectonic setting: PM-passive margin, ACM-active continental margin, ARC-volcanic arc, A1-Arc setting, A2-evolved arc setting (from Roser and Korsch, 1986).Most samples from the Tianba Flysch plot in the passive margin area while TB5 plots in arc or active continental margin, indicating a volcanic source for the upper Tianba Flysch. PAAS from Taylor and McLennan (1985).

Chapter 6. Provenance and tectonic significance of lower Tertiary clastic rocks in Tingri, southern Tibet

Abstract

The provenance of the Jidula, Youxia and Shenkeza Formations from the lower Tertiary terrigenous sections in the Tingri region, southern Tibet has been investigated using petrographic and geochemical whole-rock and single-grain techniques. Petrographic analysis of sandstones in the Jidula Formation (Paleocene) reveals that monocrystalline quartz grains of cratonic origin are dominant. In contrast, there are significant amounts of immature framework grains with a distinct ophiolitic and volcanic arc influence present in the Youxia (mid-Eocene) and Shenkeza (post mid-Eocene) Formations. Major-, trace-, and rare-earth element concentrations in both sandstones and shales complement the petrographic data and indicate that the source of the Jidula Formation consisted primarily of quartzose basement rocks, probably of Indian continental origin, whereas the Youxia and Shenkeza Formations are mainly derived from the uplifted Gangdese arc-trench system associated with the obduction of the Asian subduction complex. The compositions of Cr-rich spinels in the Youxia and Shenkeza sandstones are closely similar to those from fore-arc peridotites, and were most likely derived from the arc and ophiolite rocks along the developing Yarlung-Zangbo suture to the north. No spinels have been observed in the Jidula sandstones. Therefore the early Tertiary detrital clastics in Tingri record a marked change in provenance and sediment character between the times of the deposition of Jidula and Youxia Formations. This change indicates that the onset of India-Asia collision and development of the foreland

basin occurred at ~47 Ma in the section presented in the Tethyan Himalaya of southern Tibet.

Introduction

As the Himalayan-Tibetan orogeny is the most prominent active continent-continent collision zone (Dewey and Bird, 1970; Molnar, 1984), the geology of southern Tibet has been intensively studied for the past three decades (e.g., Allegre, et al., 1984; Burg and Chen, 1984; Tapponnier et al., 1981; Molnar and Tapponnier, 1978; Harrison et al., 1992; Hodges, 2001). However, the age of initiation of the India-Asia collision for most parts of the system is still debated, with views ranging from Late Cretaceous (>65 Ma) to as young as 37 Ma (Rowley, 1996, 1998, and references therein; Najman et al., 2000, 2002; de Sigoyer et al., 2000, 2001; Yin and Harrison, 2000; Searle, 2001). The precise timing of the start of collision between India and Asia is significant for models of mass balance in the Himalayan system due to the high rate of India-Asia motion during the 65-47 Ma interval (Patriat and Achache, 1984; Rowley, 1996).

It is well-known that the sediment composition of a foreland basin is important for constraining the tectonic evolution of the associated collision zone (Dickinson and Suczek, 1979; Ingersoll et al., 1984; Garzanti et al., 1996; Dickinson, 1985; Zuffa, 1980; Cingolani et al., 2003). Additionally it is an important method to constrain the age of the onset of collision (Rowley and Kidd, 1981), since tectonic movements change the provenance areas, influence relief and erosion, and define sediment conduits (Dewey and Mange, 1999). For example, detailed stratigraphic and petrographical analysis of the Cretaceous to Eocene Tethyan sedimentary succession (Garzanti et al., 1987, 1996) indicate that the India-Asia collision started there in the interval of late Ypresian through early Lutetian (~51 Ma) in the Zanskar region, NW Himalayas. In this chapter, new data are reported on sandstone petrology, geochemical composition, and spinel characteristics present in the lower Tertiary clastics in the Tingri region, southern Tibet, which constrain the age of the start of the collision between India and Asia in this easterly region of the Himalayan collisional zone.

Geological Framework

The Tethyan Himalaya, located between the High Himalayan belt to the south and the Indus-Yarlung-Zangbo Suture and the Lhasa block to the north (Figure 6.1), consist primarily of late Paleozoic to early Eocene sedimentary rocks, originally deposited along the northern edge of the Indian continent. Deposition began with late Paleozoic-Triassic rifting (Sengor et al., 1988; Sciunnach and Garzanti, 1996; Garzanti, 1999) during the initial development of the Neo-Tethyan Ocean, and a relatively wide passive continental margin subsequently developed along the southern margin of the Neo-Tethys (Willems et al., 1996). During the mid-Cretaceous, northward-directed subduction of the Neo-Tethyan oceanic crust beneath the southern margin of Asia resulted in the development of a magmatic arc and a fore arc-related basin (Xigaze) along the southern margin of the Lhasa block (Durr, 1996, Einsele et al., 1994). The India-Asia collision began sometime in the interval of late Cretaceous to early Tertiary and the Indus-Yarlung-Zangbo suture (IYZS) marks the site of removal of the Neo-Tethys. Therefore the strata of the Tethyan Himalaya record the closure of the Neo-Tethys and collision of India and Asia (Garzanti et al., 1987, 1996; Rowley, 1996; Pivnik and Wells, 1996; Najman et al., 1997, 2000, 2001; Qayyum et al., 2001; Wang et al., 2002; Wan et al., 2002).

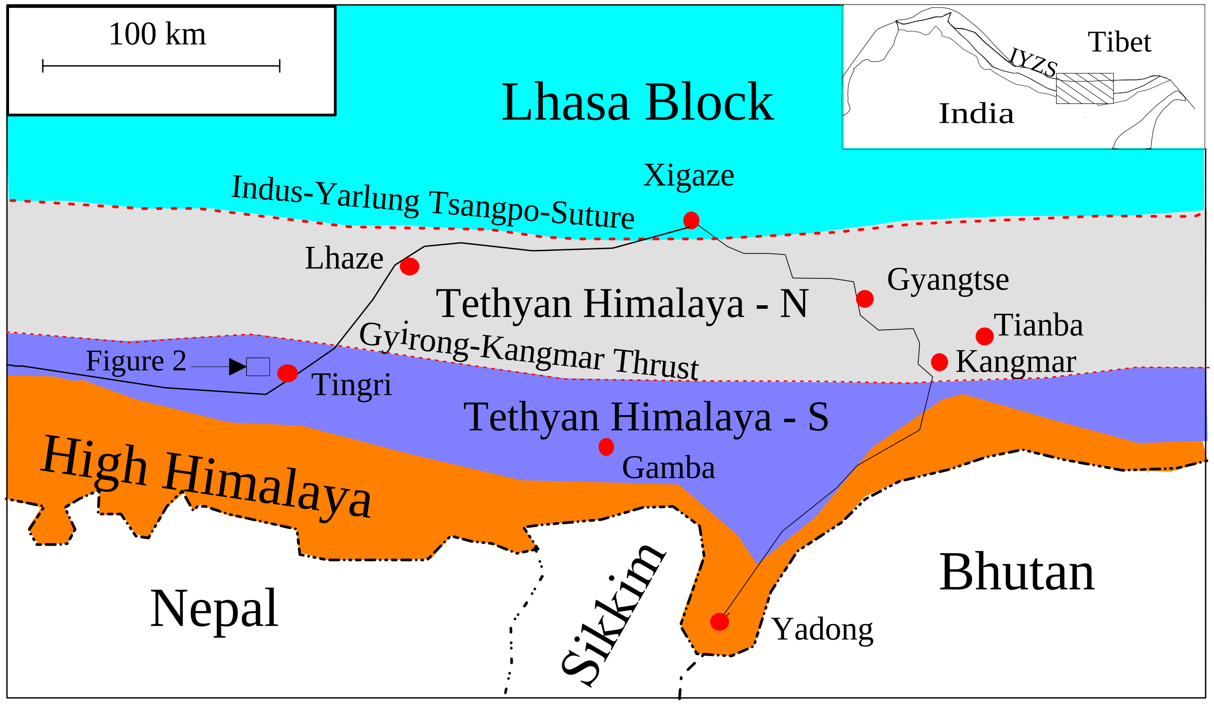

Figure 6.1 Sketch geologic map of Tingri region, southern Tibet. The inset map shows this region located in the Himalayan system. Modified after Willems et al.(1996).

In southern Tibet, the Tethyan Himalaya can be divided into two subzones having different lithological assemblages (Figure 6.1) that are separated by the East-West trending Gyirong-Kangmar thrust (Burg and Chen, 1984; Liu, 1992). The northern zone is dominated by slightly metamorphosed deposits of outer shelf, continental slope, and continental rise environments, while the southern zone is characterized by non-metamorphic, shallow water shelf calcareous and terrigenous deposits ranging from late Paleozoic to Eocene. The latest Permian is partly missing due to uplift in conjunction with the initial rift-stage of the Neo-Tethys (Wen, 1987; Willems et al., 1996; Xizang BGMR, 1992).

Lithostratigraphy in the Tingri region

This study concentrates on the well-exposed Tertiary clastic rocks near the western end of the Zhepure Shan (Figure 6.2), which belong to the southern zone of the Tethyan Himalayas. The Cretaceous-early Tertiary sequence of the southern Tethyan Himalayan zone is best exposed in the ranges east of Gamba (Khampa Dzong), and west of Shekar Dzong (or New Tingri), which are regarded as local stratotypes for the Cretaceous and lower Tertiary in southern Tibet (Zhang and Geng, 1983; Willems et al., 1996). Six stratigraphic units (Figure 6.3) have been defined in the Gongzha section on the north slope of the Zhepure Shan mountain, west of Shekar Dzong (Willems et al., 1996). They are, from oldest to youngest, the Gamba Group (late Albian-early Santonian), which consists of marls and subordinate limestones; the Zhepure Shanbei Formation (early Santonian-middle Maastrichtian), which contains well-bedded limestones interbedded with very thin layers of calcareous marl; the Zhepure Shanpo

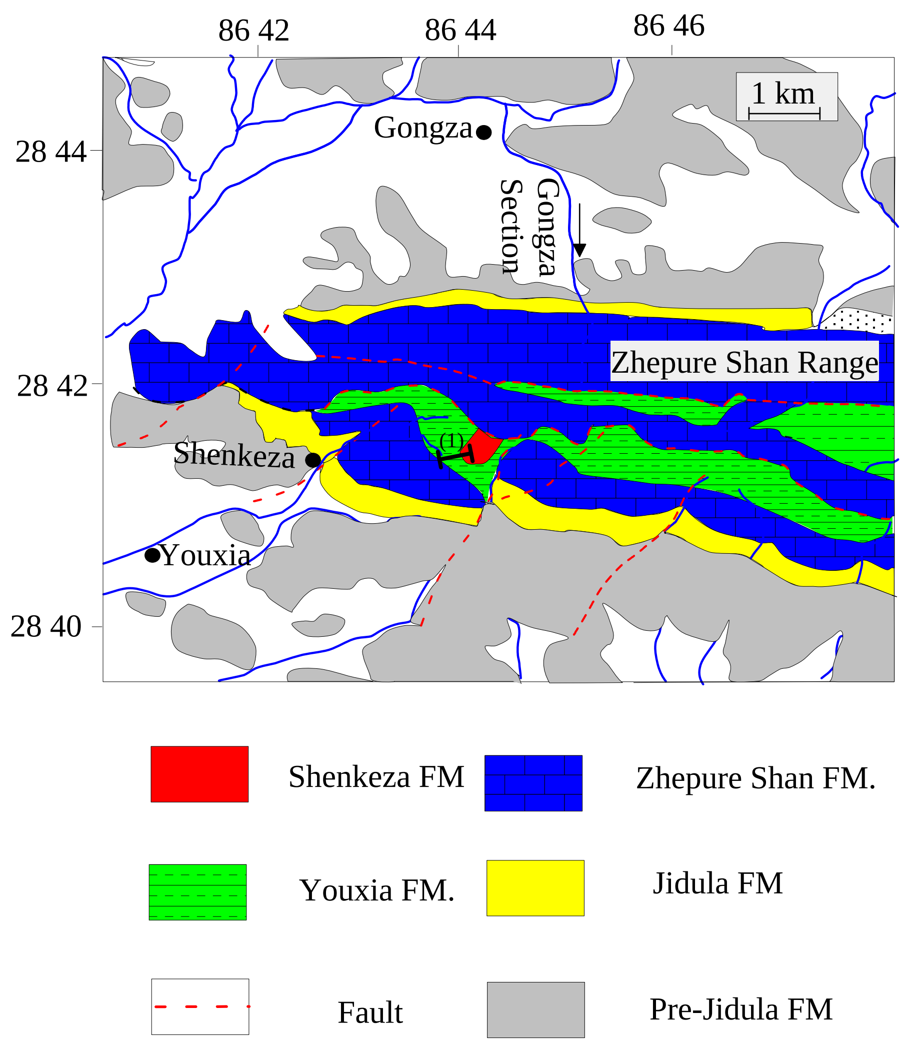

Figure 6.2 Simplified geologic map showing the location of the studied sections in the Tingri region on the western flank of Zhepure Shan Mountain.
Note: (1) is measured section at Shekeza.
Geographic coordinates in degrees, minutes.

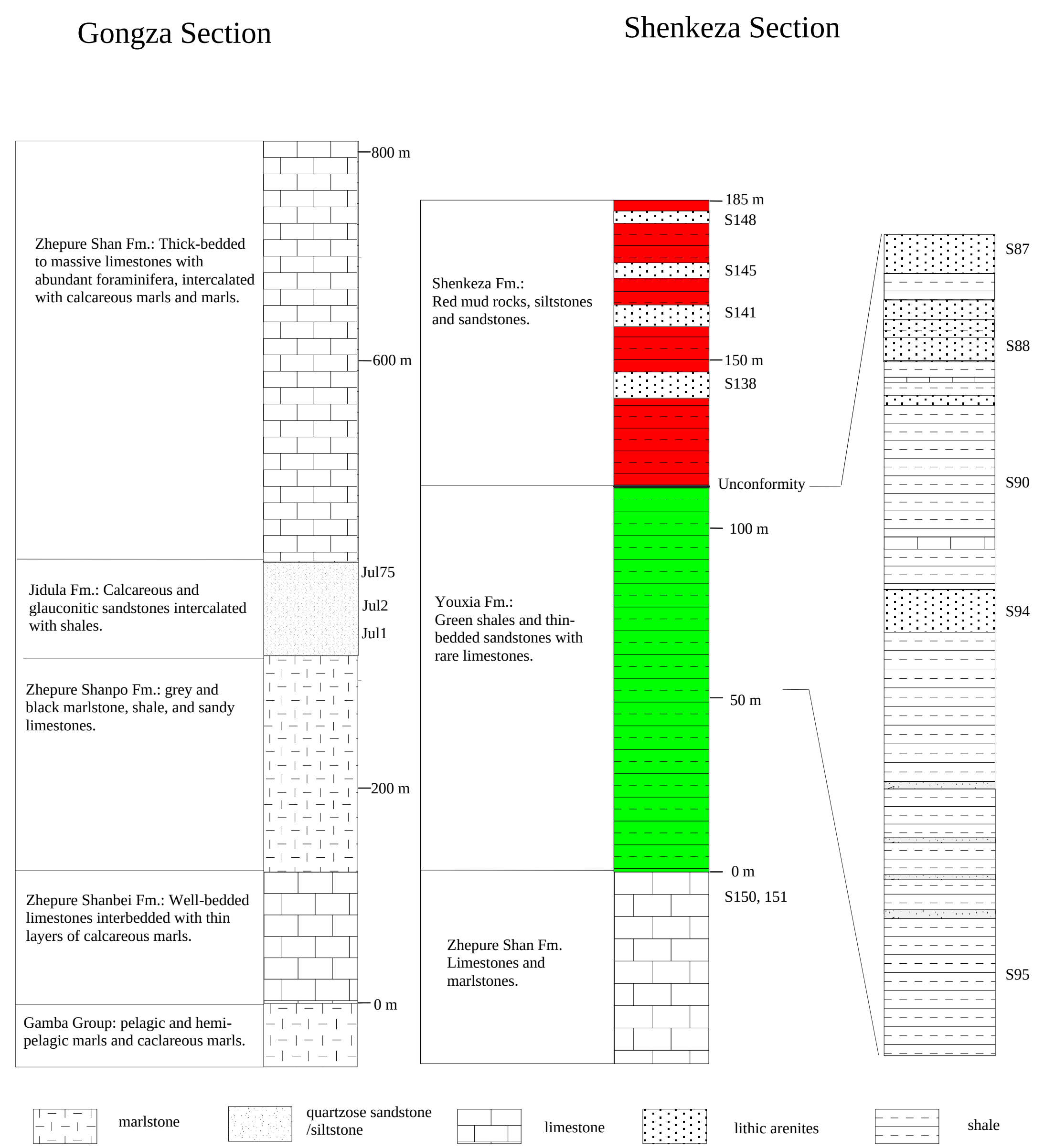

Figure 6.3 Stratigraphic columns of lower Tertiary sequence in the Tingri region. The Shenkeza section was measured by us in 2000, and the Gongza section is from Willems et al. (1996).
Section locations are shown in Figure 2. Sample locations are indicated by "Sxxx" at Shenkeza section and "Julxxx" at Gongza section.

Formation (middle Maastrichtian-early Paleocene), which consists of a lower interval dominated by siliciclastic turbidites with minor calcareous sandstones, and an upper sequence composed of pale-weathering, grey and black marlstone; the Jidula Formation (Danian) contains calcareous and glauconitic sandstones, shales and mudstones; the Zhepure Shan Formation (late Danian-Lutetian), which consists of thick-bedded to massive limestones characterized by abundant large foraminifera; and a unit called by Willems et al. (1996) the "Zongpubei Formation" (Lutetian or younger) that is made up of greenish-gray shales and some sandstones overlain by red clay and siltstone with intercalations of sandstones. These shelf deposits of the Neo-Tethys contain a relatively continuous record in the Tingri region up through the deposition of the "Zongpubei Formation". As such, Willems et al. (1996) document the youngest unequivocally dated limestones (the Zhepure Shan Formation) in this region, and the detailed study of conformably overlying clastic deposits could (and, we report below, does) provide a record of the start of Indian-Asian collision in the eastern Himalayas.

Willems et al. (1996) named the Eocene clastics in the Tingri region the "Zongpubei Fm." based on their broadly similar lithostratigraphic characteristics compared with the Zongpubei Fm. in the type section around Gamba, 180 km east of Tingri. Because we can demonstrate that the Eocene clastics near Tingri do show influence of the closure of Neo-Tethys, and that the Zongpubei Fm. at Gamba does not, we think that in this particular case it would cause significant confusion to continue to use the same lithostratigraphic unit name for these two widely separated units, even though they at first glance show similar field characteristics. Abundant fossils reported by Willems and Zhang (1993) in the basal portions of the Zongpubei Formation at Gamba indicate an age of late Paleocene (Thanetian), and we point out that this is significantly older than the age of the mid-Eocene clastic sediments in the Tingri region. Sandstones in the Zongpubei Formation at Gamba are (from our observations) relatively quartz-rich, lithic-poor arenites, and no chrome spinel grains have been observed in the heavy mineral separates of a sandstone sample from the Gamba section. This contrasts with the clastics of the Tingri region, which are lithic-rich and contain significant chrome spinel.

The Eocene clastics ("Zongpubei Formation") in the Tingri region were not well studied by Willems et al. (1996) because of poor exposure and a fault contact between the unit and the underlying Zhepure Shan Formation in the section they examined. Wang et al. (2002) described a better-exposed 180m -thick section, which they called the "Pengqu Formation", only 2.5 km southwest of the "Zongpubei Formation" in the Gongzha section studied by Willems et al. (1993, 1996). Wang et al. (2002) divided this new section into two members: the Enba Member consisting of grey and yellowish-green shale intercalated with sandstones, and red shale and sandstones they named Zhaguo Member. These strata were described as conformably overlying the massive limestones of the Zhepure Shan Formation. Nannofossils and foraminifera reported by Wang et al. (2002) in the shales were interpreted to indicate an age ranging from late early Lutetian to late Priabonian (47-34 Ma) for the "Pengqu Formation".

During field studies in the Tingri region in October 2000, our group also studied this section at Shenkeza (86˚43'39''E, 28˚41'26''N). Shenkeza is a name of a small monastery located in the same valley about 1 km west of the studied section, and Youxia village occurs a few kilometers farther down the valley. Although we observed a similar lithostratigraphic sequence consisting of green shales and thin-bedded sandstones in the lower part (Figure 6.4), and red mudstones and sandstones in the upper part (Figure 6.5), we recognize a significant erosion surface and weathering profile (unconformity) between the green and red units (Figure 6.6). We therefore reject the proposal of Wang et al. (2002) that they should be included in a single formation.

For these Eocene clastic sediments exposed in the head of the Shenkeza valley, we propose the name of Youxia Fm. for the 105-m-thick green shales and thin-bedded sandstones. This green clastic unit is widely distributed, although not commonly well-exposed, along the center of the Zhepure mountain range parallel with the Pengqu River. We reject the member names introduced by Wang et al (2002), which are those of villages in the Pengqu River Valley more than ten kilometers away from the section, and introduce the name Shenkeza Fm. to define the upper 75m-thick red mudstones and sandstones. The new name is proposed because the red unit is only exposed in the section close to Shenkeza monastery and village. The geological reason to establish two separate formations for these sedimentary rocks is that there is a significant unconformity between the two units (described in more detail below).

In the Shenkeza valley section, nummulitic grainstones of the uppermost part of the Zhepure Shan Formation are interbedded with gray shales identical to those of the lower Youxia Formation indicating a conformable contact. Abundant large foraminifera (*Nummulites atacicus, Nummulites globulis, Discocyclina dispensa, Nummulites cf. Vedenbergi, Assilina globosa, Assilina subspinosa,* etc.) in these nummulitic grainstones point to a Ypresian to early Lutetian age for the topmost limestones of the Zhepure Shan Formation. The Youxia Fm. consists of about 105 meters of greenish-grey shales

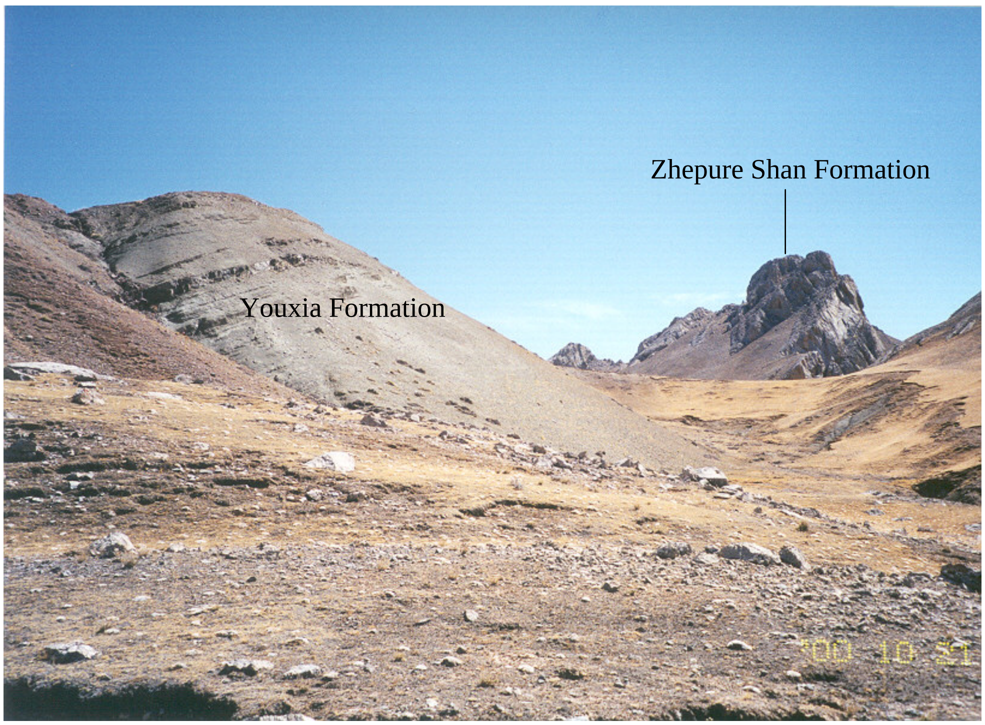

Figure 6.4 View to E of the upper part of the Youxia Formation in the head of the Shenkeza valley, made up of green shales and sandstones. The shales conformably overlie the Zhepure Shan limestones. The section of the upper Youxia Formation was measured up the gully on the left side of the photo.

Figure 6.5 View to N of Shenkeza Formation of red shales and occasional intercalations of fine-grained sandstones. The Zhepure Shan limestones above are in thrust contact with this unit.

Figure 6.6 View to NW of the unconformity between the Youxia and Shenkeza Formations. Note there is abrupt change in color from green to red. Excavation of the contact at the location of the hammer in this photo revealed a 1 m thick soil horizon of the base of the red unit, and a rubbly regolith of green sandstone fragments below it. [Professor W. Kidd stands on the unconformity, 21 Oct 2000]

intercalated with thin-bedded, green-colored sandstones and rare thin nodular limestone beds (Figure 6.3). Sandstone beds in the Youxia Formation have tabular geometry and they become more numerous, thicker, and coarser-grained up-section. Most of the sandstone beds in the unit have scoured bases that display tool marks and flute-type casts, some are normally graded, and they frequently contain horizontal and ripple-cross lamination. Several of the sandstone beds are hummocky cross-stratified, particularly those in the upper part of the unit.

We interpret the Youxia Fm. to have been deposited in an outer-shelf marine environment. Sandstones were deposited from turbid suspension currents, while the interbedded shales were deposited by suspension settling of clay between or following high-energy events. The hummocky cross-stratification seen in sandstones, particularly the thick sands in the upper part of the section (Figure 6.7), indicates later deposition occurred under the influence of storm waves (Walker, 1979). It is possible that some of the thin arenites in the middle of the section were deposited from turbidites, but the upper ones are unquestionably storm deposits, and the thinner, finer-grained ones in the middle of the section may be as well.

The green unit (Youxia Fm. as defined here) is unconformably overlain by the Shenkeza Formation, about 75m thick, consisting of mudstone and red shales and interbedded lensoid beds of sandstone. The unconformity on the green arenites of the Youxia Fm. is marked by a 25-cm thick bed of poorly sorted angular pebble/cobble-sized material derived from the underlying unit. This interpreted paleo-regolith is immediately overlain by 4m of red mudstone containing green mottles, angular/blocky pedogenic structures, argillaceous cutans, and slickensides. We interpret this lower-most mudstone

Figure 6.7 Hummocky cross-stratification in the top sandstones of the Youxia Formation, indicating a depostional environment of storm waves during the late Youxia Formation.

in the Shenkeza Formation to be a paleo-vertisol (sensu Mack et al., 1992) that formed during development of a major unconformity. Sandstone beds in the Shenkeza Fm. have lenticular geometries and range in thickness from 1-3m and are 10's-100's of meters in width. Individual sandstone beds have scoured bases, fine upwards, and contain trough cross-stratification, horizontal lamination, and ripple cross-lamination. The red mudstones within this unit also contain evidence in places for pedogenic modification including angular/blocky pedogenic structures, argillaceous cutans, and slickensides.

Wang et al. (2002) interpreted the rocks of the red Shenkeza Fm. to have been deposited in a shallow marine shelf environment, and reported marine microfossils from them. Based on our observations, however, we interpret this unit to represent fluvial channel and floodplain deposits. In addition, because of our identification of a potentially substantial unconformity at the base of the red unit, and the overall non-marine nature of the interval, we consider the late Priabonian age of the upper member reported by Wang et al. (2002) to be highly suspect. Since this age was based on the presence of calcareous marine nannofossils in the red mudstones, we suggest that the observed fossils were reworked from older marine units that lay beneath the unconformity. As such, the unit may be significantly younger than the Late Eocene-Early Oligocene age fossils identified in the unit. This interpretation is supported by the presence of older, reworked lower Tertiary marine microfauna and Mesozoic pollen also identified in the unit (Wang et al., 2002).

Sedimentary Provenance studies

Since individual provenance techniques (Humphreys et al., 1993; Johnsson, 1993) have limitations, this study took an integrated approach to determine the provenance of the Tertiary clastics in the Tingri region. This approach maximized the number of provenance indicators, and minimized the adverse effects of diagenesis and regional variations in lithology and grain size (Bhatia et al., 1983, 1985, 1986; Taylor and McLennan, 1985; Roser et al., 1986, 1988, 1996; Morton et al., 1991; McLennan et al., 1991, 1993).

Sandstone petrology

A petrographic study was conducted on sandstone samples from the Youxia and Shenkeza Formations (N=7) and from the Jidula Formation (N=3). This permitted a comparison to be made between deposits of the Indian passive margin (Jidula) with collision-related clastic rocks (Youxia and Shenkeza). Sample locations are shown in Figure 6.3 For high consistency and accuracy, 500 points were counted following the Gazzi-Dickinson point-counting method (Dickinson and Suczek, 1979; Zuffa, 1985; Ingersoll et al., 1984), whereby sand-sized minerals included within lithic fragments were counted as the mineral phase, rather than as the host lithic fragment. Given the fact that some minerals and rock fragments may be extensively altered after diagenesis and low-grade metamorphism, an effort was made to recognize those components and count them as original framework grains. Feldspar was identified on the basis of its poor optical appearance, relative relief, twinning, cleavage, and characteristic alteration. Point-counting percentages and recalculated parameters are given in Table 6.1. These values were used to plot samples on conventional triangular compositional diagrams (Figure 6.8) to infer the tectonic setting during the deposition of the early Tertiary clastics in the Tingri region.

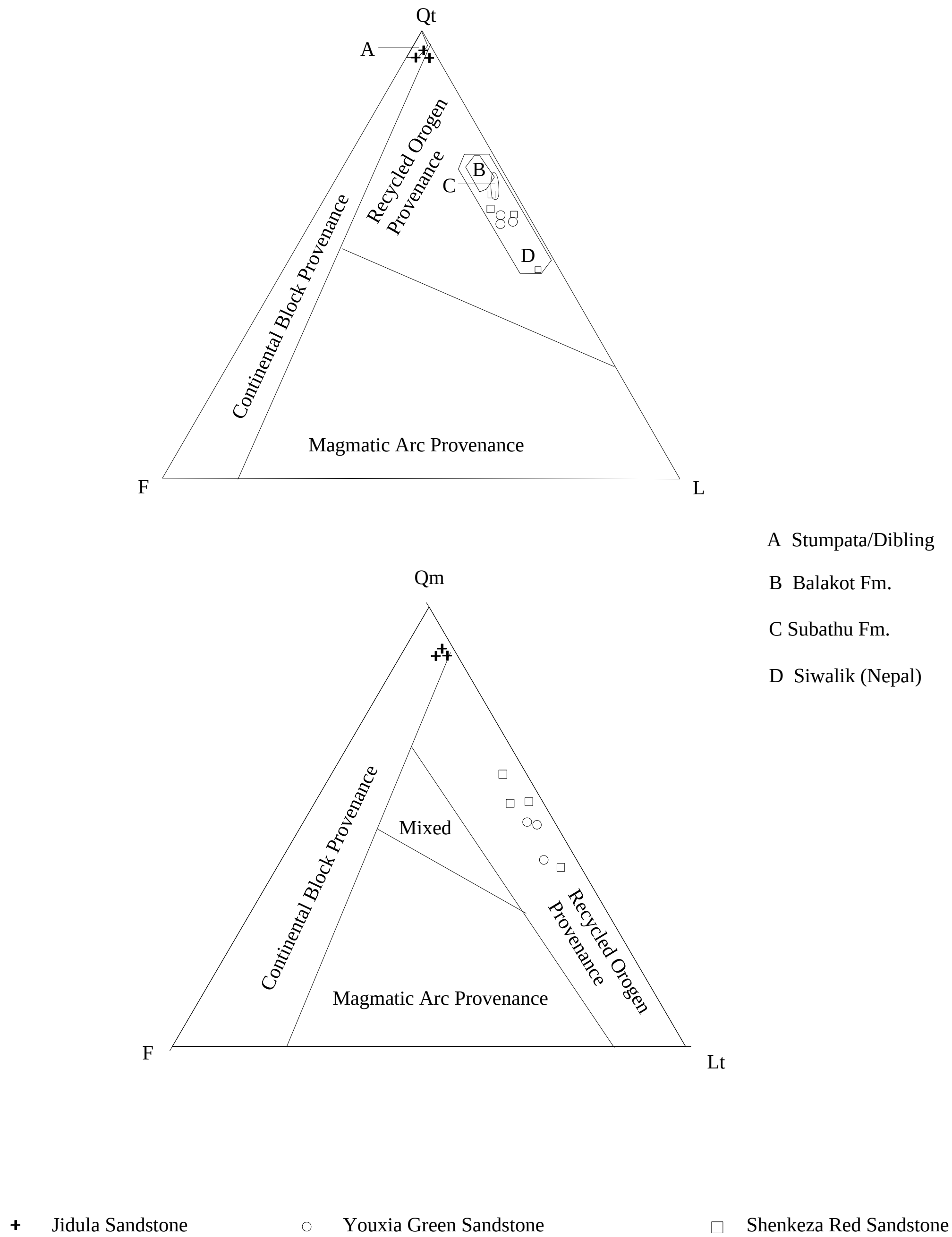

Figure 6.8 Detrital mode plot of lower Tertiary sandstones in the Tingri region Tectonic fields from Dickinson, 1985. Fields of other related Himalayan sandstones shown are from Garzanti et al. (1996)

Table 6.1. Framework grain mode parameter of sandstones from the lower Tertiary terrigenous clastics in the Tingri region.

Sample	Shen94	Shen88	Shen87	Shen148	Shen145	Shen141	Shen138	Jidula75	Jidula2	Jidula1
M-Quartz	198	242	243	207	197	145	234	302	290	250
P-Quartz	67	37	31	5	22	21	13	10	17	11
Plag	29	22	15	14	24	21	16	0	1	0
K-spar	1	4	3	0	2	0	1	8	3	4
V-lithic	55	56	46	17	26	31	9	0	0	0
M-lithic	24	22	16	5	14	18	5	4	0	2
S-lithic	93	95	126	84	102	125	151	9	9	8
Matrix	27	13	10	99	88	92	62	159	164	204
Mica	2	2	3	1	1	1	5	0	1	0
Opaque	3	3	5	66	23	44	3	7	10	19
Unknown	1	4	2	2	1	2	1	1	5	2
P/F	0.97	0.85	0.83	1.00	0.92	1.00	0.94	0.00	0.25	0.00
Qt	0.57	0.58	0.57	0.64	0.57	0.46	0.58	0.94	0.96	0.95
F	0.06	0.05	0.04	0.04	0.07	0.06	0.04	0.02	0.01	0.01
L	0.37	0.36	0.39	0.32	0.37	0.48	0.38	0.04	0.03	0.03
Qm	0.42	0.51	0.51	0.62	0.51	0.40	0.55	0.91	0.91	0.92
F	0.06	0.05	0.04	0.04	0.07	0.06	0.04	0.02	0.01	0.01
Lt	0.51	0.44	0.46	0.33	0.42	0.54	0.41	0.07	0.08	0.07

Jidula Formation

Well-sorted and subrounded to subangular quartz (> 50%) dominates over lithic fragments (~2%) and feldspar (~1%) in the calcareous sandstones of the Jidula Formation (Figure 6.9). These sandstones contain considerable calcareous matrix (32-36%), and one of them (Jidula 75) has been partially cemented by patchy micritic calcite cement (Figure 6.10). Quartz grains are mostly monocrystalline, and show considerable undulosity and strain lamellae. The lack of any common orientation to the strain shadows suggests that they were strained in the source area. Inclusions of mica, rutile and zircon within quartz are observed. Metamorphic and sedimentary lithics are the major rock fragments (Figure 6.11). No identified volcanic detritus was observed. Feldspar is a minor phase, constituting only ~1% of the total framework grains. K-feldspar with grid-iron twinning is more common than plagioclase in these sandstones. Minor heavy detrital phases include zircon, rutile, tourmaline, and magnetite. No Cr-rich spinel was observed. The dominance of monocrystalline, subangular- to -subrounded quartz grains, the presence of minor potassium feldspar with little to no plagioclase, and the paucity of lithic fragments suggest derivation from cratonic continental sources, rather than a collisional orogenic terrane.

Youxia Formation

Green sandstones in the Youxia Formation are dominated by quartzose grains (monocrystalline and polycrystalline) and lithic fragments, which are often poorly sorted with angular to subangular shapes (Figure 6.12). Well-rounded grains were rarely observed. Although most monocrystalline quartz grains (42-51%) show undulose

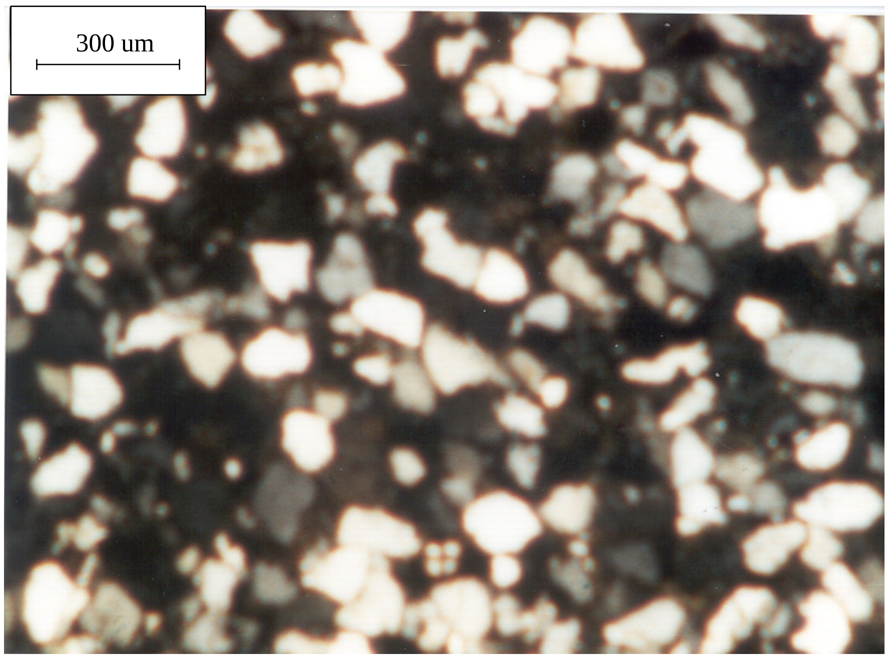

Figure 6.9 Photomicrograph (crossed polars) of quartz-rich sandstone (Jul2) in the Jidula Formation, Gongza section. Note: most quartz grains are well-sorted, unit extinguishing.

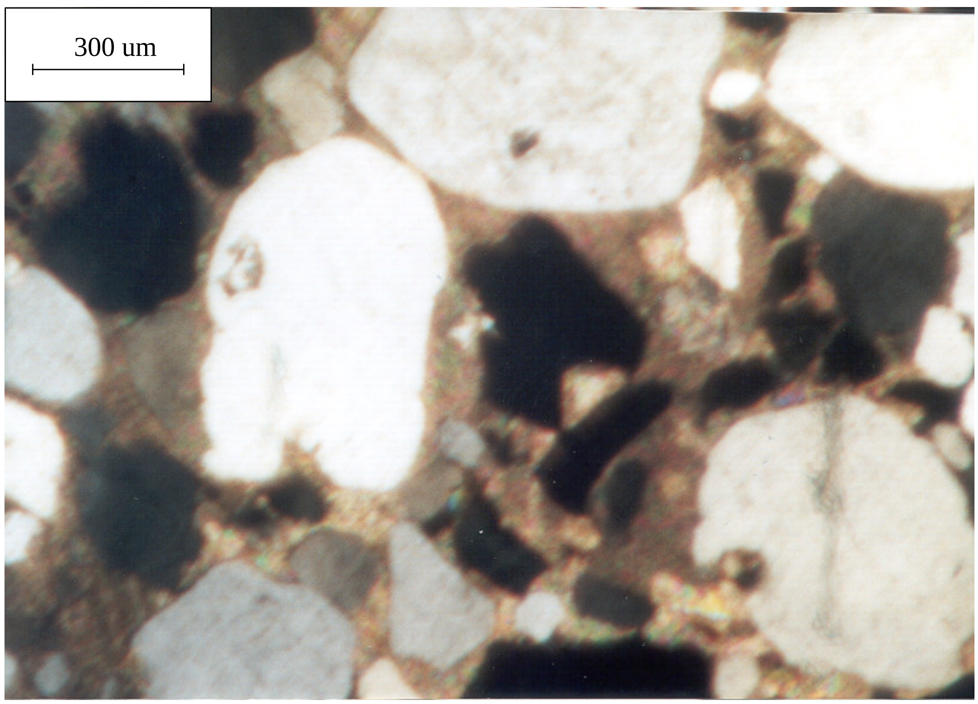

Figure 6.10 Photomicrograph of well-rounded monocrystalline quartz gains with calcite cement in the Jul 75 sandstone of Jidula Formation, Gongza Formation. Opaque minerals are magnetite or ilmenite.

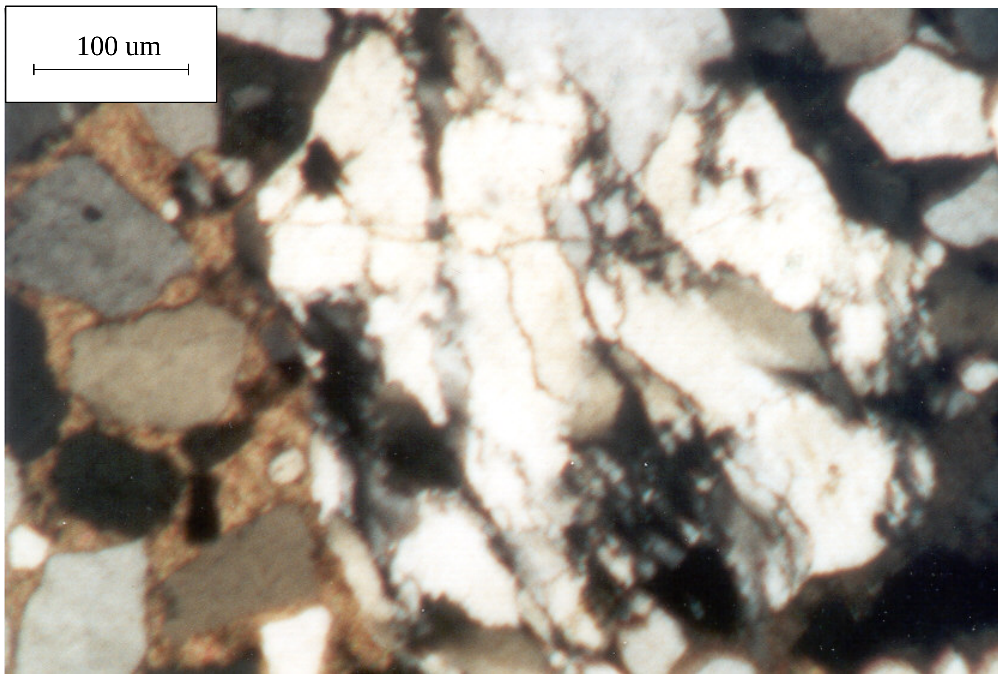

Figure 6.11 Photomicrograph (crossed polars) of a metamorphic rock fragment in Jul 75 sandstone of Jidula Formation, Gongza section.

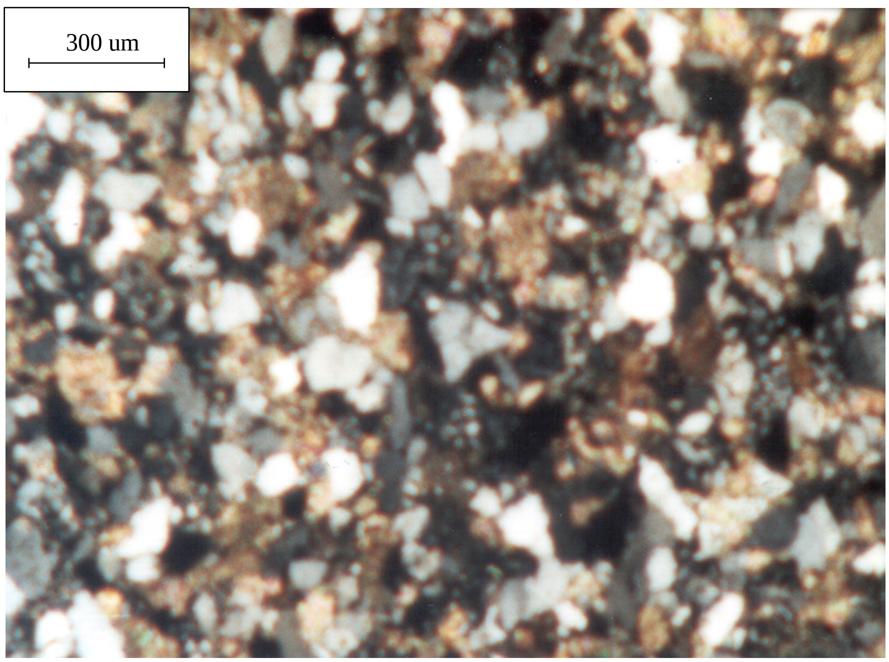

Figure 6.12 Photomicrograph (crossed polars) of lithic-rich sandstone (Shen88) in the Youxia Formation, Shenkeza section. Note most quartz grains are angular in shape.

extinction, a few uniformly extinguishing quartz grains are conspicuously clear, suggestive of a volcanic origin. Lithic fragments are abundant and constitute ~ 38% of total framework grains. Textures indicate that volcanic rock fragments are commonly intermediate or silicic in compositions composed of plagioclase phenocrysts in a fine-grained or aphanitic groundmass (Figure 6.13). Sedimentary lithics are dominantly micritic to sparitic limestone (Figure 6.14) and chert (Figure 6.15) and sporadic siltstone and shale. Quartz-mica aggregates and fine schists are the major constituents of metamorphic lithics. Feldspar (4-6%) is common and plagioclase is the dominant feldspar (Figure 6.16) in the green sandstones, with the ratios of plagioclase to total feldspar >0.83 (Table 6.1). The grains are typically fresh and unaltered, range from large euhedral crystals to subangular broken crystals commonly showing albite-Carlsbad twinning (Figure 6.17). The dominant accessory minerals present within the sandstones include muscovite, chlorite, and opaque minerals (magnetite and Cr-rich spinel) along with less common zircon, apatite, sphene, and rutile.

Shenkeza Formation

The compositions of the upper series of red sandstones (Figure 6.18) in the Shenkeza Formation are similar to the green sandstones, consisting primarily of quartz (42-50%), rock fragments (21-36%), and minor feldspar (~5%) (Figure 6.19). However, the red sandstones are very fine- to fine-grained and contain more than 10% matrix. There is a significantly higher content of opaque minerals (magnetite and Cr-rich spinel) and lower contents of polycrystalline quartz and volcanic lithic compared to the green sandstones.

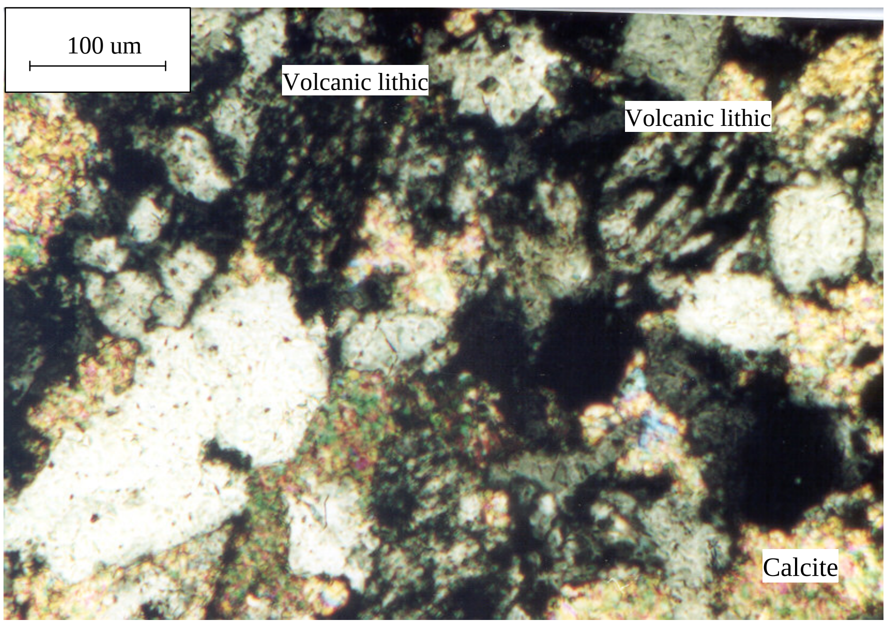

Figure 6.13 Photomicrograph (crossed polars) of volcanic rock fragments in the Shen88 sandstone of the Youxia Formation, Shenkeza section.

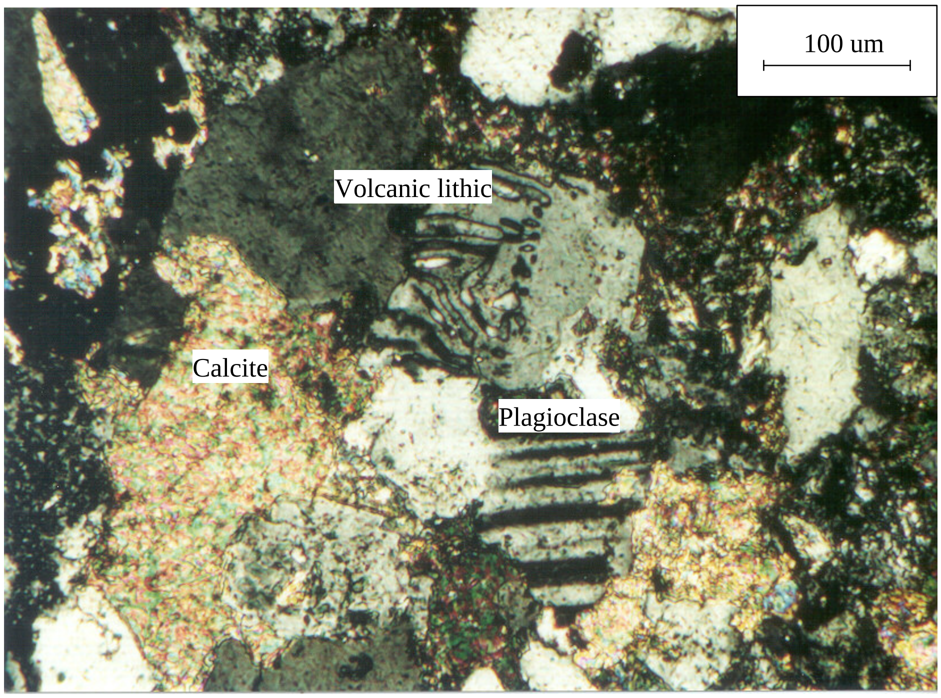

Figure 6.14 Photomicrograph (crossed polars) of Shen94 sandstone in the Youxia Formation, Shenkeza section. Note there are calcite, volcanic lithic and plagioclase grains.

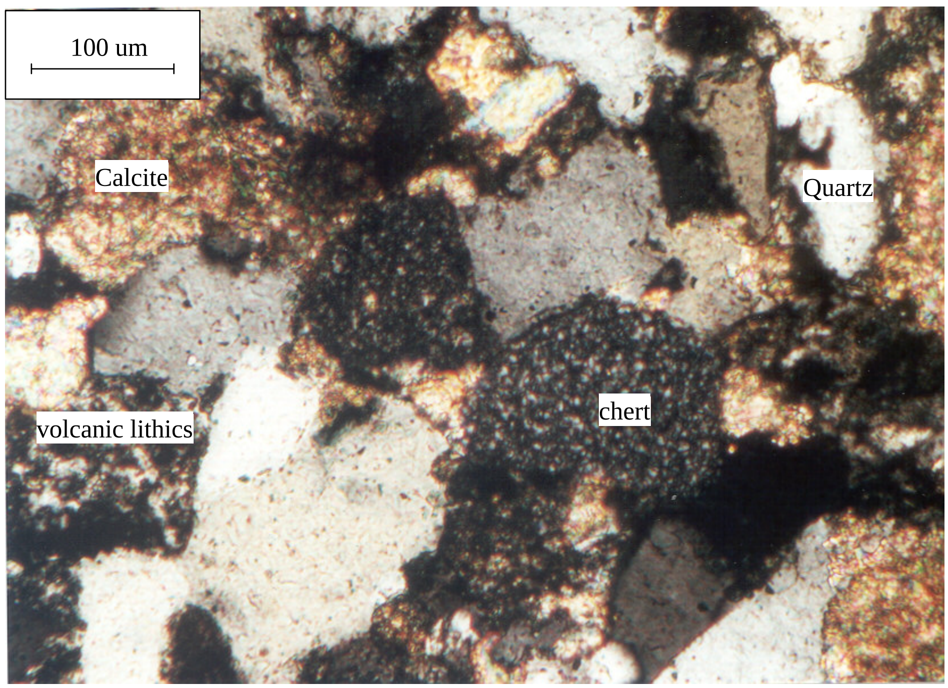

Figure 6.15 Photomicrograph (crossed polars) of volcanic and sedimentary rock fragments in the Shen87 sandstone of the Youxia Formation, Shenkeza section.

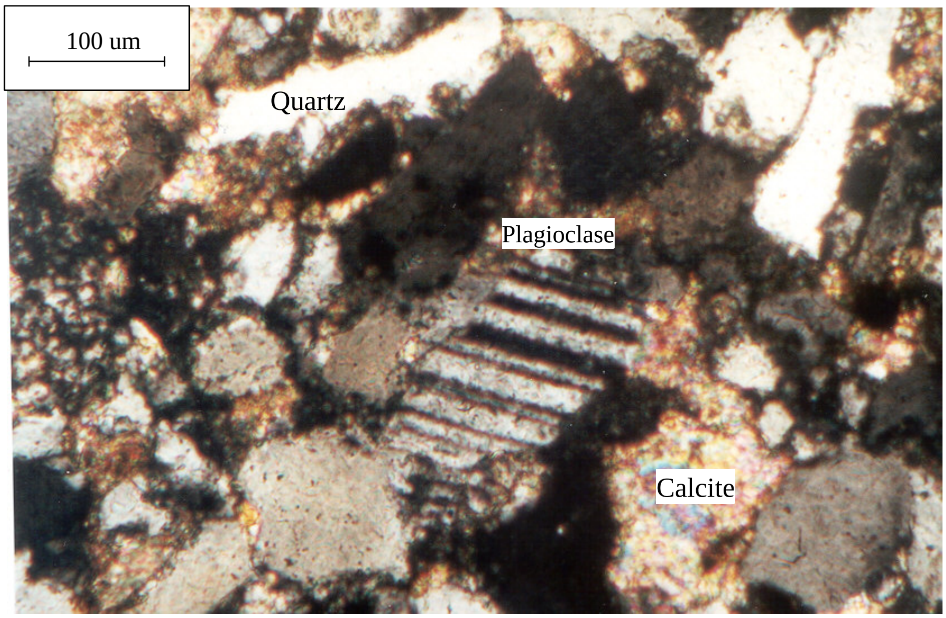

Figure 6.16 Photomicrograph (crossed polars) of a plagioclase grain in the Shen94 sandstone of the Youxia Formation, Shenkeza section.

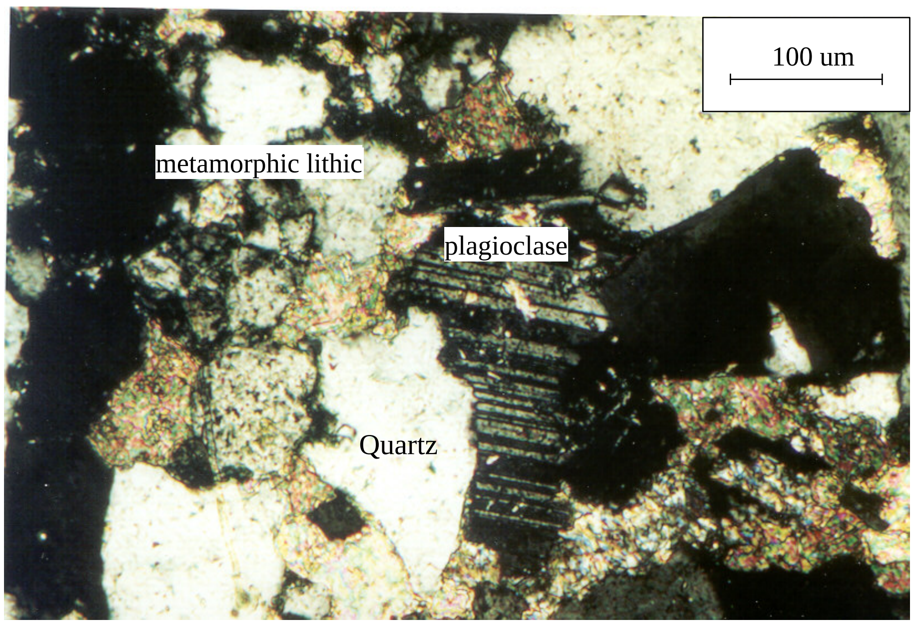

Figure 6.17 Photomicrograph (crossed polars) of a broken plagioclase and a metamorphic rock fragment in Shen88 sandstone of the Youxia Formation, Shenkeza section.

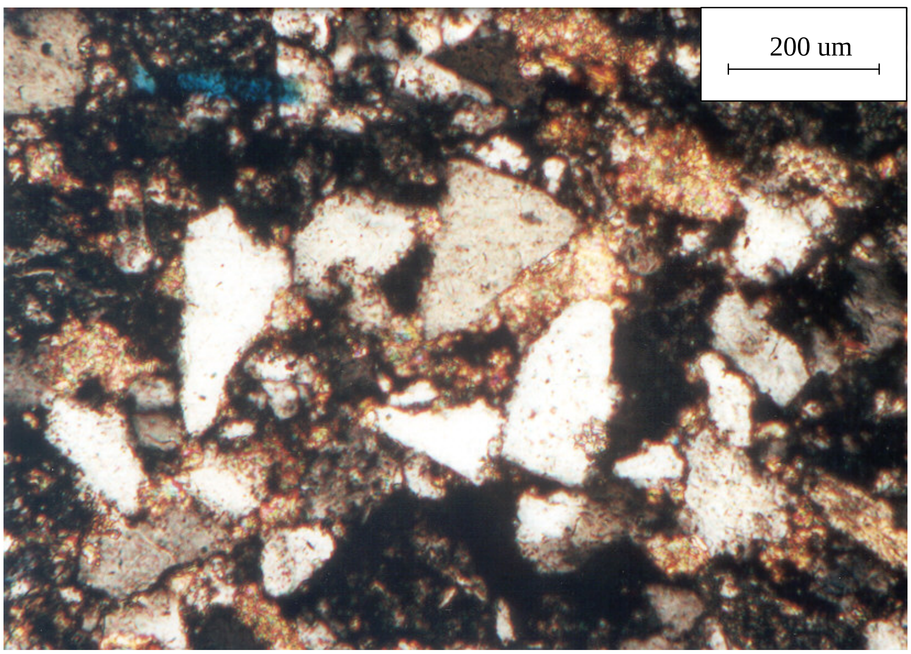

Figure 6.18 Photomicrograph (crossed polars) of angular-subangular greywackes (Shen145) of Shenkeza Formation, Shenkeza section.

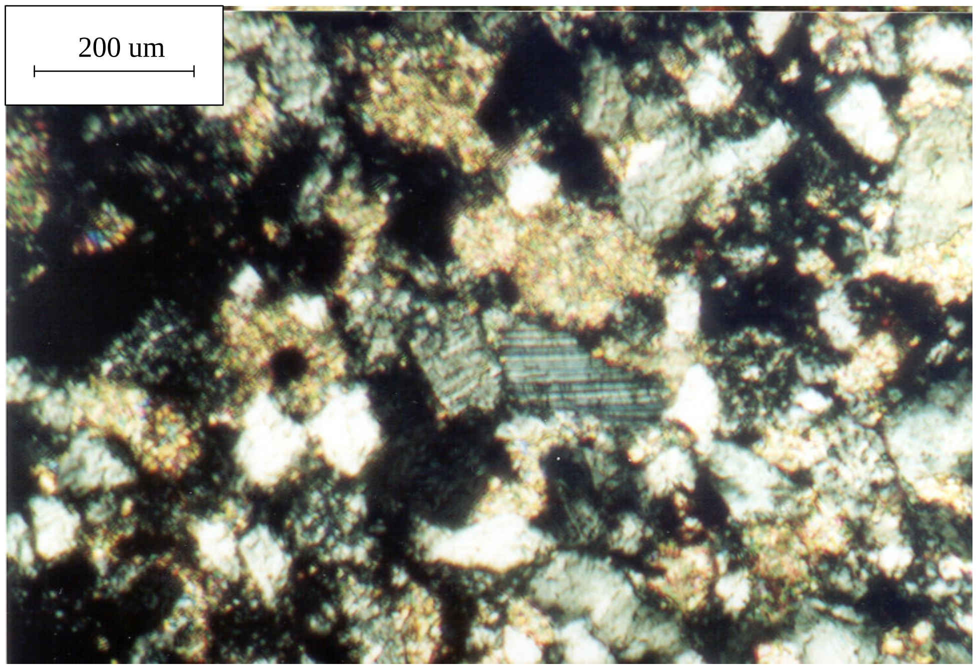

Figure 6.19 Photomicrograph (crossed polars) of angular quartz grains and a plagioclase in the Shen148 sandstone of Shenkeza Formation, Shenkeza section.

Interpretation of sandstone modes

The compositions of sandstones in the Jidula Formation are dominantly monocrystalline quartz with minor rock fragments while those in the Youxia and Shenkeza Formations are dominantly rock fragments, some of which are volcanic. The preservation of unaltered and euhedral plagioclase in the Youxia and Shenkeza sandstones suggests rapid erosion, transportation, and burial of these sandstones. These differences indicate a significant provenance-change during the deposition of lower Tertiary clastics in the Tingri region. In order to visualize the variations in sand composition and help to interpret the tectonic provenance of these sandstones, the relative contents of quartz, feldspar, and rock fragment have been plotted on the Q_tFL and $QmFL_t$ ternary diagrams (Figure 6.8) with the fields for the tectonic settings of Dickinson et al. (1983).

These figures illustrate that the quartz-rich, lithic-poor Jidula sandstones (Q_t=94-96, F=1-2, L=3-4) plot at the boundary of the continental block and recycled orogen provinces on the Q_tFL diagram, and in the continental block province (Q_m=91-92, F=1-2, L=7-8) on the Q_mFL_t diagram; while the relatively quartz-poor, lithic-rich Youxia and Shenkeza sandstones plot in the recycled orogenic provenance (Q_t=46-64, F=4-7, L=32-48, Q_m=40-62, F=4-7, L_t=33-54). According to Dickinson et al. (1983), sediment sources of the continental block are derived either from stable shields and platform or from areas of active uplift within continents, while those of the recycled orogen are mainly from sedimentary strata and subordinate volcanic rocks exposed to erosion by the orogenic uplift of fold and thrust belts. The fact that all Jidula sandstones plot in the continental block area on Q_mFL_t plot suggests that they were most likely derived from an ultimate source exclusively of a cratonic interior, consistent with the common presence of an ultra-stable dense mineral assemblage (zircon, rutile, and tourmaline). In contrast, abundant volcanic rock fragments and the presence of Cr-rich spinel in the Youxia and Shenkeza sandstones point to a volcanic setting. They consistently plot in the recycled orogen areas on the Q_mFL_t plot. It is thus likely that this abrupt provenance change was related to the arrival of the subduction complex of the Trans-Himalayas arc-trench system near the Tingri region by the end of the deposition of the Zhepure Shan limestones.

In summary, detailed petrographical studies indicate that there is a clear change in clastic provenance between the times of deposition of the Jidula and Youxia formations. The high proportion of quartz and the dominance of alkali feldspar over the more chemically unstable plagioclase in the Jidula Formation support a cratonic source. The noteworthy influx of abundant immature detritus in the Youxia Formation appears to be the first harbinger of synorogenic foreland-basin deposition of the India-Asia collision in the Tingri region.

Sandstone geochemistry

Studies (Bhatia and Crook, 1986; Cullers et al., 1988; McLennan et al., 1985, 1990, 1993) have shown that certain trace elements (e.g., Zr, Sc, Nb, Ga) are virtually insoluble during weathering, erosion, and transport. These elements are transported nearly quantitatively from sources in various tectonic settings into terrigenous clastic sediments. A few ratios of major oxides are also relatively constant from source to sink (Bhatia, 1983, 1985; Roser and Korsch, 1988; Hayashi et al., 1997; Rahman and Faupl, 2003). Accordingly, whole-rock geochemical compositions of sedimentary rocks bear a relationship to the composition of the source rocks and have often been used successfully to constrain the specific tectonic environments. Given the fact that the less resistant phases are labile and modified with burial and metamorphism (Morton, 1991), the study of geochemical compositions of clastic sediments compliments detrital modal analyses.

Geochemical analysis (Table 6.2) of the shales and sandstones from the Jidula, Youxia and Shenkeza formations has been conducted at the GeoAnalytical Laboratory of Washington State University using X-ray fluorescence (XRF) and inductively coupled plasma mass spectrometry (ICP-MS) techniques. Detailed analytical methods are given in Johnson et al. (1999) and Knaack et al. (1994), respectively. The precision was assessed through repeat analyses of samples: errors for major elements vary between 1 and 2% of the amount present. Accuracy of the trace elements and REE analyses is within 5%. All analyses discussed in this paper have been recalculated to 100% loss on a volatile-free basis.

Major elements

The effect of weathering processes on sedimentary rocks can be assessed using the chemical index of alteration (CIA, Nesbitt & Young 1982). The CIA is defined as molecular proportions: $CIA=100*Al_2O_3/(Al_2O_3+CaO*+Na_2O+K_2O)$ where CaO* is CaO in silicate minerals, as opposed to carbonates or phosphates. Details of CaO correction for bulk-rock chemistry are given by McLennan (1993). The CIA has been used to quantify the weathering history of sedimentary rocks (e.g., McLennan et al., 1993; Bock et al., 1998; Young et al., 1998, 2002). Sandstones of Jidula Fm. have higher CIA values than those of the Youxia and Shenkeza Fm., which indicates a greater weathering history or incorporation of material from mature sediments that had been through an earlier weathering cycle for the Jidula Fm. (Table 6.2). The Youxia and Shenkeza sandstones have the lowest CIA values (53-54), which are close to values of ~50 characteristic of fresh granites and rhyolites. This suggests a limited chemical weathering environment for the Youxia and Shenkeza Fm., which is consistent with the observations of feldspar grains, especially less stable plagioclase, and abundant rock fragments in the thin-sections. In the ternary plot of Al_2O_3-(CaO^*+Na_2O)-K_2O (Figure 6.20), three analyses of the Jidula sandstones display a range of CIA values (measured by height on the triangle) from about 54 to 77 and follow a linear trend parallel to the Al_2O_3-(CaO^*+Na_2O) join, which would be expected by exclusively weathering processes (Nesbitt and Young, 1982). However, four analyses in the Youxia and Shenkeza Fm. do not follow this linear trend of the Jidula Fm., neither parallel to the Al_2O_3-(CaO^*+Na_2O) join, suggesting the mixing of provenance components from different source area assemblages (McLennan et al., 1993).

Detrital sediments from the Youxia and Shenkeza Formations define a linear trend on a SiO_2-Al_2O_3 graph (Figure 6.21a), with shales of the Youxia Fm. containing lower SiO_2 and corresponding higher Al_2O_3. Three analyses in the Jidula Formation do not follow this linear trend, which may be indicative of a different provenance. In particular, Jidula75 and Jidula2 have significantly higher SiO_2/Al_2O_3 ratios (16 and 76, respectively)

Table 6.2 Geochemical analyses of the lower Tertiary terrigenous clastics in the Tingri region

	Shen95 shale	Shen90 shale	Shen148 sand	Shen94 sand	JUL2 silt	JUL2 silt	JUL75 sand
SiO_2	63.73	63.86	71.69	77.36	43.49	87.12	74.11
Al_2O_3	17.57	16.62	11.24	9.08	7.34	5.38	0.98
TiO_2	0.87	0.88	0.66	0.44	1.59	1.15	0.51
FeO*	7.73	6.73	3.20	3.05	4.74	4.37	1.18
MnO	0.16	0.16	0.31	0.16	0.07	0.01	0.02
CaO	3.39	5.04	7.48	5.45	38.27	0.21	22.24
MgO	2.56	2.67	1.71	1.40	1.61	0.54	0.28
K_2O	2.68	2.77	0.61	0.61	1.32	0.75	0.19
Na_2O	1.02	0.97	2.74	2.27	1.16	0.29	0.20
P_2O_5	0.14	0.15	0.12	0.09	0.16	0.05	0.02
LOI (%)	8.08	8.65	7.89	5.64	23.71	1.88	14.06
total	99.86	99.86	99.75	99.92	99.74	99.88	99.72
Al_2O_3/TiO_2	20.09	18.91	16.91	20.71	4.61	4.67	1.91
CIA	0.735	0.727	0.538	0.526	0.581	0.768	0.541
Ni	75	68	36	26	12	20	0
Cr	107	116	89	68	108	84	26
V	142	138	58	32	98	118	11
Zr	172	185	282	228	377	567	444
Ga	21	20	11	9	8	8	4
Cu	51	44	91	14	2	6	0
Zn	108	100	57	40	58	35	4
La	31.02	29.85	26.03	18.11	26.77	29.09	16.26
Ce	61.21	59.00	50.26	34.89	53.21	61.08	32.44
Pr	6.56	6.36	5.54	3.92	6.13	6.55	3.65
Nd	25.96	25.16	22.51	15.76	25.83	26.20	14.54
Sm	5.73	5.71	5.29	3.80	5.50	5.32	2.87
Eu	1.38	1.35	1.20	0.99	1.62	1.21	0.68
Gd	5.07	4.97	4.71	3.68	4.63	4.15	2.09
Tb	0.81	0.81	0.76	0.60	0.67	0.64	0.30
Dy	4.88	4.79	4.48	3.41	3.72	3.69	1.62
Ho	0.95	0.94	0.87	0.66	0.70	0.69	0.31
Er	2.57	2.54	2.39	1.83	1.74	1.95	0.82
Yb	2.38	2.33	2.23	1.67	1.46	1.72	0.77
Lu	0.36	0.35	0.35	0.26	0.22	0.27	0.12
Ba	198	202	1372	125	243	132	53
Th	12	10	9	6	5	9	4
Nb	13	12	10	7	16	18	7
Y	25	25	25	18	20	17	8
Hf	4.43	4.71	6.73	5.37	7.27	13.27	8.29
Ta	1.02	0.94	0.81	0.55	1.07	1.24	0.50
Pb	19	14	10	4	6	9	3
Rb	109	102	24	23	26	18	3
Cs	7.54	6.79	1.58	1.41	0.71	0.43	0.14
Sr	165	137	136	123	1143	59	1699
Sc	19.6	18.3	9.2	6.0	7.5	7.4	1.5
Tm	0.38	0.37	0.35	0.27	0.24	0.29	0.13
La/Sc	1.58	1.63	2.84	3.02	3.57	3.94	11.21
Nb/Y	0.49	0.48	0.41	0.35	0.80	1.02	0.90
LREE/HREE	7.7	7.5	6.9	6.3	8.9	9.8	11.6
Lan/Ybn	8.81	8.67	7.89	7.31	12.36	11.42	14.34
Eu/Eu*	0.78	0.78	0.74	0.81	0.98	0.79	0.85
Gdn/Ybn	1.73	1.73	1.71	1.78	2.57	1.95	2.21

Note: Total iron expressed as FeO.

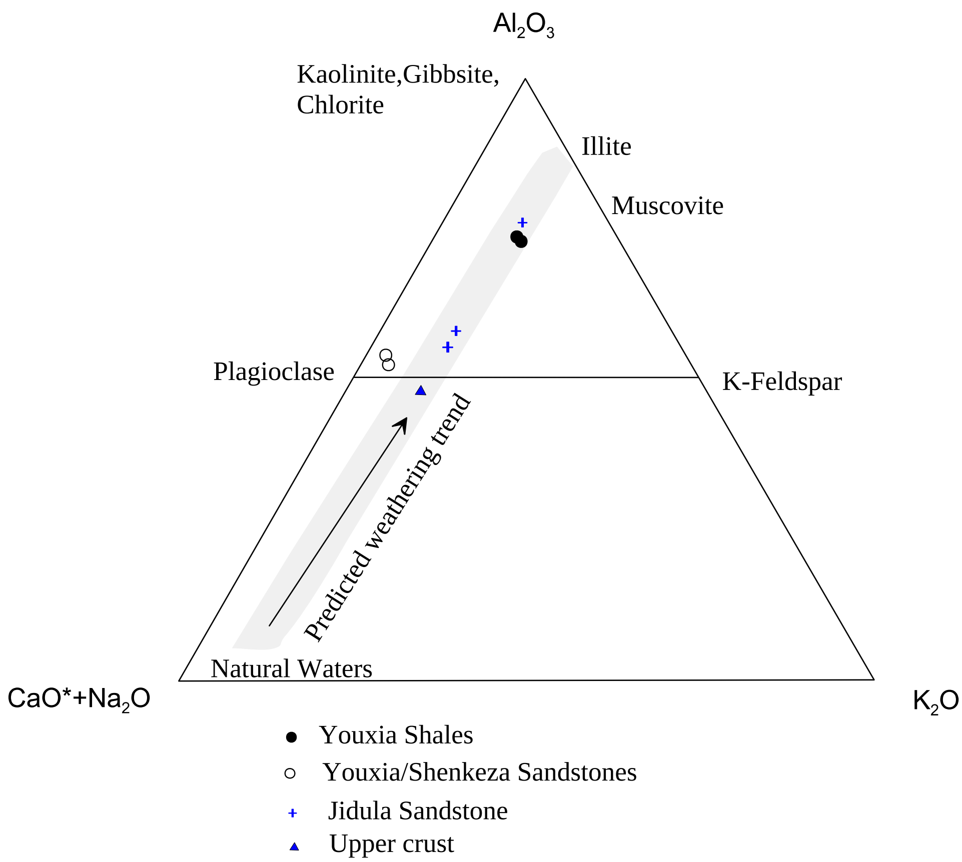

Figure 6.20 CIA ternary plot of lower Tertiary clastics in the Tingri region. Modified after Bock et al. (1998). The enrichment in Al_2O_3 and depletion of $CaO+Na_2O+K_2O$ on this plot reflects the degree of chemical weathering to which the materials have been subjected. Three analyses of the Jidula Fm. defined a linear trend encompassed in the predicted weathering trend for the average upper crustal composition while those of the Youxia Fm. do not follow the predicted weathering trend, indicating processes in addition to the weathering have affected the Youxia sediments.

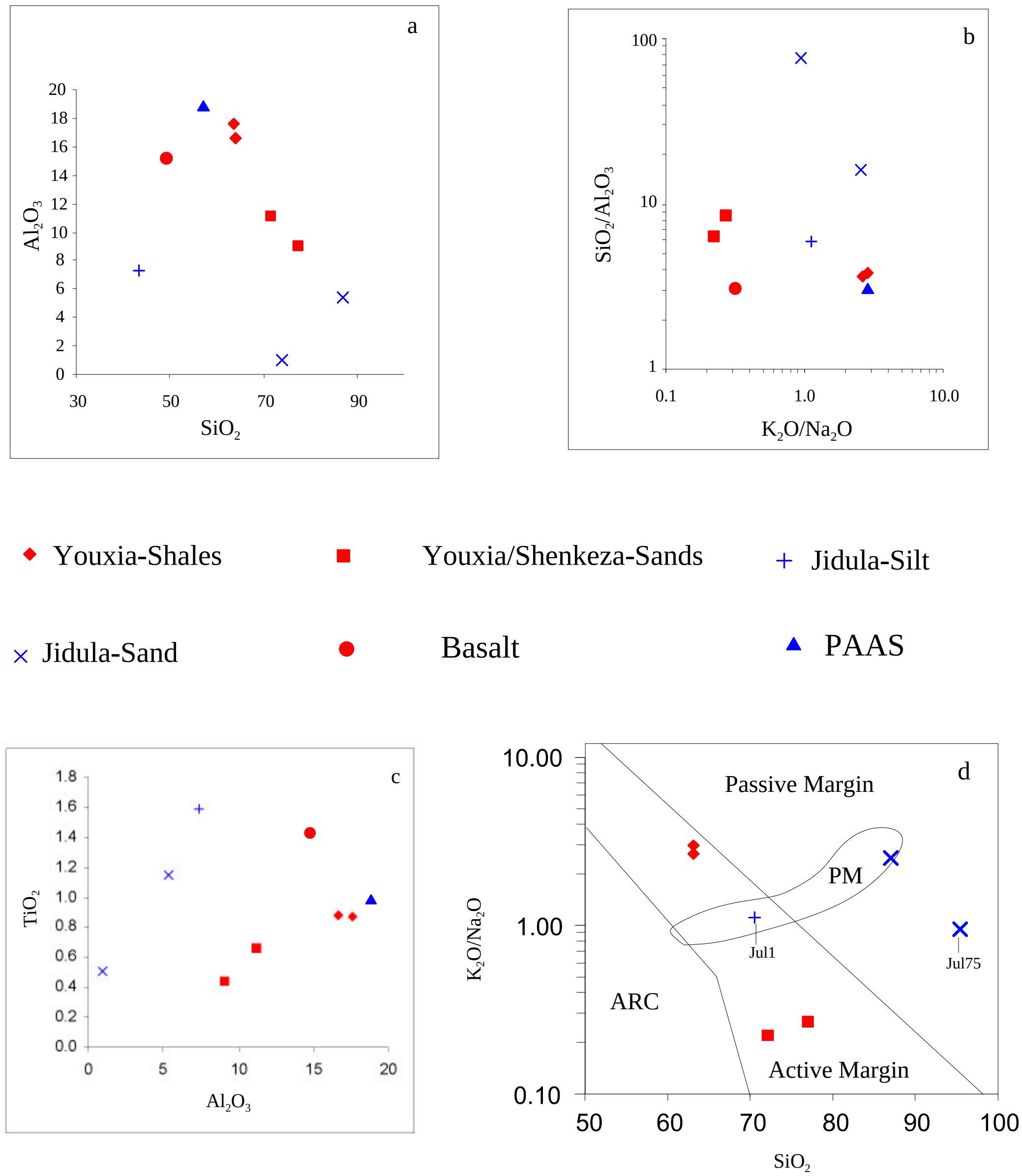

Figure 6.21 Geochemical plot of the lower Tertiary clastics in the Tingri region. a. Al_2O_3 vs. SiO_2 plot; b. SiO_2/Al_2O_3 vs. K_2O/Na_2O plot; c. Al_2O_3 vs. TiO_2 plot; d. K_2O/Na_2O vs. SiO_2 plot. Tectonic setting fields are from Roser and Korsch (1986) for Figure 6.21 d and PM is passive margin field from McLennan et al. (1990). Note in Fig 6.21d, Jul1 and Jul75 are recalcualted to 100% CaO and volatile-free because of signifcantly high CaO contents. PAAS from Taylor and McLennan (1985), basalt from Condie (1993).

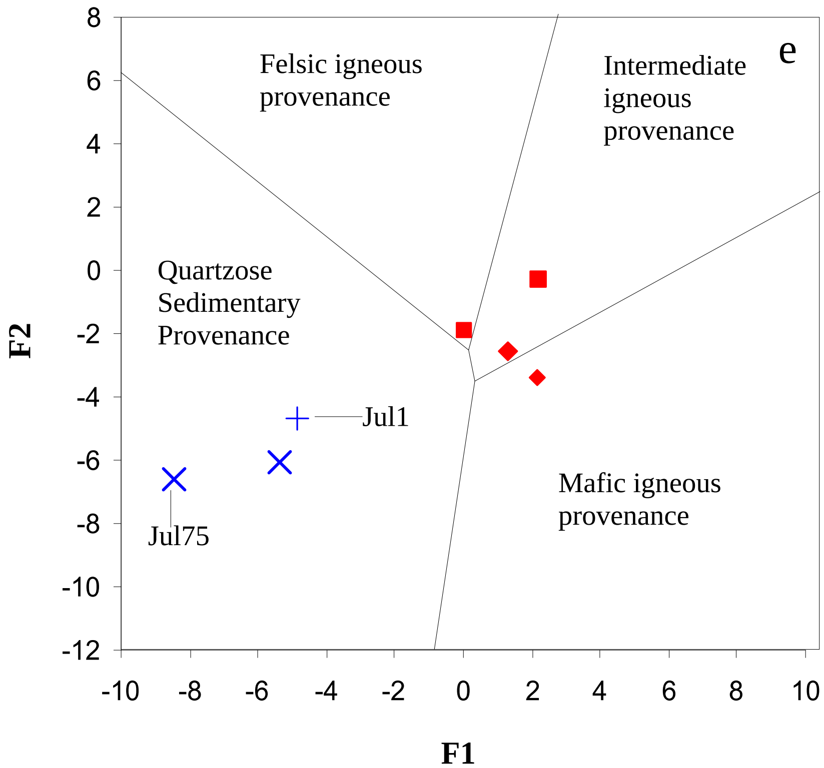

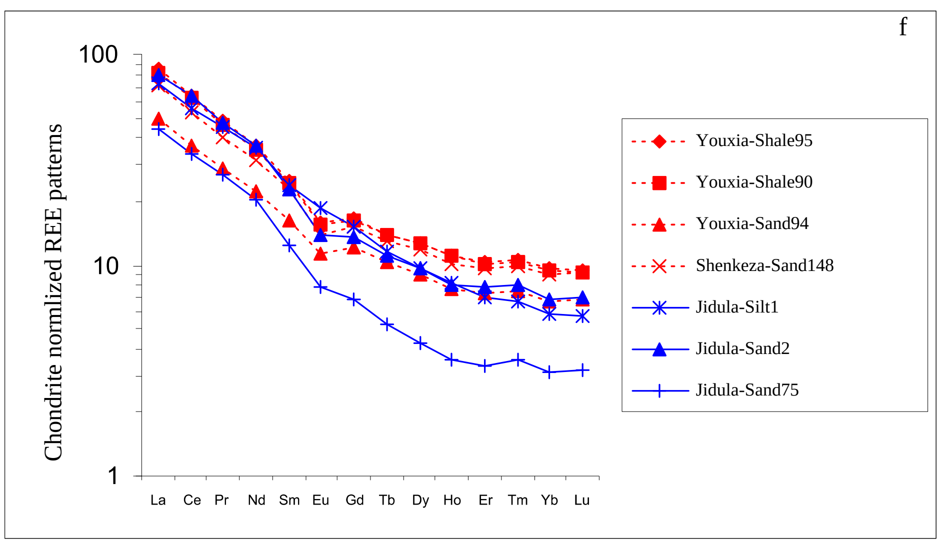

Figure 6.21(continued). Geochemical plot of the lower Tertiary clastics in the Tingri region. e. Provenance discrimination diagram; f.Chondrite-normalized REE patterns, chondritic values are those of Taylor and McLennan (1985). Tectonic setting fields are from Roser and Korsch (1988) for Figure 6.21e. Note in Figure 6.21e, Jul1 and Jul75 are recalculated to 100% CaO and volatile-free because of signficantly high CaO contents.

than those from the Youxia and Shenkeza sandstones (6 and 9, respectively) (Figure 6.21b). This may be explained by the textural maturity in the Jidula sandstones, and confirms that quartz is significantly more abundant than primary clay-sized material and labile framework grains (plagioclase and rock fragments) in these quartzose sandstones, resulting in an elevation of the SiO_2/Al_2O_3 ratio (McLennan et al., 1993). The K_2O/Na_2O ratios of the Youxia and Shenkeza sandstones (0.22 and 0.27) are significantly different from those of the Jidula sandstones (2.59 and 0.95) (Figure 6.21b). Considering that sands from volcanically active setting commonly have K_2O/Na_2O <1, whereas sands from a passive margin exhibit ratios > 1 (McLennan et al., 1990), it is concluded that there is a significant provenance change between the sandstones of the Jidula and Youxia Formations. The relative enrichments of Mg, Mn, Ni and V in the Youxia and Shenkeza sandstones compared to those in the Jidula Fm. also suggest that there was a mafic/ultramafic component in the source, such as that associated with ophiolite-obduction events (Bock et al., 1998; McLennan et al., 1990). This is in agreement with the observations described above: well-sorted and subrounded-subangular quartz is the primary framework grain in the Jidula sandstones whereas there are significant amounts labile rock fragments in the Youxia and Shenkeza sandstones. Two samples (Jul1 and Jul75) with high CaO and Sr abundances contain large amounts calcareous matrix and calcite grains as evidence in thin-section.

The Jidula and Youxia and Shenkeza Formations define two linear trends in the Al_2O_3 vs. TiO_2 plot (Figure 6.21c). The Jidula Formation has Al_2O_3/TiO_2<5 whereas the ratios of the Youxia and Shenkeza Formations vary from 16.9 to 20.7. The relatively constant Al_2O_3/TiO_2 ratios in the Youxia and Shenkeza Formations confirm that the fractionation of Al and Ti is minimal between associated sandstones and shales/mudstones (Hayashi et al., 1997; Rahman and Faupl, 2003). Hayashi et al. (1997) suggested that the Al_2O_3/TiO_2 ratio of a sedimentary rock would be essentially the same as that of its source rock, and may be used as a provenance indicator. If this is the case, the ratios of Al_2O_3/TiO_2 in the Youxia and Shenkeza Formations (16.9-20.7) are comparable to those for intermediate igneous rocks (Holland, 1984). Representative geochemical analyses for the Xigaze ophiolite show Al_2O_3/TiO_2 ratios mostly between 16.6 and 21.5 (Pearce and Deng, 1988), and the sandstones in the Xigaze fore-arc basin have similar Al_2O_3/TiO_2 ratios (typically ~18; Durr, 1996), so it is likely that both the Xigaze group and the Youxia and Shenkeza Formations have a common source rock, that is, the Gangdese andesitic arc to the north. The lower Al_2O_3/TiO_2 ratios in the Jidula Formation point to a different provenance; relatively low Al abundances may reflect a combination of weathering and reworking, and a greater level of recycling has eliminated most labile detrital minerals with high Al contents. Accordingly, the Jidula Formation was likely derived from a cratonic interior, specifically the Indian continent to the south.

Trace elements

Certain trace elements (e.g., Zr, Th, Sc, Nb, Ga) and REE are considered to be essentially constant in abundance because of their relatively low solubilities during weathering and low residence time in seawater (Bhatia and Crook, 1986; Cullers et al., 1988; McLennan et al., 1985, 1990, 1993). They are transferred quantitatively into terrigenous sediments during sedimentation, and record the signature of parent materials (Bhatia and Crook, 1986; McLennan et al., 1985, 1990).

Zr contents in the Jidula Formation rocks (377-567 ppm) are consistently higher than those in the Youxia and Shenkeza Formations (172-282 ppm). As Zr typically resides in zircon, high Zr abundance generally points to the significant presence of zircon grains (Hiscott, 1984), which is a common heavy mineral in most mature sands derived from the old continental rocks. This is consistent with the observation of a significant amount of zircon in the Jidula sandstones, and only rare zircon grains in the Youxia and Shenkeza sandstones. Cu contents in the Jidula Formation (0-6 ppm) are significantly less than those in the Youxia and Shenkeza Formations (14-91 ppm). Since Cu is generally found in sulfide minerals, commonly present in volcanic rocks (Hiscott, 1984), the relatively enrichments of Cu in the Youxia and Shenkeza Formations provides further support for the presence of significant amounts of volcanic lithologies in the source area.

In the chondrite-normalized REE diagram (Figure 6.21f), the Jidula Formation has light REE (LREE) enriched and heavy REE (HREE) depleted patterns (LREE/HREE from 8.9 to 11.6, La_n/Yb_n=11.42-14.34). Eu/Eu* values range from 0.79 to 0.98, which may by themselves suggest a source from undifferentiated arc or differentiated arc (McLennan, et al., 1990, 1993) due to the lack of Eu anomalies. However, abundant zircon indicated by high Zr (Zr=377-567 ppm) and low total REE abundances in the Jidula Formation may have significantly affected the chondrite-normalized REE patterns (Taylor and McLennan, 1985). Based on other geochemical and petrologic data presented, it is considered very unlikely that the Jidula Formation was derived from a volcanic arc. In contrast, chondrite-normalized REE distribution patterns of the Youxia and Shenkeza Formations show LREE enrichment trends with slightly depleted HREE (LREE/HREE=6.3-7.7, La_n/Yb_n=7.3-8.8) and slightly negative Eu anomalies

(Eu/Eu*=0.74-0.81). These features, coupled with different La/Sc, Nb/Y, Gd_n/Yb_n ratios, and Hf, Cs abundances (1.6-3.0, 0.4-0.5, 1.7-1.8, 4.4-6.7 ppm, 1.4-7.5 ppm in the Youxia and Shenkeza Formations, 3.6-11.2, 0.8-1.0, 2.0-2.6, 7.3-13.3 ppm, 0.1-0.7 ppm in the Jidula Formation, respectively), suggest a significant provenance change between the sandstones of the Jidula and Youxia and Shenkeza Formations. The close similarity in the average La/Sc, La_n/Yb_n, Eu/Eu* and total LREE/HREE ratios of the Youxia and Shenkeza Formations to the continental island arc values (Bhatia, 1985, 1986) supports the above inference and suggests a source from andesitic-felsic volcanic rocks within a continental island-arc tectonic setting for the Eocene clastic rocks in the Tingri region.

Geochemical discrimination of tectonic environment

In the K_2O/Na_2O-SiO_2 discrimination diagram (Roser and Korsch, 1986), four analyses of the Youxia and Shenkeza Formations fall into the active continental margin (Figure 6.21d). Jidula2 plots in the passive margin, while Jidula75 plots very close to the boundary of active/passive margins and Jidula1 not in the fields of this plot. However Jidula1 and Jidula75 contain unusually high CaO (22.24%, 38.27%, respectively), which appears to have lowered the analytical contents of SiO_2. Recalculated values on the CaO, LOI-free basis fall into the passive margin field for Jidula75, close to the boundary of active/passive margins for Jidula1. Our inference from the data suggests that the Jidula Formation was most likely deposited at a passive continental margin, while the Youxia and Shenkeza Formations were derived from erosion from an active continental margin.

Using major oxides as variables, the discriminant functions of Roser and Korsch (1988) were designed to distinguish between sediments from four provenances: mafic, intermediate and felsic igneous rocks, and quartzose sedimentary materials. Four analyses from the Youxia and Shenkeza Formations plot in the mafic-felsic igneous provenances and Jidula 2 with typical CaO content in the quartzose sedimentary provenance (Figure 6.21e). Recalculated values on the CaO, LOI-free basis of two analyses with high CaO contents from the Jidula Formation (Jidula1 and Jidula75) also plot in the quartzose sedimentary provenance.

Bhatia and Crook (1986) developed a series of discriminant diagrams based on trace element ratios from Paleozoic sandstones to allow distinction between oceanic island arc, continental island arc, active continental margin, and passive continental margin environments of deposition. On the Th-Sc-La and Th-Sc-Zr/10 ternary diagrams (Figure 6.22), the Youxia and Shenkeza Formations consistently fall in the field of continental island arcs, indicating there was a significant volcanic arc source for the Youxia and Shenkeza clastic sediments. The Jidula Formation samples plot close to, or within the passive margin field (Figure 6.22).

In summary, geochemical and petrographic data are broadly consistent with the interpretations that the Jidula Formation is dominated by mature, cratonic detritus deposited on the Indian passive margin. The relatively enriched elements (Mg, Mn, Ni and V), and high Cu and Al_2O_3/TiO_2 values in the Youxia and Shenkeza sandstones indicate a volcanic arc provenance, most likely derived from andesitic-felsic volcanic rocks in a continental island-arc tectonic setting.

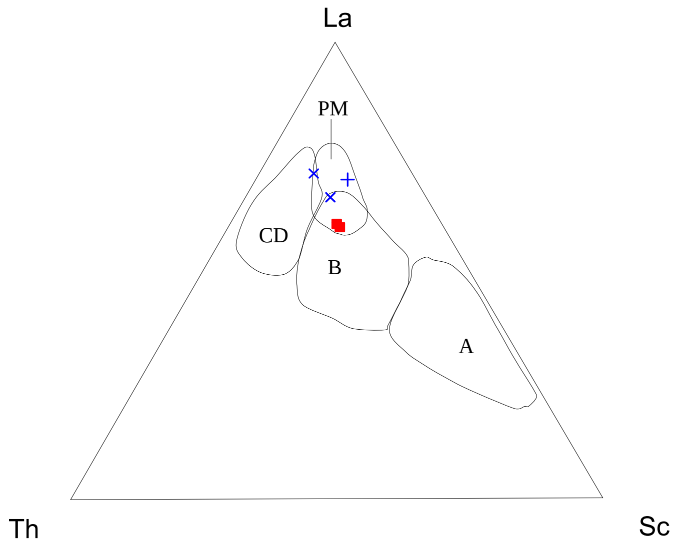

a

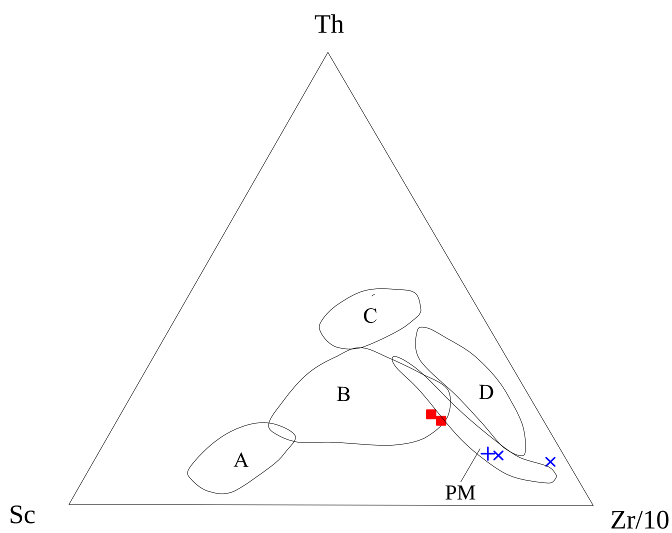

b

Figure 6.22 Tectonic discrimination plots from Bhatia and Crook (1986): a. La-Th-Sc ternary plot; b. Th-Sc-Zr/10 ternary plot. Fields are A-oceanic island arc, B-continental island arc, C-active continental margin, D-passive margin. PM is the Passive margin field from McLennan et al. (1990).

Chemical compositions of Cr-rich spinel

A large number of heavy mineral species with specific gravity >2.80 occur in sandstones, many of which are source-diagnostic (Morton, 1985, 1991; Mange and Maurer, 1992; Evans and Mange, 1991). In particular, chromium-rich spinel is unique in terms of occurrence and tectonic significance because its composition is sensitive to chemical history of the magma from which it was derived (Irvine, 1974; Roeder, 1994). The presence of Cr-rich spinels in sedimentary rocks of a basin in, and adjacent to an orogenic belt is generally interpreted as an indicator of a mantle source from ophiolitic basement (Ganssloser, 1999; Pober et al., 1988; Cookenboo et al., 1997; Lee, 1999). As such, the recognition of Cr-rich spinels has potential for constraining the tectonic setting of sedimentary basins (Garzanti et al., 1987; Bossart and Ottiger, 1989; Arai and Okada, 1991; Hisada and Arai, 1993; Najman and Garzanti, 2000; Wang et al., 2000; Barnes and Roeder, 2001; Kamenetsky et al., 2001). From petrographic work described above, dark brown to dark reddish-brown spinels were found in the Youxia and Shenkeza sandstones, but not in the Jidula sandstones. This is, to the best of our knowledge, the first report of detrital spinels found in the early Tertiary sandstones in southern Tibet. Heavy mineral separation and microprobe analyses were conducted on these spinels to provide additional constraints on the tectonic setting of the source area of the Youxia and Shenkeza Formations. Details of sample preparation and analytical methods used are given in Zhu et al. (in review).

The microprobe analyses of detrital spinels from the Youxia and Shenkeza sandstones are shown in Table 6.3. There is an inverse relationship between Cr and Al contents (Figure 6.23a), which may be indicative of different degrees of partial melting in the mantle (Dick and Bullen, 1984). Spinel grains show no obvious signs of zoning in line scans. This suggests that (1) parental lavas had undergone little or no magma mixing or significant crustal assimilation (Allan et al, 1988), (2) there was no extensive subsolidus reequilibration between spinels and other silicate minerals (Scowen et al, 1991), and (3) no major metamorphic event occurred after the crystallization of these spinels. There is no significant variation in the chemistry of Cr-rich spinels within these samples as a function of stratigraphic position.

Source of Cr-rich spinels

In terms of origin and tectonic setting, Cr-rich spinels from a variety of types of ultramafic and mafic complexes can be discriminated using major-element abundances (Irvine, 1967; Dick and Bullen, 1984; Arai, 1992; Kamenetsky et al., 2001; Barnes and Roeder, 2001). Overlaps among various tectonic settings on some plots (Dick and Bullen, 1984), however, are common because only selected aspects of the total chemical variation of the spinels are reflected in the binary plot of individual elements (Cookenboo et al., 1997). Multiple combinations of major elements therefore should be considered to determine the possible parental magma of the studied spinels.

Most spinel-peridotites have spinels with low TiO_2 abundances, whereas volcanic spinels with TiO_2 <0.2 wt% are uncommon (Kamenetsky et al., 2001). Lenaz et al. (2000), therefore, set a compositional boundary between peridotitic and volcanic spinels at TiO_2 =0.2 wt%. Since 15 of 18 analyses have TiO_2 contents <0.2, and most are near-or-below the detection limit of ~ 0.05 wt% (Figure 6.23c), the detrital spinels from the Youxia and Shenkeza Formations were most likely derived from mantle (ophiolitic) peridotites.

Table 6.3 Microprobe analyses of Cr-rich spinels from the Zongpubei Formation in the Tingri region

Sample	Al2O3	Cr2O3	MnO	MgO	TiO2	V2O5	NiO	ZnO	FeO	Fe2O3	Total	Cr/3+	Fe/3+	Al/3+	$Mg/(Mg+Fe^{2+})$	Cr/(Cr+Al)
S148	19.45	46.76	0.38	12.52	b.d.	n.a.	0.09	0.11	12.87	1.91	94.09	0.60	0.02	0.37	0.62	0.62
S148	2.45	39.19	1.95	3.68	0.05	n.a.	0.30	1.03	19.16	29.50	97.31	0.49	0.46	0.05	0.19	0.91
S148	21.42	41.24	0.53	9.00	0.33	n.a.	0.20	0.19	18.21	0.48	91.61	0.56	0.01	0.43	0.46	0.56
S148	19.57	50.51	0.63	8.16	b.d.	n.a.	0.02	0.67	24.39	-9.18	94.80	0.69	-0.08	0.40	0.43	0.63
S148	7.68	58.98	0.60	4.66	0.06	n.a.	0.03	0.60	24.25	-2.38	94.47	0.86	-0.03	0.17	0.27	0.84
S148	24.27	37.39	0.19	12.73	0.33	n.a.	0.17	0.00	12.72	5.88	93.68	0.47	0.08	0.45	0.60	0.51
S88	28.89	32.16	0.21	10.73	b.d.	n.a.	0.12	0.27	15.88	0.95	89.25	0.42	0.01	0.57	0.54	0.43
S88	11.21	53.73	0.37	5.70	0.06	n.a.	0.11	2.34	24.45	-11.57	86.40	0.85	-0.11	0.26	0.37	0.76
S87	22.44	46.19	0.26	12.67	b.d.	n.a.	0.06	0.23	14.53	3.01	99.41	0.56	0.03	0.41	0.59	0.58
S87	5.22	60.40	0.41	4.95	b.d.	n.a.	0.02	0.24	22.68	4.25	98.16	0.84	0.05	0.11	0.26	0.89
S87	2.58	66.60	0.40	7.42	b.d.	n.a.	0.03	0.19	19.41	0.78	97.42	0.94	0.01	0.05	0.40	0.95
S87	9.52	56.52	0.41	8.94	0.14	n.a.	0.03	0.15	17.39	6.15	99.24	0.74	0.08	0.18	0.44	0.80
S94	20.18	49.84	0.26	10.42	0.06	0.32	0.11	0.23	19.41	-1.73	99.09	0.63	-0.02	0.38	0.50	0.62
S94	9.05	40.13	0.66	5.37	0.39	0.13	0.11	0.64	20.12	22.26	98.85	0.50	0.33	0.17	0.26	0.75
S94	24.95	46.88	0.25	11.89	b.d.	0.18	0.08	1.04	18.72	-5.36	98.64	0.58	-0.05	0.46	0.57	0.56
S94	19.51	46.85	0.26	11.97	0.12	0.19	0.04	0.31	14.43	2.93	96.62	0.60	0.03	0.37	0.57	0.62
S94	10.96	56.99	0.45	7.18	0.05	0.27	0.02	0.80	21.44	-2.31	95.85	0.80	-0.03	0.23	0.39	0.78
S94	28.71	34.75	0.27	12.23	b.d.	0.30	0.05	0.16	14.76	2.70	93.92	0.43	0.03	0.53	0.58	0.45

note: 1. The ferric iron content of each analysis was determined by assuming stoichiometry, and an ideal XY_2O_4 formula, where $X=Fe^{2+}$, Mg, Ni, Zn, and Y=Cr, Al, Ti, Fe^{3+}, following the methods of Barnes and Roeder (2001).

2. b.d. : below detection limits

3. n.a.: no analysis

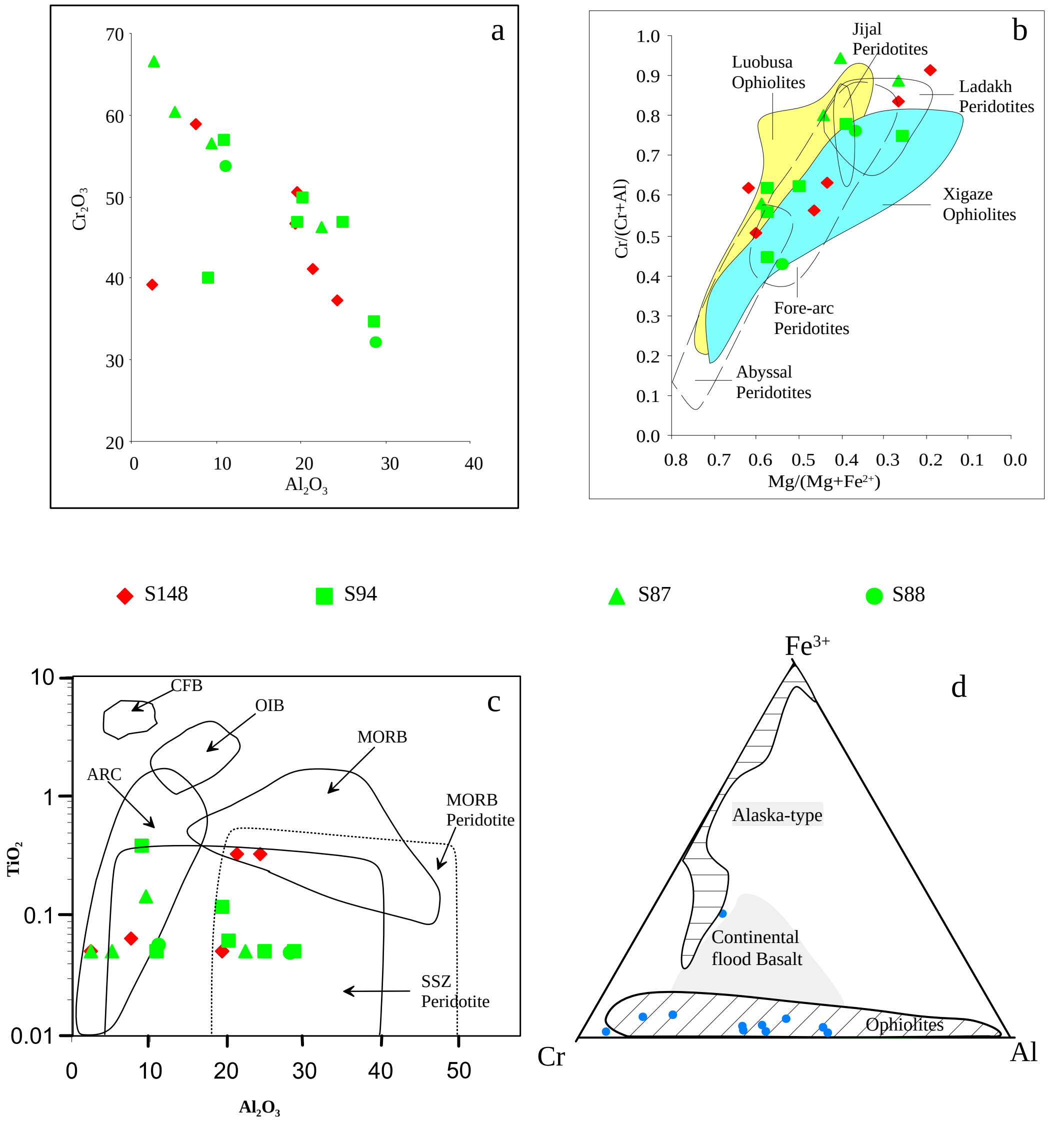

Figure 6.23 Geochemical plot of Cr-rich spinels from the Youxia and Shenkeza sandstones. a. Al_2O_3 vs. Cr_2O_3 plot, b. Cr# (Cr/(Cr+Al)) vs. Mg# (Mg/(Mg+Fe^{2+})) plot, fields displayed are: Abyssal peridotites from Brindzia and Wood (1990), Fore-arc peridotites from Parkinson and Pearce (1998), Jijal Peridotites and Ladakh peridotites from Rolland et al. (2002), Luobusa ophiolites from Zhou et al. (1996), and Xigaze ophiolites from Wang et al. (2000). c. TiO_2 vs. Al_2O_3 plot, fields displayed are from Kamenetsky et al. (2001): CFB-continental flood basalt, OIB-oceanic island basalt, MORB-mid-ocean ridge basalt, ARC-volcanic island arc, SSZ-suprasubduction zone. d. Cr-Al-Fe^{3+} ternary plot, fields displayed are from Cookenboo et al.(1997).

The detrital spinels in the Youxia and Shenkeza sandstones have Cr#(Cr/(Cr+Al)) between 0.43 and 0.94, and Mg# (Mg/(Mg+Fe^{2+})) between 0.19 and 0.62. These compositions, according to the classifications of Dick and Bullen (1984), correspond best to the spinels in transitional type II peridotites, which are transitional from volcanic arc to typical oceanic crust (Najman and Garzanti, 2000). In the plot of Cr# vs. Mg# (Figure 6.23b), there is a strong negative correlation between Cr# and Mg#, a typical Cr-Al trend (Barnes and Roeder, 2001), probably corresponding to spinels equilibrating with olivine of constant composition at constant temperature (Irvine, 1967; Roeder, 1994). The spinels vary from Al-rich spinels (*sensu stricto*) to Cr-rich chromites (*sensu stricto*). In the conventional fields (Figure 6.22b) of tectonic settings for spinels (Barnes and Roeder, 2001; Dick and Bullen, 1984), our data plot in the field of fore-arc peridotites.

In the plot of TiO_2 vs. Al_2O_3 (Figure 6.23c), assuming TiO_2~0.05 for spinels with TiO_2 abundances < 0.05, comparison of our data with the compositional fields of spinels from well-studied tectonic settings demonstrates that detrital spinels in the Youxia and Shenkeza Formations do not fall in the linear trend defined by spinels from continental flood basalts (CFB), oceanic island basalts (OIB), and mid-ocean-ridge basalts (MORB), and are best assigned to source rocks from suprasubduction zone mantle peridotites (Kamenetsky et al., 2001). It is obvious that hotspot-related basalts such as the Deccan Traps did not significantly contribute to the Zongpubei sandstones because the spinels from the Deccan Traps commonly have >1% TiO_2 and relatively constant Cr# values mostly between 0.6 and 0.7 (Barnes and Roeder, 2001; Najman and Garzanti, 2000).

It is interesting to note that 6 spinels of 18 analyses have negative ferric iron values (Table 6.3). All Fe^{3+} values were determined by assuming stoichiometry with three cations per four O atoms, following the methods of Barnes and Roeder (2001). Therefore the negative Fe^{3+} values indicate these spinels are nonstoichiometric. This may be good evidence that an arc complex is a significant source for the spinels in the Youxia and Shenkeza sandstones because nonstoichiometry is a common feature for Cr-rich spinels from primitive subducation-related magmatic suites, such as Ti-poor tholeiite from Hunter Fracture Zone, and high-Ca boninites from the Tonga Trench (Kamperman et al., 1996). 10 of 12 analyses with calculated Fe_2O_3 >0 have $Fe^{3+}/(Fe^{3+}+Al+Cr)<0.1$, plotting in the field of ophiolites in the Fe^{3+}-Al-Cr ternary diagram (Figure 6.23d). It is thus very likely that either the Gangdese arc complexes and/or associated ophiolitic rocks provided significant volcanic-related grains including Cr-rich spinels to the Youxia and Shenkeza sandstones, consistent with the petrographic observations described above.

Considered together, the plots of Mg# vs. Cr#, TiO_2 vs. Al_2O_3, and Fe^{3+}-Al-Cr demonstrate that the compositional range of the detrital spinels in the Youxia and Shenkeza sandstones closely matches that of spinels from suprasubdction-related magmatic rocks, and excludes ocean-island basalts, MORB, and continental flood basalts as major sediment sources. Also shown (figure 6.23b) are spinels from Luobusa ophiolites (Zhou et al., 1996) and Xigaze ophiolites (Wang et al., 2000) in southern Tibet, and Kohistan-Ladakh mafic-ultramafic suites in the NW Himalayas (Jan et al., 1990, 1992, 1993; Rolland et al., 2002). It is clear that there are significant overlaps between spinels from Youxia and Shenkeza sandstones and those from arc and ophiolitic rocks in this plot. Furthermore, the compositions of detrital spinels in the Youxia and Shenkeza sandstones are closely similar to those of the Chulung La Formation in Zanskar, (Garzanti et al., 1987, 1996), the Subathu Formation (Najman and Garzanti, 2000) in Himachal Pradesh, northern India and the Murree redbeds (Bossart and Ottiger, 1989; Critelli and Garzanti, 1994) in the Hazara-Kashmir Syntaxis, northern Pakistan, which are syn-collisional clastics derived from the obducting Trans-Himalayan arc-trench system. As such we conclude that the detrital spinels in the Youxia and Shenkeza sandstones were most likely derived from arc and ophiolitic sequences of the Yarlung-Zangbo suture zone to the north.

Discussion

Regional correlatives of Lower Tertiary clastic rocks

Comparisons with sedimentary sequences from the Himalayan foreland basin show that sandstone from the middle Eocene Upper Subathu Formation (Najman and Garzanti, 2000) and the middle Eocene-Miocene Murree Formation in northern Pakistan (Bossart and Ottiger, 1989; Critelli and Garzanti, 1994; Garzanti et al., 1996) are similar to the Youxia and Shenkeza sandstones (Figure 6.24). Detrital modes show that those sandstones were derived from the "recycled orogen" setting (Figure 6.8), characterized by significant amounts of immature framework grains (plagioclase, felsitic to microlitic volcanic rock fragments, serpentine schist lithics), and common spinels. The close similarity in the compositions of Cr-rich spinels also suggests that there was a common source for the lithic-rich sandstones.

This is very different from the underlying Paleocene quartzose arenites intercalated within mainly shelf carbonate deposited on the passive margin of the Indian continent, including the Stumpata and Dibling Formations (Garzanti et al., 1987) in Zanskar, the Patala Formation in Hazara-Kashmir (Bossart and Ottiger, 1989), and the Jidula Formation in southern Tibet (Willems et al., 1993, 1996). The detritial modes of the quartzose arenites consistently plot in or close to the "continental block" provenance field (Figure 6.8), characterized by abundant well-sorted monocrystalline quartz and generally lack of volcanic lithcs, plagioclase, and Cr-rich spinels.

Therefore the lower Tertiary detrital sequences in the Himalayas record an abrupt change in provenance: mature, quartz-rich sandstones (Jidula, Stumpata, Dibling and Patala Formations) indicate a provenance from the uplifted basement rocks of Indian continent to the south while immature, lithic-rich sandstones (Youxia, Shenkeza, Subathu and Murree Formations) were most likely derived from the obducting Trans-Himalayan arc-trench system to the north. This temporal evolution is consistent with the classic sequence of tectono-sedimentary episodes when an arc collides with a passive continental margin (e.g., Rowley and Kidd, 1981). Quartzose sandstones derived from the craton are first deposited on the passive margin. The start of collision is then marked by the deposition of clastics containing volcanic and ophiolitic detritus, which reflects the arrival of the arc-trench system onto the outer parts of the passive margin.

Timing of Indian-Asian collision in southern Tibet

Precise dating of the age of initiation of collision between India and Asia is an important factor in constraining the models of mass balance within the Himalayan system (Rowley, 1996, 1998). However, the start of collision is still quite poorly constrained,

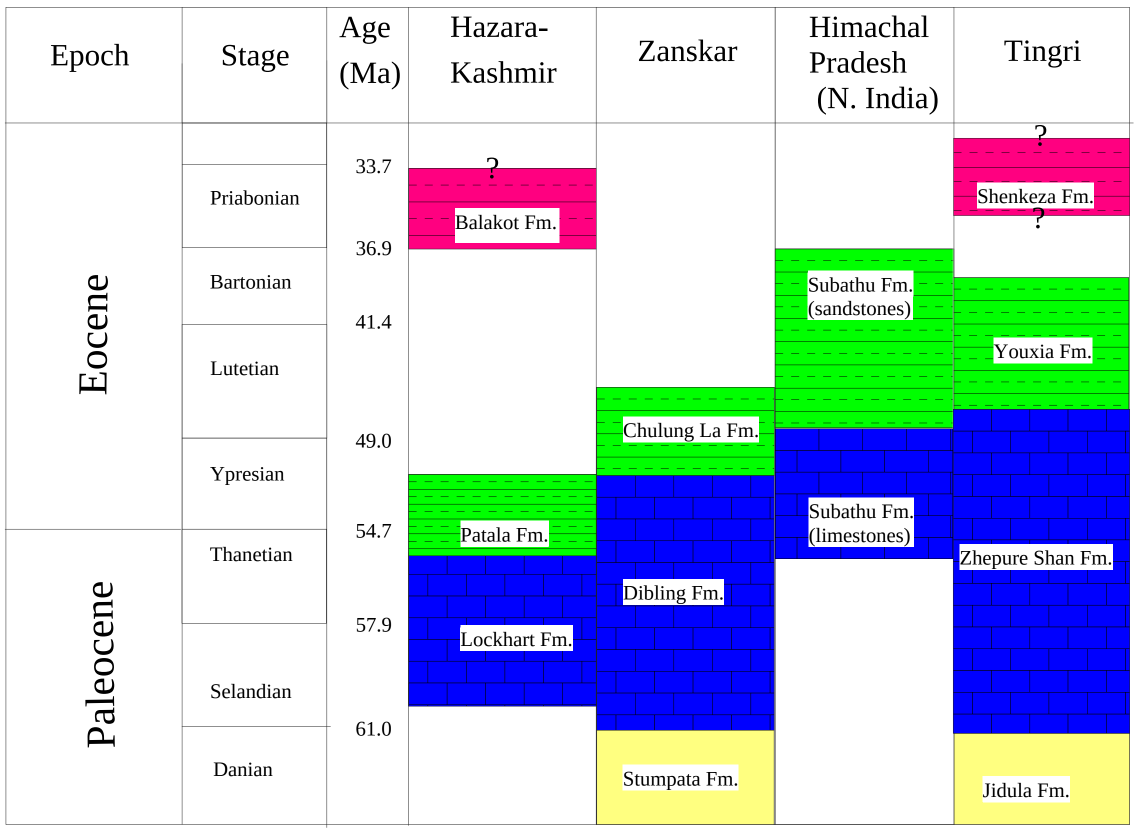

Figure 6.24 Comparison of stratigraphic columns of the Himalayan foreland basin, from Hazara-Kashmir (Bossart and Ottiger, 1989, which is modified by Najman et al. (2002)), through Zanskar (Garzanti et al., 1987, 1996), Himachal Pradesh (Najman and Garzanti, 2000), to Tingri, southern Tibet (this study). Timescale after Berggren et al. (1995).

Yellow-mature clastics of Indian passive margin; blue-carbonates of the Indian passive margin; green-marine orogenic clastics; red-non-marine redbeds.

and has been placed in a range somewhere from 65 to 37 Ma due to the different and generally indirect approaches that have been used to date it (Rowley, 1996, 1998, and references therein; Najman et al., 1997, 2001, 2002; de Sigoyer et al., 2000, 2001; Searle, 2001, Wan et al., 2002; Wang et al., 2002; Clift et al., 2002).

As mentioned above, collisions between an arc and passive margin are associated with marked changes in patterns of subsidence and sedimentation, particularly along passive margins. Therefore the sharp change of the sedimentary compositions between the times of deposition of the Jidula and Youxia formations in Tingri provides a time constraint on the initial collision of India with Asia in southern Tibet. The 1500-m-thick, well-exposed marine stratigraphy of the Zhepure Mountain in Tingri, southern Tibet shows evidence for continuous passive margin sedimentation along the north flank of the Indian continent from late Albian to early Lutetian time (Willems et al., 1996). This suggests that collision did not occur until the early Lutetian in southern Tibet, consistent with the slow subsidence inferred from the Zhepure Shan Formation deposition (Rowley, 1998). The conformable contact between the Zongpubei and Zhepure Shan Formations marks the transition from a passive margin carbonate platform (Willems et al., 1996) to a collisional foredeep, exhibiting a compositional change similar to that observed in Zanskar (Garzanti et al., 1987). The abundant nannofossils and foraminifera in the shales of the lower part of the Youxia Formation (Wang et al., 2002) point to a late early Lutetian to Bartonian age (47-37 Ma) of deposition. Therefore we conclude that the final closure of the Neo-Tethys and the onset of continental collision occurred at ~47 Ma in the Tingri region of southern Tibet.

Stratigraphic data in the Zanskar region, NW Himalaya, suggest that the age of the India-Asia collision is ~51 Ma (Garzanti et al., 1987), which is broadly consistent with other estimates in peripheral foreland basin in Pakistan and northern India (Bossart and Ottiger, 1989; DeCelles et al., 1998; Najman and Garzanti, 2000) and in the Indus Molasse (Clift et al., 2002). Recent work (Guillot et al., 2003) indicates that continent-continent collision in Zanskar has begun somewhat earlier, probably quite close to 55 Ma based on timing of early Himalayan subduction-related metamorphism. However, their new ages are from radiometric dating of metamorphic rocks, which were partially subducted during the earliest stages of collision. As they state, these rocks were not exhumed until about 50-45 Ma during the initial uplift of the incipient orogen. Accordingly, there is a lag time between initial collision and erosion of material from the collision zone delivered to the foreland basin. It is concluded that while the metamorphic ages suggest initiation of subduction of Indian crust at ~55 Ma, exhumation and foreland basin sedimentation did not begin until ~51 Ma in the Zanskar region (Garzanti et al, 1987). If this is the case, the initiation of the collision in NW Himalayas is earlier than that in southern Tibet. There is an approximately ~4 Ma difference between the onset of continental collision between the Zanskar and Tingri regions.

Yin and Harrison (2001) and Wan et al. (2002) argue that the collision of the India and Lhasa continental block was initiated at Cretaceous-Paleocene boundary time (~65 Ma) in southern Tibet. However, our data from the Jidula Formation of Zhepure Shan indicate that passive margin deposition persisted without interruption from the late Cretaceous through the Paleocene. This is demonstrated by the relative thin siliciclastic succession, the return to carbonate shelf deposition in the overlying Zhepure Shan

Formation, and from the dominance of mature, quartzose sandstones with an ultrastable heavy mineral assemblage (zircon, rutile, tourmaline) and lack of any north-derived syn-orogenic components (Cr-rich spinels, abundant labile rock fragments). The clear absence of signal in either the subsidence history (Rowley, 1998) and in details of the provenance of the Late Cretaceous and Paleocene sediments in the Zhepure Shan makes a 65 Ma collision initiation age highly improbable. Rather our data clearly support an age of initiation collision at about 47 Ma. This is marked in the stratigraphic record by the transition from the Zhepure Shan limestones to the Youxia shales, that would be associated with rapid flexural subsidence of the Zhepure Shan section of the Indian passive margin at about 47 Ma as originally argued by Rowley (1996, 1998).

Conclusions

Lower Tertiary sediments are well-exposed in the Tingri region, southern Tibet, and represents one of the few well-preserved sections containing the passive margin-peripheral foreland basin clastic facies transition in the Himalayas. The petrography and geochemistry of the Jidula and Youxia and Shenkeza Formations provide strong tools to reconstruct the early tectonic evolution of the Himalayas in southern Tibet during the early Tertiary. Sedimentation in the older Jidula Formation is dominated by mature detritus, and closely compares in geochemical composition deposited on a passive continental margin, which constrains the Jidula to have been derived from basement rocks in the Indian continent. Sandstone petrography of the younger Youxia and Shenkeza Formations shows a significant amount of immature framework grains, and plots in the "recycled orogen" provenance field, which is consistent with the geochemistry of sandstone-shale samples and the occurrence of Cr-rich spinels with typical composition of spinels in fore-arc peridotites. Therefore the sharp change of the sedimentary compositions between the times of deposition of the Jidula and Youxia and Shenkeza formations, and the persistence of carbonate shelf sedimentation to the base of the Youxia Formation, suggest that the onset of continental collision in the eastern central Himalayas near Tingri is dated at ~47 Ma.

References

Achache, J., Courtillot, V., and Zhou, Y.X., 1984. Palaeogeographic and tectonic evolution of Southern Tibet since Middle Createaceous times: New paleomagnetic data and synthesis, JGR, v. 89, 10,311-10,339.

Aitchison, J., Badengzhu, C., Davis, A.M., Liu, J., Luo, H., Malpas, J., McDermid, I., Wu, H., Ziabrev, S., and Zhou, M.F., 2000. Remnants of a Cretaceous intra-oceanic subduction system within the Yarlung-Zangbo suture (southern Tibet), Earth Planet. Sci. Lett., v. 183, 231-244.

Aitchison, J, Davis A., Badengzhu and Luo, H., 2002. New constraints on the India-Asia collision: the Lower Miocene Gangrinboche conglomerates, Yarlung Tsangpo suture zone, SE Tibet. J. Asian Earth Science, v.21, p.251-263.

Allan, J.F., Sack, R.O., and Batiza, R., 1988. Cr-rich spinels as petrogenetic indicators: MORB-type lavas from the Lamont seamount chain, eastern Pacific. American Mineralogist 73, p. 741-753.

Allegre, C., Courtillot, V., Tapponnier, P., Hirn, A., Mattauer, M., Coulon, C., Jaeger, J.J., Achache, J., Schärer, U., Marcoux, J., Burg, J.P., Girardeau, J., Armijo, R., Gariépy, C., Göpel, C., Li, T., Xiao, X., Chang, C., Li, G., Lin, B., Teng, J., Wang, N., Chen, G., Han, T., Wang, X., Den, W., Sheng, H., Cao, Y., Zhou, J., Qiu, H., Bao, P., Wang, S., Wang, B., Zhou, Y. and Xu, R., 1984. Structure and evolution of the Himalaya–Tibet orogenic belt. Nature 307, p. 17–22.

Arai, S., and Okada, H., 1991. Petrology of serpentine sandstone as a key to tectonic development of serpentine belts. Tectonophysics, 195, p.65-81.

Arai, S., 1992. Chemistry of chromian spinel in volcanic rocks as a potential guide to magma chemistry. Mineral. Mag. 56, p.173-184.

Armijo, R., Tapponnier, P., Mercier, J., and Han, T., 1986. Quaternary extension in Southern Tibet: Field observations and tectonic implications: Journal of Geophysical Research, v. 91, p. 13803-13872.

Baksi, A.K., 1995. Petrogenesis and timing of volcanism in the Rajmahal flood basalt province, NE India. Chem. Geol. 121, p.73-90.

Barnes, S.J., and Roeder, P.L., 2001. The Range of Spinel Compositions in Terrestrial mafic and ultramafic rocks. J. Petrol. 42, p. 2279-2302.

Barnes, S.J., 1998, Chromite in Komatiites, 1. Magmatic control on crystallization and composition. J. Petrol., 39, p.1689-1720.

Basu, A., and Molinaroli, E., 1989. Provenance characteristics of detrital opaque Fe-Ti oxide minerals, J. Sedimentary Petorlogy, v. 59, p.922-934.

Basu, A., and Molinaroli, E., 1991. Reliability and application of detrital opaque Fe-Ti oxide minerals in provenance determination, in Morton, A.C., Todd, S.P., and Haughton, P.D.W., eds., Developments in sedimentary provenance studies, Geol. Soc. London Special Pub. 57, p. 55-65.

Baud, A., Gaetani, M., Garzanti, E., Fois, E., Nicora, A., & Tintori, A., 1984. Geological observations in southeastern Zanskar and adjacent Lahul area (northwestern Himalaya). Ecl. Geol. Helv., v.77, n.1, p.171-197.

Beck, R., et al., 1995. Stratigraphic evidence for an early collision between northwest India and Asia, Nature, v. 373, p.55-58.
Berggren, W.A., Kent, D.V., Swisher, C.C., and Aubry, M.P., 1995. A revised Cenozoic geochronology and chronostratigraphy, in Geochronology, Time Scales and Global Stratigraphic, edited by Berggren, W. A. et al., Spec. Publ. SEPM, 54, p.129-212.
Besse, J., Courtillot, V., 1988. Paleogeographic maps of the continents bordering the Indian ocean since the Early Jurassic, J. Geophys. Res., v. 93, p.11791-11808.
Besse, J., Courtillot, V., Pozzi, J.P., Westphal, W., and Zhou, Y.X., 1984. Paleomagnetic estimates of crustal shortening in the Himalayan thrusts and Zangbo suture, Nature, 311, p.621-626.
Bhatia, M.R., 1983. Plate tectonics and geochemical composition of sandstones. J. Geol., 91, p.611-627.
Bhatia, M.R., 1985. Composition and classification of Palaeozoic flysch mudrocks of eastern Australia: implications in provenance and tectonic setting interpretation. Sedimentary Geology, 41, p.249-268.
Bhatia, M.R., Crook, K., 1986. Trace element characteristics of greywackes and tectonic setting discrimination of sedimentary basins. Contrib. Mineralogy Petrol., 92, p.181-193.
Blatt, H., Middleton, G.V., and Murray, R., 1980. Origin of sedimentary rocks, second edition, Prentice-Hall Inc., Englewood Cliffs, New Jersey, 782p.
Bock, B., Mclennan, S.M., and Hanson, G.N., 1998. Geochemistry and provenance of the middle Ordocician Austin Glen Member (Normanskill Formation) and the Taconian Orogeny in New England. Sedimentology, V.45, p.635-655.
Bossart, P., and Ottiger, R., 1989. Rocks of the Murree formation in the northern Pakistan, indicators of a descending foreland basin of late Palaeocene to middle Eocene age. Eclogae Geologicae Helvetiae. V. 82, 133-165.
Brookfield, M.E., and Andrews-Speed, C.P., 1984. Sedimentology, petrography and tectonic significance of the shelf, flysch and molasses clastic deposits across the Indus suture zone, Ladakh, NW India. Sedimentary Geology, v.40, p.249-286.
Brookfield, M.E., 1993. The Himalayan passive margin from Precambrian to Cretaceous times. Sedimentary Geology, v.84, p.1-35.
Burchfiel, B.C., and Royden, L.H., 1985. North-south extension within the convergent Himalayan region. Geology, v. 13, p. 679-682.
Burchfiel, B.C., Chen, Z., Hodges, K.V., Liu, Y., Royden, L.H., Deng, C., and Xu, J., 1992. The South Tibetan detachment system, Himalayan orogen: Extension contemporaneous with and parallel to shortening in a collisional mountain belt: Geological Society of America Special Paper 269, 41 p.
Bureau of Geology and Mineral Resources of Xizang Autonomous Region, 1994. Stratigraphy (lithostratic) of Xizang Autonomous Region, China University of Geoscience Press, 423p.
Burg, J., Chen, G., 1984. Tectonics and structural zonation of southern Tibet, China, Nature, v. 311, p.219-223.
Burke, K., Dewey, J.F., Kidd, W.S.F., 1977. World distribution of sutures-the sites of former oceans. Tectonophysics, v.40, p. 69-99.

Butler, R., 1995. Tectonics-when did India hit Asia? Nature, v. 373, p.20-21.
Caironi, V., Garzanti, E., Sciunnach, D., 1996. Typology of detrital zircon as a key to unraveling provenance in rift siliciclastic sequences (Permo-Carboniferous of Spiti, N India). Geodinamica Acta 9, p. 101-113.
Campbell, I.H., and Griffiths, R.W., 1990. Implications of mantle plume structure for the evolution of flood basalts. Earth Planet. Sci. Lett. 99, p. 79-93.
Chang, C.F., Pan, Y.S., Cheng, H.L., and Zhang, X.M., 1982. The geological structure of the Quinghai-Xizang plateau: Beijing, Science Press, 91 p.
Chemenda, A.I., Burg, J.P., and Mattauer, M., 2000. Evolutionary model of the Himalaya-Tibet system: Geopoem based on new modeling, geological and geophysical data, Earth Planet. Sci. Lett., 174, p.397-409.
Chen, Z., Burchfiel, B.C., Liu, Y., King, R.W., Royden, L.H., Tang, W., Wang, E., Zhao, J., and Zhang, X., 2000. Global Positioning System measurements from eastern Tibet and their implications for India/Eurasia intercontinental deformation. J. Geophys. Res., 105, p.16215-16277.
Clift, P.D., Shimizu, N., Layne, G., Gaedicke, C., Schlüter, H.U., Clark, M. and Amjad, S., 2001a. Development of the Indus Fan and its significance for the erosional history of the western Himalaya and Karakoram. GSA Bulletin, 113, p.1039–1051.
Clift, P.D., Shimizu, N., Layne, G., and Blusztajn, J., 2001b. Tracing patterns of unroofing in the Early Himalaya through microprobe Pb isotope analysis of detrital K-feldspars in the Indus Molasse, India, Earth and Planetary Science Letters, 188, p.475–491.
Clift, P.D., Shimizu, N., Layne, G., Gaedicke, C., Schülter, H.U., Clark, M., and Amjad, S., 2000. 55 million years of Tibetan and Karakoram evolution recorded in the Indus Fan. EOS, 81 (25), p. 277–282.
Clift, P.D., Carter, A., Krol, M., and Kirby, E., 2002a. Constraints on India-Eurasia Collision in the Arabian Sea Region taken from the Indus Group, Ladakh Himalaya, India, in The Tectonic and Climatic Evolution of the Arabian Sea Region, edited by Clift, P. D. et al., Spec. Publ. Geol. Soc. London, 195.
Clift, P. D., Lee, J.I., Hildebrand, P., Shimizu, N., Layne, G. D., Blusztajn, J., Blum, J. D., Garzanti, E., and Khan, A. A., 2002b. Nd and Pb isotope variability in the Indus River system: Implications for sediment provenance and crustal heterogeneity in the Western Himalaya. Earth and Planetary Science Letters, v. 200, p.91–106.
Condie, K.C., 1997. Plate tectonics and crustal evolution. Fourth edition, Butterworth Heinemann, Oxford, 282p.
Condie, K.C., Lee, D., and Farmer, G.L., 2001. Tectonic setting and provenance of the Neoproterozoic Uinta Mountain and big Cottonwood groups, northern Utah: constraints from geochemistry, Nd isotopes, and detrital modes. Sedimentary Geology. v.141-142, p.443-464.
Cookenboo, H.O., Bustin, R.M., Wilks, K.R., 1997. Detrital chromian spinel compostions used to reconstruct the tectonic setting of provenance: implications for orogeny in the Canadian Cordillera. J. Sediment. Res. 67, p. 116-123.

Copeland, P., Harrison, T.M., and LeFort, P., 1990. Age and cooling history of the Manaslu granite: implications for Himalayan tectonics. J. Volcanol. Geotherm. Res. 44, p.33-50.
Copeland, P., 1997. The when and where of the growth of the Himalaya and the Tibetan Plateau. In Ruddiman, W.F., (Ed.), Tectonic uplift and climate change. Plenum Press, p. 19-40.
Corfield, R.I, Searle, M.P., and Green, O.R., 1999. Photang thrust sheet: An accretionary complex structurally below the Spontang ophiolite constraining timing and tectonic environment of ophiolite obduction, Ladakh Himalaya, NW India: Geological Society [London] Journal, v. 156, p. 1031-1044.
Corfield, R. I., and Searle, M. P. 2000. Crustal shortening estimates across the north Indian continental margin, Ladakh, NW India. *In* Khan, M. A.; Treloar, P. J.; Searle, M. P.; and Jan, M. Q., eds. Tectonics of the Nanga Parbat syntaxis and the western Himalaya. Geol. Soc. Lond. Spec. Publ. 170, p.395-410.
Coward, M.P., Windley, B.F., Broughton, R., Luff, I.W., Petterson, M.G., Pudsey, C., Rex, D., and Khan, M.A., 1986. Collision tectonics in NW Himalayas, in Coward, M.P., and Ries, A.C. eds., Collision Tectonics: Geological Society [London] Special Publication 19, p.203-219.
Critelli, S., and Garzanti, E., 1994. Provenance of the lower Tertiary Murree redbeds (Hazara-Kashmir Sytaxis, Pakistan) and initial rising of the Himalayas. Sedimentary Geology. v.89, p.265-284.
Cullers, R.L., Basu, A., Suttner, L.J., 1988. Geochemical signature of provenance in sand-size material in soils and stream sediments near the Tobacco Root batholith, Montana, USA. Chem. Geol. v.70, p.335-348.
Danyushevsky, L., Della-Pasqua, and Sokolov, F.N., 2000. Re-equilibration of melt inclusions trapped by Mg olivine phenocrysts from subduction-related magmas: petrologic implications. Contributions to Mineralogy and Petrology 138, p. 68-83.
Danyushevsky, L., McNeill, A.W., Sobolev, A.V., 2002. Experimental and petrological studies of melt inclusions in phenocrysts from mantle-derived magmas: an overview of techniques, advantages and complications. Chemical Geology 183, p.4-25.
Danyushevsky, L., Sokolov, S., and Falloon, T., 2002. Melt inclusions in olivine phenocrysts: using diffusive re-equilibration to determine the cooling history of a crystal, with implications for the origin of olivine-phyric volcanic rocks. J. of Petrology. v.43, p.1651-1671.
Davis, A, Aitchison, J., Badengzhu, Luo, H., and Zyabrev, S., 2002. Paleogene island arc collision-related conglomerates, Yarlung-Tsangpo suture zone, Tibet. Sed. Geol. 150, p. 247-273.
DeCelles, P.G., Gehrels, G.E., Quade, L., and Qjha, T.P., 1998. Eocene-early Microcene foreland basin development and the history of Himalayan thrusting, western and central Nepal. Tectonics, 17, p.741-765.
DeCelles, P.G., Gehrels, G.E., Quade, J., LaReau, B., and Spurlin, M., 2000. Tectonic implications of U-Pb zircon ages of the Himalayan orogenic belt in Nepal. Science 288, p.497-499.

Delano, J.W., Schirnick, C., Bock, B., Kidd, W.S.F., Heizler, M.T., Putman, G.W., Delong, S.E., and Ohr, M., 1990. Petrology and geochemistry of Ordovician K-Nentonites in New York State: constraints on the nature of a volcanic arc. J. Geol., v. 98, p. 157-170.
De Sigoyer, J., Chavagnac, V., Blichert-Tift, J., Villa, I., Luais, B., Guillot S., Cosca, M., and Mascle, G., 2000. Dating the Indian continental subduction and collisional thickening in the northwest Himalaya: Multichronology of the Tso Morari eclogites. Geology, v.28, p.487-490.
De Sigoyer, J., Chavagnac, V., Blichert-Tift, J., Villa, I., Luais, B., Guillot, S., Cosca, M., and Mascle, G., 2001. Dating the Indian continental subduction and collisional thickening in the northwest Himalaya: Multichronology of the Tso Morari eclogites: comments and reply. Geology, v.29, p.192.
Dewey, J.F., Bird, J.M., 1970. Mountain belts and the new global tectonics, J. Geophys. Res., v. 75, p.2625-2647.
Dewey, J.F., and Burke, K.C., 1973. Tibetan, Variscan, and Precambrian basement reactivation: Products of continental collision. J. Geol., v. 81, p.683-692.
Dewey, J.F., 1974. Continental margins and ophiolite obduction: Appalachian-Caledonian system, in Burk, C.A., and Drake, C.L., eds., The geology of continental margins, Springer-Verlag, New York, p.933-950.
Dewey, J.F., Hempton, M.R., Kidd, W.S.F., Saroglu, F., and Sengor, A.M.C., 1986. Shortening of continental lithosphere: the neotectonics of eastern Anatolia- a young collision zone, in Coward, M.P., and Ries, A.C., eds., Collision Tectonics, Geol. Soc. Of London Special Pulication 19, p.3-36.
Dewey, J.F., Shackleton, R.M., Chang, C., and Sun, Y., 1988a. The tectonic development of the Tibetan plateau, in Chang, C., Shackleton, R.M., Dewey, J.F., and Yin, J., eds., The geological evolution of Tibet: Royal Society of London Philosophical Transactions, p.379-413.
Dewey, J.F., 1988b. Extensional collapse of orogens. Tectonics, 7, p.1123-1139.
Dewey, J. F., Cande, S., and Pitman, W. C., 1989. Tectonic evolution of the India-Eurasia collision zone, Eclogae. Geol. Helv., 82, p.717-734.
Dewey, J., Mange, M., 1999. Petrography of Ordovician and Silurian sediments in the western Irish Caledonides: tracers of short-lived Ordovician continent-arc collision orogeny and the evolution of the Laurentian Appalachian-Caledonian margin. In: Mac Niocaill, C., Ryan, P.D., (eds.), Continental Tectonics. Geol. Soc., London, Spec. Publ. 164, p.55-107.
Dick, H.J.B., and Bullen, T., 1984. Chromian spinel as a petrogenetic indicator in abyssal and alpine-type peridotites and spatially associated lavas. Contrib. Mineral. Petrol. v. 86, p.54-76.
Dickinson, W.R., 1970. Interpreting detrital modes of greywacke and arkose. J. Sedimentary Petrology, v.40, p.695-707.
Dickinson, W.R., Suczek, C., 1979. Plate tectonics and sandstones composition, AAPG Bulletin, v. 63, p.2164-2172.
Dickinson, W.R., Beard, L.S, Brakenridge, G.R., Erjavec, J.L., Ferguson, R.C., Inman, K.F., Knepp, R.A., Lindberg, F.A., and Ryberg, P.T., 1983. Provenance of

North American Phanerozoic sandstones in relation to tectonic setting. GSA Bulletin, v. 94, p.222-235.
Dickinson, W., 1985. Interpreting provenance relations from detrital modes of sandstones, in Zuffa, G., ed. Provenance of arenites: Dordrecht, Netherlands, D. Reidel, NATO advanced study Institute series 148, p.333-361.
Dickinson, W.R., 1988. Provenance and sediment dispersal in relation to paleotectonics and paleogeography of sedimentary basin, in Kleinspehn, K.L., and Paola, C., eds., New perspectives in basin analysis, New York Springer-Verlag, p. 3-25.
Dickinson, W.R., 1995. Forearc basin, in Busby, C.J., and Ingersoll, R.V., eds., Tectonics of sedimentary basins, Blackwell Science, Oxford, p.221-261.
Durr, S., and Gibling, M.R., 1994. Early Cretaceous volcaniclastic and quartzose sandstones from north central Nepal: composition, sedimentology and geotectonic significance. Geol. Rundsch 83, p. 62-75.
Durr, S., 1996. Provenance of Xigaze fore-arc basin clastic rocks (Cretaceous, South Tibet), GSA Bulletin, v. 108, p.669-684.
Edwards, M.A., and Harrison, T.M., 1997. When did the roof collapse? late Miocene N-S extension in the High Himalaya revealed by Th-Pb monazite dating of the Khula Kangri granite. Geology, v.25, p.543-546.
Edwards, M.A., Kidd, W.S.F., Li, J., Yue, Y., and Clark, M., 1996. Multi-stage development of the southern Tibet detachment system near Khula Kangri: new data from Gonto La. Tectonophysics, v.260, p.1-20.
Einsele, G., et al., 1994. The Xigaze forearc basin, evolution and facies architecture (Cretaceous, Tibet), Sed. Geol., v. 90, p.1-20.
Floyd, P.A., Shail, R., Leveridge, B.E., and Franke, W., 1991. Geochemistry and provenance of Rhenohercynian synorogenic sandstones: implications for tectonic environment discrimination, In: Morton, A.C., Todd, S.P., Haughton, P.D.W. (eds.), Developments in Sedimentary Provenance studies. Geol. Soc. London, Spec. Publ., 57, p.173-189.
Gaetani, M., Garzanti, E., 1991. Multicyclic history of the northern India continental margin (NW Himalaya). AAPG Bulletin, v.75, p.1427-1446.
Gansser, A., 1964. Geology of the Himalayas. London, Wiley, 284 p.
Gansser, A., 1980. The significance of the Himalayan suture zone. Tectonophysics, v. 62, p. 37-52.
Ganssloser, M., 1999. Detrital chromian spinels in Rhenohercynian greywackes and sandstones (Givetain-Visean, Variscides, Germany) as indicators of ultramafic source rocks. Geol. Mag. 136, p.437-451.
Garzanti, E., 1993. Sedimentary evolution and drowning of a passive margin shelf (Giumal Group; Zanskar Tethys Himalaya, India): Palaeoenvironmental changes during final break-up of Gondwanaland, in Himalayaa Tectonics, edited by P. J. Treloar and M. P. Searle, Geol. Soc. London Spec. Publ., 74, p.277-298.
Garzanti. E., Baud, A., and Mascle, G., 1987. Sedimentary record of the northward flight of India and its collision with Eurasia (Ladakh Himalayas, India). Geodinamica Acta 1, p. 297-312.

Garzanti, E., & Van Haver, T., 1988. The Indus clastics: forearc basin sedimentation in the Ladakh Himalaya (India). Sedim. Geol., v.59, p.237-249.
Garzanti, E., 1991. Stratigraphy of the Early Cretaceous Giumal Group (Zanskar Range, Northern India). Riv. It. Paleont. Strat., v.97, n.3-4, p.485-510.
Garzanti, E., Critelli, S., and Ingersoll, R., 1996. Paleogeographic and paleotectonic evolution of the Himalayan Range as reflected by detrital modes of Tertiary sandstones and modern sands (Indus transect, India and Pakistan). GSA Bulletin 108, p. 631-642.
Garzanti, E., 1999. Stratigraphy and sedimentary history of the Nepal Tethys Himalayan passive margin. In: Upreti & Le Fort P. (Eds.), Advances on the Geology of the Himalaya -Focus on Nepal. Journal of Asian Earth Sciences, v.17/5-6, p. 805-827.
Gibling, M.R., Gradstein, F.M., Kristiansen, I.L., Nagy, J., Sarti, M., Wiedmann, J., 1994. Early Cretaceous strata of the Nepal Himalayas: conjugate margins and rift volcanism during Gondwanan breakup. J. Geol. Soc. London, v. 151, p. 269-290.
Gnos, E., Immenhauser, A., and Peters, T., 1997. Late Cretaceous/early Tertiary convergence between the Indian and Arabian plates recorded in ophiolites and related sediments, Tectonophysics, 271(1-2), p. 1-19.
Gradstein, F.M., Gibling, M.R., Sarti, M., von Rad, U.,Thurow, J.W., Ogg., J.G., Jansa, L.F., Kaminski, M.A., and Westermann, G.E.G., 1991. Mesozoic Tethyan strata of Thakkhola, Nepal: evidence for the drift and breakup of Gondwana. Palaeogeography, Palaeoclimatology, Palaeoecology, v. 88, p. 193-218.
Girardeau, J., Marcoux, J. and Zao, Y., 1984. Lithologic and tectonic environment of the Xigaze ophiolite (Yarlung Zangbo suture zone, Southern Tibet, China): kinematics of its emplacement. Eclogae Geologicae Helvetiae 77, p. 153–170.
Girardeau, J., Mercier, J.-C.C. and Zao, Y., 1985. Structure of the Xigaze ophiolite, Yarlung Zangbo suture zone, southern Tibet, China: genetic implications. Tectonics 4, p. 267–288.
Graham, S.A., Dickinson, W.R., and Ingersoll, R.V., 1975. Himalayan Bengal model for Flysch dispersal in the Appalachian Ouachita System. GSA Bulletin, v. 86, p.273-286.
Guillot, S., Garzanti, E., Baratoux, D., Marquer, D., Maheo, G., and de Sigoyer, J., 2003. Reconstructing the total shortening history of NW Himalaya. Geochemistry, Geophysics, Geosystems, v. 4, p.1-22.
Hao, Y.C., and Wan, X.Q., 1985. The marine Cretaceous and Tertiary strata of Tingri, Xizang. Contrib. Geol. Qinghai-Xizang Plateau, v. 17, p. 227-232.
Harrison T.M., Copeland P., Kidd W.S.F., and Yin. A., 1992. Raising Tibet. Science, v.255, p.1663-1670.
Hayashi, K., Fujisawa, H., Holland, H.D., Ohmoto, H., 1997. Geochemistry of ~1.9 Ga sedimentary rocks from northeastern Labrador, Canada. Geochim. Cosmochim. Acta. v.61, p.4114-4137.
Hiscott, R.N., 1984. Ophiolitic source rocks for Taconic-age flysch: trace element evidence. GSA Bulletin, v.95, p.1261-1267.
Hodges, K.V., 2000. Tectonics of the Himalaya and southern Tibet from two perspectives. GSA Bulletin. V.112, p.324-350.

Hodges, K.V., Parrish, R.R., and Searle, M.P., 1996. Tectonic evolution of the central Annapurna Range, Nepalese Himalayas, Tectonics, 15, p.1264-1291.
Hsu, K.J., ed., 1982. Mountain building processes, Academic Press, London, 263p.
Ingersoll, R., et al., 1984. The effect of grain size on detrital modes: a test of the Gazz-Dickinsion point-counting method, J. of Sedimentary Petrology, v. 49, 103-116.
Ingersoll, R.V., 1988. Tectonics of sedimentary basins. GSA Bulletin, v.100, p. 1704-1719.
Ingersoll, R.V., 1990. Actualistic sandstone petrofacies: Discriminating modern and ancient source rocks. Geology, v. 18, p.733-736.
Ingersoll, R.V., and Busby, C.J., 1995. Tectonics of sedimentary basins, in Busby, C.J., and Ingersoll, R.V., eds., Tectonics of sedimentary basins, Blackwell Science, Oxford, p.1-51.
Irvine, T.N. 1967. Chromium spinel as a petrogenentic indicator. Part 2. Petrologic applications. Can. J. Earth Sci. v.4, p. 71-103.
Jadoul, F., Berra, F., & Garzanti, E., 1998. The Tethys Himalayan passive margin from Late Triassic to Early Cretaceous (South Tibet). Journal of Asian Earth Sciences, v.16, p.173-194.
Jaeger, J. J., Courtillot, V., and Tapponnier, P., 1989. Paelontological view of the ages of the Deccan Traps, the Cretaceous/tertiary boundary, and the India/Asia collision, Geology, 17, p.316-319.
Ji, L., 1995. Sedimentary Microfacies and Environments of Eocene Zhepure Formation in Gamba District, Xizang. Acta. Sedimentologica Sinica, v.13 supp., p.88-94.
Johnson, D.M., Hooper, P.R., and Conrey, R.M., 1999. XRF analysis of rocks and minerals for major and trace elements on a single low dilution Li-tetraborate fused bead. Advances in X-ray analysis. v.41, p.843-867.
Kamenetsky V, 1996. Methodology for the study of melt inclusions in Cr-spinel, and implications for parental melts of MORB from FAMOUS area. Earth Planet Sci. Lett. 142, p. 479-486.
Kamenetsky, V.S., Crawford, A.J., Eggins, S.M., and Mühe, R., 1997. Phenocrysts and melt inclusion chemistry of near-axis seamounts, Valu Fa Ridge, Lau Basin: insight into mantle wedge melting and the addition of subduction components. Earth Planet. Sci. Lett. 151, p. 205–223.
Kamenetsky, V. S., Eggins, S. M., Crawford, A. J., Green, D. H., Gasparon, M. & Falloon, T. J., 1998a. Calcic melt inclusions in primitive olivine at 43°N MAR: evidence for melt–rock reaction/melting involving clinopyroxene-rich lithologies during MORB generation. Earth and Planetary Science Letters 160, p.115–132.
Kamenetsky, V.S., and Crawford, A. J., 1998b. Melt–peridotite reaction recorded in the chemistry of spinel and melt inclusions in basalt from 43°N, Mid-Atlantic Ridge. Earth and Planetary Science Letters 164, p.345–352.
Kamenetsky, V.S., Eggins, S.M., Crawford, A.J., Green, D.H., Gasparon, M., and Falloon, T.J., 1999. Calcic melt inclusions in primitive olivine at 43°N MAR: Evidence for melt-rock reaction/melting involving clinopyroxene-rich lithologies during MORB generation. Earth Planet. Sci. Lett. 160, p. 115–132.

Kamenetsky, V. S., Everard, J. L., Crawford, A. J., Varne, R., Eggins, S. M., and Lanyon, R., 2000. Enriched end-member of primitive MORB melts: petrology and geochemistry of glasses from Macquarie Island (SW Pacific). Journal of Petrology 41, p. 411–430.

Kamenetsky, V., Crawford, A.J., Meffre, S., 2001. Factors controlling chemistry of magmatic spinel: an empirical study of associated olivine, Cr-spinel and melt inclusions from primitive rocks. J. Petrol 41, p. 655-671.

Kamperman, M., Danyushevsky, L.V., Taylor, W.R., and Jablonski, 1996. Direct oxygen measurement of Cr-rich spinel: Implication for spinel stoichiometry. American Mineralogist 81, p. 1186-1194.

Kent, R., 1991. Lithospheric uplift in eastern Gondwana: evidence for a long-lived mantle plume system? Geology, v. 19, p. 19-23.

Kent, R., Saunders, A.D., Kempton, P.D., Ghose, N.C., 1997. Rajmahal basalts, Eastern India: mantle sources and melt distribution at a volcanic rifted margin. In: Mahoney JJ and Coffin MF (eds.), Large igneous provinces: continental, oceanic, and planetary flood volcanism, p.145-182.

Khan, M. A.; Jan, M. Q.; and Weaver, B. L. 1993. Evolution of the lower arc crust in Kohistan, N. Pakistan: temporal arc magmatism through early, mature and intra-arc rift stages. *In* Treloar, P. J., and Searle, M. P., eds. Himalayan tectonics. Geol. Soc. Lond. Spec. Publ. 74, p.123-138.

Khan, M.A., Stern, R.J., Gribble, R.F., and Windley, B.F., 1997. Geochemical and isotopic constraints on subduction polarity, magma sources and palaeogeography of the Kohistan intra-oceanic arc, northern Pakistan Himalayas. J. Geol. Soc. Lond*.,* v.154, p. 935–946.

Klootwijk, C., Sharma, M.L., Gergan, J., Tirkey, B., Shah, S.K., and Agarwal, V., 1979. The extent of greater India: II, Palaeomagnetic data from the Ladakh intrusives in Kargil, Northwestern Himalayas. Earth Planet. Sci. Lett., 44, p. 47-64.

Knaack, C., Cornelius, S., and Hooper, P., 1994. Trace element analyses of rocks and minerals by ICP-MS, Geoanalytical Library, Washington State University: Pullman, Washington State University: http://www.wsu.edu:8080/~geology/Pages/Services/ICP.html.

Lee, Y., 1999. Geotectonic significance of detrital chromian spinel: a review. Geosciences Journal 3, p. 23-29.

Le Fort, P., 1996. Evolution of the Himalaya. In: Yin, A., and Harrison, M.(Eds.), The Tectonic Evolution of Asia, Cambridge University Press, Cambridge, p.95-109.

Lenaz, D., Kamenetsky, V., and Crawford, A.J., Princivalle, F., 2000. Melt inclusions in detrital spinel from SE Alps (Italy-Slovenial): a new approach to provenance studies of sedimentary basins. Contrib. Mineral Petrol. 139, p. 748-758.

Li, G.B., Wan, X.Q., 2003. Eocene microfossils in southern Tibet and the final closing of the Tibet-Tethys. J. of Stratigraphy, v.27, p.99-108.

Li, G.B., Wan, X.Q., Qiherige, Liang, D.Y., Liu, W.C., 2002. Eocene fossil carbonate microfacies and sedimentary environment in Gangba-Tingri, southern Tibet. Geology in China, v.29, p.401-406.

Li, X.H., Wang, C.S., Hu, X.M., Wan, X.Q., Xu, Y.L., Zhao, W.J., 2000. The Pengqu Formation: a new Eocene stratigraphical unit in Tingri area, Tibet. J. of Stratigraphy, v.24, p.243-248.

Lihou, J.C., and Mange-Rajetzky, M.A., 1996. Provenance of the Sardona Flysch, eastern Swiss Alps: examples of high-resolution heavy mineral analysis applied to an ultrastable assemblage. Sed. Geol. 105, p.141-157.

Liu, G., 1992. Permian to Eocene sediments and Indian passive margin evolution in the Tibetan Himayalas, Tub. Geowiss. Arb. v. 13.

Liu, G., Einsele, G., 1994. Sedimentary history of the Tethyan basin in the Tibetan Himalayas, Geol. Rundsch., v.83, p.32-61.

Liu, G., Einsele, G., 1996. Various types of olistostromes in a closing ocean basin, Tethyan Himalaya (Cretaceous, Tibet). Sedimentary Geology, v. 104, p. 203-226.

Mack, G.H., James, W.C. and Monger, H.C., 1992. Classification of Paleosols, GSA Bulletin, v.105, p. 129-136.

Mange, M.A., Maurer, H.F.W., 1992. Heavy mineral in color. Chapman and Hall, London. 147p.

Matte, P., Mattauer, M., Jolivet, J.M., and Griot, D.A., 1997. Continental subductions beneath Tibet and the Himalayan orogeny: A review, Terra Nova, 9, p.264-270.

McDermid, I.R.C., Aitchison, J.C., Davis, A.M., Harrison, T.M., and Grove, M., 2002. The Zedong terrane: a Late Jurassic intra-oceanic magmatic arc within the Yarlung–Tsangpo suture zone, southeastern Tibet. Chemical Geol. 187, p.267-277.

Mclennan, S.M., 1989. Rare earth elements in sedimentary rocks: Influence of provenance and sedimentary processes: Mineralogical Society of America Reviews in Mineralogy. V. 21, p.169-200.

McLennan, S.M., Taylor, S.R., McCulloch, M.T., and Maynard, J.B., 1990. Geochemical and Nd-Sr isotope composition of deep sea turbidites: crustal evolution and plate tectonic associations. Geochim. Cosmochim. Acta. v.54, p. 2015-2050.

McLennan, S.M., Hemming, S.R., McDaniel, D.K., and Hanson, G.N., 1993. Geochemical approaches to sedimentation, provenance, and tectonics. In: Processes controlling the composition of clastic sediments (Ed. By Johnsson M.J. and Base A. Geol. Soc. Am. Spec. Pap., 284, p.21-40.

Molnar, P., Tapponnier, P., 1978. Active tectonics of Tibet, JGR, v.83, p.5361-5375.

Molnar, P., Tapponnier, P., 1975. Cenozoic tectonics of Asia: effects of a continental collision, Science, v.189, p. 419-426.

Molnar, P., 1984. Structure and tectonics of the Himalaya: constraints and implications of geophysical data., Annu. Rev. Earth Planet. Sci., v. 12, p. 489-518.

Morton, A.C., 1985. Heavy minerals in provenance studies. In: Zuffa, G.G.(ed.), Provenance of Arenites. Reidel, Dordrecht, p.249-277.

Morton, A.C., 1991. Geochemical studies of detrital heavy minerals and their application to provenance studies. In: Morton, A.C., Todd, S.P., Haughton, P.D.W. (eds.), Developments in Sedimentary Provenance studies. Geol. Soc. London, Spec. Publ., 57, p.31-45.

Morton, A.C., Davies, J.R., Waters, R.A., 1992. Heavy minerals as a guide to the turbidite provenances in the lower Palaeozoic Southern Welsh Basin: a pilot study. Geol. Mag., v.129, p.573-580.
Mu, A.Z., Wen, S.X., Wang, Y.G., Zhang, B.G., Ying, J.X., 1973. Stratigraphy of the Mount Jolmo Lungma region in southern Tibet. China Sci. Sinica16, p.96-111.
Najman, Y., and Garzanti, E., 2000. An integrated approach to provenance studies: reconstructing early Himalayan paleogeography and tectonic evolution from Tertiary foredeep sediments, N. India. GSA Bulletin 112, p.435-449.
Najman, Y.M.R., Pringle, M.S., Johnson, M.R.W., Robertson, A.H.F., and Wijbrans, J.R., 1997. Laser 40Ar/39Ar dating of single detrital muscovite grains from early foreland basin sediments in India: Implications for early Himalayan evolution. Geology, v. 25, p.535-538.
Najman, Y., Pringle, M., Godin, L., and Oliver, G., 2001. New dating of the oldest Himalayan continental foreland basin sediments forces reconsideration of current models of India-Eurasia collision. Nature 410, p.194-197.
Najman, Y., Pringle, M., Godin, L., and Oliver, G., 2002. A reinterpretation of the Balakot Formation; implications for the tectonic evolution of the NW Himalaya, Pakistan. Tectonics, v.21, p.9-1-9-18.
Nelson, K. D., et al., 1996. Partially molten middle crust beneath Southern Tibet: Synthesis of project INDEPTH results., Science, 274, p.1684-1896.
Nesbitt, H.W., Young, G.M., 1982. Early Proterozoic climates and plate motions inferred from major element chemistry of lutites. Nature 299, p.715-717.
Nicolas, A., 1989. Structures of Ophiolites and Dynamics of Oceanic Lithosphere, Kluwer Academic Publishers, Dordrecht, 368 p.
Nicolas, A., Girardeau, J., Marcoux, J., Dupre, B., Wang, X., Cao, Y., Zheng, H. and Xiao, X., 1981. The Xigaze ophiolite (Tibet): a peculiar oceanic lithosphere. Nature 294, p. 414–417.
Paktunc, A.D., Cabri, L.J., 1995. A proton- and electron-microprobe study of gallium, nickel and zinc distribution in chromian spinel. Lithos 35, p. 261-282.
Patriat, P., Achache, J., 1984. India-Eurasia collision chronology has implications for crustal shortening and driving mechanism of plates, Nature, v. 311, p.615-621.
Pazelt, A., Li, H., Wang, J., and Appel, E., 1996. Pleomagnetism of Cretaceous to Tertiary sediments from southern Tibet: Evidence for the extent of the northern margin of India prior to the collision with Eurasia, Tectonophysics, 259, p.259-284.
Pearce, J.A., Lippard, S.J. and Roberts, S., 1984. Characteristics and tectonic significance of supra-subduction zone ophiolites. Geological Society of London Special Publication 16, p. 77–94.
Pearce, J.A., 1987. An expert system for the tectonic characterization of ancient volcanic rocks. J. Volcanol. Geothern. Res. 32, p.51-65.
Pearce, J.A., Mei, H., 1988. Volcanic rocks of the 1985. Tibet Geotraverse: Lhasa to Golmud. in Chang, C., Shackleton, R.M., Dewey, J.F., and Yin, J., eds., The geological evolution of Tibet: Royal Society of London Philosophical Transactions, p.169-201.

Pettijohn, F.J., Potter, P.E., and Siever, R., 1987. Sand and Sandstone, second edition, Springer-Verlag, 553p.
Pivnik, D.A., Johnson, G.D., 1995. Depositional response to Pliocene-Pleistocene foreland partitioning in northwest Pakistan. GSA Bulletin, v.107, p.1037-1053.
Pivnik, D.A., Wells, N.A., 1996. The transition from Tethys to the Himalaya as recorded in northwest Pakistan. GSA Bulletin, v.108, p.1295-1313.
Pober, E., Faupl, P., 1988. The Chemistry of detrital spinels and its application for the geodynamic evolution of the Eastern Alps. Geol Rundsch 77, p.641-670.
Qayyum, M., et al., 2001. Detrital modes and provenance of the Paleogene Khojak Formation in the Pakistan: Implications for early Himalayan orogeny and unroofing, GSA Bulletin, v.113, p.320-332.
Rage, J.C., Cappetta, H., Hartenberger, J.L., Jaeger, J.J., Sudre, J., Vianeyliaud, M., Kumar, K., Prasad, G.V.R., and Sahni, A., 1995. Collision age. Nature, v. 375, p. 286.
Ratschbacher, L., Frisch, W., Liu, G., Chen, C., 1994. Distributed deformation in southern and western Tibet during and after India-Asia collision. JGR, v.99, p.19917-19945.
Reuber, I., 1986. Geometry of accretion and oceanic thrusting on the Spongtang ophiolite, Ladakh-Himalaya. Nature, v.321, p.592-596.
Richter, F., Rowley, D.B., and DePaolo, D.J., 1992. Sr isotope evolution of seawater: the role of tectonics. Earth Planet. Sci. Lett., v. 109, p. 11-23.
Robertson, A.H.F., and Degnan, P.J., 1993. Sedimentology and tectonics implications of the Lamayuru Complex: Deep-water facies of the Indian passive margin, Indus suture zone, Ladakh Himalaya, in Treloar, P.J., and Searle, M.P., eds., Himalayan tectonics, London, Geological Society Special Pub. 74, p. 299-321.
Roeder, P.L. and Reynolds, I., 1991, Crystallization of chromite and chromium solubility in basaltic melts. J. Petrol. 32, p. 909-934.
Roeder, P.L., 1994. Chromite: from the fiery rain of chondrules to the Kilauea Iki lava lake. Can. Mineral. 32, p. 729-746.
Roeder, P.L. and Poustovetov, A., 2001. Growth Forms and Composition of chromian spinel in MORB magma: diffusion-controlled crystallization of chromian spinel. Canadian Mineralogist. V. 39, p. 397-416.
Rolland, Y., Picard, C., Pecher, A., Lapierre, H., Bosch, D., Keller, F. 2002. The Cretaceous Ladakh arc of NW Himalaya-slab melting and melt-mantle interaction during fast northward drift if Indian plate. Chem. Geol. V.182, p. 139-178.
Roser, B.P., and Korsch, R.J., 1986. Determination of tectonic setting of sandstone-mudstone suites using SiO2 content and K2O/Na2O ratio. J. Geol., v.94, p. 635-650.
Roser, B.P., Korsch, R.J., 1988. Provenance signatures of sandstone-mudstone suites determined using discrimination function analysis of major element data. Chemical Geology, 67, p. 119-139.
Rowley, D., and Kidd, W.S.F., 1981. Stratigraphic relationships and detrital composition of the medial Ordovician flysch of western New England: implications for the tectonic evolution of the Taconic Orogeny. J. Geol., 89, p. 199-218.

Rowley, D., 1996. Age of initiation of collision between India and Asia; a review of stratigraphic data, Earth Planet. Sci. Lett., v. 145, p.1-13.
Rowley, D., 1998. Minimum age of initiation of collision between India and Asia north of Everest based on the subsidence history of the Zhepure Mountain section, J. Geol., v. 106, p. 229-235.
Schiano, P., Clocchiatti, R., Lorand, J.P., Massare, D., Deloule, E., and Chaussidon, M., 1997. Primitive basaltic melts included in podiform chromites from the Oman Ophiolite. Earth and Planetary Science Letters, v.146, p. 489-497.
Schwab, F.L., 1975. Framework mineralogy and chemical composition of continental margin-type sandstone, Geology, v.3, p.487-390.
Sciunnach, D., Garzanti, E., 1996. Sedimentary record of Late Paleozoic rift and break-up in Northern Gondwana (Thini Chu Group and Tamba-Kurkur Fm.; Dolpo Tethys Himalaya, Nepal). Geodinamica Acta, v.9, n.1, p.41-56.
Sciunnach, D., and Garzanti, E., 1996. Detrital chromian spinels record tectono-magmatic evolution from Carboniferous rifting to Permian spreading in Neotethys (India, Nepal and Tibet). Ofioliti 22, p. 101-110.
Scowen, P.A.H., Roeder, P.L., and Helz, R.T., 1991. Reequilibration of chromite within Kilauea Iki lava lake, Hawaii. Contrib. Mineral. Petrol. 107, p. 8-20.
Searle, M. P.; Windley, B. F.; Coward, M. P.; Cooper, D. J. W.; Rex, A. J.; Rex, D. C.; Li Tingdong; Xiao Xuchang; Jan, M. Q.; Thakur, V. C.; and Kumar, S. 1987.The closing of the Tethys and the tectonics of the Himalayas, GSA Bulletin, v. 98, p.678-701.
Searle, M.P., Pickering, K.T., and Cooper, D.J.W., 1990. Restoration and evolution of the intermontane Indus molasses basin, Ladakh Himalaya, India. Tectonophysics, v.174, p.301-314.
Searle, M.P., 1991. Geology and Tectonics of the Karakoram Mountains, Wiley, New York, 358p.
Searle, M., 1995. The rise and fall of Tibet. Nature, v.374, p.17-18.
Searle, M.P., Khan, M.A., Fraser, J.E., and Gough, S.J., 1999. The tectonic evolution of the Kohistan-Karakoram collision belt along the Karakoram Highway transect, north Pakistan. Tectonics, v.18, p.929-949.
Searle M., 2001. Dating the Indian continental subduction and collisional thickening in the northwest Himalaya: Multichronology of the Tso Morari eclogites: comments and reply. Geology, v.29, p.191.
Sengor, A.M.C., et al., 1988. Original assembly of the Tethyside orogenic collage at the expense of Gondwanaland. In: Audley-Charles MG, Hallame A (eds) Gondwana and Tethys. Geol. Soc. Spec. Pub. 37, p.119-181.
Shimizu, N., Sobolev, A. V., and Layne, G. D., 1998. In-situ Pb isotope analysis of olivine-hosted melt inclusions from mid-ocean ridges. EOS Transactions, American Geophysical Union, F950.
Sigurdsson, I.A., Steinthorsson, S., and Gronvold, K., 2000. Calcium-rich melt inclusions in Cr-spinels from Borgarhraun, northern Iceland. Earth Planet. Sci. Lett., v.183, p.15-26.
Sinha, A., 1988. Geology of the Higher Central Himalaya, New York, John Wiley &Sons, 219p.

Sobolev, A.V., Danyushevsky, L.V., 1994. Petrology and geochemistry of boninites from the north termination of the Tonga Trench: constraints on the generation conditions of primary high Ca boninite magmas. Journal of Petrology 35, p.1183-1211.

Sobolev, A.V., 1996. Melt inclusions in minerals as a source of principle petrological information. Petrology v.4, p. 209-211.

Sobolev, A.V., Hofmann, A.W., and Nikogosian, I.K., 2000. Recycled oceanic crust observed in 'ghost plagioclase' within the source of Mauna Loa lavas. Nature 404, p. 986-990.

Stosch, H.G., 1981. Sc, Cr, Co and Ni partitioning between minerals from spinel peridotite xenoliths. Contrib. Mineral. Petrol. 78, p.166-174.

Stowe, C.W., 1994. Compositions and Tectonic settings of chromite deposits through time. Economic Geol. 89, p.528-546.

Sun, S.S. and McDonough, W.F., 1989. Chemical and isotopic systematics of oceanic basalts: implications for mantle composition and processes. Geological Society Special Publication 42, p. 313–345.

Tapponnier, P., Mercier, J.L., Proust, F., Andrieux, J., Armijo, R., Bassoullet, J.P., Brunel, M., Burg, J.P., Colchen, M., Dupré, B., Girardeau, J., Marcoux, J., Mascle, G., Matte, P., Nicolas, A., Li, T., Xiao, X., Chang, C., Lin, P., Li, G., Wang, N., Chen, G., Han, T., Wang, X., Den, W., Zhen, H., Sheng, H., Cao, Y., Zhou, J. and Qiu, H., 1981a. The Tibetan side of the India–Eurasia collision. Nature 294, p. 405–410.

Tapponnier, P., Mattauer, M., Proust, F., Cassaigneau, C., 1981c. Mesozoic ophiolites, sutures and large-scale tectonic movements in Afghanistan. Earth & Planetary Science Lett., v.52, p.355-371.

Taylor S.R. and McLennan S.M., 1985. The continental crust: its composition and evolution. Black-wells, Oxford, 312p.

Treloar, P.J., and Coward, M.P., 1991. Indian plate motion and shape: Constraints on the geometry of the Himalaya orogen, Tectonophysics, 191, p.189-198.

Tucker, M.E., 2001. Sedimentary petrology: an introduction to the origin of sedimentary rocks, third edition, Blackwell Science, 262p.

Uddin, A., and Lundberg, N., 1998. Cenozoic history of the Himalayan-Bengal system: sand composition in the Bengal basin, Bangladesh. GSA Bulletin, v.110, p.497-511.

Valloni, R., and Maynard, J.B., 1981. Detrital modes of recent deep-sea sands and their relation to tectonic setting: a frist approximation. Sedimentology, v.28, p.75-83.

Van der Voo, R., Spakman, W., and Bijwaard, H., 1999. Tethyan subducted slabs under India, Earth Planet. Sci. Lett. 171, p.7-20.

Walker, R.G., (ed.), 1979. Facies Models. Geosci. Can. Reprint Series 1, Geol. Assoc. Can., 211p.

Wan, X., Jansa, L.F., Sarti M., 2002. Cretaceous and Paleogene boundary strata in southern Tibet and their implication for the India-Eurasia collision. Lethaia. v. 36, p. 131-146.

Wang, C., et al., 2000, The Cretaceous in Gyangze, Southern Xizang (Tibet): Redefined, Acta Geological Sinica, v. 74, p. 97-107.
Wang, C., Liu, Z. and Hébert, R., 2000. The Yarlung-Zangbo paleo-ophiolite, southern Tibet: implications for the dynamic evolution of the Yarlung-Zangbo Suture Zone. Journal of Asian Earth Sciences 18, p. 651–661.
Wang, C., Li, X., Hu, X., Jansa, L.F., 2002. Latest marine horizon north Qomolangma (Mt Everest): implications for closure of Tethys seaway and collision tectonics. Terra Nova. v. 14, p.114-120.
Watson, B., 1976. Glass inclusions as samples of early magmatic liquid: determinative method and application to a south Atlantic basalt. J. of Volcanology and Geothermal Research. 1, p.73-84.
Weinberg, R.F., and W. J. Dunlap, W.J., 2000. Growth and deformation of the Ladakh Batholith, Northwest Himalayas; implications for timing of continental collision and origin of calc-alkaline batholiths, J. Geol., 108, p.303-320.
Wen, S., 1987a. Cretaceous-Tertiary system. In: Stratigraphy of the Mount Qomolangma Region. Science Press, Beijing, p.130-180.
Willems, H., Zhang, B.G., 1993a. Cretaceous and lower Tertiary sediments of the Tethys Himalaya in the area Gamba (South Tibet, PR China). Ber FB Geowiss Univ Bremen 38, p.3-27.
Willems, H., Zhang, B.G., 1993b. Cretaceous and lower Tertiary sediments of the Tibetan Tethys Himalaya in the area Tingri (South Tibet, PR China). Ber FB Geowiss Univ Bremen 38, p.29-47.
Willems, H., Zhou, Z.C., Zhang, B.G., Grafe, K.U., 1996. Stratigraphy of the Upper Cretaceous and Lower Tertiary strata in the Tethyan Himalayas of Tibet (Tingri area, China), Geol. Rundsch., v.85, 723-754.
Xizang BGMR (Xizang Bureau of Geology and Mineral Resources), 1992. Regional Geology of the Xizang Autonomous Region. Beijing: Geological Publishing House.
Xu, Y.L., 2000. Early Tertiary calcareous nannofossils from southern Tibet and the closing time of east Tethys in Tibet. Geoscience, v.14, p.255-264.
Yerino, L.N., and Maynard, J.B., 1984. Petrography of modern marine sands from Peru-Chile Trench and adjacent area, Sedimentology, v. 31, p.83-89.
Yin, A., and Harrison, M., 2000, Geologic evolution of the Himalayan-Tibetan orogen, Annu. Rev. Earth Planet. Sci., v. 28, 211-280.
Ying, J.X., 1988. The evolutionary outline on Stratigraphy and geology of southern Tethyan domain in the Qinghai-Xizang Plateau. Bull. Inst. Geol. 3, p.1-25.
Young, G.M., Brunn, V., Gold, D.J.C., and Minter, W.E.L., 1998. Earth's oldest reported glaciation: physical and chemical evidence from the Archean Mozaan Group (~2.9 Ga) of South Africa. J. Geol., v. 106, p.523-538.
Zhang B.G., 1979. The Cretaceous/Tertiary boundary of southern Tibet in China, in Christensen, W.K.,Birkelund, T., eds., Proc. Symp. Cretaceous-Tertiary boundary events. University of Copenhagen, Copenhagen, p.258-262.
Zhang, B.G., 1980. Latest marine sediments in Xizang and process of Early Tertiary regression, in Proc. Symp. Qinghai-Xizang Plateau. Academia Sinica, Beijing, p. 329-332.

Zhu, B., Kidd, W.S.F., Rowley, D., Currie, B. Chemical compositions and tectonic significance of chrome-rich spinels in Tianba Flysch, southern Tibet. In review.
Zuffa, G.G., 1980. Optical analysis of arenites: their composition and classification, J. of Sedimentary Petrology, v. 50, p.21-29.
Zuffa, G.G., 1985. Optical analysis of arenites: influence of methodology on computational results, in Zuffa, G.G., ed., Provenance of arenites, Reidel, Dordrecht, p. 165-189.